INVARIANCES AND CONTROLLED VARIABLES IN HUMAN ARM MOVEMENT

Doctoral thesis presented by

Adam Matić

Thesis director:

Dr. Alejandro Gómez Marín

PhD Program in Neuroscience

Instituto de Neurociencias, UMH-CSIC

Universidad Miguel Hernández de Elche

- 2022 –

Sant Joan d'Alacant, 2022

DOCTORAL THESIS BY COMPENDIUM OF PUBLICATIONS

This doctoral thesis, entitled "*Invariances and controlled variables in human arm movement*" is presented as a compendium of the following publications where I am the first or co-first author:

Matic, A., & Gomez-Marin, A. (2019). A customizable tablet app for hand movement research outside the lab. *Journal of neuroscience methods*, *328*, 108398. PMID: 31412268 DOI: 10.1016/j.jneumeth.2019.108398

Zago, M., Matic, A., Flash, T., Gomez-Marin, A., & Lacquaniti, F. (2017). The speed-curvature power law of movements: a reappraisal. *Experimental brain research*, *236*(1), 69-82. PMID: 29071361 DOI: 10.1007/s00221-017-5108-z

Matic, A., & Gomez-Marin, A. (2020). Geometric purity, kinematic scaling and dynamic optimality in drawing movements beyond ellipses. *Journal of Mathemathical Psychology*, *99*, 102453. DOI: 10.1016/j.jmp.2020.102453

Matić, A., Valerjev, P., & Gomez-Marin, A. (2021). Hierarchical control of visually-guided movements in a 3D-printed robot arm. *Frontiers in Neurorobotics*, 149. PMID: 34776921 DOI: 10.3389/fnbot.2021.755723

ADDITIONAL PUBLICATIONS INCLUDED IN THE THESIS

Matić, A., & Gomez-Marin, A. (2022). Angular speed should be avoided when assessing the speed-curvature power law of movement. bioRxiv. DOI: 10.1101/2022.06.27.497695

Matić, A., & Gomez-Marin, A. (2021). Elbow angle and stiffness control by twisted string actuators and nested feedback. *The 9.5th international symposium on Adaptive Motion of Animals and Machines. Ottawa Canada (Virtual Platform)*, DOI 10.18910/84845

Matić, A. (2022). Visuomotor phase-locked loop reproduces elliptic hand trajectories across different rhythms. bioRxiv. DOI: 10.1101/2022.07.20.500761

Sant Joan d'Alacant, 2022

Dr. Alejandro Gómez Marín, director of the doctoral thesis entitled *"Invariances and controlled variables in human arm movement"*

CERTIFIES:

That Mr. Adam Matić has carried out under my supervision the work entitled "*Invariances and controlled variables in human arm movement*" in accordance with the terms and conditions defined in their Research Plan and in accordance with the Code of Good Practice of the University Miguel Hernández of Elche, and has fulfilled in a satisfactory manner the objectives needed for its public defense as a doctoral thesis.

I sign for the appropriate purposes, in Sant Joan d'Alacant _____

Thesis director

Dr. Alejandro Gómez Marín

Sant Joan d'Alacant, 2022

Ms. Elvira de la Peña García, Coordinator of the Neuroscience PhD Program at the Institute of Neurosciences in Alicante, a joint center of the Miguel Hernández University (UMH) and the Spanish National Research Council (CSIC),

INFORMS:

That Mr. Adam Matić has carried out under the supervision of our PhD Program the work entitled "*Invariances and controlled variables in human arm movement*" in accordance with the terms and conditions defined in the Research Plan and in accordance with the Code of Good Practice of the University Miguel Hernández de Elche, fulfilling, in a satisfactory manner, the objectives for its public defense as a doctoral thesis.

I sign for the appropriate purposes,

in Sant Joan d'Alacant _____

Dra. Elvira de la Peña García

Coordinator of the PhD Program in Neuroscience

Av Ramón y Cajal s/n
CAMPUS DE SANT JOAN
03550 SANT JOAN D'ALACANT–
ESPAÑA

E-mail : elvirap@umh.es
www.in.umh.es

Tel: +34 965 919533
Fax: +34 965 919549

Sant Joan d'Alacant, 2022

To whom it may concern:

The doctoral thesis entitled: "*Invariances and controlled variables in human arm movement*", developed by myself, Adam Matić, presented as a compendium of publications, based on experimental studies undertaken at the Instituto de Neurociencias UMH-CSIC during the PhD program in Neuroscience of the Miguel Hernández University, has been partially supported by *Formación del Personal Investigador* (FPI) grant with reference BES-2016-077608, and a CSIC-Severo Ochoa grant of the Instituto de Neurociencias UMH-CSIC with reference SEV-2013-0317-16-1

Adam Matić

Table of contents

Abbreviations 3

Acknowledgements 4

Abstract 6

Resumen 7

1. Introduction 9

1.1. Why motor control 10
1.2. In natural hand movement, speed is related to curvature 11
1.3. The 2/3 power law and the kinematics of curved movements 12
1.4. Theories explaining the origins of the speed-curvature power law 15
1.4.1. Central origin 15
1.4.2. Interaction hypotheses 17
1.4.3. Statistical artifacts 18
1.5. Control theory and the target tracking task 18
1.5.1. Target tracking task 19
1.5.2. The controlled variable 20
1.5.3. Approximating controlled variables 22
1.5.4. More than tracking targets 24
1.6. Objectives 25

2. Materials and Methods 27

2.1. Movement recording application for Android tablet 28
2.2. Recording of movement trajectories in the lab 28
2.2.1. Hardware 28
2.2.2. Software 29
2.3. Generating trajectories with arbitrary speed-curvature power laws 29
2.4. Robot arm with hierarchical control 29
2.5. Control of joint angle and tone with antagonistic muscles 32

3. Discussion 35

3.1. Understanding the problem 36
3.1.1. An android app for recording finger movement outside of the lab 36
3.1.2. A reappraisal of the speed-curvature power law 37
3.1.3. Mechanical work is not minimal in the speed-curvature power law 38
3.1.4. Angular speed should be avoided when assessing the speed-curvature power law 39
3.2. Proposing solutions 40
3.2.1. Robot arm produces power law trajectories, and other invariances 40
3.2.2. Robot model of antagonistic muscles 42
3.2.3. Visuomotor phase-locked loop reproduces elliptic hand trajectories 43

4. Conclusions 47

5. References 51

6. Annex 57

Annex 1: Matic, A., & Gomez-Marin, A. (2019). A customizable tablet app for hand movement research outside the lab.....
Annex 2: Zago, M., Matic, A., Flash, T., Gomez-Marin, A., & Lacquaniti, F. (2017). The speed-curvature power law of movements: a reappraisal.....
Annex 3: Matic, A., & Gomez-Marin, A. (2020). Geometric purity, kinematic scaling and dynamic optimality in drawing movements beyond ellipses.....
Annex 4: Matić, A., & Gomez-Marin, A. (2022). Angular speed should be avoided when assessing the speed-curvature power law of movement. .....
Annex 5: Matić, A., Valerjev, P., & Gomez-Marin, A. (2021). Hierarchical control of visually-guided movements in a 3D-printed robot arm.....
Annex 6: Matić, A., & Gomez-Marin, A. (2021). Elbow angle and stiffness control by twisted string actuators and nested feedback.....
Annex 7: Matić, A. (2022). Visuomotor phase-locked loop reproduces elliptic hand trajectories across different rhythms .....

Abbreviations

AC power law – angular speed and curvature power law

CV – controlled variable

DOF – degree of freedom

GTO – Golgi tendon organ

OFC – optimal feedback control

PCT – perceptual control theory

qc – controlled quantity

qi – input quantity

qo – output quantity

TSA – twisted string actuators

VC power law – tangential speed and curvature power law

Acknowledgements

I would like to thank the people who have helped me during doctoral studies. First, to my thesis director Alex, for giving me the freedom to explore the ideas I thought were important and for providing me with guidance when I needed it.

For their help in all administrative matters, a big thanks to Virtudes and Maite.

I would like to thank all my lab mates from the Behavior of Organisms lab - Saurabh, Chema, Marina, and Gina, for their help in work and for their friendship. I would also like to thank the members of the Hub Lab – Roberto, Maria, Javi and Alicia; and the Social Lab – Aroa, Diana, Helena, Joan, Michael and Kevin. Thank you all for the tireless drawing of ellipses, for making the cafeteria lunches fun and for being great friends and colleagues.

Finally, I thank Raquel from the Canals Lab for her wisdom and support.

...

*To understand a system, we must be able to see that it **must**, because of its inner nature, behave as we see it behaving. Its properties must grow out of its inner organization; its behavior must arise from its properties.*

...

*The best way to prove that an explanation actually explains something is to cast is as a working simulation, turn it on, and let it operate by the rules you have put in it. If you can't do that, then you don't have a model **or** an explanation. All you have is more or less persuasive rhetoric.*

W.T. Powers, Preface to *Living Control Systems* (1989, p. *xv*)

Abstract

The main question of this thesis is the origin of the correlation between speed and curvature in human hand movement, or *why does the hand move slower in curves*? The phenomenon is known since the late 19th century, and was formalized in the late 20th century as the "speed-curvature power law" or "the 2/3 power law". It has often been studied, since it is one of the few invariances found in hand movement. There is no consensus about its origin, and the attempts to explain it can be placed into roughly three approaches. First, the cortical origin hypotheses assume that the cortical structures optimize movement trajectories according to a criterion (such as minimal jerk) and the movement system then executes the planned trajectory. The second group of approaches assumes interaction: the power law depends on the interaction between the brain, the hand, and the environment; it arises from low-pass filtering properties of the arm or from differences in the environment, such as moving the hand through air or water. Finally, the third approach attempts to explain away the power law as a purely statistical artifact, arising from mistakes in the measurement process or the calculation of variables.

To answer this question, we have considered all three approaches, using mathematical analysis of generated trajectories, human behavioral experiments, and numerical and robotic modelling. We showed that the power law is not mathematically trivial, but that there is a statistical artifact if angular speed is used instead of tangential speed. We argued against the claim that mechanical work is minimal in the 2/3 power law, and explored the relationship between the angular frequency of a curve, its power law exponent and the minimization of jerk. Applying the theory of hierarchical control, we built a robot arm and showed how the interaction between the artificial perception, simple controllers, low-pass-filtering physical arm, and the unpredictable environment may result in the power law when drawing ellipses. The robot, however, produced smaller and phase-delayed elliptic trajectories compared to humans in similar tasks. In behavioral experiments with humans, we found that the most likely visual features used when tracking targets along elliptic trajectories are the phase and size difference. We created a numerical simulation of sensorimotor feedback loops using those features as controlled variables. When performing the same tasks as human participants, the simulation drew ellipses of the correct size and without phase delay, and also reproduced the exponents of the speed-curvature power law.

Taken together, the papers show significant progress toward understanding the origins of the speed-curvature power law, and suggest further testable hypotheses on the neural mechanisms of sensorimotor control in human arm and hand movement. Specifically, it appears that the power law in drawing ellipses can be explained by a hypothesis in the interaction approach - the power law emerges in the interaction of the low-pass filtering in the sensorimotor system, and higher-level visual controlled variables, such as the phase difference and the size difference.

Additionally, we developed a free open-source movement tracking application for Android tablets to facilitate hand movement research outside the lab. Further, we built a prototype robot model of two antagonistic muscles for simultaneous control of joint angle and muscle tone. This is an initial step toward a more complex electromechanical model of the human arm that could be used to integrate and further verify the hypotheses generated by the present thesis.

Resumen

La pregunta principal de esta tesis es el origen de la correlación entre la velocidad y la curvatura en el movimiento de la mano humana, o ¿por qué la mano se mueve más despacio en las curvas? El fenómeno se conoce desde finales del siglo XIX y se formalizó a finales del siglo XX como la "ley de potencia de curvatura de velocidad" o "ley de potencia de 2/3". Se ha estudiado a menudo, ya que es una de las pocas invariancias encontradas en el movimiento de la mano. No hay consenso sobre su origen, y los intentos de explicarlo se pueden encontrar en, principalmente, tres enfoques. Primero, las hipótesis del origen cortical asumen que las estructuras corticales optimizan las trayectorias de movimiento de acuerdo con un criterio (como sacudida mínima) y luego el sistema de movimiento ejecuta la trayectoria planificada. El segundo enfoque asume la presencia de interacción: la ley de potencia depende de la interacción entre el cerebro, la mano y el entorno: surge de las propiedades de filtrado de paso bajo del brazo o de las diferencias en el entorno, como mover la mano a través del aire o el agua. Finalmente, el tercer enfoque intenta explicar la ley de potencia como un artefacto puramente estadístico, que emerge de errores en el proceso de medición o el cálculo de variables.

Para responder a esta pregunta, hemos considerado los tres enfoques, utilizando análisis matemáticos de trayectorias generadas, experimentos de comportamiento en humanos y modelos numéricos y robóticos. Mostramos que la ley de potencia no es matemáticamente trivial, pero que existe un artefacto estadístico si se usa la velocidad angular en lugar de la velocidad tangencial para su medida. Argumentamos que el trabajo mecánico no es mínimo en la ley de potencia de 2/3, y exploramos la relación entre la frecuencia angular de una curva, su exponente de ley de potencia y la minimización de la sacudida. Aplicando la teoría del control jerárquico, construimos un brazo robótico y mostramos cómo la interacción entre la percepción artificial, los controladores simples y el brazo físico de filtrado de paso bajo con el entorno impredecible puede dar como resultado la ley de potencia al dibujar elipses. El robot, sin embargo, produjo trayectorias elípticas más pequeñas y con retraso de fase en comparación con los humanos en tareas similares. En experimentos de comportamiento con humanos, descubrimos que las características visuales más probables que se utilizan al rastrear objetivos a lo largo de trayectorias elípticas son la diferencia de fase y tamaño. Creamos una simulación numérica de bucles de retroalimentación sensoriomotora usando estas características como variables controladas. Al realizar las mismas tareas que los participantes humanos, la simulación dibujó elipses del tamaño correcto y sin retraso de fase, reproduciendo también los exponentes de la ley de potencia de velocidad-curvatura.

En conjunto, los artículos muestran un progreso significativo hacia la comprensión de los orígenes de la ley de potencia de velocidad-curvatura y sugieren más hipótesis comprobables sobre los mecanismos neurales del control sensoriomotor en el movimiento del brazo y la mano humana. Específicamente, sugiere que la ley de potencia al dibujar elipses puede explicarse mediante la hipótesis en el enfoque de interacción: la ley de potencia surge de la interacción del filtrado de paso bajo en el sistema sensoriomotor con las variables visuales controladas de nivel superior, como la diferencia de fase y la diferencia de tamaño.

Además, desarrollamos una aplicación de seguimiento del movimiento de código abierto para tabletas Android con el fin de facilitar la investigación del movimiento de las manos fuera del laboratorio. Adicionalmente, construimos un modelo de robot prototipo de dos

músculos antagónicos para el control simultáneo del ángulo articular y el tono muscular. Este es un paso inicial hacia un modelo electromecánico más complejo del brazo humano que podría usarse para integrar y verificar aún más las hipótesis generadas por la presente tesis.

1. Introduction

1.1. Why motor control

Research in motor control is plagued (or perhaps blessed) with controversies, some of which involve quite fundamental questions (Flash and Sejnowski, 2001).

Most of our interactions with the world are mediated by muscles – obviously locomotion and limb movements, but also chewing, breathing, speaking, eye movements, iris dilation and contraction, and noise dampening in the ear. When we get goosebumps, there are tiny muscles, attached to hair follicles, that contract and move a small bundle of hairs. Internally, muscles pump our blood and help regulate our digestion. Inevitably, a large part of nervous system activity is going to be directly related to muscles.

In evolution, locomotion seems to be one of the earliest functions of neurons. The first neurons are believed to have been similar to neurons of modern sea animals such as the amphioxus and larval ascidians (Striedter and Northcutt, 2019, p. 64, 90). The amphioxus, for example, does not have a heart. Its few muscles are used in gill movement, swimming and burrowing into sand. Ascidians, also known as sea squirts, swim during their larval phase in search of a place to attach themselves and they lose most of their neurons during metamorphosis to the adult, sedentary form. The entire evolution of the vertebrate nervous system may be seen as an elaboration of the movement repertoire from simple patterns toward more complex ones, owing to the elaboration and diversification of the underlying neural structures (Cisek, 2019).

In robotics and AI, movement was once considered an easy problem and logical reasoning was considered hard. As it turned out, logical reasoning was solved much sooner than movement. The observation that the easy problems are hard, and the hard problems easy is known as the *Moravec paradox*, and it still holds – AI systems can beat the best human players in chess, go and StarCraft, and we do have fairly constant progress in robot motor skills, but, arguably, they are nowhere near the capabilities of a human child.

Our problems with movement stem from the seemingly impossible conditions the motor control systems have to deal with. The sensory apparatus is noisy, imprecise and delivers the information about limb states with significant delay, so we don't always have an accurate or timely information about their state. Our muscles are nonlinear, fatigable, and asymmetrically arranged around joints, so the same 'commands' to muscles will not create the same forces or the same movements at different times, or from different starting positions. On top of all that, the environment is constantly changing in unpredictable ways. Even a perfect movement plan, taking into account limb dynamics, muscle states, noise, delays and requirements of the task, will at some point fail and might need to be recalculated because it was impossible to predict the environmental disturbances and perturbations. And yet, humans move and perform everyday tasks with ease, neutralizing disturbances as they go, and only rarely stumble, fall or drop objects. Some of this ability is probably owed to our large brains, but, even insects, with much smaller brains, easily move around. The skilled ones, like the praying mantis, can use their arm-like limbs to catch pray and manipulate it to their mouths.

This gap between the apparent structural limitations of the elements of our sensorimotor loops and our obvious motor abilities gave rise to a myriad of different approaches in

theoretical motor control. As in other sciences, research in motor control begins with observation and measurement. Any regularities are noted and expressed precisely and unambiguously in the form of mathematical laws. These regularities, also called invariances, may then serve as starting points for mechanistic models of sensorimotor loops, that represent its elements at different levels of detail. Competing models may hold different implications for the structure of the neural controllers, and may predict different behavioral performance in experiments - those are the main criteria for comparing the models. A model explaining human motor behavior should be composed of biologically realistic or plausible elements; it should explain and predict neural activity during movement; and it should reproduce the kinematic and dynamic invariances measured in experiments with human participants. Different approaches in theoretical motor control seem to emphasize the importance of different criteria.

Historically, there have not been a large number of invariances found in human movement. There are, for example, the speed-accuracy tradeoff, where the precision of movement falls with the increase in speed or rhythm (Woodworth, 1899); the Fitts' Law, where the duration of point-to-point movement decreases with the increase of target area size (Fitts, 1954); bell-shaped speed profiles in point-to-point movements, where the speed initially rises, reaches a peak near the middle of the movement, and then falls toward the endpoint (Morasso, 1981); and the speed-curvature power law (Lacquaniti et al. 1983) that I will elaborate below, as the main topic of this thesis.

1.2. In natural hand movement, speed is related to curvature

In a study of the speed of hand movement during writing, Binet and Courtier (1893) noticed several curious phenomena that are not entirely explained to this day. They used a late-19th century technological innovation called the Edison pen, made for copying documents. The interesting property of the pen was the constant frequency of vibrations of its tip, since its traces could be used to infer movement speed. The segments of the path traced at higher speeds appear as dots separated further apart than the dots in segments traced at lower speeds (Figure 1).

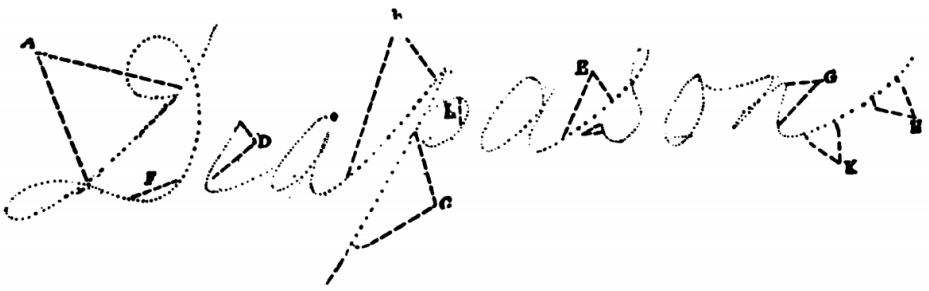

***Figure 1. Handwriting sample, from Binet and Courtier (1893)**. The sample was made with an Edison pen, a forerunner to modern tattooing pens. The tip of the pen oscillates at a constant frequency, so faster movements leave dots further apart than slower movements. Segments A-K are straight and drawn at higher speeds than the curved segments. The text is "Diapason", meaning "tuning fork" in French.*

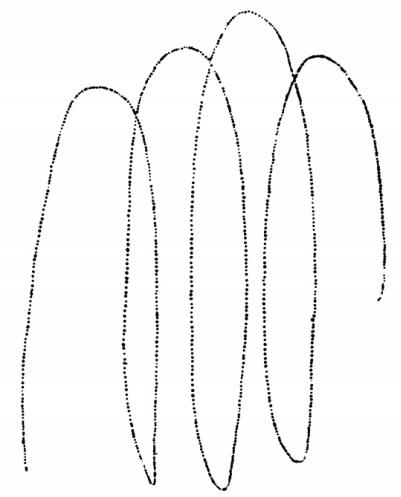

Figure 2. Drawing loops, from Binet and Courtier (1893). *The participants could not draw the loops at a uniform speed along the whole path, and instead always moved at a lower speed on the curves in the top and bottom and higher speed on the straight vertical segments.*

They noticed that the speed of writing is generally higher in the straight segments of letters, and lower in the curved segments; that the speed in circular segments seemed to depend on the radius of the circle – larger circles or arcs were drawn at higher speeds (Figure 2). These phenomena were present in the writing of all the participants and appeared even when they attempted to maintain uniform natural speed. Interpreting this result, Binet and Courtier suggested that participants did not have a great deal of voluntary control over the instantaneous speed during natural handwriting. The term 'natural' here refers to the speed commonly used when writing – neither too slow or too fast.

Another late-19th century researcher noticed a similar thing. Jack (1895), after analyzing the samples made by participants writing with a tuning fork that vibrated at a constant frequency, leaving traces on a smoked glass slide, wrote: "*the curved parts of letters and figures are more slowly formed than the rectilinear parts"* and *"the velocity of a curve varies, roughly speaking, with the radius of curvature*."

The correlation between speed and curvature is one of the most researched invariances found in human movement. The research has gained momentum with the invention of modern recording equipment, such as digitizing tables and electronic pens and tablets, as well as the spread of computers that aided data recording and analysis. In one of the papers of this thesis, we describe a novel software packet for Android tablets, free and open-source, that can be used for recording finger movements in drawing or tracing on the tablet (**Annex 1**).

1.3. The 2/3 power law and the kinematics of curved movements

Almost a century after Binet, Courtier and Jack, the phenomenon was studied by Viviani and Terzuolo (1982), who noticed that in some curved movements, tangential velocity is proportional to curvature, or that angular speed was constant with a different value in

different movement segments. A different formulation was offered as the 'speed-curvature power law' by Lacquaniti, Viviani and Terzuolo (1983). They've noticed that the speed of the pen, while tracing ellipses, can be approximated by a power function of curvature with a constant exponent. The name "power law" comes from the empirical relationship:

$$V \approx kC^{\beta} \quad (1)$$

where speed V is approximately equal to curvature C raised to the power β, times a constant k, related to rhythm or average speed.

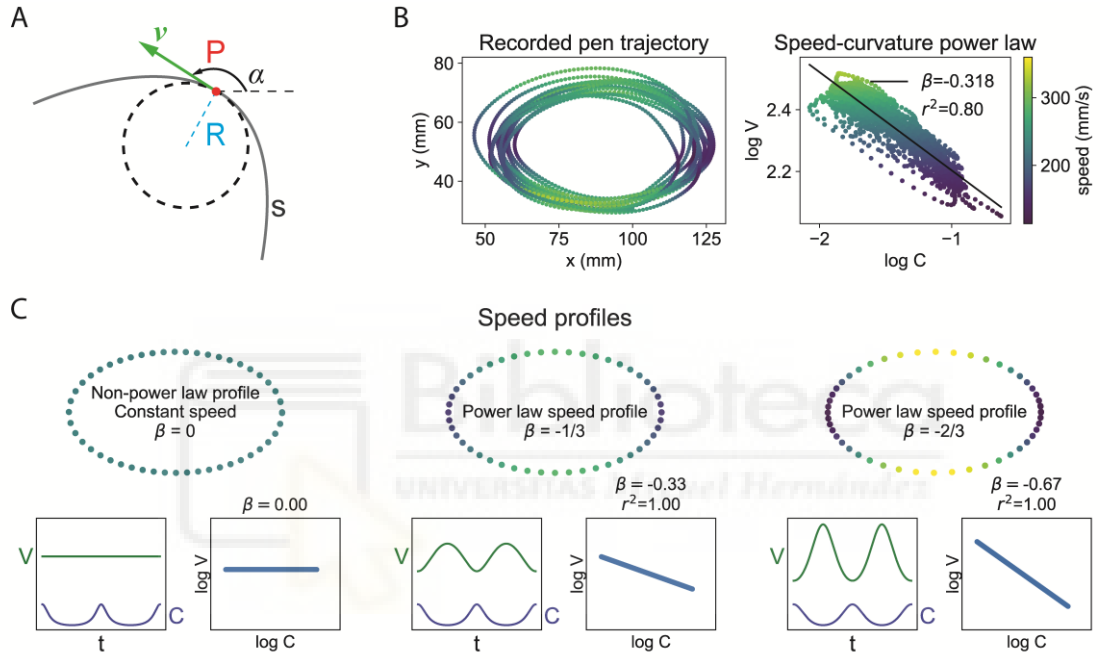

Figure 3. The speed-curvature power law in hand movement, *$V \approx kC^{\beta}$, or* $\log V \approx \log k + \beta \log C$. ***A)*** *Geometric and kinematic definitions of the variables: the point P moves along the curve s; at each instant of time, its velocity can be described by the vector v, speed V by the magnitude of velocity, and curvature C as the reciprocal of the radius R of the osculating circle (C = 1/R). The direction of movement with respect to the x-axis is α, and its first time-derivative is the angular velocity A. The variable k is a constant related to average speed.* ***B)*** *An example of an empirical trajectory conforming to a speed-curvature power law: a participant moves the pen faster (bright green) in areas of low curvature and slower (dark green) in areas of high curvature. On a log-log plot, the relationship between speed and curvature is linear, with the slope β, intercept log k and coefficient of determination r^2.* ***C)*** *Examples of the speed-curvature relationships for equal curvature profiles, but different speed profiles. In the first case, the speed is constant, and there is no power law. In the second case, the speed is slightly lower in areas of high curvature, with the exponent β= -1/3 (~0.33) and r^2=1. This profile is often found in elliptic human hand movements. In the third case, the speed is much lower in areas of high curvature than in areas of low curvature, with the exponent β= -2/3 (~0.67) and r^2=1.*

The exponent β in drawing ellipses at a "natural" speed was found to be β=-1/3, and the law is sometimes called the "1/3 power law". The phenomenon is also known as the "2/3 power law", since the *angular* speed in drawing ellipses varies approximately in proportion to curvature raised to the power of 2/3:

$$A \approx kC^{2/3} \quad (2)$$

The formulations using tangential speed or angular speed have been considered equivalent; the -1/3 speed-curvature power law and the 2/3 angular speed-curvature power law are thought to be the same phenomenon described by different variables. In further text we use both names, indicating explicitly which formulation we are using: VC power law for the speed and curvature, and AC for the angular speed and curvature power law.

Tangential speed or just speed, from equation (1) is defined as the magnitude of the velocity vector of the moving point P with coordinates (x, y) (see also Figure 3A):

$$V = |\boldsymbol{v}| = \sqrt{\dot{x}^2 + \dot{y}^2} \quad (3)$$

Curvature C is the reciprocal of the radius R of the osculating circle (Figure 3A), and can be approximated using the first and second derivatives of position:

$$C = \frac{1}{R} = \frac{|\dot{y}\dot{x} - \ddot{x}\dot{y}|}{V^3} \quad (4)$$

where x and y are coordinates of the point P in the Cartesian plane. Angular velocity is defined in a moving frame as the rate of change in the direction α of the velocity vector, $A = \frac{d\alpha}{dt}$. The exponent β is approximated as the slope of the linear regression line of the model:

$$\log V \approx \log k + \beta \log C \quad (5)$$

This linear model is found by taking the logarithm of both sides of the equation (1).

The values of the exponents in the VC power law indicate the "degree of slowing down in curves" or the difference between the fastest and slowest speed (Figure 3C). For $\beta = 0$, the speed is constant. Technically, the correlation of a constant with a variable is not defined because it involves a division with zero, so this a non-power-law trajectory. For β=-1/3, what is most commonly found in human movement, the speed is slightly lower in curved parts than straight parts (Figure 3B), and for more negative values of the exponent β, the speed is even more low if curved pars relative to straight parts.

The exponents of the AC power law are different, as and constant speed trajectories have the exponent β=1 and an r^2 of 1. Most commonly found exponent in empirically recorded elliptic trajectories is 2/3, and smaller values indicate more relative slowing in curves.

The phenomenon of the power law is interesting as it is one of the rare behavioral invariances found in various types of human movement, as well as the movement of some animals. The power law with the exponent β=-1/3 has been found in planar elliptic trajectories (Viviani and Schneider, 1991; Viviani and Flash, 1995; Richardson and Flash, 2002; Flash and Handzel, 2007; Huh and Sejnowski 2015; Catavitello et al, 2016), as well as in trajectories in 3D space (Maoz et al, 2009). Similar speed-curvature relationships were found in human walking trajectories (Vieilledent et al, 2001; Ivanenko et al, 2002),

and smooth pursuit eye movements (de'Sperati and Viviani, 1997). Different values of the exponent were found in drawing other shapes instead of ellipses (Schaal and Sternad, 2001; Richardson and Flash, 2002; Huh and Sejnowski, 2015). It was also found in the movements of hands of monkeys (Schwarts, 1994; Abeles et al, 2013), movements of the *drosophila* larvae (Zago et al, 2016), and elephant trunks (Dagenais et al, 2021).

Mathematically, an object moving along a given path could take any of the infinite possible speed profiles, and yet the speed of the human hand in natural movements is correlated with curvature. The invariance poses an interesting problem for movement theories: does the nervous system create a plan of the whole trajectory in preparation for the movement; or is the speed profile a non-intended consequence of some constant properties of the movement subsystems?

The fact that its origin is not entirely explained points to unanswered fundamental questions in theoretical motor control – we still do not exactly and quantitatively know how the brain, the spinal cord, the bones and muscles interact with the unpredictable environment to create fluid and seemingly effortless movements such as drawing a circle or an ellipse. During the past 40 years, there have been many approaches to explaining the power law, and they can be divided in roughly three groups: central origin theories, brain-body-environment interaction theories, and attempts to explain away the power law as a purely statistical artifact. These approaches are used to explain multiple phenomena in motor control, but here we focus specifically on the phenomenon of the speed-curvature power law.

1.4. Theories explaining the origins of the speed-curvature power law

1.4.1. Central origin

Hypotheses or theories in the central origin group propose that the invariances in movements imply the existence of explicit planning of the movement trajectory. A *trajectory* is understood to be the full profile of positions in time, simultaneously defining the geometry and kinematics of the movement at each point in time. A planned trajectory, or a *desired trajectory* is imagined as a trajectory originating in the central nervous system, in the higher-level, planning phase of the movement. It may be executed either open-loop or by some form of closed-loop trajectory servo-followers on the lower levels. This kind of control architecture is often seen in industrial robot arms.

Since the realized trajectory is considered equal or nearly equal to the desired trajectory, the question of explaining the power law requires answering *why is the desired trajectory following the speed-curvature power law?* Presumably, the brain is choosing power law trajectories, from the set of all possible ones, because they are beneficial in some way. Mathematically, this process can be expressed as the optimization of different cost functions, and selecting some specific cost functions leads to the 2/3 power law.

A commonly proposed cost is squared jerk, the third derivative of position. Minimization of jerk is considered equivalent to maximization of smoothness. By minimizing jerk over a given path and duration, researchers can predict a large class of movement trajectories (Wann et al. 1988; Viviani and Flash, 1995; Todorov and Jordan 1998; Richardson and Flash, 2002). It is defined as minimization of the magnitude of squared jerk of a point with position vector *x*, integrated over the duration of movement, T:

$$J = \int_0^T |\dddot{x}|^2 dt \qquad (5)$$

Huh and Sejnowski (2015), predict a wide range of exponents in hand trajectories that follow different 'pure frequency curves' (Huh 2015), and demonstrate that trajectories of human participants, when moving in a fast and smooth manner, behave as predicted by the optimization of jerk. We have replicated this finding (**Annex 2**).

Lebedev et al (2001) argued that the power law emerges because of the principle of least action and the minimization of work. We have argued that Lebedev and colleagues made a mistake in their calculations and that work is not minimal in power law trajectories (**Annex 3**).

Another perspective uses non-Euclidean geometrical representations of movement to explain the power law (Flash and Handzel, 2007; Bennequin et al, 2009; Polyakov et al, 2009). According to their analyses, maintaining a variable such as affine speed at a constant value, leads to the speed-curvature power law.

The main problem of central origin hypotheses is the relatively complex process leading to the generation of desired trajectories, involving calculus of variations and detailed knowledge of limb dynamics, encoded in internal models. This process if sometimes criticized for not being biologically plausible, implying that it could not possibly be executed in real time by the central nervous system (Ostry and Feldman, 2015; Powers, 2008)**.**

The existence of the desired trajectory itself was also questioned (e.g. Cisek, 2005). Some experiments seem to imply that the desired trajectory does not exist (Liu and Todorov, 2007). As an alternative to pre-planned desired trajectories, Todorov and Jordan (2002) proposed optimal feedback control theory (OFC). The theory proposes continuous use of sensory feedback and optimization of cost functions that result in different control laws or policies, with time-varying gains. The theory predicts a wide range of observed phenomena, such as muscle synergies and movement invariances, but it still requires internal models of limb dynamics and optimal state estimation from sensory data. As summarized by Haith and Krakauer (2013), among movement researchers, OFC seems to be a most widely accepted model of movement, as it describes a large number of phenomena using a relatively small number of principles, and a small set of cost function.

Its main drawback is the implication of an omniscient brain (Haith and Krakauer, 2013). This weakness means that even though OFC predicts behavior very well, it is a normative model – it describes how participants behave, but not necessarily how the nervous system achieves these behaviors (Pruszynski and Scott, 2012). The general problem in the field

of motor control is then to find mechanistic models with biologically plausible elements that still predict behavior as good or better than OFC.

1.4.2. Interaction hypotheses

As a counter to hypotheses of central origin, the second group of hypotheses aims to explain the power law as a consequence of the physical interactions of the human hand and the environment. When controllers are proposed, they are simple and biologically plausible.

For example, Catavittelo et al (2016) show that drawing ellipses in water results in hand trajectories with a different power law exponent than when drawing ellipses in the air, suggesting a major role for environmental dynamical factors instead of neural determinism. Gribble and Ostry (1996) show that a simulated neural control signal does not have to contain a power-law profile for the final hand trajectory to obey the power law. They explain their findings as the effects of spring-damper-like properties of the musculoskeletal system. Further, Schaal and Sternad (2001) showed that even a simple low-pass filter with an appropriate cutoff frequency can lead to the power law.

Consistent with above, we constructed a robot arm with artificial vision and showed that, because of its mass, processing delays, and explicit signal-smoothing algorithms, it acts as a low pass filter, and can create a speed-curvature power law when drawing ellipses at a high speed, even when the reference trajectory has a non-power-law, constant speed profile (**Annex 5**).

One problem with the low-pass filter hypothesis is that it does not address the signal attenuation and phase delays. In low-pass filters, as their name implies, amplitudes of frequencies lower than the cutoff go through the filter unchanged, while amplitudes of frequencies higher than the cutoff get removed or attenuated, and there is also some frequency-dependent phase delay. However, when human participants follow targets along elliptic trajectories, they maintain the amplitudes of the x and y sinusoids forming the elliptic shapes, and produce cursor trajectories with, on average, very low phase delay relative to the transport delay in the loop (Viviani et al. 1990). However, methods employed by Gribble and Ostry (1996), Schaal and Sternad (2001) and also our robot arm, result in lower output (cursor) amplitudes and strongly phase-delayed trajectories of the cursor.

To address this issue, we proposed two high-level controllers that directly, visually, measure ellipse shape size and phase delay, and then generate an oscillatory reference signal for the downstream movement control systems, maintaining simplicity of controllers, and reproducing participant behavior (**Annex 7**).

1.4.3. Statistical artifacts

In an analysis of trajectories composed of points distributed as white gaussian noise, Maoz and colleagues (2005) show that those trajectories conform to the VC power law, given that we consider coefficient of determination of $r^2 \approx 0.57$ an acceptable indicator of conformity. Further, if we take a non-power-law trajectory, and add gaussian noise, simulating measurement noise or movement noise and muscle tremor, this may again result in a trajectory conforming to the power law. With proper filtering, the analysis showed the 'true' state of not conforming to the power law. They point to a possible origin of the power law as an artifact of white or non-white noise, or of improper smoothing. We may also interpret their results as suggesting that only relatively high values of the coefficient of determination, higher than about $r^2 = 0.6$ or 0.7 should be taken as indicative of conformity to the speed-curvature power law.

More recently, and perhaps with more controversy, Marken and Schaffer (2017) argued that both the VC and the AC power laws are purely statistical artifacts, arising from failure to include a third predictor variable, the cross-product of acceleration and velocity *D*, into the regression analysis. According the them, the 2/3 power law is a mathematically necessary consequence of the way speed and curvature are calculated, and how the fit to the power law is estimated.

In response to Marken and Schaffer, we showed (**Annex 2**) that the speed-curvature power law is not mathematically necessary, we simulated physical systems where it does not appear, and showed empirical data from human drawing of different shapes where the exponents change with the change in the shape.

However, we have later found a mistake in our reasoning, not mentioned by Marken and Shaffer – we have assumed, as all the researchers since Lacquaniti and colleagues (1983), that the VC and AC power are equivalent. However, they are not equivalent, and angular speed should be avoided when assessing the speed-curvature power law (**Annex 4**).

1.5. Control theory and the target tracking task

In this section, I will describe the theoretical background we used in the design of behavioral experiments and computational and robotic models of behavior. The general framework is control theory, a field of applied mathematics used in analysis and design of feedback processes and devices. More specifically, we took a lot of inspiration from the writings and computer programs of W. T. Powers, for example Powers (1973, 1976, 1978, 2008). This approach is sometimes called *Perceptual Control Theory* (PCT) because of the emphasis on explaining behavior as control of variables generated by the perceptual apparatus of organisms. It features relatively simple controllers, arranged in a hierarchy, and most of the complexity is contained in the perceptual functions. We have

also used modern developments in fields such as theoretical control, robotics, control engineering, and engineering psychology.

Why control theory? For billions of years, evolution has been designing negative feedback loops. Some of those mechanisms are known as homeostatic loops, they can be found inside organisms, where they sense and maintain variables of the *milieu intérieur* – body temperature, blood glucose levels, oxygen and carbon dioxide levels, and many others.

The central assumption in the basis of applying control theory to the analysis of behavior is that there are also feedback loops closed through the *external* environment. Certain variables are sensed, and if their values are not at their respective reference values, organisms *behave* in ways that reduce the difference. The stated assumption is not particularly controversial. However, exploring the implications of this assumption leads to novel experimental methods, combining control theory, computer simulations and behavioral measurements. During the thesis, we've designed and performed several types of tracking, tracing and drawing experiments, with a similar design and approach.

1.5.1. Target tracking task

The approach can be illustrated with the example of target tracking (Figure 4), where the participant is holding an electronic pen in his hand and moving a cursor on the screen, following a target. Depending on the instructions and the patterns of target movement, the participant might be controlling different visual variables, such as the distance between the cursor and the target, expressed in the Cartesian coordinate system, or their angular separation, or a difference in cursor and target amplitudes if they are moving in sinusoidal patterns, etc. At this point the researcher and the participant don't necessarily know the exact controlled variable – it is often not obvious from the task definition or observable behavior.

The task of the researchers is then, to create a mathematical model of the sensorimotor loops involved in the process, verify their proposal in experiments and progressively improve it, by comparing the behavior of the participant to the behavior of the model.

Mathematically, a sensorimotor behavioral process is a negative feedback loop – the participant is controlling a visually perceived variable, comparing its state to some desired state, and performing actions that reduce the difference. Crucially, the visually perceived variable is always a result of the interaction between the environmental disturbances and participant's own behavior. In the terminology of industrial process control: behavior is the manipulated variable, and perception is the measured variable (or the *process output* variable).

There are two independent variables in the loop. One is the reference signal, representing the desired state of the controlled variable. It is internal to the participant and the researcher does not have direct control over it, but it may be influenced by giving

instructions the participant. The other independent variable is the disturbance, or what is commonly called the stimulus. All the other variables are dependent on the disturbance and the reference signal.

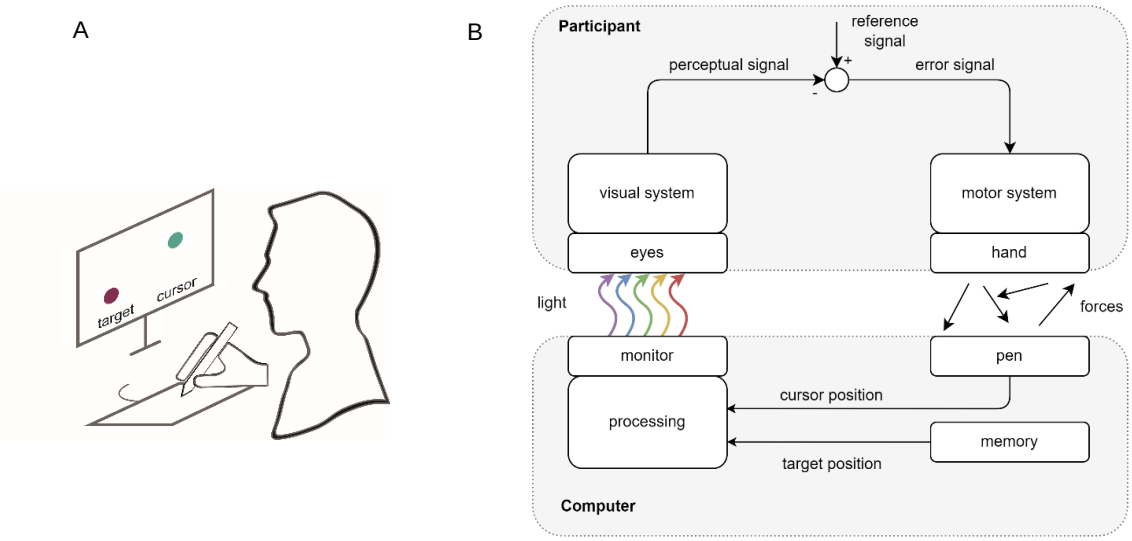

Figure 4. Target tracking task. A) *Sketch of the participant performing a target tracking task.* ***B)*** *Diagram of variables and functions in the participant–environment feedback loop.*

The sketch and the feedback loop (Figure 4A and 4B) are drawn from the perspective of the researcher. This means that the researcher could, in principle, observe and measure all of the variables in the diagram. Cursor and target positions are discrete variables in the computer, and the researcher may also see their correlates on the monitor. The *perceptual*, *reference* and *error* signals are assumed to be time-varying quantities in the nervous system of the participant. Powers (1973) speculated they could each be average rates of firing over a bundle of neural fibers. Comparator, the element calculating the difference between the reference and the perceptual signal, would be implemented by a set of neurons receiving both excitatory and inhibitory inputs, and generating a "difference" output signal. They would be implemented separately for positive and negative values of the signals, since firing rates are always positive. Though, of course, other implementations of the neural computations are possible.

1.5.2. The controlled variable

Strictly speaking, the perceptual signal, constructed from raw light waves, and across multiple levels of perceptual abstraction by the participant's visual system, is the controlled variable. It is the variable maintained at its reference level despite disturbances. In order to understand the behavior of the participant, we must start from understanding the nature of the controlled variable.

As we illustrate in Figure 5A, in a tracking task, the perceptual signal is expressed in some neural units and is ultimately a function of cursor and target positions. From the perspective of the researcher, we could observe and measure the target and cursor positions. In theory, we could observe the perceptual signal in the participant's brain to determine the nature of this function – if we had the tools to measure the signal in real time, with sufficient resolution, and if we knew exactly where to look, and what kind of neural code is relevant. In practice, this might be very difficult.

Alternatively, we can replace the system in Figure 5A with an equivalent system, shown in Figure 5B. As proposed by Powers (1978), the controlled quantity may be modelled as a linear combination of the effects of the disturbance (target) and the participants own behavior (cursor). The effect of the disturbance is called the disturbance quantity and is a function of the target position, here named G. The effect of the participants behavior is called the feedback quantity, here named F. The input function is a simple unit converter, and a pure delay may be added.

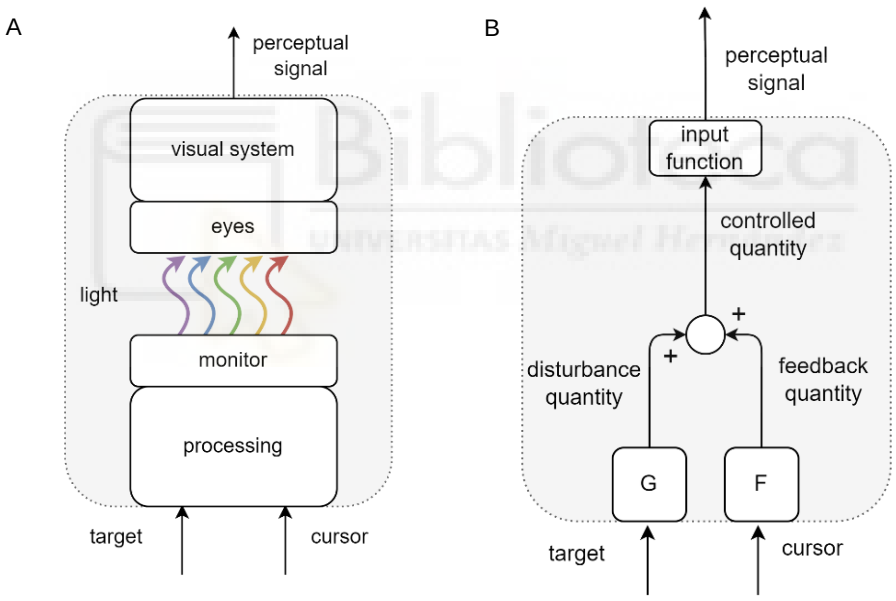

Figure 5. Equivalent systems. A) *The computer converts the cursor and target position, in pixels, to light patterns emitted by the monitor. Starting from the light patterns, the visual system constructs a perceptual signal, represented in some neural units.* ***B)*** *In an equivalent system, the disturbance function G converts the target position to the disturbance quantity, and the feedback function F converts the cursor position to the feedback quantity. Disturbance and feedback quantities are added to form the controlled quantity, units depend on functions F and G. The input function converts the controlled quantity to neural units, and may be as simple as a constant multiplier, or may also have a pure delay element.*

We can also replace the system converting the error signal to the cursor position with an equivalent system (Figure 6). The output function is modelling the conversion of participant's visual error signal to the observed cursor position. In tracking tasks, the output function is often modelled as an amplifier in series with a low-pass filter, or as a multiplier and a leaky integrator.

Finally, replacing both systems with their equivalents, we get the canonical diagram of the feedback loop in the tracking task, as shown in Figure 7.

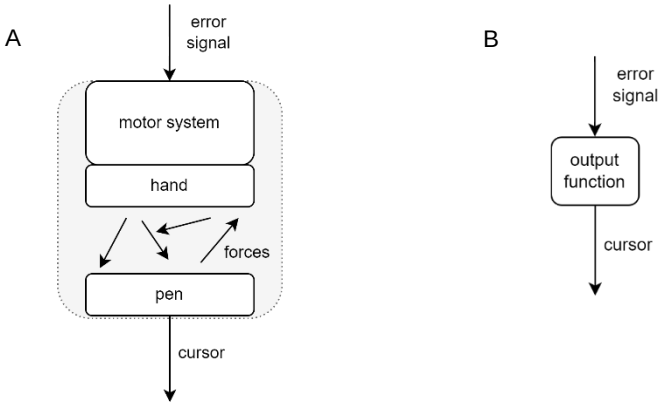

***Figure 6. Equivalent systems**. **A)** The visual error signal is passed on to the motor system, where it generates muscle forces, joint torques and movement of the hand, which in turn moves the pen, and the cursor on the screen. **B)** An equivalent function converts the error signal to cursor position.*

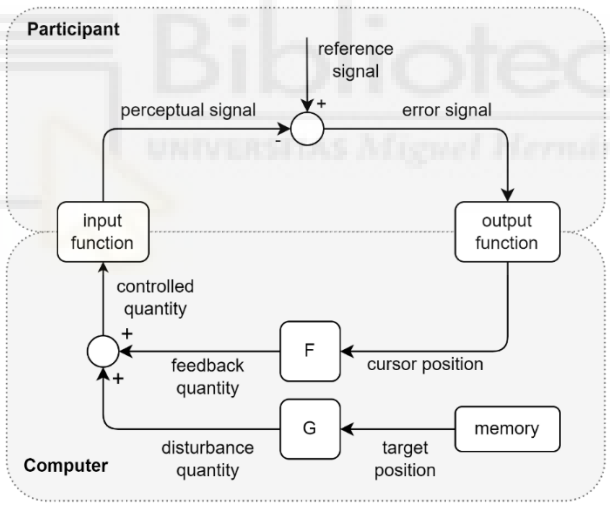

***Figure 7. Diagram of the feedback loop in the target tracking task.** Replacing 'cursor' and 'target' with different output and disturbance variables, this diagram represents any negative feedback control system*

1.5.3. Approximating controlled variables

In any control loop, the controlled variable is maintained equal to or near the reference level and is unaffected by the disturbances: if the reference level is constant, the controlled variable will also be constant (Figure 8). This fact forms the basis of *the test for the controlled variable*, or the process of searching for the best definition of the controlled quantity. Here, I will describe a version of the test used in target tracking; for a more general version see Powers (1978) or Runkel (1991).

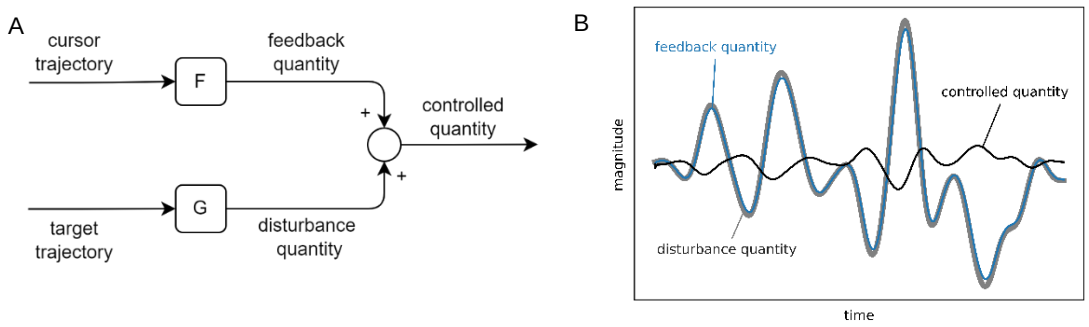

Figure 8. The test for the controlled variable in the tracking task. A) *When applied to the tracking task, the test can be seen as varying the definitions of functions F and G in order to minimize the correlation between the controlled quantity and the disturbance quantity, and to minimize the variance of the controlled quantity with respect to the disturbance quantity* ***B)*** *Assuming a stable reference, the controlled quantity will be stable, and the feedback quantity will track or oppose the disturbance, depending on the sign.*

When the researcher disturbs a variable controlled by the participant, the participant will counteract the disturbance and return the controlled variable to its reference state. Out of different hypotheses of the controlled variable, assuming the reference signal is stable, the best candidate is the most stable one. A stable variable, unaffected by the disturbance will have a low correlation with the disturbance quantity, and its variance will be small in relation to the variance of the disturbance. This process of searching for the best definition of the controlled variable can be described as the search for the definitions of functions F and G (Figure 8A) that minimize the correlations, in absolute value, between the controlled quantity and the disturbance quantity; and minimize the variance of the controlled quantity with respect to the variance of the disturbance. In other words, the best approximation to the controlled variable will have the lowest correlation between disturbance and controlled quantities, and the highest stability of the controlled quantity relative to the disturbance.

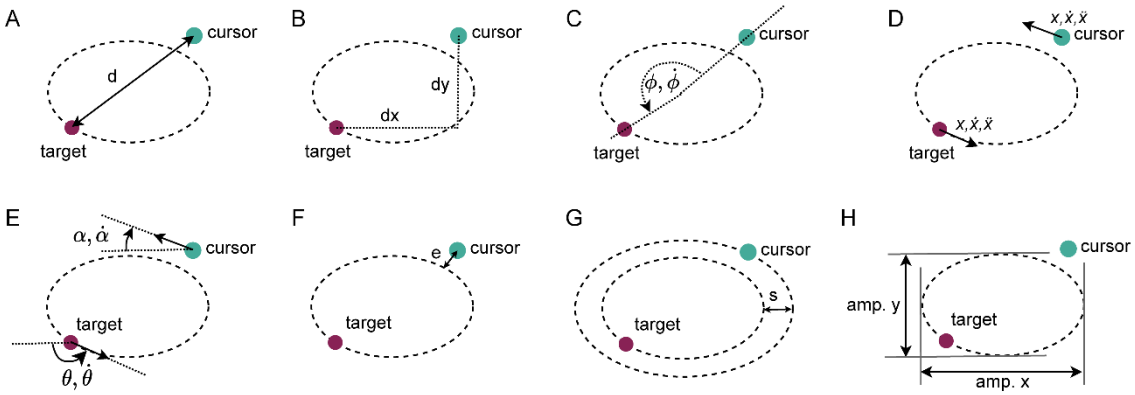

Figure 9. Potential visual features used in tracking a target along an elliptic trajectory. A*) Euclidean distance.* ***B)*** *x and y components of the Euclidean distance* ***C****) Relative angle and angular velocity.* ***D)*** *Position, speed and acceleration of the cursor and target.* ***E)*** *Direction of movement and its rate of change.* ***F)*** *Distance of the cursor from the path* ***G)*** *Ellipse size difference.* ***H)*** *The amplitude of movement in x and y dimensions.*

In a task of tracking targets along elliptical trajectories, one of the tasks we used in testing phenomena related to the speed-curvature power law, there are many candidates for the controlled variable (Figure 9). The participant might be controlling the cursor-target Euclidean distance, the angular difference, some function of positions, speeds and accelerations, the amplitude of vertical and horizontal movements, etc. These are some of the definitions we came up with, though there could be others.

1.5.4. More than tracking targets

On the abstract level of mathematical approximations and box-and-arrows diagrams, controlling the cursor-target distance is analogous to the body's blood glucose concentration control, or to the control of the individual's social status in a group. All these processes involve sensing a particular variable, comparing it to the desired state, and acting to reduce the error. There are differences in implementation and dynamic characteristics, but the basic relationships between the variables are the same – the controlled quantity will tend to be equal to the reference level, the error will tend to zero, and the behavior will tend to neutralize the effects of perturbations on the controlled variable. So far, the methodology of searching for controlled variables has been applied mostly to visual tracking tasks, and it remains to be seen how to apply it to different tasks and behaviors.

In principle, regardless of the modality of control, or even the organism, the search for controlled variables will follow the same "make a hypothesis and verify existence of control" procedure described above. The significance of this procedure for neuroscience is the possibility of using purely behavioral experiments to generate hypotheses about environmental quantities that correlate with neural quantities. When we are dealing with negative feedback systems, the stimuli generated by the experimenter may not be perceived by the organism, but only acts as disturbances to the variables controlled by the organism. This is especially relevant for experiments with behaving participants, where the feedback loop is closed. Finding exact definitions of controlled variables may contribute to explaining, first the behavior, and second the neural processes that generate them.

In robotics, a theory that explains human sensorimotor loops can be used to help construct artificial devices that will match human abilities. We showed that a robot arm with artificial vision, constructed with a hierarchical control architecture based on Powers (2008) reproduces some human behavioral features in tracking tasks, shows joint synergies, and motor equivalence; all with very simple controllers (**Annex 5**).

Additionally, we developed a robotic prototype modelling a spinal reflex loop involving artificial muscles, tendon tension sensors and muscle length sensors (**Annex 6**).

1.6. Objectives

The main objective of this thesis was to improve our understanding of processes and structures underlying the production of the invariance known as the speed-curvature power law in human hand and arm movement. While the field of motor control is often focused on the recorded behavioral outputs, we focused on inferring perceptual inputs and, from there, started to build the understanding of the entire sensorimotor loop. We have proposed the following specific objectives:

- Deepen our understanding of the geometry and kinematics of curved trajectories, as well as mathematics and statistics used in the estimation of the speed-curvature power law
- Identify visually controlled variables in elliptic target tracking tasks
- Identify or hypothesize about proprioceptive controlled variables involved in arm and hand control in humans
- Create simulation models and robot models of human sensorimotor loops that can produce the speed-curvature power law in situations where humans produce it, in order to generate hypotheses relevant for understanding the neural mechanisms of hand and arm control

2. Materials and Methods

2.1. Movement recording application for Android tablet

The Android tablet we used was Samsung SM-T580 tablet, dimensions 254x164x8mm, PLS LCD screen 10.1″, 1920x1200px resolution. The tablet has a capacitive touch screen and can register finger or stylus movements. The screen refresh rate is 60Hz and the touch sampling rate 85Hz.

The app was programmed in Android Studio (version 3.3.2) in the Kotlin programming language. The combination of relative simplicity and the ability to use existing Java libraries makes Kotlin a practical choice.

We used a Windows 10 PC, with 8GB of RAM and Intel i5 CPU. A notable feature of the software is recording of finger movements at the rate of 85Hz. The software is free and open-source, and can be found on github.com. Figure 10 shows a workflow diagram from design of the experiment to the analysis of the results.

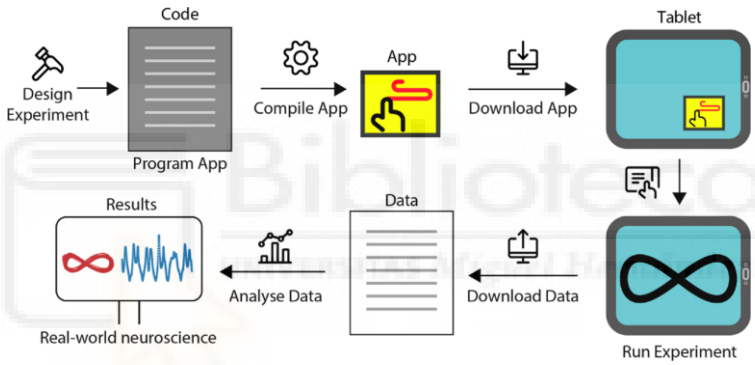

Figure 10. The workflow diagram: from design of the experiment to the analysis of results. *Using our app simplifies the process by providing the template code for new experiments.*

2.2. Recording of movement trajectories in the lab

2.2.1. Hardware

In recording human hand movement trajectories, we used several different graphics tablets with dedicated electronic pens or touchscreens to record finger movements:

Wacom Intuos Pro S, PTH-451, spatial resolution 0.08mm, sampling rate: 200 samples/s. Active surface: 15x10cm

Wacom Intuos Pro Paper PTH-860, resolution 0.08mm, sampling rate: 120 samples/s. Active surface: 30x21cm.

Wacom Cintiq 27QHD, interactive graphics monitor. The screen refresh rate is 60hz, and the pen position sampling rate 150Hz, resolution 2560x1440px.

2.2.2. Software

Our hand trajectory recording software is written in Python with the pygame library or the qt library for simple graphics, often just two circles for the target and cursor, or the cursor and a path for following. The trajectories were recorded with maximal temporal and spatial resolution afforded by the devices used. The analysis of recorded trajectories was performed using Jupyter Notebooks.

2.3. Generating trajectories with arbitrary speed-curvature power laws

Starting from the equation $V = kC^{\beta}$, since $V = ds/dt$, where dt is the time differential, and ds the arc-length differential, we can write $ds/dt = kC^{\beta}$. Curvature C can be numerically calculated as $d\alpha/ds$, where α is the local angle between the tangent line at any given point and the x axis, and $d\alpha$ its differential, the equation of time-dilation that allows to transform any trajectory into desired power law kinematics is: $dt = k^{-1}ds^{1-\beta}d\alpha^{\beta}$.

The numerical procedure for generating a trajectory with an arbitrary power law exponent from a given trajectory is 1) sample the given trajectory using a constant dt; 2) calculate the arc-length ds_i, and direction $d\alpha_i$ differential at each point (x_i, y_i) of the trajectory; 3) construct a new time-difference vector, where each dt_i follows the equation $dt_i = ds_i^{1-\beta}d\alpha_i^{\beta}$; 4) construct a time vector as a cumulative sum of all dt_i, and scale it by the desired duration divided by the total duration of the original time vector, to set the total duration equal to the desired duration; 5) using a cubic spline, fit the existing (x_i, y_i) points to the new time vector; 6) finally, sample the splined trajectory again with constant dt, obtaining a new vector of points (x_j, y_j) as a discrete approximation of an arbitrary power law trajectory.

2.4. Robot arm with hierarchical control

We designed and built a robot arm with four degrees of freedom, visual control of hand tip position, and pen pressure control (Figure 11). The control architecture of the robot arm was adapted from computer simulations (Powers, 1999; 2008). Each joint was actuated by a geared DC motor, and had a potentiometer for measuring the joint angle. The angle measurements were collected by a Teensy 3.1 microcontroller which also implemented the fast 200Hz lower-order control systems, analogous to spinal-level control systems in the human arm. Slower, high-level, visual and touch control loops were implemented on the PC. The image was recorded by a webcam at 30Hz and 640x480px, and after each frame, the visual perception system found the location of the green marker on the hand tip, and sent the information to visual control loops. Similarly, the pressure of the pen tip on the tablet was recorded at 30Hz and sent to the PC as pressure perception

to the pressure control loop. Higher level loops provided reference signals for the lower-level loops (Figure 12).

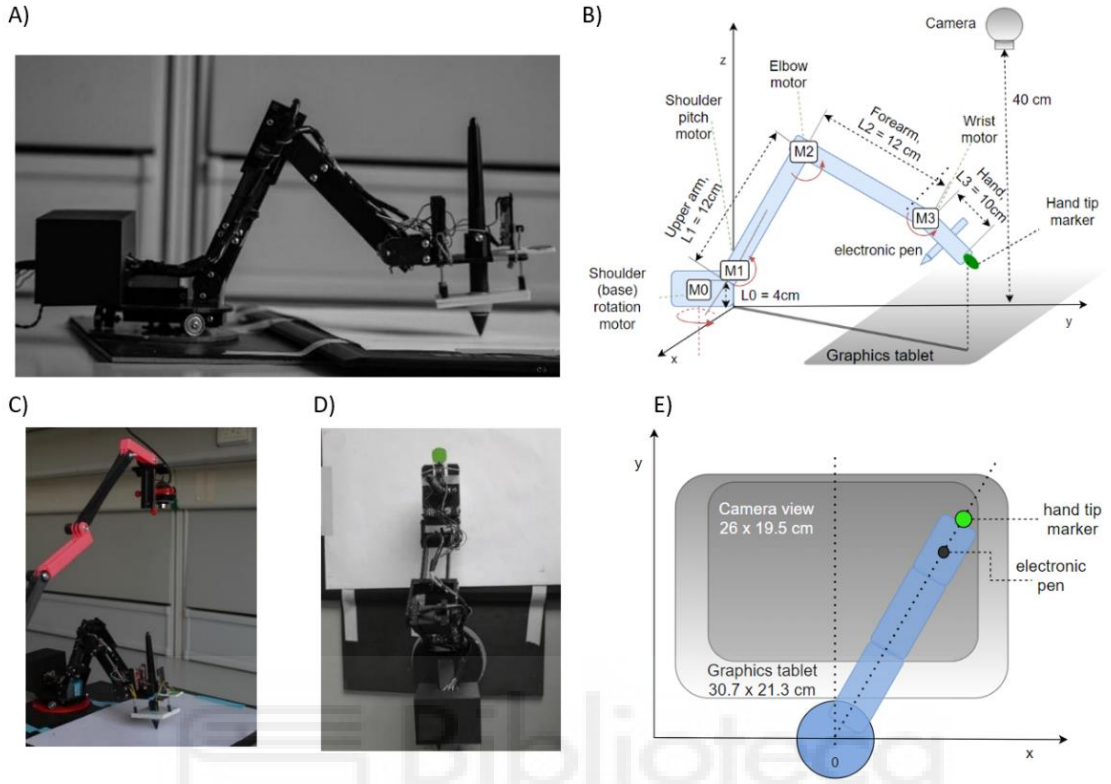

Figure 11. The robot arm system design and implementation. *(**A**) Side view showing the body of the robot, enclosed microcontroller, electronic pen and tablet. (**B**) Diagram of the robot arm in perspective view with arm segments L0 – L3, motors M0 - M3, camera, tablet, pen and marker of tip position. (**C**) Photo of the experimental setup, including the top camera. (**D**) Top view photo (camera's viewpoint), the green circle is used by the visual system as the marker of hand tip position. (**E**) Diagram of the robot from the top view.*

The control architecture was based on simulations (Powers, 1999; 2008), but was not identical to them since we needed to adapt it to the robot arm hardware, and we added touch-pressure sensors and pressure control not found in the simulations. The control architecture shown here (Figure 12A) is simpler than the simulations, since it avoids the whole layer of explicit control of joint angles.

Higher-level loops take visual information to construct controlled variables – x and y location of the cursor in the visual field, and also pressure and orientation of the pen while writing. They are slower and more precise than proprioceptive loops. The errors from the higher-level loops propagate to lower levels as reference signals.

The lower-level loops are designed to be analogous to the spinal or brainstem-level control systems in humans, as they work with imprecise proprioceptive information, with low signal transport delays, and high frequency sampling. The controlled variables are: *xp*, the proprioceptive lateral displacement of the finger; *R*, or reach is the distance of the fingertip to the shoulder; z is the elevation of the fingertip, and δ (delta) the angle of the wrist with respect to the x-y plane (Figure 12B).

Finally, the four proprioceptive control loops directly set voltages on shoulder rotation, shoulder pitch, elbow and wrist motors, combining their outputs, resembling multiple muscle output schemes found in the human spinal cord.

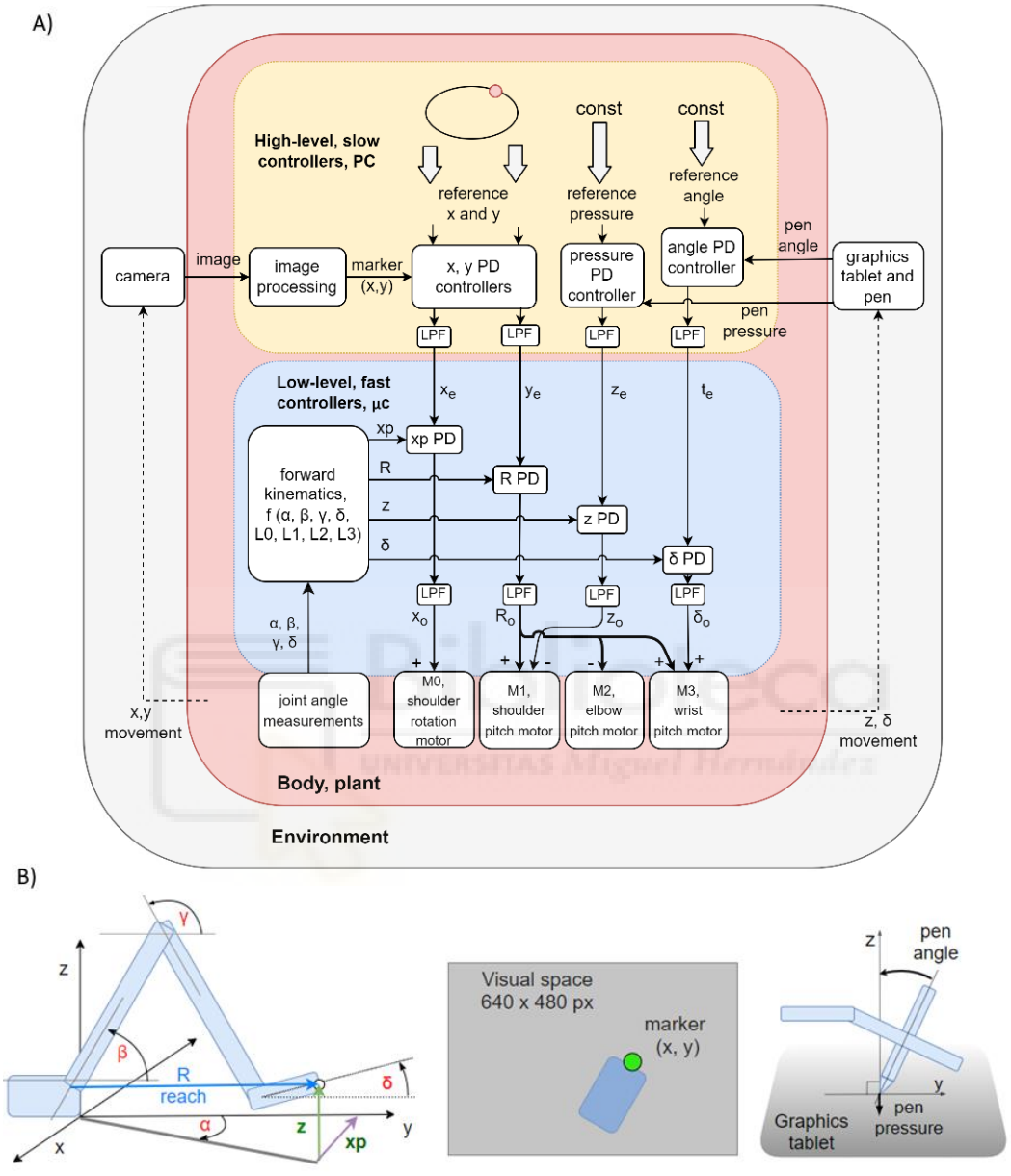

Figure 12. Control diagrams of the robot arm system. *(**A**) Block diagram of two levels of feedback loops, high level (yellow) and low level (blue). There are four high-level controlled variables: position of the marker in x and y dimensions in the visual field, angle of the pen to the tablet, and pressure of the pen to the tablet. The references are supplied by the experimenter. The outputs from top-level loops are references for the lower-level loops controlling proprioceptive variables: xp, the x coordinate of the hand tip in proprioceptive space; reach, the distance from the shoulder base to the hand tip; z as the height of the hand tip; and delta (δ) as the angle between the x-y plane and the hand. All controllers are proportional-derivative (PD) with a low-pass filter (LPF) in controller output. (**B**) Diagrams showing the geometric definitions of variables in the block diagram, the visual space and a diagram of the pen angle and pressure variables.*

2.5. Control of joint angle and tone with antagonistic muscles

This robotic prototype is a model of the elbow joint (Figure 13). It includes mechanical analogs of antagonist muscles, and electro-mechanical analogs of muscle tension and muscle length receptors. The two muscles were modelled by twisted string actuators (TSA). Each TSA was composed of a geared DC motor (N20) that was rotating a loop of string approximately 1mm in profile diameter. Rotation of the motor would twist the string and shorten its length. When untwisting, the string would lengthen if there was a force pulling in the opposite direction. This arrangement removed the backlash from the joint. Two antagonistic TSAs could only pull in one direction, and it was important to coordinate simultaneous pulling in opposite directions to maintain total muscle tone and generate desired torque on the joint.

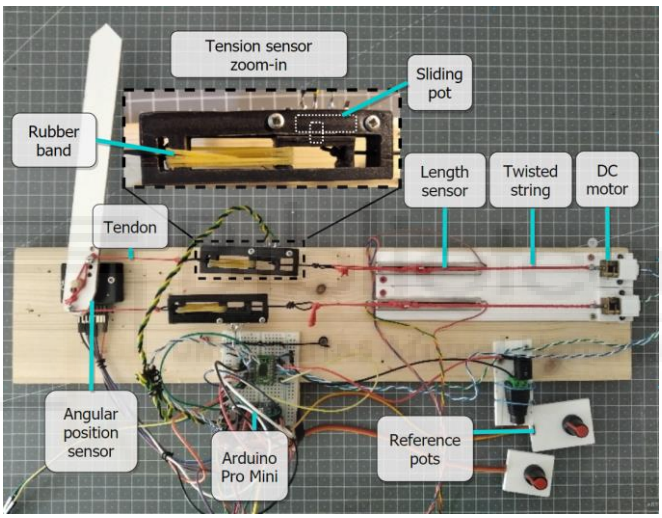

Figure 13. Elbow joint angle and tone control by antagonistic muscles, modelled as TSAs. *Each muscle unit contains a geared DC motor, a string for twisting, slide potentiometer for length measurements, rubber-band tension sensor and a high-precision angular position sensor.*

The coordination was achieved by a nested (or cascaded, hierarchical) control scheme (Figure 14). On the first level, the controlled variables were string lengths measured by a sliding potentiometer. On the second level, the controlled variables were the sum of two muscle tensions, named the muscle tone or joint stiffness, and the difference in muscle tensions, named the joint torque. On the third level, the controlled variables are the joint angle and angular speed.

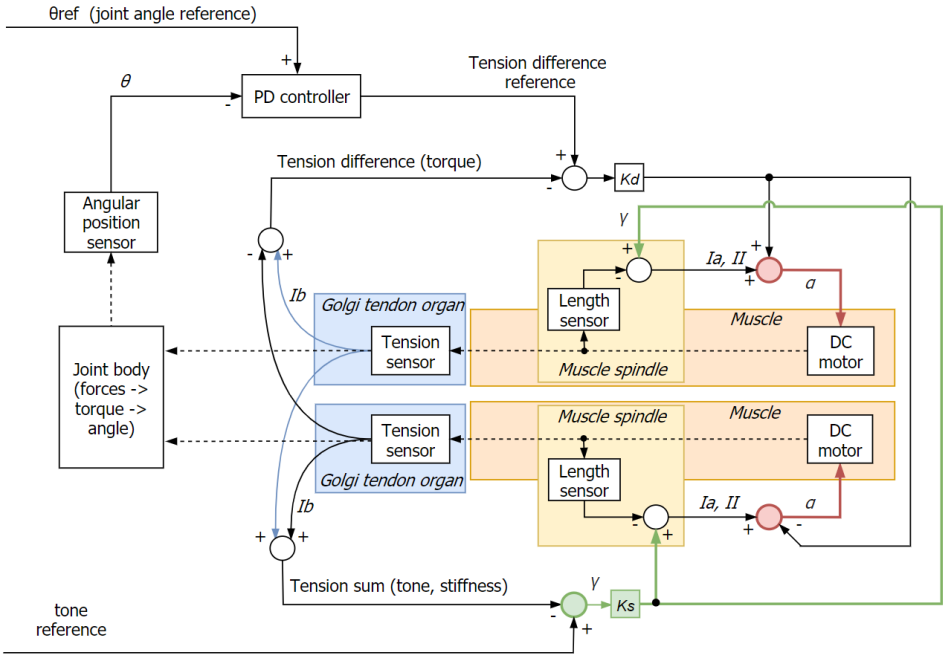

Figure 14. Block diagram of the control architecture for two antagonist muscles, biological analogs in cursive. *The lowest level of control are the spindle-muscle loops controlling muscle lengths. The spindle is a combination of a length sensor and comparator.*

2.6. Identifying visually controlled variables in the task of tracking elliptical targets

The controlled variable (CV) is the variable in a negative feedback control loop that is measured and maintained equal or near equal to the reference variable. If a variable is controlled by a system, directly perturbing it will result in an action that removes the effect of the perturbance, and restores the level of the controlled variable back to the reference level. The speed of this restoration depends on the dynamic characteristic of the loop. These facts form the basis for inferring unknown controlled variables in different behavioral tasks: the participant is controlling an unknown variable or a set of variables, and the researcher attempts to identify the best approximations to the variables controlled by the participant. First, the researcher forms a specific quantitative hypothesis of the controlled variable, and defines an appropriate perturbation inside the bandwidth of the system. The participant performs the task while the researcher applies the disturbance, predicting that if the variable is controlled it will stay stable despite the perturbations, and the behavior of the participant will negate the effects of the disturbance. When the CV is inferred from behavioral experiments, it is always an approximation and, theoretically, can always be improved. Quantitatively, one approximation is better than another if, for the same task, the CV has a smaller variance relative to the variance of the effects of the perturbation; and if the correlation between the CV and the effects of the perturbation is lower (Powers, 1978).

In the task of tracking elliptic trajectories, we have compared the cartesian cursor-target distance in x and y dimensions with the angular separation of the cursor and the target, where the center of angle is in the center of the ellipse, as well as the difference in sizes of the ellipses, where size is defined as the semi-major axis of an ellipse passing through the cursor or the target.

3. Discussion

3.1. Understanding the problem

The first group of four papers are all about *understanding the problem* of the invariance in human movement known as the speed-curvature power law. We developed an instrument for recording movement outside of the lab, explored the mathematical properties of curves conforming to the power law, and of curves created by physical and mathematical systems that do not conform to the power law. We have deepened our understanding of the statistical procedures used to estimate the correlation and regression coefficients relating different kinematic and geometric variables.

3.1.1. An android app for recording finger movement outside of the lab

Our contribution to the methods for recording human hand movement is a free and open-source Android app that can be used for designing tracking, tracing and drawing experiments outside of the lab, using an android tablet or a smartphone. We have provided the source code of the app (https://github.com/adam-matic/KinematicCognition) written in the programming language Kotlin, and a demonstration of an experimental protocol and analysis of the results (https://github.com/adam-matic/KinematicCognition-Analysis) written in Phyton.

The app was optimized for high temporal resolution in trajectory measurements, and can achieve up to 85Hz sampling rate for finger touch event recording on the tested tablet, the Samsung T-580. For simple graphics, the screen display can be refreshed at 60Hz, which is on par with standard computer monitors.

The analysis of recorded trajectories revealed that the results are in accordance with previous experiments. Tracing the lemniscate figure (**Annex 1,** Figure 4A, 4B and 4C) is consistent with an experiment reported by Viviani and McCollum (1983). The lead-follow analysis shows, similar to Viviani and Mounoud (1990), that for one participant, the cursor followed the target with a variable phase delay, sometimes following and sometimes overtaking the target (**Annex 1:** Figure 4D, 4E). We analyzed recorded pure frequency curve traces to get the spectrum of curvature (**Annex 1**: Figure 4F) and found that the curvature profiles of the traced trajectories have single peaks at the same frequencies as the displayed pure curves, and we note that the traces were performed at a relatively high speed in a fast and fluid manner. In scribbling movements, we demonstrated an analysis of clockwise and counter-clockwise turning directions of the unwrapped direction angle (**Annex 1**: Figure 4G) and the number of complete rotations in either direction (**Annex 1**: Figure 4H). Finally, we show a discrete segmentation analysis of different paths that can be taken to draw the shape in **Annex 1**: Figure 4J.

In conclusion, the app with its source code can be used in experiments in its current state, directly downloaded from the code repository; or it can be used to help the development

of state-of-the-art recording apparatus for research on finger and hand movement outside of the lab, using a portable Android tablet.

3.1.2. A reappraisal of the speed-curvature power law

This study was motivated by a claim of Marken and Shaffer (2017) that the speed-curvature power law is purely a statistical artifact, arising from neglecting to include a second predictor variable, the cross-product of speed and acceleration into the regression analysis. They also claimed that speed is necessarily correlated to curvature, because of their 'mathematical relationship'.

First, we demonstrated that in trajectories of human participants drawing different shapes, the exponent of the AC power law is not always 2/3. We replicated an experiment from a study by Huh and Sejnowski (2015) where participants traced the so-called pure frequency curves. Huh and Sejnowski used tangential speed and curvature – and we obtained equivalent results using angular speed and curvature (**Annex 2**: Figure 2C). The exponent of the AC power law ranged from 0.4 for the spiral shape (ν=2/33) up to 0.8 for the hexagonal shape (ν = 6).

Second, we demonstrated that the power law does not depend on the way curvature is calculated. Using data from Drosophila larvae movement (Zago et al. 2016), we calculated curvature with three different methods, using time parametrization of the trajectory; using the spatial derivative of the angle coordinate, and using the inverse of the radius of the osculating circle, and we found no statistically significant differences in the regression parameters in the angular speed and curvature power law (**Annex 2**: Figure 3).

Our third point was that the speed-curvature power law, in the VC or AC form, is not necessarily present in any given trajectory. To demonstrate, we generated different speed profiles for the same elliptical path (**Annex 2**: Figure 4). We showed one trajectory with a perfect 2/3 power law where the ellipse parameter θ was proportional to time, and two trajectories that were not fitting to a power law: in the first one, θ was proportional to time squared, and in the second to the integral of the absolute sine of time (**Annex 2**: Figure 4A). The exact exponent of 2/3 in the AC power law appears only when the second derivative of θ is 0, or when the magnitude of the cross-product of speed and acceleration (D) is constant (**Annex 2:** Figure 4E)

Finally, we simulated several physical systems to show how different physical interactions may lead to non-power law trajectories. In **Annex 2**: Figure 5A, we show that two bodies attracted by gravitational force do not conform to a power law – their speed depends on how close they are to their barycenter, not on the curvature of their paths. The speed of a projectile depends on initial conditions and forces that act on it, such as drag; and we show a power law trajectory for a no-drag situation, and a non-power-law trajectory when there is drag (**Annex 2**: Figure 5B). In **Annex 2:** Figure 5C,

the speed of the pendulum changes from zero at the peaks, to maximum at the bottom, while curvature stays constant, again showing that speed is not related to curvature in this physical system. Two coupled springs in the plane with no friction, in **Annex 2**: Figure 5D, show the behavior of a coupled harmonic oscillator may lead to power law trajectories.

In conclusion, we have refuted the claim of Marken and Shaffer (2017) that the speed-curvature power law is necessary mathematically or physically, or that it is an artifact coming out of the way curvature is calculated. We maintain that it is a real, non-trivial phenomenon in movement and that it needs to be explained by movement control theories.

3.1.3. Mechanical work is not minimal in the speed-curvature power law

Lebedev and colleagues (2001) proposed that the 2/3 power law results from the principle of least action: given a path and the duration of movement, the mechanical work is minimal. According to them, the nervous system chooses the most economical trajectory; the neural controllers implementing the principle of least action are acquired through training, and they are minimizing the mechanical work needed to perform motor tasks.

However, we noticed that they made a mistake in deriving their conclusions. The variable *D* is defined as the magnitude of the cross product of velocity and acceleration. We can rewrite the 2/3 power law as $V = D^{1/3}R^{1/3}$, and from this find that $D = V^3/R = V(V^2R)$. The term in the parenthesis is centripetal acceleration A_n, so we have $D = VA_n$. The error by Lebedev and colleagues (2001, their equation 5) was to equate this product D with mechanical power P. However, mechanical power P is not equal to D, the magnitude of the *cross-product* of velocity and acceleration. Instead, mechanical power is the amount of mechanical work per unit of time, and mechanical work is proportional to the *dot product* of velocity and acceleration vectors. Consequently, mechanical work is not constant and mechanical power is not minimal in the 2/3 power law, so the principle of least action is not related to the 2/3 power law.

We show in **Annex 3**: Figure 3 how different trajectories that conform to the 2/3 power law all have a constant magnitude of the cross-product D, and they do not have constant mechanical work or mechanical power. We further reasoned that if the variable D is constant, then the integral of D is minimal. We analyzed the same four trajectories over a 6s segment, across different power law kinematics. We show that the integral of D is locally minimal for β=2/3 (**Annex 3**: Figure 4). According to Pollick et al (2009), the variable D is the cube of equi-affine speed, and if D is constant, the equi-affine speed is constant. We found that the integral of equi-affine speed, the equi-affine arc-length, is invariant to the exponent of the power law (**Annex 3**: Figure 5). It is known from previous research that 2/3 power law trajectories also have minimal jerk (Wann et al., 1988; Viviani and Flash, 1995). We confirmed these finding for non-elliptic trajectories that

were also quasi-pure in the curvature spectrum, with the peak at frequency ν=2 (**Annex 3**: Figure 6).

This study was an exploration of the properties of numerically generated trajectories, of their geometric purity, optimality and conformity to the speed-curvature power laws. We have discovered and corrected a mistake by Lebedev and colleagues (2001), where we showed that the trajectories conforming to the 2/3 power law do not have minimal mechanical power or work, and cannot be derived from the principle of least action. Instead, we show that the variable D, magnitude of the cross-product between velocity and acceleration, and also related to affine velocity, is constant in the 2/3 power law.

The main limitation of the study is the use numerically generated trajectories, and not exploring human-drawn trajectories, which should be performed in future studies.

3.1.4. Angular speed should be avoided when assessing the speed-curvature power law

In our power law reappraisal paper (**Annex 2**), we assumed that the AC and VC forms of the speed-curvature power law were *equivalent*, where the A is angular speed, and V is tangential speed; We showed that the AC and the VC power law are not *necessary* mathematically, statistically or physically. We have demonstrated analytically and numerically generated trajectories that do *not* conform to the power law, and we showed empirically measured trajectories that fit to different values of the exponent of the power law. However, it appears we made a mistake in assuming equivalence of the two laws. In this paper (**Annex 4**) we examine the differences in using angular speed to estimate the exponent of the power law, versus using tangential speed.

We explore this difference by analyzing empirical data using the AC and the VC power law. We used data from another experiment (**Annex 7**) where participants tracked targets moving along elliptic trajectories with increasing frequency across tasks, and with three different speed profiles. In the case of the VC form of the power law, only the fast movements, with frequency above 1 Hz resulted in a good fit to the power law, while the slower ones were not fitting to the power law (**Annex 4**: Figure 2). In contrast, in the case of the AC power law, nearly all of the trajectories appear to have a strong power law (**Annex 4**: Figure 3).

We explain this difference as a mistake in the initial assumptions: *the VC and AC power laws are not equivalent*. They are equivalent in exponents of the law, but not in the strength of the correlation. Tangential speed (V) is a purely kinematic variable, and curvature (C) a purely geometric variable, but angular speed is a mixed geometric-kinematic variable (A=VC); it depends on both curvature and speed. Angular speed is not necessarily correlated to curvature, but is often trivially correlated to curvature simply because small-curvature segments tend to be associated with a low angular speed (rate of

turning). In fact, the strength of the correlation will depend on the range of curvature (**Annex 4**: Figure 6, 7).

To illustrate this mistake, we used the analogy with a set of rectangles of different widths. Considering a set of rectangles of random, uncorrelated widths (w) and heights (h); their area (a=wh) will be correlated with width simply because the smaller width rectangles will tend to have smaller areas, and larger width rectangles will tend to have larger areas; not necessarily because the widths and heights are systematically related.

In sum, while the speed-curvature power law is not trivial – not given by mathematics, physics or statistics – we should only be using tangential speed and not angular speed as the kinematic variable when approximating the fit of trajectories to the power law.

3.2. Proposing solutions

In the second group of papers we gather proposals for the solutions to the problem elaborated in the first group of papers. Namely, we build robotic and simulation models of human sensorimotor loops. The models are aimed to be generative - the elements of the model represent simplified elements of human sensorimotor loops, and they should perform the same tasks human participants can perform. If indeed, the models behave similar to human participants, and the elements of the model are biologically plausible, the model may be said to explain the behavior.

3.2.1. Robot arm produces power law trajectories and other invariances

The purpose of the robot arm was two-fold: to see what kinds of invariances will emerge in simple target tracking tasks performed by a physical robot arm interacting with the real environment; and to test a hierarchical control architecture on real-world, noisy artificial sensors, geared electrical motors, and the unpredictable external environment. For these purposes, we built a 4-joint robot arm with a camera for visual perception, pressure sensing and angle sensing from the electronic (see Methods). We subjected the robot to tasks inspired by tasks commonly performed by humans and monkeys, such as center-out reaching, tracking elliptical targets and random pursuit tracking. We used direct and indirect perturbations to simulate situations encountered by humans in everyday tasks, such as using a tool, writing on a tilted surface, rotation of the visual field and blocking of a joint.

The main finding, relating to the power law, is that the robot arm produced power-law trajectories at high rhythms of movement even when the reference was a constant-speed non-power-law trajectory (**Annex 5**: Figure 4). For slow rhythms, the robot arm followed the reference, keeping the speed low and constant. At mid-range rhythms, the speed of the robot arm was on average lower than the speed of the reference and it was oscillating. At very high rhythms, the robot's trajectory followed the speed-curvature power law,

while the target had constant-speed non-power law trajectory. The speed profile of the robot arm is very similar to the profile of speed of the human hand when drawing ellipses, however, the size of the ellipse drawn by the robot is much smaller, and is showing an increasing phase delay. We can explain this phenomenon if we look at the robot as a dynamical system that takes the reference signal as an input and returns the robot hand position as output. When we create an input-output ratio vs frequency and phase-delay vs frequency plots (Bode plot, **Annex 5**: Figure 5), we can see that the robot arm acts as a low-pass filter: attenuating all amplitudes above 0.1Hz and creating frequency-dependent phase delays. Gribble and Ostry (1996) and Schaal and Sternad (2001) also show that the speed-curvature power law can emerge out of low-pass filtering. A non-power law reference may contain high frequency components, but when it passes through the filter, only the low-frequency components remain, and pure sinusoids in x and y dimensions create trajectories fitting to the power law (Lacquaniti et al, 1983).

These results suggest that, in humans, the speed-curvature power law may emerge out of the *failure* to track a given reference trajectory – as opposed to successfully tracking a pre-planned power-law reference trajectory. Indeed, when human participants track constant speed targets along elliptic trajectories, they can follow the instantaneous speeds when the average speed is low, while at high speeds they always go slower in the curves, following the speed-curvature power law (Viviani and Mounoud, 1990, see also **Annex 7**).

However, if the low-pass filter hypothesis is correct, we need to explain how the human visuo-motor system compensates for the difference in the sizes of the reference and the drawn ellipses, as well as the phase delay between them. In the framework of hierarchical control (Powers, 2008), the proposed solutions, in principle, are higher-level feedback loops systems that control more abstract visual variables, and set lower-level references. For example, these variables might be directly related to the visually perceived size of the drawn ellipses and the angular (phase) separation between the cursor and target, as we elaborate in a different paper (**Annex 7**).

Unrelated to the speed-curvature power law, we also found the invariance known as the bell-shaped speed profile in center-out reaching (**Annex 5**: Figure 3). In humans, straight-line movements have a characteristic speed profile – starting from zero speed, the hand quickly accelerates to a peak, and gradually decelerates to a stop, forming the shape of a bell (Morasso, 1981; Viviani and McCollum, 1983). This invariance is maintained regardless of direction or extent of movement, prompting the hypothesis that the straight-line trajectories must be pre-planned. Minimizing jerk over a given path and duration, for example, results in a bell-shaped speed profile (Atkeson and Hollerbach, 1985). However, we get the bell-shaped speed profile without any trajectory planning. The speed profile emerges out of the simple structural relationship - the acceleration of the hand is directly related to the visual separation between the cursor and the target. A lot of second-order systems behave in this way. A limitation of our solution is that it always behaves isochronously – the durations of reaching are the same regardless of reaching extent. This

suggest there might be a higher-level system managing movement speed, perhaps related to maintaining accuracy or the speed-accuracy tradeoff.

The performance under the blocked-wrist condition may be interpreted as the phenomenon of motor equivalence – humans can perform the same movement, such as drawing a letter, with the left of their right hand, on a horizontal or vertical surface, holding a pen or stick, or in many other different ways. This ability in the robot is a direct consequence of the synergistic, multi-input, multi-output arrangement of control systems. These control systems resemble the definition synergy of Latash et al. (2007) – the controlled variables such as *reach* are the performance variables, and the activations of motors are elemental variables. This arrangement is a proposal for the computational basis of synergies in human arm control, not just at the level of muscles, but perhaps on multiple levels of control (**Annex 5:** Figure 6).

The robot arm has proven to be resilient to different perturbations, and has performed elliptic target tracking, reaching and random pursuit tracking with similar effectiveness under normal conditions and under conditions of: a) blocked wrist, b) tablet tilted by 30° from horizontal, c) the hand-tip marker placed on a 'tool' extension, d) camera rotated by 30° (**Annex 5**: Figure 7). This resilience comes from the hierarchical arrangement of control systems – the higher-level systems specify the reference, the desired value of the lower-level perceptions; they do not specify actions or how the lower-level systems should achieve their references.

In summary, even though the robot arm is modest in precision and speed, the robustness to direct and indirect perturbations, combined with the computational simplicity of the controllers, is suggesting that similar multi-level control architectures might be implemented in the basis of biological control. With regards to the speed-curvature power law, we confirmed that low-pass filtering in the high-level visual sensorimotor loop may be an important element in the origin of the power law, but the system is still missing size and phase compensation. Taken together, the goal for future research is to attempt to design a hierarchical control system with a low-pass filter element that can compensate for the differences in size and phase when tracking elliptical targets.

3.2.2. Robot model of antagonistic muscles

One important observation made during the testing of the hierarchically controlled robot arm was related to the backlash in the gears and precision of movement. Backlash is one of 'hard nonlinearities' in robot control, coming from the small spaces between transmission gears. It is a known phenomenon in robotic engineering that backlash in the gears may cause instabilities and self-sustained oscillations (Slotine and Li, 1991, p. 172), and because of it, the gains need to be reduced, impacting final precision of movement. Common solutions to avoiding backlash are using direct-drive arms or cables in the drive train, such as twisted string actuators (TSAs). TSAs are an emerging technology in

robotics (Palli et al, 2012; Popov et al. 2013; Rodriguez et al. 2020), they can be placed in a variety of configurations and controlled by different architectures.

We designed and build a pair of antagonistic TSAs as a model of the elbow joint (see Methods). The robotic prototype also contained a model of the Golgi tendon organ as a force or tension sensor made from a potentiometer and some rubber bands, and the model of the muscle spindle as a muscle length sensor or comparator. The controlled variables at the first level were muscle lengths, at the second level had simultaneous control of sums of tendon tensions and differences of the tensions; while the joint angle and angular speed were controlled at the third level. The control architecture was inspired by a simulation by Powers (1979) intended to model spinal control systems.

The analysis of the response to a step input in joint angle shows that the removal of backlash from the joint had very good effects on joint precision: the steady-state error was very low, only +/-0.03 degrees in low stiffness and +/-0.04 degrees in the high stiffness situation. On the other hand, since the motors used in the TSAs were small and slow, the bandwidth was only about 0.2 Hz (**Annex 6:** Figure 3).

Overall, the extremely simple control architecture, using only summing and differentiating elements in the computational part of the controller, is still working very precisely despite being built from very inaccurate elements. This architecture shows promise as a model of the spinal control architecture; however, it is still a very early prototype. In future development, the simple antagonist muscle arrangement might be extended to multiple muscles and joints, with added realistic delays and faster motors to improve bandwidth. A system like that might be used to build affordable, precise, and easily controllable prosthetic arms. Likewise, it may be more directly compared to human arms, functioning as a robotic platform for testing hypotheses about the spinal and supra-spinal motor control systems.

3.2.3. Visuomotor phase-locked loop reproduces elliptic hand trajectories

In the experiments with the hierarchically controlled robot arm, we confirmed and further explored the idea that low-pass filtering in the visuo-motor loop may be responsible for the speed-curvature power law. The robot arm could follow a low-frequency constant-speed reference, but at higher frequencies, it could not follow the reference. Specifically, the robot arm it did not follow the high frequency components of the reference trajectory. Consequently, the hand trajectory contained mostly pure sinusoids in position and speed profiles, and conformed to the power law. However – the sinusoids had a smaller amplitude, causing the drawn ellipses to be much smaller than required, and also causing phase shifts not observed in tasks with human participants.

In this study **(Annex 7)**, we designed an experiment where the participants tracked a target along an elliptic trajectory, across a range of frequencies and different speed profiles, and

we designed a numerical, generative model that aims to predict and explain participant behavior in this task.

In experiment 1, we found that the participants, like the robot, could accurately follow only low frequency references. The participants followed the path of the target (**Annex 7**: Figure 2B, 2E), and the speed (**Annex 7**: Figure 2C, left panel, and Figure 2E). Participant trajectories did not conform to the power law because of high noise in the curvature estimate. The curvature is estimated using the first and second derivative of position, making it sensitive to measurement noise and movement tremor, and they are apparently not entirely removed with the second-order Butterworth low-pass filter with a 10Hz cutoff.

At high speeds we have a different situation. Participants don't follow the path of the target exactly, and there are large errors in instantaneous speed (**Annex 7**: Figure 2B, 2E). In fact, the speed profiles of the participants' hands are nearly identical across different situations for the same cycle frequency, even though the target profiles were different (**Annex** 7: Figure 2D). The targets had profiles with exponents $\beta=0$, $\beta=-1/3$ and $\beta=-2/3$, while all the participant's trajectories had the exponent $\beta=-1/3$. At high frequencies, or high average speeds of movement, participants don't have a lot of control over their instantaneous speeds, confirming the observation of Binet and Courtier (1893). After about 1Hz and faster movements, all participant trajectories were following the -1/3 VC power law. This suggests that participants have relatively poor trajectory control at high speeds – apparently, they *cannot* produce constant speed trajectories at cycle frequencies larger than 1Hz even what that is the task, and they can *only* produce trajectories conforming to the -1/3 power law.

The first question we wanted to answer was the nature of the visually controlled variables in elliptic target tracking. First, we demonstrated that the participants are *not* controlling the linear cursor-target distance in x and y dimensions. We fitted a model controlling cursor-target distances dx and dy to human behavior in a random pursuit tracking task. Clearly, in the random pursuit task, this model explains participant behavior very well, in accordance with previous research (reviewed in Parker et al, 2020). However, in the ellipse tracking task, this model was drawing the ellipses of different sizes than participants, and introduced a large phase delay not present in human-made trajectories (**Annex 7**: Figure 3). However, when looked in the frequency domain, the model can be seen as a low-pass filter, and still produces -1/3 power-law elliptic trajectories. This suggested that, even if the model does not explain the behavior of the participants entirely, it could be used as a low-pass filter element in a lager, multi-level loop that also compensated for the observed differences in the size of the drawn ellipses and the phase delay.

We proposed that these higher-level systems are perceiving the phase difference between the cursor and the target; and the size difference between the cursor-drawn ellipse and the target-drawn ellipse, using them as a controlled variable in a negative feedback loop. We conducted a preliminary experiment (experiment 2, **Annex 7**: Figure 4) where we directly disturbed these two variables simultaneously with a random-smoothed disturbance. The

results of the experiment confirmed that the participant (N=1) maintained both variables stable and uncorrelated to the disturbance quantity (**Annex** 7: Figure 4), supporting our proposal.

Next, we created a generative numerical model with size and phase difference as high-level controlled variables. The phase difference modified the frequency of a 2D harmonic oscillator, and the size difference modified the amplitude. This arrangement is similar to a phase-locked loop (PLL), used very commonly in signal processing and communication technologies. The output of the oscillator served as the reference, or a kind of virtual target, for the lower-level target tracking system, that also performed low-pass filtering. (**Annex 7:** Figure 5).

The model replicated many important features of participant behavior: (i) the power law emerged only for fast-drawn ellipses (frequency $f \geq 0.84$Hz), (ii) the speed profiles were similar to participant's speed profiles across all frequencies, (iii) the position profiles were nearly identical for all frequencies, (iv) the sizes of the drawn ellipses were similar to the size of participant drawn ellipses in the same task, (v) the phase differences were maintained near zero radians (**Annex 7**: Figures 5 and 6). The model also replicated participant behavior from experiment 2 with simultaneous random changes in phase and size of the ellipse (**Annex 7**: Figure 6C and 6D).

The limitation of the study is, primarily, the small number of participants and this should be improved in future research. There could also be alternative models with similar or better performance in the same tasks. For example, the oscillator might not be located in the higher-level loop, suggesting a cortical structure, but perhaps in a lower-level loops, suggesting a spinal level structure; as indicated by fitting of the delay parameter in the model.

Overall, the model presented here explains the origins of the speed-curvature power law in terms of a hierarchical sensorimotor control system. The high-level perceptually controlled variables are ellipse size difference and phase difference. These variables and their implicit references are used to manipulate the frequency and amplitude of an internal oscillator. The oscillator, in turn, sets the reference of a target-tracking system that also performs low-pass filtering. The similarities in the behavioral performance of the model to the participants, taken together with the computational simplicity of the model elements, may be suggesting the existence of neural perceptuomotor mechanisms that perform the task in a similar way.

4. Conclusions

1. The speed-curvature power law is a real, non-trivial phenomenon in human movement, and not a statistical artifact.

2. Angular speed should not be used to estimate the speed-curvature power law since it is often trivially correlated to curvature, and instead tangential speed can be used.

3. The principle of least action, as suggested by Lebedev et al. (2001) cannot explain the origin of the speed-curvature power law.

4. The power law may be created by low-pass filtering non-power-law elliptic trajectories. However, the drawn ellipses will be smaller and phase-delayed compared to the referent trajectory and also compared to the trajectories created by human participants in the same situation.

5. A hierarchical control architecture with simple elements produces flexible and adaptive behavior in a physical robot system, despite noise, delays and non-linearities. This suggests that the architecture of neural systems in the control of arm movement may be hierarchical.

6. The removal of backlash by tension-controlled antagonistic twisted string actuators allows for very precise angular position control, despite non-precise individual elements of the robotic prototype.

7. Phase and size difference are the most likely visual features controlled by human participants when tracking targets along elliptic trajectories, also underlying the generation of the power law at high frequency tasks. This claim is supported by further behavioral experiments, when participants keep both phase and size difference stable even under direct perturbation. It is also supported by a numerical model that replicates participant trajectories in tracking targets across multiple frequencies.

1. La ley de potencia de velocidad-curvatura es un fenómeno real y no trivial en el movimiento humano, y no un artefacto estadístico.

2. La velocidad angular no debe utilizarse para estimar la ley de potencia, dado que suele estar trivialmente correlacionada con la curvatura. En su lugar, puede utilizarse la velocidad tangencial.

3. El principio de mínima acción, como sugieren Lebedev et al. (2001), no puede explicar el origen de la ley de potencia.

4. La ley de potencia puede crearse mediante el filtrado de paso bajo de trayectorias elípticas sin ley de potencia. No obstante, las elipses dibujadas serán más pequeñas y con retraso de fase en comparación con la trayectoria de referencia y con las creadas por los participantes humanos en la misma situación.

5. Una arquitectura de control jerárquica con elementos simples produce un comportamiento flexible y adaptativo en un sistema de robot físico, a pesar del ruido, los retrasos y las no linealidades. Esto implica que los sistemas neuronales en el control del movimiento del brazo pueden ser jerárquicas.

6. La eliminación de la holgura mediante actuadores de cuerda torcida antagónicos controlados por tensión permite un control de posición angular muy preciso, a pesar de la falta de precisión de los elementos individuales del prototipo robótico.

7. Las diferencias de fase y de tamaño son los rasgos visuales más probablemente controlados por los participantes humanos cuando siguen visualmente objetivos a lo largo de trayectorias elípticas, lo que también subyace a la generación de la ley de potencia en tareas de alta frecuencia. Esta afirmación está respaldada por experimentos de comportamiento adicionales, en los que los participantes mantienen estables tanto la diferencia de fase como la de tamaño incluso bajo una perturbación directa. Además, está respaldada por un modelo numérico que reproduce las trayectorias de los participantes en el seguimiento de objetivos a través de múltiples frecuencias.

5. References

Abeles, M., Diesmann, M., Flash, T., Geisel, T., Herrmann, M., & Teicher, M. (2013). Compositionality in neural control: an interdisciplinary study of scribbling movements in primates. *Frontiers in computational neuroscience*, *7*, 103.

Atkeson, C. G., and Hollerbach, J. M. (1985). Kinematic features of unrestrained vertical arm movements. *Journal of Neuroscience*, *5*(9), 2318-2330.

Bennequin, D., Fuchs, R., Berthoz, A., & Flash, T. (2009). Movement timing and invariance arise from several geometries. *PLoS computational biology*, *5*(7), e1000426.

Binet, A., & Courtier, J. (1893). Sur la vitesse des gestes graphiques [On the speed of voluntary movements]. Revue Philosophique, 35, 664-671

Catavitello, G., Ivanenko, Y. P., Lacquaniti, F., & Viviani, P. (2016). Drawing ellipses in water: evidence for dynamic constraints in the relation between velocity and path curvature. *Experimental brain research*, *234*(6), 1649-1657. https://doi.org/10.1007/s00221-016-4569-9

Cisek, P. (2005). Neural representations of motor plans, desired trajectories, and controlled objects. *Cognitive Processing*, *6*(1), 15-24.

Dagenais, P., Hensman, S., Haechler, V., & Milinkovitch, M. C. (2021). Elephants evolved strategies reducing the biomechanical complexity of their trunk. *Current Biology*, *31*(21), 4727-4737.

Cisek, P. (2019). Resynthesizing behavior through phylogenetic refinement. Attention, Perception, & Psychophysics, 81(7), 2265-2287.

de'Sperati, C., & Viviani, P. (1997). The relationship between curvature and velocity in two-dimensional smooth pursuit eye movements. *Journal of Neuroscience*, *17*(10), 3932-3945.

Fitts, P. M. (1954). The information capacity of the human motor system in controlling the amplitude of movement. Journal of experimental psychology, 47(6), 381.

Flash, T., & Handzel, A. A. (2007). Affine differential geometry analysis of human arm movements. *Biological cybernetics*, *96*(6), 577-601.

Flash, T., & Sejnowski, T. J. (2001). Computational approaches to motor control. *Current opinion in neurobiology*, *11*(6), 655-662.

Gribble, P. L., & Ostry, D. J. (1996). Origins of the power law relation between movement velocity and curvature: modeling the effects of muscle mechanics and limb dynamics. *Journal of Neurophysiology*, *76*(5), 2853-2860.

Haith, A. M., & Krakauer, J. W. (2013). Theoretical models of motor control and motor learning. *Routledge handbook of motor control and motor learning*, 1-28.

Harris, C. M., & Wolpert, D. M. (1998). Signal-dependent noise determines motor planning. *Nature*, *394*(6695), 780-784.

Huh, D. (2015). The vector space of convex curves: How to mix shapes. *arXiv preprint arXiv:1506.07515*.

Huh, D., & Sejnowski, T. J. (2015). Spectrum of power laws for curved hand movements. *Proceedings of the National Academy of Sciences*, *112*(29), E3950-E3958.

Ivanenko, Y. P., Grasso, R., Macellari, V., & Lacquaniti, F. (2002). Control of foot trajectory in human locomotion: role of ground contact forces in simulated reduced gravity. *Journal of neurophysiology*, *87*(6), 3070-3089.

Jack, W. R. (1895). On the analysis of voluntary muscular movements by certain new instruments. Journal of Anatomy and Physiology, 29, 473-478.

Lacquaniti, F., Terzuolo, C., & Viviani, P. (1983). The law relating the kinematic and figural aspects of drawing movements. *Acta psychologica*, *54*(1-3), 115-130.

Latash, M. L., Scholz, J. P., & Schöner, G. (2007). Toward a new theory of motor synergies. *Motor control*, *11*(3), 276-308.

Lebedev, S., Tsui, W. H., & Van Gelder, P. (2001). Drawing movements as an outcome of the principle of least action. *Journal of mathematical psychology*, *45*(1), 43-52.

Liu, D., & Todorov, E. (2007). Evidence for the flexible sensorimotor strategies predicted by optimal feedback control. *Journal of Neuroscience*, *27*(35), 9354-9368.

Maoz, U., Portugaly, E., Flash, T., & Weiss, Y. (2005). Noise and the two-thirds power law. Advances in Neural Information Processing Systems, 18.

Maoz, U., Berthoz, A., & Flash, T. (2009). Complex unconstrained three-dimensional hand movement and constant equi-affine speed. *Journal of neurophysiology*, *101*(2), 1002-1015.

Marken, R. S., & Shaffer, D. M. (2017). The power law of movement: an example of a behavioral illusion. *Experimental Brain Research*, *235*(6), 1835-1842.

Morasso (1981) bell-shaped speed profile

Morasso, P. (1981). Spatial control of arm movements. *Experimental brain research*, 42(2), 223-227.

Ostry, D. J., & Feldman, A. G. (2003). A critical evaluation of the force control hypothesis in motor control. *Experimental brain research*, *153*(3), 275-288.

Palli, G., Natale, C., May, C., Melchiorri, C., & Wurtz, T. (2012). Modeling and control of the twisted string actuation system. *IEEE/ASME Transactions on Mechatronics*, *18*(2), 664-673.

Pollick, F. E., Maoz, U., Handzel, A. A., Giblin, P. J., Sapiro, G., & Flash, T. (2009). Three-dimensional arm movements at constant equi-affine speed. *Cortex*, *45*(3), 325-339.

Popov, D., Gaponov, I., & Ryu, J. H. (2013, November). Bidirectional elbow exoskeleton based on twisted-string actuators. In *2013 IEEE/RSJ International Conference on Intelligent Robots and Systems* (pp. 5853-5858). IEEE.

Powers,W. T. (1973). Behavior: The Control of Perception. Chicago, IL: Aldine.

Powers, W. T. (1976). The cybernetic revolution in psychology. In *Cybernetics Forum* (Vol. 8, pp. 72-86).

Powers, W. T. (1978). Quantitative analysis of purposive systems: Some spadework at the foundations of scientific psychology. *Psychological Review*, *85*(5), 417.

Powers, W. T. (1999). A model of kinesthetically and visually controlled arm movement. *International journal of human-computer studies*, *50*(6), 463-479.

Powers, W.T (1979). The nature of robots. Part 3: A closer look at human behavior. Byte. Aug;4(8):94-116

Powers, W. T. (2008). Living control systems III: The fact of control.

Pruszynski, J. A., & Scott, S. H. (2012). Optimal feedback control and the long-latency stretch response. *Experimental brain research*, *218*(3), 341-359.

Richardson, M. J., & Flash, T. (2002). Comparing smooth arm movements with the two-thirds power law and the related segmented-control hypothesis. *Journal of neuroscience*, *22*(18), 8201-8211.

Rodriguez, A. S. M., Hosseini, M., & Paik, J. (2020). Hybrid Control Strategy for Force and Precise End Effector Positioning of a Twisted String Actuator. *IEEE/ASME Transactions on Mechatronics*, *26*(5), 2791-2802.

Runkel, P. J. (1990). Research method for control theory. *American Behavioral Scientist*, *34*(1), 14-23.

Schaal, S., & Sternad, D. (2001). Origins and violations of the 2/3 power law in rhythmic three-dimensional arm movements. *Experimental brain research*, *136*(1), 60-72.

Schwartz, A. B. (1994). Direct cortical representation of drawing. *Science*, *265*(5171), 540-542.

Slotine, J. J. E., & Li, W. (1991). *Applied nonlinear control* (Vol. 199, No. 1, p. 705). Englewood Cliffs, NJ: Prentice hall.

Striedter, G. F., & Northcutt, R. G. (2019). *Brains through time: a natural history of vertebrates*. Oxford University Press.

Todorov, E., & Jordan, M. I. (1998). Smoothness maximization along a predefined path accurately predicts the speed profiles of complex arm movements. *Journal of Neurophysiology*, 80(2), 696-714.

Todorov, E., & Jordan, M. I. (2002). Optimal feedback control as a theory of motor coordination. *Nature neuroscience*, *5*(11), 1226-1235.

Vieilledent, S., Kerlirzin, Y., Dalbera, S., & Berthoz, A. (2001). Relationship between velocity and curvature of a human locomotor trajectory. *Neuroscience letters*, *305*(1), 65-69.

Viviani, P., & Terzuolo, C. (1982). Trajectory determines movement dynamics. *Neuroscience*, 7(2), 431-437.

Viviani, P., & McCollum, G. (1983). The relation between linear extent and velocity in drawing movements. *Neuroscience*, *10*(1), 211-218.

Viviani, P., & Mounoud, P. (1990). Perceptuomotor compatibility in pursuit tracking of two-dimensional movements. *Journal of motor behavior*, *22*(3), 407-443.

Viviani, P., & Schneider, R. (1991). A developmental study of the relationship between geometry and kinematics in drawing movements. *Journal of Experimental Psychology*: Human Perception and Performance, 17(1), 198.

Viviani, P., & Flash, T. (1995). Minimum-jerk, two-thirds power law, and isochrony: converging approaches to movement planning. *Journal of Experimental Psychology*: Human Perception and Performance, 21(1), 32.

Wann, J., Nimmo-Smith, I., & Wing, A. M. (1988). Relation between velocity and curvature in movement: Equivalence and divergence between a power law and a minimum-jerk model. *Journal of Experimental Psychology: Human Perception and Performance*, 14(4), 622–637.

Woodworth, R.S., 1899. Accuracy of voluntary movement. Psychol. Rev.: Monogr. Suppl. 3 (3), i–114. https://doi.org/10.1037/h0092992.

Zago, M., Lacquaniti, F., & Gomez-Marin, A. (2016). The speed–curvature power law in Drosophila larval locomotion. *Biology letters*, *12*(10), 20160597.

6. Annex

Annex 1: Matic, A., & Gomez-Marin, A. (2019). A customizable tablet app for hand movement research outside the lab. *Journal of neuroscience methods*, *328*, 108398. PMID: 31412268 DOI: 10.1016/j.jneumeth.2019.108398

Annex 2: Zago, M., Matic, A., Flash, T., Gomez-Marin, A., & Lacquaniti, F. (2017). The speed-curvature power law of movements: a reappraisal. *Experimental brain research*, *236*(1), 69-82. PMID: 29071361 DOI: 10.1007/s00221-017-5108-z

Annex 3: Matic, A., & Gomez-Marin, A. (2020). Geometric purity, kinematic scaling and dynamic optimality in drawing movements beyond ellipses. *Journal of Mathematical Psychology*, *99*, 102453. DOI: 10.1016/j.jmp.2020.102453

Annex 4: Matić, A., & Gomez-Marin, A. (2022). Angular speed should be avoided when assessing the speed-curvature power law of movement. bioRxiv. DOI: 10.1101/2022.06.27.497695

Annex 5: Matić, A., Valerjev, P., & Gomez-Marin, A. (2021). Hierarchical control of visually-guided movements in a 3D-printed robot arm. *Frontiers in Neurorobotics*, 149. PMID: 34776921 DOI: 10.3389/fnbot.2021.755723

Annex 6: Matić, A., & Gomez-Marin, A. (2021). Elbow angle and stiffness control by twisted string actuators and nested feedback. *The 9.5th international symposium on Adaptive Motion of Animals and Machines. Ottawa Canada (Virtual Platform)*, DOI 10.18910/84845

Annex 7: Matić, A. (2022). Visuomotor phase-locked loop reproduces elliptic hand trajectories across different rhythms. bioRxiv. DOI: 10.1101/2022.07.20.500761

Annex 1:

Matic, A., & Gomez-Marin, A. (2019). A customizable tablet app for hand movement research outside the lab. Journal of neuroscience methods, 328, 108398.
PMID: 31412268 DOI: 10.1016/j.jneumeth.2019.108398

A customizable tablet app for hand movement research outside the lab

Adam Matic, Alex Gomez-Marin*

Behavior of Organisms Laboratory, Instituto de Neurociencias CSIC-UMH, Alicante, Spain

A B S T R A C T

Background: Precise behavioral measurements allow the discovery of movement constraints that provide insights into sensory-motor processes and their underlying neural mechanisms. For instance, when humans draw an ellipse on a piece of paper, the instantaneous speed of the pen co-varies tightly with the local curvature of the path. Known as the speed-curvature power law, this phenomenon relates to fundamental questions of motor control.

New method: We have developed a software app for displaying static curves or dynamic targets while recording finger or stylus movements on Android touch-screen tablets. Designed for human hand movement research, the app is free, ready-to-use, open-source and customizable.

Results: We provide a template experimental protocol, and detailed explanations to use it and flexibly modify the code for different kinds of tasks. Our validation of the app demonstrates laboratory-quality results outside the laboratory. We also provide raw data and analysis scripts.

Comparison with existing methods: Commonly used laboratory devices for recording hand movement trajectories are large, heavy and expensive. In turn, software apps are often not published, nor customizable. Our app running on tablets becomes an affordable, flexible, and portable tool suited for quantitative and robust behavioral studies with large number of participants and outside the laboratory (e.g. in a classroom, a hospital, or at home).

Conclusions: The affordability, flexibility, and resolution of our tablet app provide an effective tool to study behavior quantitatively in the real world.

* Corresponding author.
E-mail address: agomezmarin@gmail.com (A. Gomez-Marin).

"A drawing is simply a line going for a walk." (Paul Klee)

1. Introduction

It has been argued that nothing makes sense in neuroscience except in the light of behavior (Krakauer et al., 2017). Yet, even when we carefully measure the behavior of organisms, the promise that the discoveries found in the laboratory will generalize in real-world situations is often hard to fulfill. This is in part due to the simplicity of experimental designs which, in turn, allow to maximize control by the experimenter, taming the complexity and context that is natural to the behaving subject under study (Gomez-Marin and Mainen, 2016). For instance, writing on a piece of paper or simply drawing with our finger on a tablet are everyday activities, but the quantitative study of the processes and mechanisms generating such complex hand trajectories is nearly always done in laboratory conditions.

Another main reason for laboratory research is the necessary involvement of expensive, sophisticated, and usually massive technological devices for manipulation and measurement. In fact, measuring behavior has a rich history in hand movement research, where the development of recording instruments has played a central role. These include graph paper, cameras, robot arms, motorized linkages, and other clever gadgets to store hand position over time. While it is not our aim here to present a exhaustive account, let us list several influential methods in movement research that illustrate the advancement of a field with more than a century of history.

An early instrument in recording movement was the Edison pen, where a needle at the tip of the pen was oscillating at constant frequency. The needle made marks on the paper so that movements at higher speed left marks spaced further apart than movements at lower speed. With such device, the speed of the pen in curved parts of a trajectory was observed to be lower than the speed in straight parts (Binet and Courtier, 1893). A middle-sized model was priced at 50$ in the 1890's, which is on the order of 1500$ in today's dollars. A few years later, Woodworth used a simple method of graph paper and metronome-synchronized movements to measure the relationship between speed and accuracy (Woodworth, 1899). As he notes, the method was easy to use and he recorded more than 125 K individual trajectories for a study. The difficult part was analyzing the recorded data, and this was done by his assistants. During the 1930's, Bernstein invented a highly sophisticated method called cyclography, utilizing high-speed film cameras with shutter speeds of 150–200 Hz and light-bulb markers placed on the bodies of his participants (Bernstein, 1984; Gurfinkel and Cordo, 1998). Using multiple cameras or a single camera and a system of mirrors, the three-dimensional trajectories of joints and limbs of participants could be reconstructed. Bernstein formulated the so-called degrees of freedom problem, and an early theory of movement control hierarchy. Regarding handwriting analysis with digitizers in the 1960's, an overview of devices used can be found in (Schoemaker, 1998).

In the 1980's, a puzzling constraint between instantaneous speed and local curvature of end-point hand trajectories was discovered in data recorded with an ultrasonic device called the Graph Pen (Lacquaniti et al., 1983; Soechting et al., 1986), which was capable of 100 Hz sampling and 0.1 mm accuracy in measuring pen position on a plane. Another device used by (Lacquaniti et al., 1983) was a Calcomp electromagnetic digitizing table, 100 Hz sampling and 0.025 mm accuracy. It was then established that in human hand movement, the instantaneous angular velocity is proportional to the local curvature raised to the 2/3 power ($A = k \cdot C^{\beta}$ with $\beta = 0.66$); the so-called two-thirds power law.

Further investigations of the coordination of arm movements used two-link mechanical manipulanda. Built with two joints and precision potentiometers calibrated to measure joint angles, and sampling at 100 Hz, it achieved 1 mm resolution in the endpoint position measurement (Flash and Hogan, 1985). Another class of measuring technologies consisted of pressure sensitive pads, which can be used with ordinary pens. For example, a Quest Micropad pressure sensitive device can reach 200 Hz, and achieve 0.2 mm accuracy (Wann et al., 1988). Furthermore, for free movement in three dimensions, the use high-speed cameras together with visual markers placed on the body of the participant facilitate computerized analysis. For instance, in (Dounskaia et al., 2002) an Optotrack 3D optoelectronic camera system achieved 100 Hz frequency using infrared LED lights as markers.

More recently, researchers have been using digitizing graphics tablets like the Wacom Cintiq and Intuos. In particular, using such devices it has been empirically found (and theoretically predicted) that humans produce a spectrum of speed-curvature power laws while tracing pure frequency curves (Huh and Sejnowski, 2015). These devices provide very high temporal and spatial resolution of recording pen or finger position, up to 140 Hz in sampling rates for Cintiq and up to 200 Hz for Intuos models, and reported 0.005 mm of spatial resolution (5080 lines per inch; but accuracy may be lower), while displaying any curve geometry and target kinematics on the very surface where the participant draws. We have recently reproduced such findings with the same devices (Zago, Matic et al., 2018). However, note that the Wacom Cintiq 27QHD is a 27" monitor weighing 13 kg, and priced around 2750$. Its size and cost, and the requirement of a separate computer to record the data can be a limitation in experimental settings that require affordable, portable, and high-throughput data collection. This has prompted us to explore other solutions that are more efficient and inexpensive without compromising the quality of the data.

In the last years, small-size autonomous computers such as iPad tablets, Android tablets, touch-screen laptops or even smart-phones are increasingly used in movement control and development research (Accardo et al., 2013; Lee et al., 2014; Hill et al., 2014), as well as in clinical settings (Anzulewicz et al., 2016; Sisti et al., 2017; Vianello et al., 2017). Tablet computers are affordable and transportable, which in principle makes them ideal for large-scale experiments outside of the laboratory, in natural settings for humans such as classrooms, homes, or hospitals. Actually, the spatial and temporal resolution of recording movement trajectories in the tablets is becoming on par with larger, specialized graphics digitizing tablets, thus becoming a reasonable and practical alternative. We have exploited this fact here.

In this article we report on creating a free and open source application for an Android tablet made to facilitate large-scale hand movement experiments in situations not necessarily constrained to laboratory settings. Our application can be used in its current form, or as a template and code base for designing applications for new experiments. Currently, there are three main task types available in the code: (i) tracing figure shapes, (ii) tracking target trajectories and (iii) free scribbling or drawing. Each task type invites to constraint certain aspects of trajectory production. For instance, in tracing, participants are invited to move their finger following a particular geometry statically displayed on the screen, but with kinematics being free. In tracking, participants are invited to follow the particular kinematics displayed by a moving target. And in scribbling, participants can draw in space (geometry) and time (kinematics) as they please. We have developed an experimental protocol for high-throughput experimentation outside the lab, and we have tested the validity of the app for generating laboratory-quality motor control data. In sum, our app is ready to use, open, customizable, and suitable for human movement research.

2. Materials and methods

2.1. Hardware

We have used a fairly common and affordable tablet, the Samsung Galaxy Tab A6 (alternative name SM-T580) whose price is around 170€. Physical dimensions are 254 × 164 × 8 mm. It comes with the Android operating system, version 8.1.0 (Oreo) and API level 26. The display is a 10.1" PLS LCD screen, with dimensions 216 × 135 mm, and a resolution of 1920 × 1200px. The tablet has a capacitive touch-

screen, and registers touch by a finger or a capacitive stylus, with resolution equal to the display resolution, which is 226ppi or 8.89 px/mm in pixel density. Maximum screen refresh rate is 60 Hz. Maximum sampling rate of touch events is not published, but we have found it to be close to 85 Hz.

2.2. Software

The app was programmed in Android Studio (version 3.3.2), a free integrated development environment (IDE), officially supported by Google, intended for development of Android OS applications on multiple platforms. Android Studio enables development in programming languages Java, C++, Go. For this application we used Kotlin, which is a recently designed general-purpose programming language fully interoperable with Java, can freely use Java libraries, and compiles to the JVM, but features a simpler and more concise syntax. The combination of relative simplicity and the ability to use existing Java libraries makes Kotlin a practical choice. To program the app, we have used a Windows 10 PC, with 8GB of RAM and Intel i5 CPU. But there are no stringent constraints on the PC needed to do so.

2.3. Experiments

The proof-of-concept validation behavioral experiments were performed by one of the authors. They involved tracing, tracking and drawing different geometric and kinematic tasks with the finger on the tablet. The total duration of the experimental protocol coded in the app was 15 min. Default instructions were to produce fast and fluid movements without corrections. Procedures were approved by the Institutional Review Board.

3. Results

We have created an application software (an "app") for Android tablets to be used in hand movement and sensory-motor control research, with a focus on the speed-curvature power law. The application is ready for use in its current form. We also provide the source code together with an easy way of designing other tasks to be encoded in the app, as well as a deconstruction of an effective experimental protocol, which we demonstrate. We also validate the quality of the data collected for motor control science, and share the raw data as well as analysis scripts. See Fig. 1 for a general methodological scheme, whose steps we now explain:

3.1. The app is ready to run and easy to install

The application can be installed on any Android tablet. It can be run in its original form by simply downloading it the app in a tablet. This would install the app with predesigned template experiments and its default settings. An ordinary route for Android applications is the Google Play Store, but it is not necessary, as it might involve fees and delays, and add another layer of complexity to the process. Distributing the *apk* file can be done via USB cable, copying it from the PC to each tablet, or more simply via email, by sending the *apk* file or a link for its download to each tablet's email address. The app can then be downloaded and installed on the tablets.

3.2. An effective experimental protocol has been designed and validated

As diagrammed in Fig. 2, when participants start the app the first panel they see is the data entry panel. They are asked to enter the year and month of birth, gender, and dominant hand. This information is stored as metadata, and used to construct the filename with the trajectory data. The participant can then start a "practice" sequence or an "experiment" sequence, following the instructions previously programmed in the app by the experimenter. The practice sequence serves to familiarize the participant with the tasks and can be repeated as many times as needed. By default, the data is not recorded in the practice sequence (but this can be modified in the *Experiment.kt* file; see next subsection). The experiment sequence contains a series of tracing, tracking and scribbling tasks, as defined in the program. Data is recorded after each task in the experimental sequence. The experiment ends after all tasks have been run.

After a concise verbal instruction to the participant about the experiment, we found practice to be important in ensuring that the experiment takes place smoothly. We also found that it is effective to present the various (tracing, tracking, and scribbling) tasks consecutively with a brief pause, rather than providing a general menu where the participant clicks back and forth the corresponding task or curve to execute. This protocol coded in the app should be particularly useful to perform high-throughput experiments in groups of children or adults by having the app installed in several tablets and running the practice and experiment phases synchronized across participants.

When the experimental sequence is finished, the application ends and the movement data (x position, y position, time) is saved in a *txt* file together with the type of task and metadata (age, gender, hand) as the file name, so that each file self-contains all the necessary information for further analyses (see section 3.6).

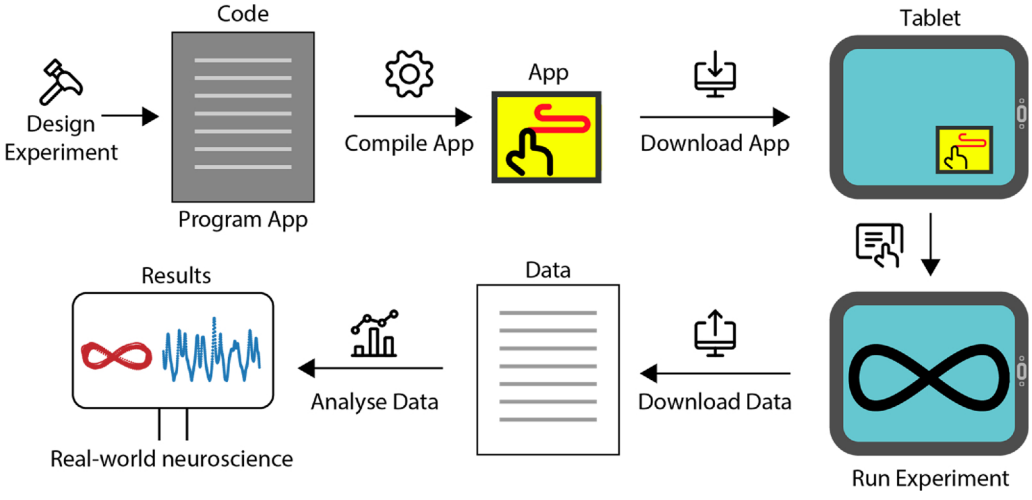

Fig. 1. General methodological scheme of the tablet app: from experimental design to data analyses. The app is compiled and ready to be used (*app-release.apk* file). It simply needs to be downloaded to the Android tablet via USB from a desktop computer or by email. Its deployment consists of three phases: basic data entry, practice and experiment sections (see Fig. 2). When the experiment is finished, the raw data (movement trajectories, experimental templates, and participant metadata) can again be easily transferred from each tablet to a desktop computer via USB or email. It is also possible to customize the app for other experimental designs involving sequences of tracing, drawing or scribbling tasks (see Fig. 3). This is implemented in the source code of the app (editing the *Experiment.kt* file; see scripts in supplementary material). Quantitative data analyses (which can be performed in Python files we share within a Jupyter Notebook; see *Analysis_KinematicCognition.ipynb* file in supplementary material) yield state-of-the-art motor control results as demonstrated in Fig. 4. The potential of the app for real-world behavioral neuroscience experiments is summarized in Fig. 5.

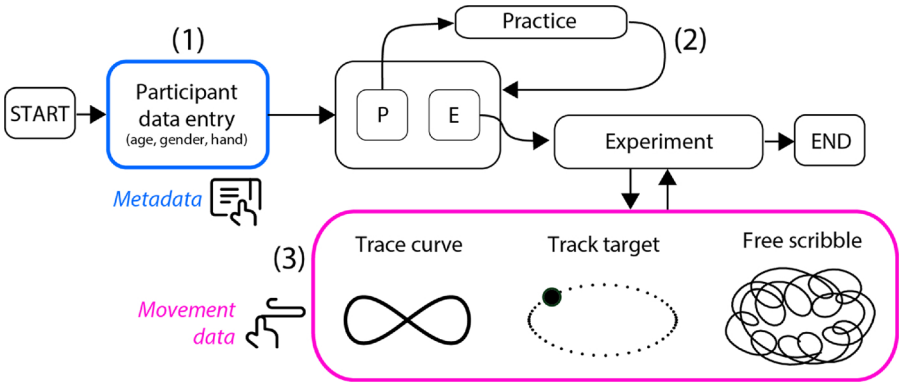

Fig. 2. Application flow diagram during an experiment. Upon clicking on the app icon on the tablet desktop, the app starts with the data entry panel (**1**), which is saved as metadata. Next the participant can choose to run a practice sequence (**2**) one or more times by pressing the "practice" button (**P**). Then the participant may click the "experiment" button (**E**) so as to be presented with a sequence of tracing, tracking and scribbling tasks (**3**) for which data is recorded.

3.3. The app can be edited by non-professionals to customize experimental protocols

The source code is provided and can be edited in order to accommodate the particular needs of the experimenter. To facilitate the customization process, we have designed the code to allow editing of a single file in order to change the most important protocol elements: the type of task, duration, sequence of appearance, and pause in between tasks.

After the experimental design is implemented in code, tested, and debugged, the code needs to be compiled into an Android package file (*apk*) using the Android Studio IDE. Note that the code is written in the Kotlin programming language. To make it accessible to nonprofessionals, the file *Experiment.kt* in the project source is the only one that needs to be edited (see supplementary material). It contains definitions of all the curves used in tracing tasks, all target trajectories used in tracking tasks, the duration of each task and their ordering in the practice sequence and the experiment sequence.

The definitions of the curves are at the top of the file *Experiment.kt*. Curves for tracing tasks, such as ellipses or lemniscates, are defined as lists of x–y points. For future reference and comparison with participant trajectories, points for each curve are saved into a text file named after the curve (e.g. *Lemniscate.txt* contains a list of x–y points used to draw the shape on the screen). Target trajectories are defined as functions that return point coordinates at a particular time t measured from the task start. Currently implemented code enables design of target trajectories following pure frequency curves (specifying geometry) and velocities defined by a speed-curvature power law with an arbitrary exponent (specifying kinematics).

Next, each task or event needs to be defined with a name, type and duration. The name is arbitrary, the type is one of "trace", "track", "scribble" or "pause", and duration is the number of seconds after which the task will automatically end and proceed to the next task. Finally, ordering and duration of tasks are defined for the practice sequence and the experiment sequence.

In sum, in order to customize the app, one needs to download the project from Github (clone the repository), and open it in Android Studio to edit the file named *Experiment.kt*. As depicted in Fig. 3, this allows a handy composition of new "practice" and "experiment" tasks.

3.4. The app can be thoroughly customized by advanced programmers

We provide all the necessary source-code files as Supplementary Material. In particular, one needs to access the "KinematicCognition" folder. The files therein (and also inside the "idea" folder) are the build instructions for Android Studio and configurations for the project. They are mostly in Kotlin programming language. In the "gradle" folder one finds additional files for the building process. There is no need for the user to modify any of these files. The Android Studio actually generates and modifies them as one compiles the app. In the "app" folder one finds two main folders. In the "release" folder one can find the app ready to be installed as an *app-release.apk*. The "src/main" folder contains all the scripts needed to customize the app. In the "java/com/example/kinematiccognition" are the Kotlin (*.kt*) files corresponding to the so-called 'activities' (screens, routines for recording the trajectories, saving files, generating trajectories). For basic editing as described in the previous section, one does not need to worry about any of such files. But advanced programmers can of course make use of their editing. In the "res" folder there are many folders automatically managed by Android Studio. They comprise icons, layouts of the screens, connections between layouts, additional libraries, and dependencies. Let us also remind to select the appropriate API level for compilation in Android Studio so that it matches the particular tablet model to be used. Note that if the application is intended for a tablet with different screen resolution (ours was 1920×1200px), the shapes and trajectories should be adapted by adjusting their size in pixels in *Experiment.pk* file.

3.5. The app is optimized for temporal resolution of trajectory recording

In the Android operating system, the touch location and the timestamp are not usually provided in their raw form, as recorded by the touch-screen driver. To improve user experience during normal use, finger touch locations are by default recorded in batches of events, synchronized to display refresh events, and passed through an interpolation and estimation algorithm. These touch events are available to the programmer through methods *event.X*, *event.Y* for the location, and *event.getTime* for the timestamp. Maximal temporal resolution is equal to the screen refresh rate, which is 60 Hz (for the SM-T580 Samsung model we used). These methods are useful in general user interface programming, gesture recognition and similar uses. However, the interpolation and estimation algorithms may distort finger touch position and timestamp. Similarly, because the touch events will be synchronized to screen refresh events, the rate of touch events may be lower than recorded in its raw form.

To acquire more accurate and non-processed raw location and timestamp data at maximal possible temporal resolution, we access the recorded batches of events through the *event.historicalX*, *event.historicalY* and *event.historicalTime* methods. Trajectory recording methods are implemented in each of the task classes in the code. In target tracking tasks, trajectories are defined as functions of time. This method allows for correct positioning of the target, independent of the drawing frame rate or lags in the running of the app during the task. Synchronization of the target and finger trajectories in data analysis can be made using this target trajectory data. In free scribbling tasks, only the last one second of the trajectory is shown, as a disappearing trail. This minimizes the effect of drawing on the frame rate, keeping it near maximum 60 Hz.

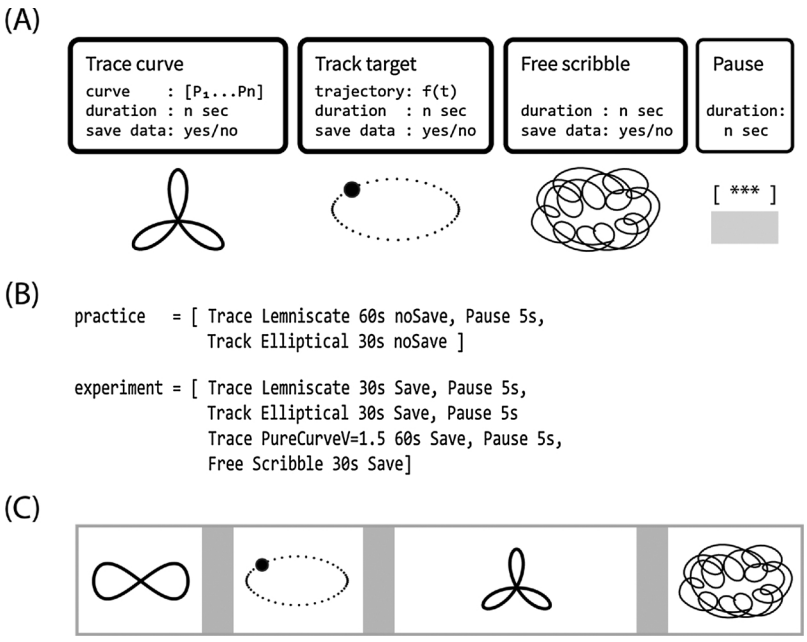

Fig. 3. Composing task elements to easily and flexibly create an experimental protocol in the app. The *Experiment.kt* file contains: (**A**) the definitions of curves and trajectories to specify the geometry and kinematics used as experimental tasks, as well as definitions of each task specifying duration and whether to save the data or not; and (**B**) definitions of practice and experimental sequence of tasks as one wishes to make them appear in the application. For instance, the "experiment" vector in (B) would generate the sequence of tasks depicted in (**C**).

3.6. Movement data and metadata file formats allow efficient management and analysis

Each tablet will contain the data of the experiments that were run on it, stored by default to the folder "/internal storage/download". The data is composed of text files containing participant trajectories, target trajectories, and default curve points. As we mentioned, they can be copied to the desktop computer over a USB cable, or sent to an email address from each tablet.

The filename of each recorded trajectory contains the metadata of the participant information collected in the data entry panel (year and month of birth, gender, and dominant hand), as well as the type of the task performed, and the time and date of the experiment. For example, file *February1986MaleRight scribble 10.4.2019. 16.10.57.txt* contains the movement data of a scribbling task performed at the noted date and time by a right-handed male born in February 1986. In this way, all the relevant information of each experiment is centralized in a single file.

Raw trajectory data is stored in text files, with each file containing three columns, a timestamp in milliseconds since the start of the task, and x and y coordinates in pixels. Note that the upper left corner is the coordinate (0, 0), x is increasing from left to right, and is y increasing from top to bottom. This may result in reversing the y coordinate if the data is plotted in the traditional Cartesian coordinate system.

Curve tracing and scribbling tasks save the participant movement coordinates only, while the tracking tasks save two files: one with participant data, with the filename prefixed "user", and one with target positions prefixed "target". Target participant data are saved in different files because of their different sampling rate. Target position is saved at the rate of screen refreshing, while the participant data at the rate of touch event recording. For the tablet Samsung T580 used in developing this application, the timestamp differences were are approximately 16.66 ms (60 Hz refresh rate) for screen refresh, and 11.8 ms (85 Hz sampling rate) for touch events. While the rate of data sampling for participant trajectories is reasonably constant at near 85 Hz, it is useful to spline/interpolate and re-sample the participant and target trajectory data, or participant data from different tasks to the same sampling frequency. For target tracking tasks, the target trajectory can be synchronized to participant finger trajectory by the timestamp variable, since the timestamps measure time in ms since the start of the task, for both movements.

3.7. The data collected with the app yields state-of-the-art scientific results

To evaluate the data collection potential of the app and to demonstrate the range and quality of possible types of analysis, we performed a pilot study consisting of several tracing, tracking and scribbling tasks. All data was filtered with a low-pass Butterworth filter with a cutoff frequency of 8 Hz. The analyses we performed are characteristic of the study of the speed-curvature power law, as well as of other quantitative aspects of movement research. The results, shown in Fig. 4, illustrate the usefulness of our method in hand movement research.

First, when tracing of a lemniscate figure (Fig. 4A), the trajectory shows a strong covariance between angular speed and curvature (Fig. 4B), which yields a power law with the exponent $\beta = 0.82$ and $r^2 = 0.977$ (Fig. 4C). This is consistent with the law and exponent found in the literature for a lemniscate (Viviani and McCollum, 1983). Other curves tested (data not shown) yielded power laws with the exponents reported in (Lacquaniti et al., 1983) and (Huh and Sejnowski, 2015).

Second, we analyzed the lead-and-follow dynamics when the finger tracks a moving target along an elliptical trajectory with hypo-natural kinematics (Fig. 4D). Hypo-natural movement trajectories are defined as those for which the angular speed and curvature power law has an exponent lower than 2/3 (in this case we imposed $\beta = 1/3$) so that the target slows down in high-curvature parts of the path much more than in the movements naturally performed by participants. The angular difference between the target and participant positions is measured from the center of the ellipse, at each point along the trajectory. Consistent with a similar analysis in the literature (Viviani and Mounoud, 1990), we find that the participant is not merely following the target, but getting closer and further away periodically, with more difficulty to track it at certain regions, and with certain trajectory segments even overtaking the target (Fig. 4E).

Third, a set of pure frequency curves (Huh, 2015) with parameters $\nu = 0.8$, $\nu = 1.5$ and $\nu = 2.0$ (respectively corresponding to four-lobe, three-lobe and ellipse curves) were shown on the tablet screen as static templates and the participant traced those figures in a fast and fluid manner. For participant traces of those curves, Fig. 4F shows the amplitude of the curvature spectrum, which is the Fourier transform of the logarithm of the curvature profile but parametrized in angle rather than in length or time (Huh and Sejnowski, 2015). Remarkably, the curvature profiles of the traced trajectories have single peaks at the precise

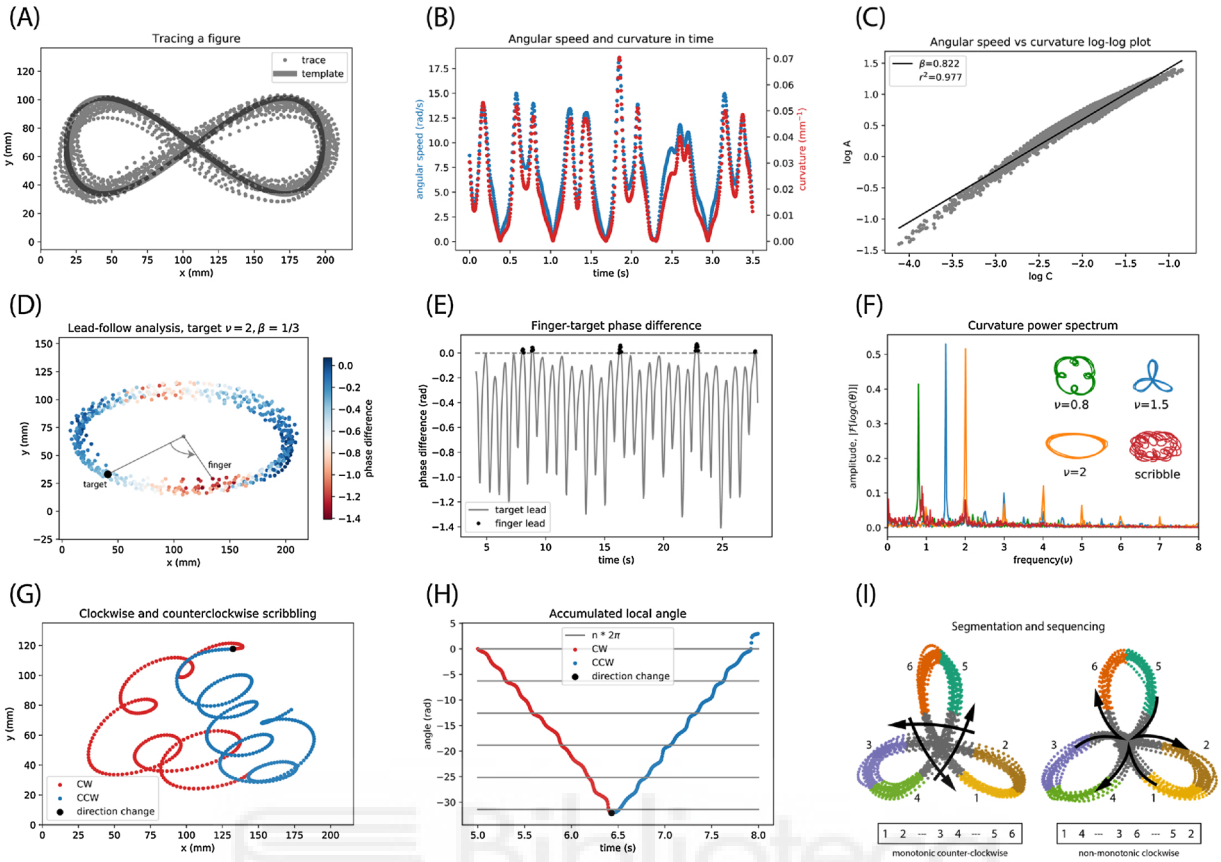

Fig. 4. Analyses of the data collected with the app produce state-of-the-art results: Five main situations are shown: power-law constraint during tracing (**A-C**); lead-follow dynamics during tracking (**D-E**); geometrical accuracy in pure-frequency curves (**F**); clockwise scribbling (**G-H**); and action segmentation degeneracy (**I**). **(A)** Tracing a lemniscate figure with the finger on the tablet. **(B)** Instantaneous angular speed and local curvature as a function of time for a short interval. Both appear tightly correlated. **(C)** The trajectory of the participant's finger complies with the speed-curvature power law ($r^2 = 0.977$), with an exponent $\beta = 0.82$. **(D)** Tracking a moving target along an ellipse. The color of the dots depicts the relative phase angle (measured from the center of the ellipse) between target and the finger, which is minimal in the most curved parts of the trajectory. **(E)** Lead-follow analysis reveals that the participant is behind the target most of the time, only leading in front of the target at some points that coincide with maximal curvature. **(F)** Amplitude of the power spectrum of the curvature profile in tracing pure frequency curves shows strongest peaks at the frequency of the template, while the scribble has a much broader distribution. **(G)** Direction analysis during free scribbling shows clockwise turning (in red) for the first part of the analyzed trajectory, followed by counter-clockwise turning (in blue) in the second part. **(H)** Accumulated angle over time reveals five full windings before changing direction. **(I)** Discrete segmentation of a continuous path produced while tracing a three-lobe flower-like shape can reveal different choice sequences in drawing of the same path across different trials or individuals. Apart from clock-wise or counter-clockwise directions, one can also choose to trace the pattern with monotonic changes in curvature, or sharply changing direction at the center.

pure frequencies of the template curves displayed. One also sees harmonics. In contrast, the log curvature profile of a free scribbling trajectory does not show sharp peaks (except some dominant contributions at $\nu = 2$ and also a bit below $\nu = 1$) as it is not a pure-frequency curve. Overall, this analysis illustrates how such spectra can be a powerful and principled measure of geometrical accuracy during tracing.

Fourth, in a segment of scribbling movements (Fig. 4G) we examined the direction of movement as the accumulated unwrapped local angle over time. We can clearly distinguish between clock-wise and counter-clockwise movements, and quantify the number of complete rotations (gray lines in Fig. 4H) during free scribbling.

Fifth, we can discretize a continuous trajectory by means of a segmentation analysis. As shown in Fig. 4I, there are actually different ways to draw the same simple figure. The three-lobe pattern helps illustrate such degeneracy. In the left one, the trajectory crosses the center without changing the direction of movement (thus, monotonically) and this is all done counter-clockwise. In the right one, each 'petal' is drawn separately (non-monotonic curvature changes) with the direction of movement changing in the middle of the figure, while this is done clockwise. In sum, the tracing of such a simple figure can betray handedness and decision-making differences across participants, and within participants in time.

3.8. Scripts for data analyses are available as a Jupyter notebook

The raw data and a python scripts to analyze it are also available as supplementary information. In particular, the "KinematicCognition-Analysis" folder contains the files *power_law_analysis.py* and *power_spectrum.py* which correspond, respectively, to the scripts that estimate speed and curvature to test the power-law constraint and it exponent, and the scripts that calculate the power spectrum of any trajectory. The file *Analysis_KinematicCognition.ipynb* is a Jupyter Notebook that facilitates the visualization and generation of the analyses corresponding to those shown in each plot of Fig. 4. In the "data-new" folder is the raw data of the pilot study corresponding to different curves traced, targets tracked and scribbling. Note that for local use, one must match the paths to local folders.

4. Discussion

Android tablets are widely available and affordable today. The reader may even have one or two at home. We have created an app and deployed it on a commercial tablet, demonstrating that it allows sufficiently high temporal and spatial resolution for state-of-the-art motor control laboratory research. We have provided a ready-to-use version of

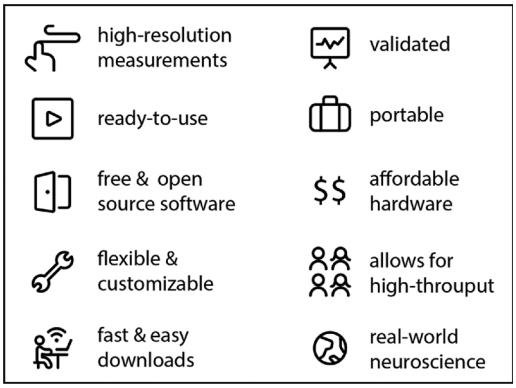

Fig. 5. Main advantages of the app for real-world behavioral neuroscience. Our app is ready to use, free, open source, and designed to be flexibly customizable for users who are not programming experts. The app and the data collected can easily be downloaded via USB or email. We include scripts not only for re-programming the app but also for data analyses. Our experimental protocol has been designed for simultaneous high-throughput data collection with several tablets, and validated to reproduce state-of-the-art laboratory results in the real world.

the app, with an experimental protocol design that is suited for high-throughput effective data collection outside the laboratory. We have also shared the source code and organized it so as to facilitate researchers to design their own experiments, and to be able to compile new app versions.

As summarized in Fig. 5, our app has plenty of advantages. Let us also remark now some of its limitations. First, it is worth stating that the spatial and temporal resolution of digitizing tables and similar devices a few decades ago was on the same level (or better) than today's Android tablets. For instance, in (Lacquaniti et al., 1983) a resolution of 100 Hz is reported for an electromagnetic digitizing table with 0.025 mm of accuracy, and in (Wann et al., 1988) a pressure sensitive pad achieved 200 Hz sampling rate, though with somewhat lower accuracy of 0.2 mm. Nevertheless, the sampling rate of movement recording for the tablet used in the present manuscript is fast enough to enable the quantitative analysis of kinematics and geometry of human movement while drawing. The price of the tablet we used here is easily an order of magnitude cheaper than typical recording devices used in the lab. Second, we did not program the app to be run on cell phones since this would considerably limit the spatial range and resolution of most of the motor control experiments one is interested in. Third, note as well that our app cannot be run on an Apple iPad. Yet, nothing prevents other users to use the code, design, and analyses employed here to extend it to other platforms or uses.

Our custom-made app running on a commercial tablet is a sweet spot between the precision of laboratory equipment and the usability of mobile devices. It is a fact that tinkering with the source code requires some considerable programming knowledge. Yet, our goal here has been to design the code to significantly simplify the task of creating a movement-recording app, specially in comparison with creating it from scratch. Additionally, we have solved some more involved technical issues regarding the access of maximal temporal resolution of touch events and maximal rate of screen refreshing during experiments. In sum, we expect our app (and modifications of it) not only to be usable but actually used.

Broadening the scope, we hope that the methods presented here will be of value to study motor control phenomena outside the laboratory. This may include educational programmes at schools, improving health in hospitals, scientifically studying artistic practices, and even recreational purposes at home. Let us emphasize the potential of our App and method in the study of Parkinson's disease. Being one of the most common chronic neurological diseases in advanced ages, tests for early-sign detection and quantification of progression are certainly established but at times too subjective or cumbersome to perform. It is not unfeasible that one could manifest some subtle motor signs of the disease while drawing simple shapes or writing one's name on the tablet. Given the accuracy of measurement of our app, one may even test it for early diagnosis and also to follow up on the improvements —or at least lack of progression— of the disease upon medical and complementary treatment (such as the one realized in Parkinson Associations, with whom we are starting to collaborate). If so, our app could become a low-cost, objective and simple-to-use evaluation tool.

Neuroscience has needed a considerable amount of time to realize the imperative to go "out of the head". Conceding a certain dose of behavioral "chauvinism" in the face of 21st century "neuralism" (Gomez-Marin, 2017), one must take seriously the idea that in order to understand how the brain works we must also ask what it is for (aka, behavior). At the end of the day, everyone willing to spend some time with our App scripts and with 200$ to spend on a tablet can now do high-resolution human behavioral science of laboratory-quality in the real world. The time is ripe to move "out of the lab".

Supplementary material

All codes (and data) used in this study are available. The app in release form (app-release.apk) and the source codes to edit it can be obtained from the authors directly in the following online repository: https://github.com/adam-matic/KinematicCognition. The raw behavioral data used in this study together with the scripts used to analyze it in Python within a Jupyter notebook can be found here: https://github.com/adam-matic/KinematicCognition-Analysis.

Contributions

Idea and conceptualization: AGM; experimental design: AM and AGM; app development: AM; experiments: AM; data analysis: AM; figures: AM and AGM; first manuscript draft: AM, final manuscript: AGM.

Funding

The authors declare no competing financial interests. The work was supported by the Spanish Ministry of Science (grant BFU-2015-74241-JIN to AGM; pre-doctoral contract BES-2016-077608 to AM) and by the Severo Ochoa Center of Excellence programs (SEV-2013-0317 start-up funds to AGM).

Acknowledgements

We thank María Regina Zaghi Lara, Roberto Morollón, and María del Carmen Lillo Navarro for valuable suggestions on the experimental protocol and for help in testing the app. We acknowledge Streamline for figure icons.

References

Accardo, A.P., Genna, M., Borean, M., 2013. Development, maturation and learning influence on handwriting kinematics. Hum. Mov. Sci. 32 (1), 136–146. https://doi.org/10.1016/j.humov.2012.10.004.

Anzulewicz, A., Sobota, K., Delafield-Butt, J.T., 2016. Toward the autism motor signature: gesture patterns during smart tablet gameplay identify children with autism. Sci. Rep. 6, 31107. https://doi.org/10.1038/srep31107.

Binet, A., Courtier, J., 1893. Sur la vitesse des mouvements graphiques ("On the speed of drawing movements"). Rev. Philos. France l'Etranger 35, 664–671. http://www.jstor.org/stable/41075629.

Bernstein, N., 1984. The Techniques of the Study of Movements. Human Motor Actions — Bernstein Reassessed. pp. 1–26. https://doi.org/10.1016/s0166-4115(08)61367-9.

Dounskaia, N., Ketcham, C.J., Stelmach, G.E., 2002. Commonalities and differences in control of various drawing movements. Exp. Brain Res. 146 (1), 11–25. https://doi.org/10.1007/s00221-002-1144-3.

Flash, T., Hogan, N., 1985. The coordination of arm movements: an experimentally confirmed mathematical model. J. Neurosci. 5 (7), 1688–1703. https://doi.org/10.1523/JNEUROSCI.05-07-01688.1985.

Gomez-Marin, A., Mainen, Z.F., 2016. Expanding perspectives on cognition in humans,

animals, and machines. Curr. Opin. Neurobiol. 37, 85–91. https://doi.org/10.1016/j.conb.2016.01.011.
Gomez-Marin, A., 2017. Causal Circuit Explanations of Behavior: Are Necessity and Sufficiency Necessary and Sufficient? Decoding Neural Circuit Structure and Function. Springer, pp. 283–306. https://link.springer.com/chapter/10.1007/978-3-319-57363-2_11.
Gurfinkel, V.S., Cordo, P.J., 1998. The scientific legacy of Nikolai Bernstein. Progress Motor Control 1, 1–19.
Hill, L.J., Culmer, P.R., Mon-Williams, M., 2014. Lags in measuring eye–hand coordination. J. Neurosci. Methods 232, 150–151. https://doi.org/10.1016/j.jneumeth.2014.05.016.
Huh, D., 2015. The Vector Space of Convex Curves: How to Mix Shapes. arXiv preprint. https://arxiv.org/abs/1506.07515.
Huh, D., Sejnowski, T.J., 2015. Spectrum of power laws for curved hand movements. Proc. Natl. Acad. Sci. 112 (29), E3950–E3958. https://doi.org/10.1073/pnas.1510208112.
Lacquaniti, F., Terzuolo, C., Viviani, P., 1983. The law relating the kinematic and figural aspects of drawing movements. Acta Psychol. 54 (1–3), 115–130. https://doi.org/10.1016/0001-6918(83)90027-6.
Lee, K., Junghans, B.M., Ryan, M., Khuu, S., Suttle, C.M., 2014. Development of a novel approach to the assessment of eye–hand coordination. J. Neurosci. Methods 228, 50–56. https://doi.org/10.1016/j.jneumeth.2014.02.012.
Krakauer, J.W., Ghazanfar, A.A., Gomez-Marin, A., MacIver, M.A., Poeppel, D., 2017. Neuroscience needs behavior: correcting a reductionist bias. Neuron 93 (3), 480–490. https://doi.org/10.1016/j.neuron.2016.12.041.
Sisti, J.A., Christophe, B., Seville, A.R., Garton, A.L., Gupta, V.P., Bandin, A.J., Yu, Q., Pullman, S.L., 2017. Computerized spiral analysis using the iPad. J. Neurosci. Methods 275, 50–54. https://doi.org/10.1016/j.jneumeth.2016.11.004.
Soechting, J.F., Lacquaniti, F., Terzuolo, C.A., 1986. Coordination of arm movements in three-dimensional space. Sensorimotor mapping during drawing movement. Neuroscience 17 (2), 295–311. https://doi.org/10.1016/0306-4522(86)90248-4.
Vianello, A., Chittaro, L., Burigat, S., Budai, R., 2017. MotorBrain: a mobile app for the assessment of users' motor performance in neurology. Comput. Methods Programs Biomed. 143, 35–47. https://doi.org/10.1016/j.cmpb.2017.02.012.
Viviani, P., McCollum, G., 1983. The relation between linear extent and velocity in drawing movements. Neuroscience 10 (1), 211–218. https://doi.org/10.1016/0306-4522(83)90094-5.
Viviani, P., Mounoud, P., 1990. Perceptuomotor compatibility in pursuit tracking of two-dimensional movements. J. Mot. Behav. 22 (3), 407–443. https://doi.org/10.1080/00222895.1990.10735521.
Wann, J., Nimmo-Smith, I., Wing, A.M., 1988. Relation between velocity and curvature in movement: equivalence and divergence between a power law and a minimum-jerk model. J. Exp. Psychol. Hum. Percept. Perform. 14 (4), 622. https://doi.org/10.1037/0096-1523.14.4.622.
Woodworth, R.S., 1899. Accuracy of voluntary movement. Psychol. Rev.: Monogr. Suppl. 3 (3), i–114. https://doi.org/10.1037/h0092992.
Zago, M., Matic, A., Flash, T., Gomez-Marin, A., Lacquaniti, F., 2018. The speed-curvature power law of movements: a reappraisal. Exp. Brain Res. 236 (1), 69–82. https://doi.org/10.1007/s00221-017-5108-z.

Annex 2:

Zago, M., Matic, A., Flash, T., Gomez-Marin, A., & Lacquaniti, F. (2017). The speed-curvature power law of movements: a reappraisal. Experimental brain research, 236(1), 69-82.
PMID: 29071361 DOI: 10.1007/s00221-017-5108-z

The speed-curvature power law of movements: a reappraisal

Myrka Zago[1] · Adam Matic[2] · Tamar Flash[3] · Alex Gomez-Marin[2] · Francesco Lacquaniti[1,4,5]

Abstract Several types of curvilinear movements obey approximately the so called 2/3 power law, according to which the angular speed varies proportionally to the 2/3 power of the curvature. The origin of the law is debated but it is generally thought to depend on physiological mechanisms. However, a recent paper (Marken and Shaffer, Exp Brain Res 88:685–690, 2017) claims that this power law is simply a statistical artifact, being a mathematical consequence of the way speed and curvature are calculated. Here we reject this hypothesis by showing that the speed-curvature power law of biological movements is non-trivial. First, we confirm that the power exponent varies with the shape of human drawing movements and with environmental factors. Second, we report experimental data from *Drosophila larvae* demonstrating that the power law does not depend on how curvature is calculated. Third, we prove that the law can be violated by means of several mathematical and physical examples. Finally, we discuss biological constraints that may underlie speed-curvature power laws discovered in empirical studies.

Keywords Motor control · Drawing · Two-thirds power law · Statistical analysis

Introduction

One of the best-studied characteristics of human voluntary movements is the empirical relationship between instantaneous speed and local path curvature. Speed—distance divided by time—is a spatio-temporal property of movement, while curvature is a purely spatial property, corresponding to the extent to which the trajectory bends relative to a straight line. Although a given trajectory can be traced with infinitely many different speed profiles, biological constraints restrict the degrees of freedom with the result that speed generally co-varies with curvature throughout a given continuous movement (Viviani and Terzuolo 1982). Specifically, in a planar drawing of elliptic shapes, the angular speed of the pen tip varies in close proportion to the 2/3 power of the curvature of the trace (so called 2/3 power law, Lacquaniti et al. 1983).

Since the original demonstration, the 2/3 power law has been largely confirmed for elliptic trajectories drawn in 2D space (Viviani and Schneider 1991; Viviani and Flash 1995; Richardson and Flash 2002; Flash and Handzel 2007; Huh and Sejnowski 2015; Catavitello et al. 2016) or 3D space (Soechting and Terzuolo 1986; Flanders et al. 2006; Maoz et al. 2009). Moreover, speed-curvature power relationships have been reported for many other types of movements, including isometric 3D force trajectories (Massey et al. 1992), walking trajectories (Vieilledent et al. 2001; Ivanenko et al. 2002; Hicheur et al. 2005), and smooth pursuit eye

Myrka Zago and Adam Matic contributed equally to the work.

✉ Francesco Lacquaniti
lacquaniti@med.uniroma2.it

[1] Laboratory of Neuromotor Physiology, IRCCS Santa Lucia Foundation, Via Ardeatina 306, 00179 Rome, Italy

[2] Behavior of Organisms Laboratory, Instituto de Neurociencias CSIC-UMH, Av Ramón y Cajal, Alicante, Spain

[3] Department of Applied Mathematics and Computer Science, Weizmann Institute of Science, Rehovot 76100, Israel

[4] Department of Systems Medicine, Medical School, University of Rome Tor Vergata, Via Montpellier 1, 00133 Rome, Italy

[5] Centre of Space Bio-medicine, University of Rome Tor Vergata, Via Montpellier 1, 00133 Rome, Italy

movements (de'Sperati and Viviani 1997). Deviations from the 2/3 value of the exponent occur at inflection points of the trajectory where the prescribed tangential speed would become infinite, but they also occur for some trajectories without inflection points, such as ellipses with low eccentricities or large sizes (Wann et al. 1988; Schaal and Sternad 2001), or other shapes (Massey et al. 1992; Schaal and Sternad 2001; Richardson and Flash 2002; Dounskaia 2007; Flash and Handzel 2007; Bennequin et al. 2009; Huh and Sejnowski 2015).

The power law has been studied mainly in humans, but it also applies to drawings made by monkeys (Schwartz 1994; Abeles et al. 2013) and to crawling movements of Drosophila larvae (Zago et al. 2016). Thus, the power law might be a recurrent law underlying several biological movements. It is generally thought to depend on physiological mechanisms, although its exact origin remains debated. In particular, it has been suggested that the law might be due to kinematic or dynamic constraints arising at some level of the neuro-musculo-skeletal chain (Schwartz 1994; Viviani and Flash 1995; Gribble and Ostry 1996; Harris and Wolpert 1998; Schaal and Sternad 2001; Dounskaia 2007; Flash and Handzel 2007; Bennequin et al. 2009; Polyakov et al. 2009; Huh and Sejnowski 2015; Zago et al. 2016).

Now, a paper recently published in this journal (Marken and Shaffer 2017, in the following abbreviated as M/S) claims that the 2/3 power law is just an artifact, being a mathematical consequence of the way the critical variables of speed and curvature are calculated. If true, the contention put forth by M/S would have a significant impact on the field of motor control, since the power law is often considered as one of the hallmarks of curvilinear movements (e.g., Wolpert et al. 2013).

Here we reassess the validity of the speed-curvature power law by considering previous work as well as new data. In particular, we show that (a) the power law is not a trivial relationship given by mathematics or physics, (b) it does not depend on the methods used to compute the critical variables, and (c) the exponent of the power law is not fixed to 2/3 but varies with the shape of movement and with environmental factors. Based on these points, we reject the hypothesis that the empirical power law is a mathematical or statistical artifact.

Basic notions on the geometry of curves

As remarked at the outset of this article, a priori any given path of movement can be traced with infinitely many speed profiles, since the path specifies the instantaneous movement direction but not the speed. Moreover, any path can be defined independently of the law of motion. Speed and path become jointly determined only when a specific kinematic law is provided.

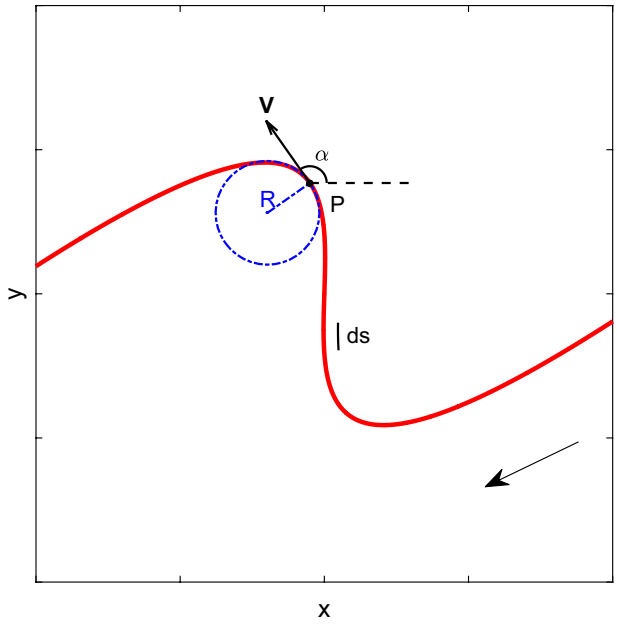

Fig. 1 Schematic illustration of kinematic and geometric variables for an arbitrary trajectory described by a moving point P (see text for details). $\mathbf{V}$ is the vector of tangential velocity, α the tangential angle, R the radius of curvature (radius of the osculating circle)

We first review the definitions of the critical variables from elementary differential geometry of planar, continuous, differentiable, regular curves (for 3D curves, see for example Struik 2012; Gielen et al. 2009; Pollick et al. 2009). The position of a point P moving along the curve (Fig. 1) can be described by the functions of time $x = f(t)$ and $y = g(t)$, as well as by the arc-length s along the curve measured from a starting point (x_0, y_0). Then, given unit vectors $\mathbf{i}$[1] and $\mathbf{j}$ along the x and y axis, respectively, the vector from the origin to P is $\mathbf{R} = \mathbf{i}x + \mathbf{j}y = \mathbf{i}f(t) + \mathbf{j}g(t) = \mathbf{R}(s)$, the tangential velocity vector is $\mathbf{V} = \frac{\mathrm{d}\mathbf{R}}{\mathrm{d}t} = \mathbf{i}\frac{\mathrm{d}x}{\mathrm{d}t} + \mathbf{j}\frac{\mathrm{d}y}{\mathrm{d}t}$, with magnitude (speed[2]) $V = |\mathbf{V}| = \left|\frac{\mathrm{d}\mathbf{R}}{\mathrm{d}t}\right| = \sqrt{\left(\frac{\mathrm{d}x}{\mathrm{d}t}\right)^2 + \left(\frac{\mathrm{d}y}{\mathrm{d}t}\right)^2} = \left|\frac{\mathrm{d}s}{\mathrm{d}t}\right|$. We can associate to P a moving frame (Frenet-Serret frame) composed of tangent and normal unit vectors, $\mathbf{T}$ and $\mathbf{N}$ respectively. $\mathbf{T} = \frac{\mathrm{d}\mathbf{R}}{\mathrm{d}s} = \mathbf{i}\frac{\mathrm{d}x}{\mathrm{d}s} + \mathbf{j}\frac{\mathrm{d}y}{\mathrm{d}s} = \frac{\mathbf{V}}{|\mathbf{V}|}$, $\mathbf{N} = \frac{\mathrm{d}\mathbf{T}/\mathrm{d}s}{|\mathrm{d}\mathbf{T}/\mathrm{d}s|}$. Thus, $\mathbf{V} = \mathbf{T}|\mathbf{V}|$ and $\mathbf{V} = \boldsymbol{\Omega} \times \mathbf{R}$ where $\boldsymbol{\Omega}$ is the vector of angular velocity. We can measure the direction of $\mathbf{T}$ by means of the tangential angle α, that is, the angle between the tangent line to the

[1] Bold characters denote vector quantities throughout.

[2] Although the terms velocity and speed are often used interchangeably in the literature (including M/S), the former denotes the vector with a magnitude and direction while the latter denotes the magnitude only.

curve at the given point and the x-axis. Angular speed (magnitude of angular velocity vector) corresponds to the absolute value of the rate of change of α with respect to time $A = |\mathbf{\Omega}| = \left|\frac{d\alpha}{dt}\right|$. Curvature C corresponds to the absolute value of the rate of change of α with respect to arc-length $C = \left|\frac{d\alpha}{ds}\right| = \left|\frac{d\mathbf{T}}{ds}\right| = \left|\frac{d^2\mathbf{R}}{ds^2}\right|$, and $C\mathbf{N} = \frac{d\mathbf{T}}{ds}$. Radius of curvature R is the inverse of C and corresponds to the radius of the osculating circle, i.e., the circle passing through the point P and two other points on the curve infinitesimally close to P.

From the above equations $V = \left|\frac{ds}{dt}\right|$, $A = \left|\frac{d\alpha}{dt}\right|$, $C = \left|\frac{d\alpha}{ds}\right|$, it can be seen that speed (whether tangential or angular) is independent of curvature (or radius of curvature) in the absence of constraints. In other words, the curvature profile uniquely specifies the shape of a movement, independently of the speed profile (Bennequin et al. 2009; Huh and Sejnowski 2015).

Empirical speed-curvature power laws for human drawing have different exponents

As is the case for all biological power laws (West 2017), also the speed-curvature power law is an approximation. Most previous studies investigating speed-curvature relationships in biological movements tested the hypothesis that angular speed A is approximately proportional to curvature C raised to an exponent β:

$$A \approx KC^{\beta} \tag{1}$$

where A and C are measured at each instant of time at the endpoint that traces the trajectory (the pen tip for hand-drawing). A different but mathematically equivalent formulation of speed-curvature relationships involves V instead of A, and R instead of C. Because $A = V/R$ and $R = 1/C$, Eq. 1 is equivalent to:

$$V \approx KC^{-(1-\beta)} = KR^{(1-\beta)} \tag{2}$$

The relationships of Eqs. 1–2 can also be expressed using logarithms, yielding respectively:

$$\log A \approx \log K + \beta \log C \tag{3}$$

$$\log V \approx \log K + (1-\beta) \log R \tag{4}$$

In the case of normal hand-drawing of ellipses, the exponent β is approximately equal to 2/3 and K is roughly constant throughout the drawing, being related to the overall tempo of the movement and increasing proportionally to the average speed (Lacquaniti et al. 1983). For more complex trajectories such as the scribbles, K is piecewise constant (Lacquaniti et al. 1983, 1984; Viviani and Cenzato 1985; Richardson and Flash 2002).

In general, however, the power exponent β is not invariant. Dynamic factors may affect its value (Wann et al. 1988; Gribble and Ostry 1996), as shown by a recent study comparing elliptic drawing movements performed in air and water at the same average speed (Catavitello et al. 2016). The speed-curvature law held in both conditions, but the exponent was close to 2/3 in air and 3/4 in water, indicating that the speed-curvature coupling is affected by the viscosity of the medium where the movement unfolds.

A major factor affecting the specific value of the exponent β is determined by the shape of the drawn trajectory. Thus, deviations from the 2/3 value of the exponent were noticed for specific curves such as the asymmetrical lemniscate (Viviani and Flash 1995; Richardson and Flash 2002; Flash and Handzel 2007). Several models based on the optimization of different kinematic costs (Richardson and Flash 2002, Huh and Sejnowski 2015) or on assuming non-Euclidean geometrical representations of movements (Flash and Handzel 2007; Bennequin et al. 2009; Polyakov et al. 2009) were developed to account for such deviations. A thorough investigation of the shape dependency of the exponent has recently been carried out by Huh and Sejnowski (2015). They considered a wide set of planar convex curves that differ in terms of the spatial angular frequency (Huh 2015). Angular frequency ν of a curve is the number of curvature oscillations per cycle. For instance, ν is equal to 2 for an ellipse, because the curvature profile fluctuates twice per cycle. At integer frequencies $\nu > 2$, the curves resemble rounded regular polygons. In general, a convex curve with a rational frequency $\nu = m/n$, where m and n are coprime integers (i.e., no common factors) and $m \neq 1$, has a closed shape of period $2\pi n$, and exhibits m degrees of rotational symmetry. For such pure frequency curves, Huh and Sejnowski (2015) described a spectrum of power laws with exponents covering a wide range. The exponent of the angular speed-curvature power law ranged from about 0.34 for a curve with $\nu = 2/33$ up to about 0.90 for a curve with $\nu = 6$, and including an exponent of 0.65 for the ellipse ($\nu = 2$), close to the value reported in previous studies for the latter curve.

The finding that drawing different shapes results in very different values of the power exponent is important because it reveals potential physiological mechanisms underlying movement generation (see section Biological constraints on speed-curvature relationships). Given the relevance of this issue for the present discussion, here we replicated part of the protocol by Huh and Sejnowski (2015) to verify the strong shape-dependency of the power exponent.

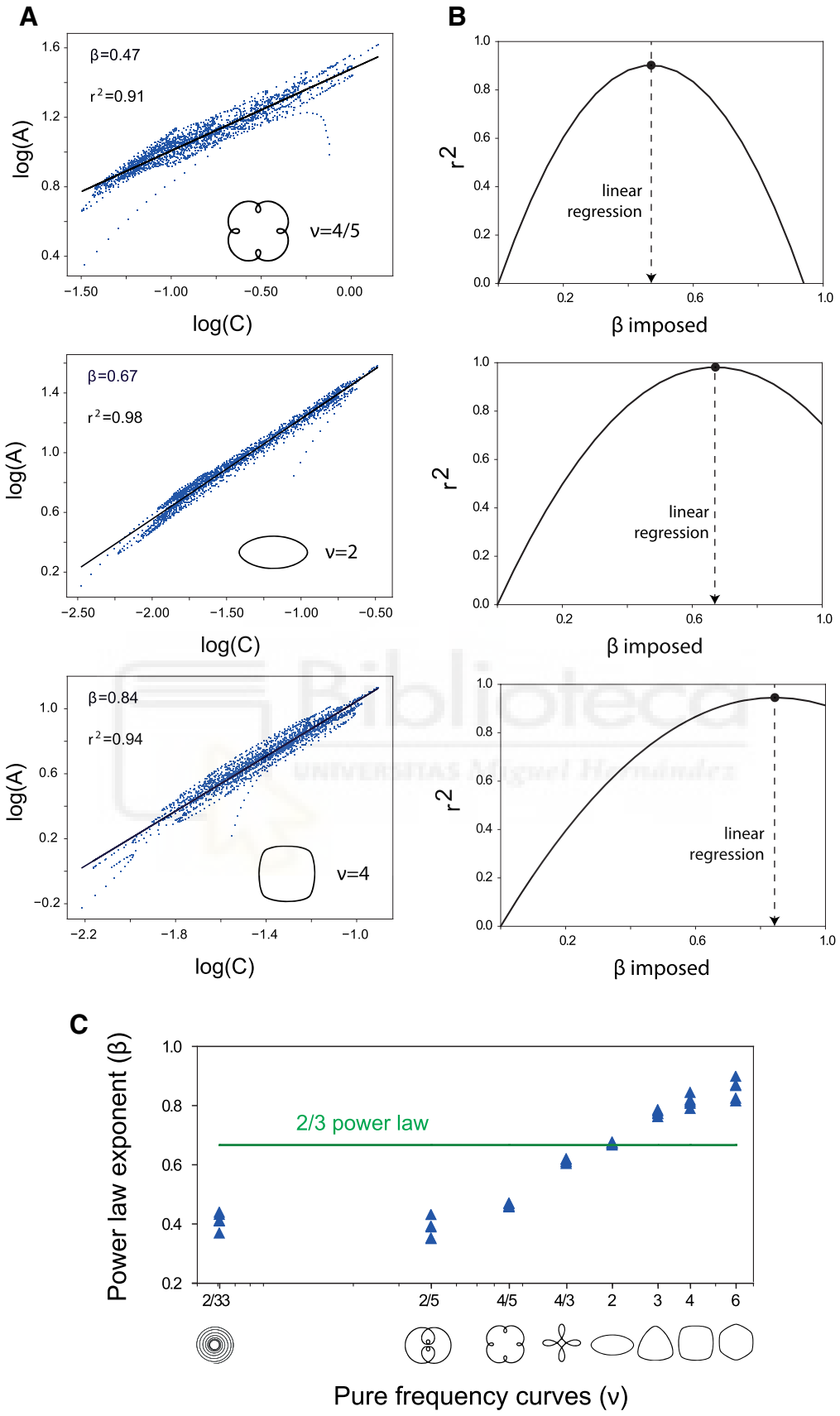
A
B
β=0.47
r²=0.91
log(A)
log(C)
ν=4/5
r2
linear
regression
β imposed
β=0.67
r²=0.98
ν=2
β=0.84
r²=0.94
ν=4
C
Power law exponent (β)
2/3 power law
2/33
2/5
4/5
4/3
2
3
4
6
Pure frequency curves (ν)

◂**Fig. 2** Dependence of the power exponent on the shape of human drawings. **a** Power laws for movement trajectories characterized by angular frequency (ν) equal to 4/5 (four-leaf), 2 (ellipse) and 4 (rounded square), from top to bottom. Scatter plots of instantaneous angular speed and curvature on log–log scale. The data were best-fitted (black line), with β-exponent and variance accounted for (r^2) as indicated in the insets. **b** Plots of r^2 resulting from imposing β-exponents in the range 0–1 in the power function for the corresponding drawings of panel (A). The best-fitting β-exponent is indicated by the vertical dashed line. **c** Best-fitting exponents (blue triangles) as a function of angular frequency (ν) of all eight drawn shapes

Methods and results

We used the same eight curves included in Fig. 5 of Huh and Sejnowski (2015). The angular frequency ν of these curves was 2/33, 2/5, 4/5, 4/3, 2, 3, 4, and 6. These curves (typical size 10 cm) were presented on a sheet of paper that was placed on top of a digitizing tablet (Wacom Intuos ProS PTH-451, spatial resolution: 0.08 mm, sampling rate: 200 samples/s). Three participants traced the curves continuously over 30 s with the tablet stylus (leaving no trace behind). They had previously given written informed consent to procedures approved by the Institutional Review Board, and had been instructed to draw with fast and fluid movements without corrections. The tempo of the movements (average speed) was indicated by a metronome with a period of 0.6 s. The x, y position-samples of the stylus tip were low-pass filtered (5 Hz cut-off, second-order, zero-phase-lag Butterworth filter), and interpolated using cubic splines to obtain the first and second time derivatives. Linear regressions of log A versus log C (Eq. 3) was used to estimate the exponent (β) of a power law $A = KC^{\beta}$. Here and throughout the article, log denotes base 10 logarithm ($\log_{10}$).

Figure 2a shows the results for three different curves. Data were well fitted by a power law, but the power exponent β systematically increased with the angular frequency of the curve, in agreement with Huh and Sejnowski (2015). Only for the ellipse did the exponent comply with the 2/3 power law, while for the other two curves the exponents deviated substantially from 2/3. Notice that the fit of the power relationships was quite sensitive to the specific value of β, as shown by forcing other β values (Fig. 2b).

Figure 2c shows the best-fitting exponents for all eight drawn shapes plotted as a function of the respective angular frequency (ν). Again in agreement with Huh and Sejnowski (2015), the overall β versus ν relationship was S-shaped. The variance accounted for (r^2) by the log–log linear regressions in each trial of each curve was greater than 0.83 ($\nu = 6$), 0.86 ($\nu = 4$), 0.93 ($\nu = 3$), 0.97 ($\nu = 2$), 0.94 ($\nu = 4/3$), 0.87 ($\nu = 4/5$), 0.72 ($\nu = 2/5$) and 0.55 ($\nu = 2/33$). Participants had some difficulty to trace accurately the curves with very high or very low angular frequencies, and the log–log regressions fitted the data less well than those at intermediate frequencies, as also reported in Huh and Sejnowski (2015).

In sum, the present results confirm the strong shape dependency of the exponent of the speed-curvature power law, consistent with Bennequin et al. (2009) and Huh and Sejnowski (2015).

Empirical power laws do not depend on how curvature is computed

Although speed and curvature are mathematically independent (see above), in practice some spurious correlation between the two measured variables might result from the time discretization due to a finite sampling rate and from using temporal derivatives in the calculation of both speed and curvature. In other words, the time-sampled spatial coordinates used to estimate local curvature might reflect to some extent also the speed of movement. This can be seen by re-parametrizing curvature first with respect to x, y coordinates and then with respect to time. Thus, from $C = \left|\frac{d\alpha/dx}{ds/dx}\right| = \frac{|d^2y/dx^2|}{[1+dy/dx^2]^{3/2}} = \left|\frac{d\alpha/dt}{ds/dt}\right|$, $x = f(t)$ and $y = g(t)$, $\alpha = \tan^{-1}\left(\frac{dy/dt}{dx/dt}\right)$, we can derive $C = \frac{\left|\frac{dx}{dt}\frac{d^2y}{dt^2} - \frac{dy}{dt}\frac{d^2x}{dt^2}\right|}{\left[\frac{dx}{dt}^2 + \frac{dy}{dt}^2\right]^{3/2}}$ or using the dot notation for time derivatives.

$$C = \frac{|\dot{x}\ddot{y} - \ddot{x}\dot{y}|}{(\dot{x}^2 + \dot{y}^2)^{3/2}} \tag{5}$$

In this section, we compare empirical speed-curvature relationships for crawling larvae using different sampling rates and different methods to calculate path curvature. To this end, we re-analyzed data presented in Zago et al. (2016).

Methods and results

For details on the experimental procedures and tracking of larvae behavior, see Gomez-Marin et al. (2011, 2012) and Zago et al. (2016). All procedures were in accordance with the ethical standards of the institution at which the experimental recordings were performed. Briefly, *Drosophila melanogaster* larvae in the foraging stage crawled on a viscous medium and were tracked at 7 frames/s, 90 µm/pixel. These sampling parameters have been shown to be fully adequate for the slow, small movements of these animals (Gomez-Marin et al. 2011, 2012). Three groups of larvae were exposed to different sensory environments, resulting in three different types of crawling trajectories, overshoot ($n = 42$ larvae), approach ($n = 40$), and dispersal ($n = 41$). The x, y position-samples of the larvae centroid were low-pass filtered (0.07 Hz cut-off, second-order, zero-phase-lag Butterworth filter), and interpolated with cubic splines.

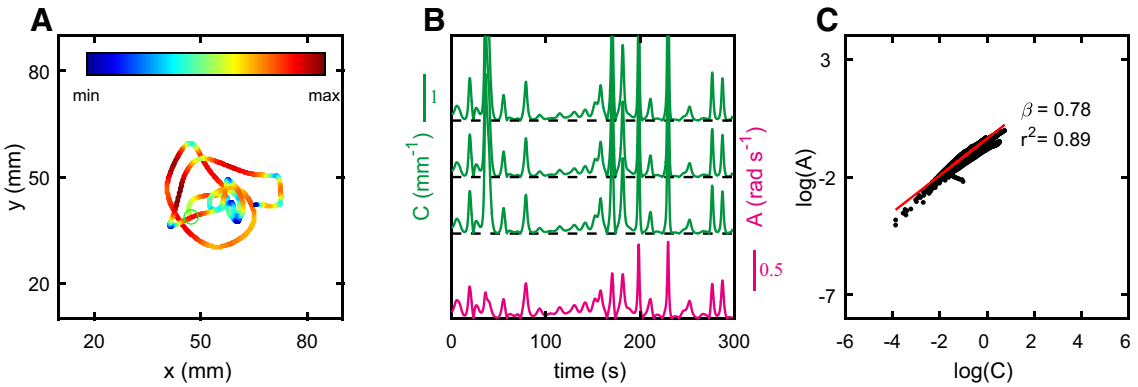

Fig. 3 Empirical relation between angular speed and curvature in a crawling larva. **a** Trajectory of the larva centroid. Green circle indicates starting position. Each point of the trajectory is colored according to the instantaneous tangential speed. **b** Time course of the angular speed (A, red) and curvature (C, green) for the trajectory plotted in panel A. The three traces of curvature are plotted with an offset between each other and correspond to curvature computed as in Eq. 5 (top), as the spatial derivative of the angle coordinate (middle), and as the inverse of the radius of the osculating circle (bottom). The dashed horizontal lines correspond to $C = 0$ in all three cases. **c** Scatter-plot of instantaneous angular speed A and curvature C on log–log scale. The data were best-fitted (red line) with β-exponent and variance accounted for (r^2) as indicated in the inset. These data refer to curvature computed according to method 1) above. In this example, β and r^2 values differed by $< 10^{-4}$ between the three methods

Curvature was then computed using three different methods: (1) as $C = \frac{|\dot{x}\ddot{y}-\ddot{x}\dot{y}|}{(\dot{x}^2+\dot{y}^2)^{3/2}}$ with the time parametrization (Eq. 5), (2) as the spatial derivative of the angle coordinate $C = \left|\frac{d\alpha}{ds}\right|$, (3) as the inverse of the radius of the osculating circle. Before computing $d\alpha/ds$ (method 2), we oversampled the original data by a factor 1000 (corresponding to a rate of 7000 samples/s) in order to dilute any time dependence of the spatial coordinates. To compute the osculating circle (method 3), we oversampled the data by a factor of 10, and then we best fitted a circle to any 3 consecutive x, y samples. Next, we performed least-squares orthogonal-regression of log angular speed A versus log curvature C (Eq. 3), the latter being computed with one of the three methods described above.

Figure 3a shows a typical trajectory traced by a crawling larva in the overshoot condition. These trajectories were not associated with a constant progression speed or any simple kinematic pattern. Both the instantaneous angular speed and the local path curvature were widely modulated, yet they co-varied throughout (Fig. 3b). Notice that the time profiles of curvature derived with the three methods described above are essentially identical (for clarity, they are plotted with an offset in Fig. 3b). A log–log plot of angular speed versus curvature revealed a power law as a straight line whose slope corresponds to the power-exponent β (Fig. 3c). We found no statistically significant difference in the linear regression parameters (slope β and r^2) between the results obtained with the three methods used to compute curvature (Kruskal–Wallis ANOVA by ranks followed by multiple comparisons, $P > 0.95$ in all three groups of larvae). The median value of β was 0.78 (interquartile-range = 0.06), 0.78 (interquartile-range = 0.08), and 0.76 (interquartile-range = 0.06) for the overshoot, approach, and dispersal conditions, respectively. The maximum difference between the slope β computed with one of the three methods and the slope computed with the other two methods was $< 0.1\%$ of the maximum value. Median value of r^2 was > 0.91 for all three methods.

These results show that the empirical speed-curvature relationships of the crawling larvae are very little affected by the specific method used to estimate path curvature, indicating that the numerical calculations typically used are unlikely to introduce any significant cross-talk between curvature estimates and speed estimates, irrespective of the specific parametrization.

A power exponent close to 3/4 in crawling larvae is reminiscent of the value found for human drawing movements in water (Catavitello et al. 2016), and thus it might depend on the viscosity of the medium (Zago et al. 2016). Alternatively, it could be attributed to the complex shape of the trajectories traced by the larvae. Irrespective of the origin, the deviation of the exponent from 2/3 reinforces the notion that the power exponent is not constant in biological movements.

Zago et al. (2016) also checked for the potential contamination of speed-curvature relationships by noise in the data (Maoz et al. 2006). Their Fig. S1 shows that the values of β and r^2 of the log–log regression of speed versus curvature depend little on the specific value of the low-pass frequency cut-off used to filter the position data of the crawling larvae.

A different way to look at speed-curvature relationships

Since $V = (\dot{x}^2 + \dot{y}^2)^{1/2} = A/C$ and $C = \frac{|\dot{x}\ddot{y} - \ddot{x}\dot{y}|}{(\dot{x}^2+\dot{y}^2)^{3/2}} = \frac{|\dot{x}\ddot{y} - \ddot{x}\dot{y}|}{V^3}$, by substitution we obtain $A = |\dot{x}\ddot{y} - \ddot{x}\dot{y}|^{1/3} C^{2/3}$. For brevity, we denote the term $|\dot{x}\ddot{y} - \ddot{x}\dot{y}|$ as D (same notation as in M/S):

$$A = D^{1/3} C^{2/3} \tag{6}$$

or equivalently $V = D^{1/3} C^{-1/3}$. In logarithmic units, $\log A = \frac{1}{3}\log D + \frac{2}{3}\log C$ or $\log V = \frac{1}{3}\log D - \frac{1}{3}\log C$. Notice that, in Eq. 6, D depends simultaneously on both speed and curvature. In fact, using the formulas by de L'Hôpital and Faà di Bruno, we can rewrite:

$$\dot{x}\ddot{y} - \ddot{x}\dot{y} = \frac{dx}{ds}\frac{ds}{dt}\frac{d^2y}{dt^2} - \frac{dy}{ds}\frac{ds}{dt}\frac{d^2x}{dt^2} = \left(\frac{ds}{dt}\right)^3 \left(\frac{dx}{ds}\frac{d^2y}{ds^2} - \frac{dy}{ds}\frac{d^2x}{ds^2}\right) \tag{7}$$

Equation 7 makes explicit the simultaneous dependence of D on speed and curvature, since the term $\left(\frac{ds}{dt}\right)^3$ is the third power of the tangential speed, while the term $\left(\frac{dx}{ds}\frac{d^2y}{ds^2} - \frac{dy}{ds}\frac{d^2x}{ds^2}\right)$ is the curvature.

Therefore, Eq. 6 represents a simple mathematical identity and does not imply that A depends on two independent variables, D and C, because in the absence of constraints A and V remain mathematically independent of C and R. Moreover, D cannot be considered an independent predictor of V (or A) because D itself depends on V (or A).

For an arbitrary motion, in Eq. 6, A, D and C are all time-varying functions along the traced curve. However, in the special case in which D does not vary with time throughout the movement, that is, when $D^{1/3} = K =$ constant, Eq. 6 satisfies Eq. 1 with a power exponent of β exactly equal to 2/3. In other words, the special condition of $D^{1/3} = K$ yields the 2/3 power law for the speed-curvature consistently found for elliptic drawings (see above). In the following, we will consider conditions that either satisfy or violate $D^{1/3} =$ constant. First, we describe mathematical and physical examples, and then we consider biological constraints that result in a nearly constant value of $D^{1/3}$.

The power law is not obligatory mathematically

Before we have used formal arguments to show that a given path of movement can be traced with different speed profiles, since the path specifies the instantaneous movement direction but not the speed. In this section we provide analytical and numerical calculations to demonstrate the same fact. To this end, we use the prototypical case of an elliptic path that, when drawn by humans or monkeys, typically complies with the 2/3 power law. In our simulations, the geometry of the curve is constant, while the kinematics is specified by means of the usual parametric representation in sine and cosine functions of the angle θ_t. However, we define different time profiles for θ_t, with the result of obtaining for the same geometry different kinematics, and therefore different relationships between angular speed and curvature.

Methods and results

Figure 4 shows the results of three different simulations of elliptic motion. We present both the analytical solutions and the results of numerical calculations (Fig. 4d). For the latter, the time-discrete trajectories were interpolated (cubic splines) to obtain first and second time derivatives, which were then used to calculate curvature C and angular speed A.

In all three simulations, the kinematics is defined by the equations:

$$x = a\sin\left(2\pi\theta_t\right), y = b\cos\left(2\pi\theta_t\right) \tag{8}$$

Only in the first simulation (top panel, Fig. 4b) does the angle θ_t have a simple, linear dependence on time ($\theta_t = t$). In the other two cases, θ_t has a more complex, non-linear time-dependence (middle and bottom, Fig. 4b). In particular, the target slows down as curvature increases (toward the vertices), progressively accelerates, and slows down as curvature decreases, in the first, second and third simulation, respectively. As a result, the angular speed A and curvature C co-vary throughout the movement in the first case (top, Fig. 4c), whereas the relationship between A and C changes over one cycle for the other two cases (middle and bottom, Fig. 4c). Accordingly, log$A$ is linearly related to log$C$ with an exponent β equal to 2/3 in the first case (top, Fig. 4d), whereas the relationship log$A$ versus log$C$ is complex and the 2/3 power law is violated in the other two cases (middle and bottom, Fig. 4d).

To see why this happens, we remind that the critical condition to satisfy exactly the 2/3 power law is given by $D = |\dot{x}\ddot{y} - \ddot{x}\dot{y}| =$ constant. By taking the time derivatives of Eq. 8 and performing straightforward calculations, we find that $D = ab\left(2\pi\left|\dot{\theta}\right|\right)^3$. Now, for the first case we considered ($\theta_t = t$), we find that $D = ab(2\pi)^3 =$ constant, and $A = KC^{2/3}$ is satisfied exactly. In fact, the notion that orthogonal harmonic oscillations (such as those of Eq. 8 with $\theta_t = t$) generate motions that comply with the 2/3 power law has long been established (Lacquaniti et al. 1983). Notice further that, if we scale up the motion speed by a constant ($\theta_t = ct$), then D scales up with c^3 and the 2/3 power law still holds but the A–C curve is shifted upwards, consistent with the published results of the effects of changes in average speed of human hand-drawing (Lacquaniti et al. 1983). In contrast with the previous cases, in the elliptic trajectories in which θ_t has a non-linear time-dependence (as in the second and

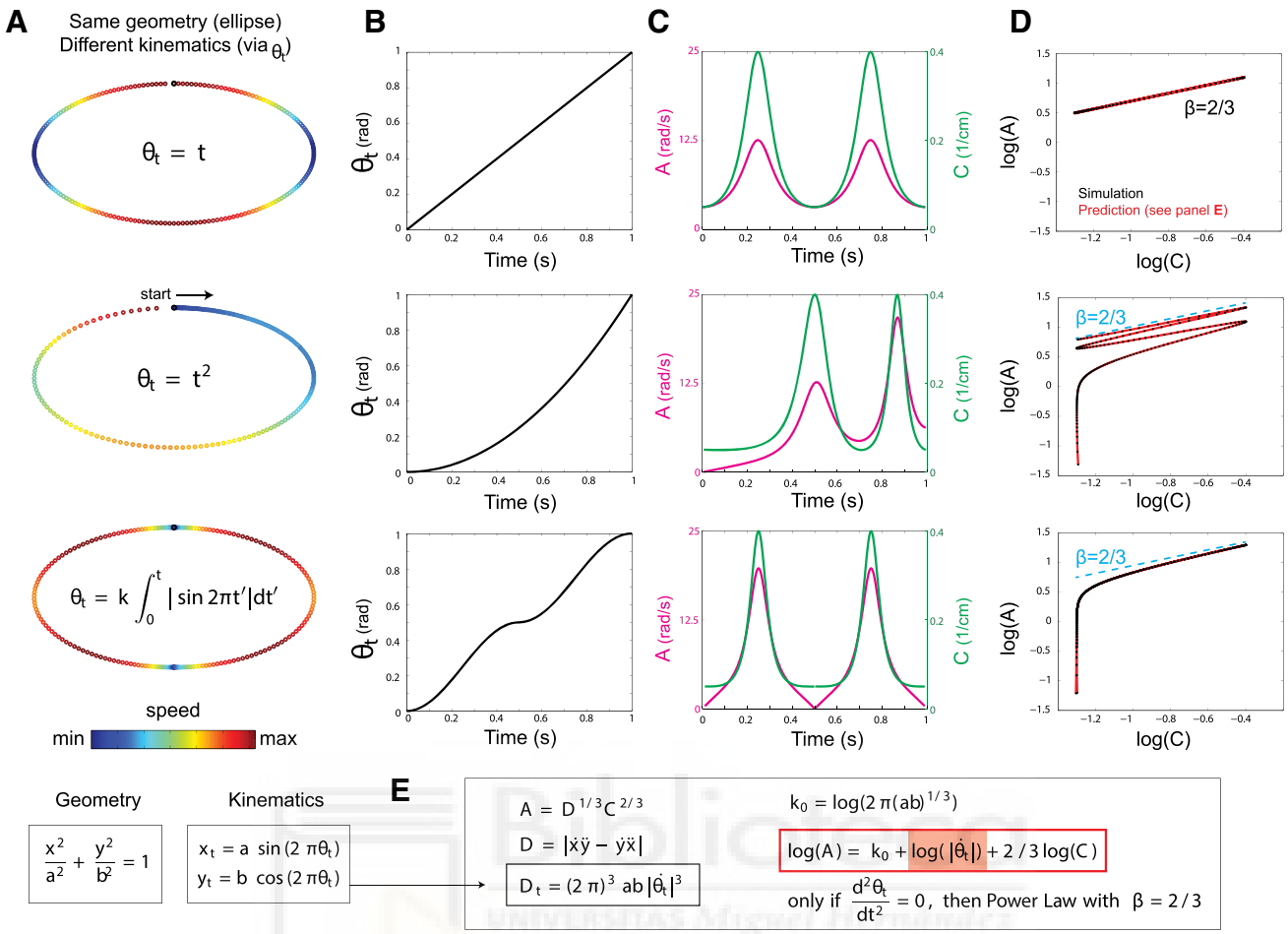

Fig. 4 Mathematical models and numerical simulations of one ellipse traced with three different kinematics (top, middle, bottom row). **a** Each point of the ellipses is colored according to the instantaneous tangential speed. The defining equations for the angles θ_t are in the insets. The moving point slows down with increasing curvature, progressively accelerates over one cycle, and slows down with decreasing curvature in the top, middle and bottom panels, respectively. The bottom inset reports the general parametric equations for the geometry and kinematics of the ellipses, with $a = 10$, $b = 5$ cm. **b** Time course of θ_t for the three kinematic cases depicted in (A) over one cycle. **c** The corresponding time profiles of angular speed A (magenta) and curvature C (green). **d** Log–log plots of A and C, for both the analytical (red) and the numerical (black) solutions. For comparison, blue dashed lines with 2/3 slope are shown in the middle and bottom panels. **e** Summary of the main mathematical expressions for the speed-curvature relation of ellipses traced with different kinematics

third simulations of Fig. 4), D is not constant any more but changes drastically (with the 3rd power of the rate of change of the angle θ_t). Therefore, in all such cases, the 2/3 power law is mathematically violated.

The power law is not obligatory in physical systems

In this section, we address another theoretical issue about the nature of the speed-curvature power-law: Does any object obey necessarily the law irrespective of the underlying forces because of the way the law is derived? If this were the case, we should be able to derive the law also for the motion of any arbitrary, inanimate body subjected to non-biological forces. In the following, we provide examples of the motion of objects affected by gravitational, drag or elastic forces, and we show that most of them violate the speed-curvature power law, while one example complies with the law.

Methods and results

Figures 5a–d show the results of simulations of a few different systems whose kinematics is dictated by the dynamic equations provided in Fig. 5e. In all cases, the dynamic equations of motion were numerically integrated by means of time-step Euler integration. The time-discrete, unfiltered trajectories were interpolated (cubic splines) to obtain first and

second time derivatives, which were then used to calculate curvature and angular speed.

The first physical system we consider is given by an ideal binary star consisting of two bodies of equal mass, under Newton's law of universal gravitation (Fig. 5a). The gravitational pull between the two bodies causes them to move in elliptic orbits around their common center of mass. Unsurprisingly, we find that the instantaneous angular speed of each body can be either very large or very small for the same values of local curvature. The log–log plot of angular speed and curvature shows that the power law is clearly violated. Once more, the result can be predicted by considering that $D = |\dot{x}\ddot{y} - \ddot{x}\dot{y}|$ is not constant for this system (Fig. 5e). Similar results are obtained (data not shown) when we consider the case where one body is massive, such as the Sun, and the other one is much less massive, such as a planet orbiting around the Sun. We then rediscover Kepler's observation that in perihelion (the point closest to the Sun) the planet is moving faster than in aphelion (the point farthest from the Sun). Since these two points have the same curvature, it is clear that speed and curvature do not co-vary, violating the power-law.

The second physical system consists of a projectile launched in ballistic trajectory under the action of gravity (Fig. 5b). We consider two cases, namely that the projectile motion is affected (thin line) or unaffected (thick line) by a drag force proportional to speed. Without drag, angular speed and curvature co-vary, and the 2/3 power law is obeyed. With drag, instead, the law is violated. In fact, by considering the corresponding dynamic equations (Fig. 5e), we see that D is constant without drag, but is non-constant with linear drag. Notice that D is non-constant also with quadratic drag (valid at high speeds): $D = \left|-g\dot{x} - k(\dot{x}\dot{y}^2 - \dot{y}\dot{x}^2)\right|$.

The third physical system is a simple pendulum under gravity, without drag (Fig. 5c). This system provides a dramatic violation of the speed-curvature power-law (La Scaleia et al. 2014). The oscillations of the pendulum trace a circle and thus curvature is constant throughout, while angular speed changes throughout, being zero at the extremes of the swing and maximal in the middle point. Accordingly, the log–log plot of angular speed vs. curvature yields a line parallel to the ordinates axis.

Finally, we consider a system consisting of a mass connected to two orthogonal linear springs, whose elastic force is proportional to the distance from equilibrium length (Fig. 5d). Depending on the initial conditions and parameter values, speed and curvature can approximate a power law, but in general the power law is not obeyed exactly.

Different biological constraints may give rise to the speed-curvature power law

We have previously argued that the power law is not a trivial relationship given by mathematics or physics. Here we consider a number of potential physiological constraints that may underlie non-trivial speed-curvature power laws found in empirical studies of biological movements. One approach consists in investigating specific kinematic conditions under which D in Eq. 6 is constant or nearly constant, thus yielding speed-curvature relationships closely obeying the 2/3 power law. As we mentioned above, Lacquaniti et al. (1983) showed that orthogonal harmonic oscillations at the same frequency generate 2D elliptic drawings that always comply with the 2/3 power and, for such condition, D in Eq. 6 is exactly constant.[3] Even in the case of harmonic oscillations that are not orthogonal, such as those generated by coupled angular motions at the limb joints, D can vary little with time. Thus, Soechting and Terzuolo (1986) and Schaal and Sternad (2001) showed that, for periodic drawings of ellipses in 3D, the condition $D \approx$ constant is satisfied by sinusoidal motion of the limb segments with appropriate inter-segmental phase shifts. Dounskaia (2007) elaborated further on the implications of sinusoidal angular motions using a simplified model of planar 2D drawing movements. She showed that the condition $D^{1/3} \approx$ constant holds when the shoulder and elbow perform sinusoidal angular motions of moderate amplitudes with a substantial phase offset, whereas the condition is violated ($D^{1/3}$ widely time-varying) when the angular motions are very large or very small (consistent with previous experimental observations by Wann et al. 1988 and Schaal and Sternad 2001).

However, only some biological movements are subserved by simple sinusoidal motions. For instance, the small hand drawing movements of the convex curves that we described earlier (see Empirical speed-curvature power laws for human drawing have different exponents) involve important contributions by wrist and fingers (in addition to shoulder and elbow), which exhibit considerable harmonic distortion and whose phase is quite variable (Lacquaniti et al. 1987). Since the different convex curves of Fig. 2 (as well as those of Huh and Sejnowski 2015) were all of about the same size and were performed at about the same average speed, the different values of the exponent β as a function of curve shape cannot be explained on the basis of the average speed and amplitude of oscillation at the shoulder and elbow joints (Dounskaia 2007).

[3] Notice, however, that orthogonal harmonic oscillations at a different frequency generate Lissajous motions that do not comply necessarily with the 2/3 power law (Lebedev et al. 2001).

A GRAVITATION

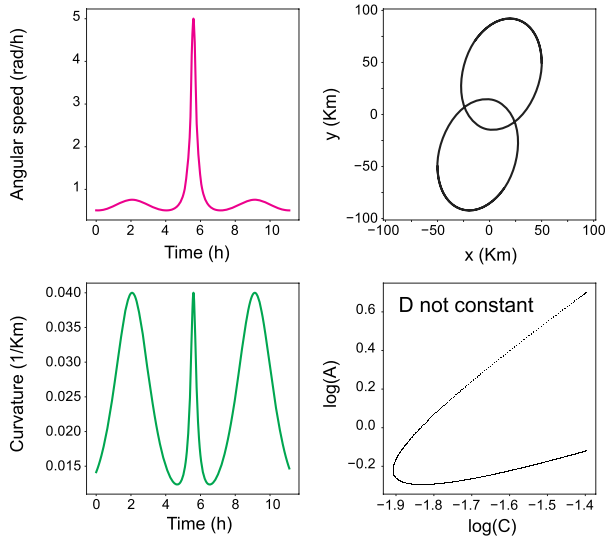

B PROJECTILE

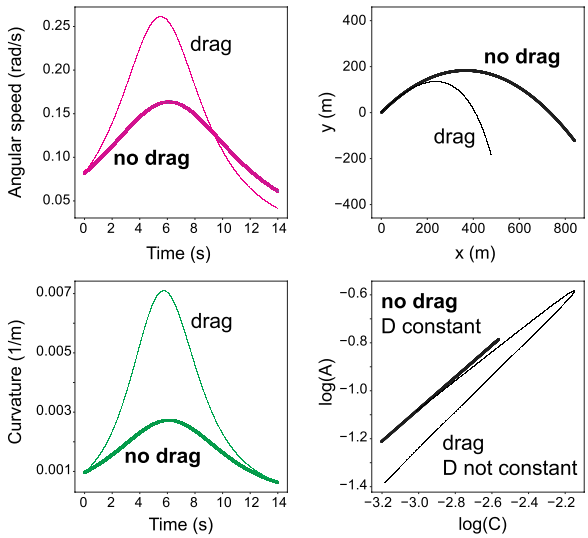

C PENDULUM

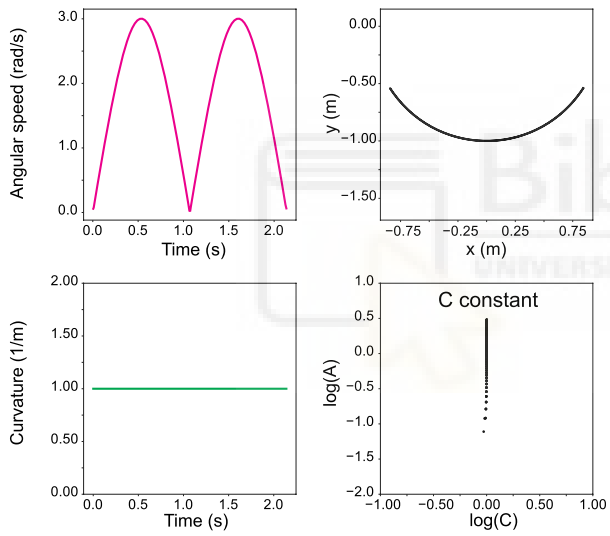

D SPRINGS

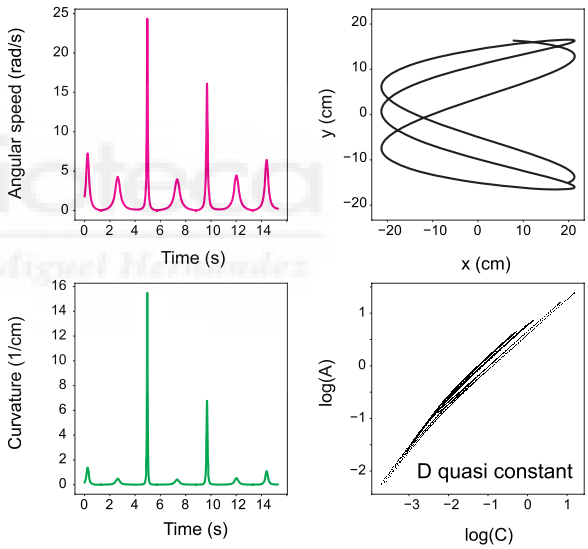

E

GRAVITATION

$$\ddot{x}_1 = -k(x_1 - x_2)/r^3$$
$$\ddot{y}_1 = -k(y_1 - y_2)/r^3$$

$D = |\dot{x}\ddot{y} - \dot{y}\ddot{x}| \neq$ constant

PROJECTILE

$$\ddot{x} = -k\dot{x}$$
$$\ddot{y} = -g - k\dot{y}$$

$D_{k=0} = |0 + g\dot{x}| = |gv_0| =$ constant (no drag)

PENDULUM

$$\ddot{\theta} = -(g/L)\sin\theta$$
$$x = L\sin(\theta)$$
$$y = -L\cos(\theta)$$

$D = L^2|\dot{\theta}|^3$ so $C = 1/L =$ constant

SPRINGS

$$\ddot{x} = -k_x x$$
$$\ddot{y} = -k_y y$$

$D = |k_x x\dot{y} - k_y y\dot{x}| \simeq$ constant

◂**Fig. 5** Physical models and numerical simulations of the kinematics of different systems subject to gravitational, drag or elastic forces. **a** Two gravitating bodies of equal mass, such as two equal stars orbiting around their common barycenter. **b** Ballistic projectiles thrown with an initial speed and accelerated downwards by gravity in the presence (thin lines) or absence (thick lines) of drag. **c** Simple pendulum accelerated by gravity in the absence of drag. **d** Two uncoupled linear springs. Subpanels in A–D show in clockwise order: angular speed (magenta) versus time, x coordinate versus y coordinate of the moving object, log–log plot of angular speed and curvature, and curvature (green) versus time. **e** Differential equations used to simulate the different physical systems, together with the analytical assessment of whether or not the term D = constant and the 2/3 power law is satisfied. Parameters are: $k = 0.04$, r = instantaneous distance between the two bodies for gravitation; $k = 0.09$ and $g = 9.81$ m s^{-2} for the projectiles; $L = 1$ m and $g = 9.81$ m s^{-2} for the pendulum; $k_x = 1.78$ and $k_y = 0.33$ s^{-2} for the springs

A different perspective on the significance of the constraint was brought up by consideration of the geometrical structure of the internal representations of human movements and perceptions (Pollick and Sapiro 1997; Flash and Handzel 2007; Polyakov et al. 2009; Bennequin et al. 2009). Although Euclidean geometrical representations are often assumed, there is growing evidence that both movement planning and visual perception may rely on representations drastically departing from Euclidean geometry, such as affine and equi-affine geometries (Koenderink and van Doorn 1991; Bennequin et al. 2009). Following this approach, Pollick and Sapiro (1997) and Flash and Handzel (2007) showed that $D^{1/3}$ = constant implies that the equi-affine speed V_{ea} is constant, since $V_{ea} = |\dot{x}\ddot{y} - \ddot{x}\dot{y}|^{1/3}$ (Guggenheimer 1977). Therefore, the 2/3 power law is predicted by assuming a constant equi-affine speed throughout the movement. On the other hand, a combination of Euclidean, affine, and equiaffine geometries can generate variable power law exponents, depending on the shape of the trajectory, consistent with the observations by Huh and Sejnowski (2015), replicated in our earlier section of this article.

Still a different approach relies on the assumption that the motor system optimizes a given cost function along the trajectory. In particular, the minimum-jerk model has frequently been associated with the speed-curvature power law (Wann et al. 1988; Viviani and Flash 1995; Todorov and Jordan 1998; Richardson and Flash 2002; Huh and Sejnowski 2015). This model assumes the minimization of squared hand jerk (the rate of change of acceleration) summed over movement duration T: $\int_0^T (\dddot{x}^2 + \dddot{y}^2)dt$. Todorov and Jordan (1998) argued that the constraint of the 2/3 power law provides an efficient solution to the minimization of the total jerk along a prescribed trajectory, since it sets the normal component of jerk to zero. Indeed, by taking time derivatives and canceling terms, the expression $\dot{x}\ddot{y} - \ddot{x}\dot{y}$ = constant is shown to be equivalent to $\frac{\dot{x}}{\dot{y}} = \frac{\ddot{x}}{\ddot{y}}$, which implies that the jerk vector should be parallel to the tangential velocity vector, so that the jerk component in the normal direction is zero (Soechting and Terzuolo 1986; Todorov and Jordan 1998). Huh and Sejnowski (2015) expressed the total squared-jerk cost to be minimized in the Frenet–Serret moving frame. Remarkably, this model revealed scale-invariant features of 2D curved movements and accounted for a spectrum of power laws with a wide range of exponents for different pure frequency curves (see above), as well as for mixtures of power laws for multi-frequency curves such as those associated with scribbling. This approach is related to the Cartan's moving frame method used by Bennequin et al. (2009), which also predicts a mixture of geometries compatible with a spectrum of power exponents, not just the 2/3 power exponent. Lebedev et al. (2001) argued instead that the 2/3 power law arises from the principle of least action; viz. if a movement between two points of a given path obeys the 2/3 power law, then the amount of work required to execute a trajectory in a fixed time is minimal. In fact, the principle of least action states that the integral $\int_0^T \dot{x}^3(\frac{d^2y}{dx^2})dt$ must be minimal over movement duration T, and this condition is satisfied when $\dot{x}^3\left(\frac{d^2y}{dx^2}\right)$ = constant. Since $\dot{x}\ddot{y} - \ddot{x}\dot{y} = \dot{x}^3(\frac{d^2y}{dx^2})$, it follows that a movement obeying the 2/3 power law satisfies the principle of least action (Lebedev et al. 2001).

Omitted variable bias hypothesis

M/S argue that the Equation $A \approx KC^{\beta}$ (Eq. 1) and the equivalent ones (Eqs. 2–4) typically used to assess speed-curvature relationships in biological movements are inappropriate, because these equations omit the predictor variable $D^{1/3}$ that is included in the expression $A = D^{1/3}C^{2/3}$ (Eq. 6). However, this argument is flawed since D of Eq. 6 is not an independent variable, but depends on both A and C (or V and R), as we showed in an earlier section (A different way to look at speed-curvature relationships). Therefore, D cannot be considered an independent predictor of A (or V), because D itself depends on A (or V). If one applied to experimental data a statistical regression based on Eq. 6 (as M/S do), one would learn nothing at all about the physiological underpinnings of the relationship between speed and curvature, because Eq. 6 is a mathematical identity that must always be satisfied, apart from measurement errors. In fact, the only interest in performing a statistical regression on Eq. 6 (or its log–log equivalent) would lie in the study of noise effects (see below). This is acknowledged by M/S when they state that a statistical regression analysis that included $D^{1/3}$ as a predictor variable would always find the exponent of C in Eq. 6 to be exactly equal to its true value 2/3. Accordingly, their application of the principles of omitted variable bias

(OVB, see Wooldridge 2012) to the speed-curvature relationship is ill-grounded, since OVB applies to linear regressions of a dependent variable on one or more independent variables, and here C is an independent variable but D is not.

Given the circularity of M/S argument based on a mathematical identity, it is totally unsurprising that M/S are able to calculate the value of the deviation of the exponent β of Eq. 1 from the 2/3 value based on Eq. 6. Indeed, this had already been shown by Maoz et al. (2006), who performed the statistical regressions to show the potential effects of measurement noise. Maoz et al. (2006) showed that, if one considers all variables as random variables affected by measurement noise, $A = D^{1/3}C^{2/3}$ (Eq. 6) implies that $\beta = \frac{2}{3} + \frac{\xi}{3}$, where β denotes the linear regression coefficient of log$A$ versus log$C$ and ξ denotes the linear regression coefficient of log$D$ versus log$C$. In turn, $\xi = \frac{\mathrm{Cov}(\log C, \log D)}{\mathrm{Var}(\log C)}$ where Cov and Var are the covariance and variance of the indicated variables. Therefore, if log$D$ and log$C$ (as derived from experimental measurements) are statistically uncorrelated, $Cov(\log C, \log D) = 0$, $\xi = 0$ and $\beta = 2/3$, thus fulfilling exactly the 2/3 power law. For all other cases, instead, $Cov(\log C, \log D) \neq 0$, $\xi \neq 0$ and $\beta \neq 2/3$. Therefore, the experimental finding of a range of β values (including the special case of $\beta = 2/3$) for different kinds of biological movements implies that the control systems are able of establishing non-trivial co-regulations of path geometry and kinematics.

As we discussed at length before (see Different biological constraints may give rise to the speed-curvature power law), D is not a predictor variable but its behavior, whether it is nearly constant or widely time-varying throughout a movement, can tell us something about the physiological mechanisms underlying the generation of a given biological movement (Lacquaniti et al. 1983; Soechting and Terzuolo 1986; Viviani and Flash 1995; Pollick and Sapiro 1997; Todorov and Jordan 1998; Maoz et al. 2006; Dounskaia 2007; Flash and Handzel 2007; Polyakov et al. 2009; Bennequin et al. 2009). Interestingly, the message stemming from these previous studies goes in the opposite direction to that of M/S. Rather than being mathematical/statistical artifacts, empirical speed-curvature power laws are real and require a critical investigation of the properties of D to account for compliance or deviation of empirical β values relative to the prototypical 2/3 value found in elliptic drawings, and to test different hypotheses about the physiological origin of the speed-curvature relationships.

Real statistical issues with the power law analysis

A general caveat is that caution is necessary before claiming that experimental measurements conform to a power law, unless a mechanistic model of the system dynamics specifically predicts such a law (Stumpf and Porter 2012). In theory, a power law should be scale invariant, that is, the functional relationship between the two variables should be independent of their magnitude. In practice, few empirical phenomena obey power laws for all values of the variables, and therefore the corresponding law should be defined only over a specified domain.

Statistical support for a power law is often searched using log–log plots, given the simplicity of this analysis (the exponent of the law being found by linear regression). This is also the case for most studies of the speed-curvature power law. A common rule of thumb to assess a candidate power law is that it should exhibit an approximately linear relationship on a log–log plot over at least two orders of magnitude in both the x and y axes (Stumpf and Porter 2012). For instance, Fig. 3 shows that the log–log regressions of speed versus curvature for the experimental data with crawling larvae comply with this criterion (see also Zago et al. 2016). When this criterion is not fulfilled, there are additional statistical tests that can be used to validate power law distributions (Clauset et al. 2009).

One drawback of using log–log regressions is that they tend to de-emphasize the error of data points at the higher ends of the range of values, i.e. higher speeds and curvatures in the present case. Schaal and Sternad (2001) compared log–log regressions and nonlinear regressions of speed versus curvature for drawing of ellipses in 3D space, and found that log–log regressions slightly but systematically underestimated the absolute deviations from the coefficient expected from the 2/3 power law. Therefore, when high speeds and curvatures are important for a specific study, nonlinear regressions should be used instead of log–log regressions.

Correlation versus causation

In several experiments dealing with the speed-curvature power law, the path was unconstrained, so that both instantaneous curvature and speed can vary freely, and indeed the point of the law is that their changes are tightly correlated (coupled) between each other. On the other hand, it is incorrect to state that "Since neither of these variables [i.e., curvature or speed, our note] is manipulated under controlled conditions, any observed relationship between them cannot be considered to be causal" (M/S, pg. 1836). In fact, in a series of previous experiments, movement was guided by asking participants to follow with the pen tip the inner edge of a Plexiglas template cut by a numerical control milling machine (Lacquaniti et al. 1983; Catavitello et al. 2016). Each template resembled an ellipse but consisted of two pairs of circular arcs with different radii. A set of 11 such templates was built by varying the radii so that the shape of

the templates varied progressively from a circle to a very elongated pseudo-ellipsis, while the perimeter was kept constant. This step-response paradigm allowed to address the relation between the geometry of the trajectory and the speed of execution in a controlled manner. Recordings from each template resulted in a pair of data points in the log angular speed versus log curvature plot, one for the more curved and the other one for the less curved portions of the trajectory. All data points were well fitted by power functions, but the power exponents decreased with increasing average speed of execution (Fig. 4 in Lacquaniti et al. 1983). Using the same templates, Catavitello et al. (2016) investigated the speed changes occurring at the transitions between the two circular arcs and found that they occurred before the radius changed from large to small, possibly reflecting an anticipatory control of path trajectory (Tramper and Flanders 2013), but the reverse transition (small to large radius) did not involve a similar anticipation. Several other studies have explored the manual tracing of template figures, thus manipulating curvature under controlled conditions (e.g., Wann et al. 1988; Viviani and Flash 1995; Todorov and Jordan 1998; Richardson and Flash 2002; Flash and Handzel 2007; Huh and Sejnowski 2015).

On a theoretical basis, the causal relationship between curvature and speed is predicted by models assuming that the geometrical shape of a given movement is pre-planned while the speed profile results from movement optimization (Wann et al. 1988; Viviani and Flash 1995; Todorov and Jordan 1998; Richardson and Flash 2002; Flash and Handzel 2007; Huh and Sejnowski 2015) or non-Euclidean implementations of the plan (Pollick and Sapiro 1997; Flash and Handzel 2007; Polyakov et al. 2009; Bennequin et al. 2009). Specifically, Huh and Sejnowksi (2015) showed that movement speed depends not only on the instantaneous curvature, but also on the nearby curvature within 1 rad of the angle coordinate α, suggesting that the angle coordinate and therefore curvature only need to be planned 1 rad ahead. This is consistent with the result of Tramper and Flanders (2013) that planning (or anticipation) takes over longer distance and time when the radius changes from large to small, and shorter distance and time when the radius changes from small to large.

M/S rightly point out that "muscle forces will not be consistently related to the curvature and velocity of the movement" (pg. 1836). Indeed, it has been long known that the changes in electrical muscle activity (EMG) and joint torques follow a time course different from that of hand or joint kinematics. For instance, drawing of ellipses in 3D tends to comply with the 2/3 power law and involves sinusoidal angular motions at the shoulder and elbow joints (Soechting et al. 1986; Schaal and Sternad 2001). Instead the corresponding joint torques and EMG activities deviate substantially from sinewaves (Soechting et al. 1986). The relationship between neural commands, muscle forces, joint torques, and hand kinematics is very complex, being stochastic, non-linear, and closed-loop. For instance, due to the existence of sensory feedbacks with substantial time delays, the muscle forces do not simply affect movement output, but in turn they are affected by the movement via the feedback loops. Therefore, the inference drawn by M/S that "An alternative to a causal explanation of the power law is that the law is an inherent characteristic of the mathematical relationship between measures of curvature and velocity obtained during any curved movement" (pg. 1836) is logically a non sequitur, given the complex relationship between muscle forces and movement kinematics.

Conclusion

Although some of the arguments and simulations we presented probably appear trivial to mathematically oriented readers, they are important to be clarified since illusory issues are still lingering around the speed-curvature power law, as demonstrated by M/S paper. We believe that our analyses are sufficient to refute the argument that "the power law of movement is an observation forced by the mathematical relationship between measures of the curvature and velocity of movement that are used in power law research" (M/S, pg. 1841).

Contrary to M/S conclusion, we maintain that the speed-curvature power law is real and it applies to a wide variety of biological movements with different values of the exponent. The issue that remains to be solved concerns the physiological origins of the power law. But this is a different topic to be covered in a forthcoming article.

References

Abeles M, Diesmann M, Flash T, Geisel T, Herrmann M, Teicher M (2013) Compositionality in neural control: an interdisciplinary study of scribbling movements in primates. Front Comput Neurosci 7:103. doi:10.3389/fncom.2013.00103

Bennequin D, Fuchs R, Berthoz A, Flash T (2009) Movement timing and invariance arise from several geometries. PLoS Comput Biol 5(7):e1000426

Catavitello G, Ivanenko YP, Lacquaniti F, Viviani P (2016) Drawing ellipses in water: evidence for dynamic constraints in the relation between speed and path curvature. Exp Brain Res 234:1649–1657

Clauset A, Shalizi CR, Newman ME (2009) Power-law distributions in empirical data. SIAM Rev 51(4):661–703

de'Sperati C, Viviani P (1997) The relationship between curvature and speed in two-dimensional smooth pursuit eye movements. J Neurosci 17:3932–3945

Dounskaia N (2007) Kinematic invariants during cyclical arm movements. Biol Cybern 96:147–163

Flanders M, Mrotek LA, Gielen CC (2006) Planning and drawing complex shapes. Exp Brain Res 171:116–128

Flash T, Handzel AA (2007) Affine differential geometry analysis of human arm movements. Biol Cybern 96:577–601
Gielen CC, Dijkstra TM, Roozen IJ, Welten J (2009) Coordination of gaze and hand movements for tracking and tracing in 3D. Cortex 45:340–355
Gomez-Marin A, Stephens GJ, Louis M (2011) Active sampling and decision making in Drosophila chemotaxis. Nat Commun 2:441
Gomez-Marin A, Partoune N, Stephens GJ, Louis M (2012) Automated tracking of animal posture and movement during exploration and sensory orientation behaviors. PLoS One 7:e41642
Gribble PL, Ostry DJ (1996) Origins of the power law relation between movement speed and curvature: modeling the effects of muscle mechanics and limb dynamics. J Neurophysiol 76:2853–2860
Guggenheimer HW (1977) Differential geometry. Dover, New York, p 378
Harris CM, Wolpert DM (1998) Signal-dependent noise determines motor planning. Nature 394:780–784
Hicheur H, Vieilledent S, Richardson MJE, Flash T, Berthoz A (2005) Speed and curvature in human locomotion along complex curved paths: a comparison with hand movements. Exp Brain Res 162:145–154
Huh D (2015) The vector space of convex curves: how to mix shapes. arXiv:1506.07515
Huh D, Sejnowski TJ (2015) Spectrum of power laws for curved hand movements. Proc Natl Acad Sci 112:E3950–E3958
Ivanenko YP, Grasso R, Macellari V, Lacquaniti F (2002) Two-thirds power law in human locomotion: role of ground contact forces. NeuroReport 13:1171–1174
Koenderink JJ, van Doorn AJ (1991) Affine structure from motion. J Opt Soc Am A 8:377–385
La Scaleia B, Zago M, Moscatelli A, Lacquaniti F, Viviani P (2014) Implied dynamics biases the visual perception of speed. PLoS One 9(3):e93020
Lacquaniti F, Terzuolo C, Viviani P (1983) The law relating the kinematic and figural aspects of drawing movements. Acta Psychol (Amst) 54:115–130
Lacquaniti F, Terzuolo C, Viviani P (1984) Global metric properties and preparatory processes in drawing movements. In: Kornblum S, Requin J (eds) Preparatory states and processes. Erlbaum, Hillsdale, pp 357–370
Lacquaniti F, Ferrigno G, Pedotti A, Soechting JF, Terzuolo C (1987) Changes in spatial scale in drawing and handwriting: kinematic contributions by proximal and distal joints. J Neurosci 7:819–828
Lebedev S, Tsui WH, Van Gelder P (2001) Drawing movements as an outcome of the principle of least action. J Math Psychol 45:43–52
Maoz U, Portugaly E, Flash T, Weiss Y (2006) Noise and the 2/3 power law. Adv Neural Inf Proc Syst 18:851–858
Maoz U, Berthoz A, Flash T (2009) Complex unconstrained three-dimensional hand movement and constant equi-affine speed. J Neurophysiol 101:1002–1015
Marken RS, Shaffer DM (2017) The power law of movement: an example of a behavioral illusion. Exp Brain Res 235:1835–1842
Massey JT, Lurito JT, Pellizzer G, Georgopoulos AP (1992) Three-dimensional drawings in isometric conditions: relation between geometry and kinematics. Exp Brain Res 88:685–690
Pollick FE, Sapiro G (1997) Constant affine speed predicts the 1/3 power law of planar motion perception and generation. Vision Res 37:347–353
Pollick FE, Maoz U, Handzel AA, Giblin P, Sapiro G, Flash T (2009) Three-dimensional arm movements at constant equi-affine speed. Cortex 45:325–339
Polyakov F, Stark E, Drori R, Abeles M, Flash T (2009) Parabolic movement primitives and cortical states: merging optimality with geometric invariance. Biol Cybern 100:159–184
Richardson MJE, Flash T (2002) Comparing smooth arm movements with the 2/3 power law and the related segmented-control hypothesis. J Neurosci 22:8201–8211
Schaal S, Sternad D (2001) Origins and violations of the 2/3 power law in rhythmic three-dimensional arm movements. Exp Brain Res 136:60–72
Schwartz AB (1994) Direct cortical representation of drawing. Science 265:540–542
Soechting JF, Terzuolo CA (1986) An algorithm for the generation of curvilinear wrist motion in an arbitrary plane in three-dimensional space. Neuroscience 19:1393–1405
Soechting JF, Lacquaniti F, Terzuolo CA (1986) Coordination of arm movements in three-dimensional space. Sensorimotor mapping during drawing movement. Neuroscience 17:295–311
Struik DJ (2012) Lectures on classical differential geometry. Dover Publ, New York
Stumpf MP, Porter MA (2012) Critical truths about power laws. Science 335:665–666
Todorov E, Jordan MI (1998) Smoothness maximization along a predefined path accurately predicts the speed profiles of complex arm movements. J Neurophysiol 80:696–714
Tramper JJ, Flanders M (2013) Predictive mechanisms in the control of contour following. Exp Brain Res 227:535–546
Vieilledent S, Kerlirzin Y, Dalbera S, Berthoz A (2001) Relationship between speed and curvature of a human locomotor trajectory. Neurosci Lett 305:65–69
Viviani P, Cenzato M (1985) Segmentation and coupling in complex movements. J Exp Psychol Hum Percept Perform 11:828–845
Viviani P, Flash T (1995) Minimum-jerk, 2/3 power law, and isochrony: converging approaches to movement planning. J Exp Psychol Hum Percept Perform 21:32–53
Viviani P, Schneider R (1991) A developmental study of the relationship between geometry and kinematics in drawing movements. J Exp Psychol Hum Percept Perform 17:198–218
Viviani P, Terzuolo C (1982) Trajectory determines movement dynamics. Neuroscience 7:431–437
Wann J, Nimmo-Smith I, Wing AM (1988) Relation between speed and curvature in movement: equivalence and divergence between a power law and a minimum-jerk model. J Exp Psychol Hum Percept Perform 14:622–637
West G (2017) Scale. Penguin, New York, p 479
Wolpert DM, Pearson KG, Ghez CPJ (2013) The organization and planning of movement. Princ Neural Sci 5:743–766
Wooldridge JM (2012) Introductory econometrics: a modern approach. South-Western Cengage Learning, Mason, pp 88–93
Zago M, Lacquaniti F, Gomez-Marin A (2016) The speed-curvature power law in *Drosophila* larval locomotion. Biol Lett 12(10):20160597

Annex 3:

Matic, A., & Gomez-Marin, A. (2020). Geometric purity, kinematic scaling and dynamic optimality in drawing movements beyond ellipses. Journal of Mathematical Psychology, 99, 102453.
DOI: 10.1016/j.jmp.2020.102453

Geometric purity, kinematic scaling and dynamic optimality in drawing movements beyond ellipses

Adam Matic, Alex Gomez-Marin *

Behavior of Organisms Laboratory, Instituto de Neurociencias CSIC-UMH, Alicante, Spain

A B S T R A C T

Drawing movements have been shown to comply with a power law constraining local curvature and instantaneous speed. In particular, ellipses have been extensively studied, enjoying a 2/3 exponent. While the origin of such a non-trivial relationship remains debated, it has been proposed to be an outcome of the least action principle whereby mechanical work is minimized along 2/3 power law trajectories. Here we demonstrate that this claim is flawed. We then study a wider range of curves beyond ellipses that can have 2/3 power law scaling. We show that all such geometries are quasi-pure and with the same spectral frequency. We then numerically estimate that their dynamics produce minimum jerk. Finally, using variational calculus and simulations, we discover that equi-affine displacement is invariant across different kinematics, power law or otherwise. In sum, we deepen and clarify the relationship between geometric purity, kinematic scaling and dynamic optimality for trajectories beyond ellipses. It is enticing to realize that we still do not fully understand why we move our pen on a piece of paper the way we do.

We must represent any change, any movement, as absolutely indivisible. — Henri Bergson

1. Introduction

In 1609 Kepler published in the book *Astronomia Nova* (Kepler, 1609) his celebrated First Law of planetary motion: Mars moves along an elliptical trajectory with the sun at one of its foci. This left behind Ptolemaic and Copernican models; not circles, but ellipses. In the same book we find Kepler's Second Law, which specifies an invariant (which was later understood as conservation of angular momentum): the area between the Sun, Mars and any previous point of Mars is constant along the motion of the planet. In sum: equal areas in equal times. This was generalized to all other planets. We move faster when we are close to the sun (fastest when nearest, at the perihelion), and slower when far away (slowest when furthest, at the aphelion).

Ten years later, Kepler published in *Harmonices Mundi* (Kepler, 1619) his Third Law of motion: the semi-major axis A is related to the period P of a planet by means of the following relation: $A = k \cdot P^{2/3}$ (the parameter k is a constant, which can be renormalized using the semi-major axis of the Earth and the number of years as units). It was Kepler's big achievement to establish such a lawful regularity despite the fact that nobody understood why planets would care to follow it. No one could derive Kepler's two-thirds power law until Newton's Law of Universal Gravitation (Newton, 1687) was proposed nearly seventy years later. From geometric properties and kinematic laws one would then strive to "climb up" in order to establish dynamic laws that frame the former.

Physics is full of celebrated examples of this sort, where constraints of motion are first discovered and later explained by other more general empirical laws, which in turn are then shown to derive from even more fundamental theoretical principles (such as symmetries). Such is a hallmark understanding phenomena, from the motion of planets across the solar system to the movement of Picasso's brush along a canvas. However, when it comes to "living matter", the explanatory work seems to have been accomplished when molecules or circuits are shown to be "necessary and sufficient" for the appearance (or disappearance) of the phenomenon under investigation (Gomez-Marin, 2017).

In the midst of the dominant reductionistic zeitgeist obsessed with efficient mechanical causes in the form of counterfactual reasoning within purely interventionist approaches (Krakauer et al., 2017), it is conceptually refreshing (and empirically exciting) to realize that relationships like Kepler's laws could be understood as formal causes. Science is actually the art of interpreting correlations, be it in terms of efficient causation or, in arguably more mature sciences (in physics), by actually giving up causation (or, rather, by framing it in) the notion of invariance (Bailly & Longo, 2011). Is it not ironic that, while the stone falls for symmetry reasons, the insect is thought to fly for neural reasons?

* Corresponding author.
E-mail address: agomezmarin@gmail.com (A. Gomez-Marin).

Scaling laws are a particularly relevant sub-class of deep relations, ranging from physics to psychophysics, ecology or language. They all point to unifying principles in complex systems (West, 2011). Note that not all power laws are necessarily statistical, namely, expressing a constraint or a functional dependency on probability distributions (such as $p(x) = x^a$). Others relate one degree of freedom to another (in the form $x = y^b$), like the speed-curvature power law studied here.

In fast elliptical hand movements, the instantaneous angular speed also scales with local curvature via a power law, whose exponent is 2/3 (Lacquaniti et al., 1983). This relationship, simple as it seems, is not a trivial mathematical fact, nor a statistical artifact, nor is it given by physics (Zago et al., 2018). Cortical computations have been proposed as the controlling mechanism (Schwartz, 1994). However, it is still unclear how the neuro-musculo-skeletal system may actually do so. Moreover, the trajectories of insects also comply with the speed-curvature power law (Zago et al., 2016), suggesting that a much simpler explanation – perhaps via simple central pattern generators – may be at work (at least in the humble fruit fly). Nearly forty years later, the origins of the law remain debated.

Most theoretical and phenomenological studies of the power-law have concentrated on ellipses, also decomposing scribbling into monotonic segments (Lacquaniti et al., 1983). On a few occasions shapes other than ellipses have been studied, such as the cloverleaf, lemniscate or limaçon (Flash et al., 2018). Invoking optimality as a normative explanation, one can derive the power law by powerful mathematical frameworks. Requiring that the trajectory produces minimum jerk (jerk is the time derivative of acceleration, or equivalently the second derivative or speed, or the third derivative of position) naturally implies such speed-curvature constraints (Flash & Hogan, 1985). Also recently, a spectrum of power laws with different exponents has been empirically demonstrated when tracing a whole range of "pure frequency" curves beyond ellipses, and shown to theoretically derive from minimization of jerk (Huh & Sejnowski, 2015).

Notably, it has also been proposed that the 2/3 power-law is an outcome of the least action principle, namely, that imposing mechanical work to be minimal along the trajectory naturally produces the power law with its well-known 2/3 exponent (Lebedev et al., 2001). Here we correct this mistaken statement. In turn, this allows us to deepen our knowledge of the relationship between geometrical purity, kinematic scaling and dynamic optimality beyond elliptical trajectories. Planets do not move at constant speed along their (quasi) elliptical trajectories around the Sun. Nor does your finger when tracing an ellipse on a tablet (Matic & Gomez-Marin, 2019). And yet, while planets do not follow the speed-curvature power law (Zago et al., 2018), nor do finger movements derive from the physical principle of least action, as we hope to show in what follows.

2. Materials and methods

2.1. Mathematical relations

Basic notation and equations. Let us use the following notation: A is the angular speed ($A = V/R$), where V is the instantaneous speed (the module of the velocity vector) and R is the local radius of curvature. Curvature is then defined as $C = 1/R$. The speed-curvature power law then reads: $A = kC^{\beta}$, where k is a constant and β is the power law exponent. By definition, the power law can also be written as $V = kC^{\beta-1}$ or $V = kR^{1-\beta}$

Space–time dilation for arbitrary power-law generation. Since $V = ds/dt$ (where dt is the time differential, and ds the arc-length differential), then one can obtain an explicit relation for how time dilates with space at every infinitesimal increment along the trajectory: $ds/dt = kC^{\beta-1}$. Since C can be numerically calculated as $d\alpha/ds$ (where α is the local angle between the tangent line at any given point and the x axis, and $d\alpha$ its differential), we arrive at the final equation that allows to transform any trajectory into a power law kinematics that respects the original geometry: $dt = (1/k)ds^{\beta}d\alpha^{1-\beta}$.

2.2. Numerical simulations

Trajectory generation. Trajectories were generated by numerically integrating (with a $dt = 0.001s$) the x and y positions and their derivatives for curves expressed and governed via the following differential equation: $d^3x/dt^3+q(t)x = 0$ for x(t), and also for y(t): $d^3y/dt^3+q(t)y = 0$. Note that the initial conditions can be different but both x and y are governed by the same equation with the same time-dependent coefficient q(t). The four different curves explored in this manuscript were generated by choosing the function q(t) as follows: $q(t) = 1$ corresponds to the ellipse, $q(t) = t$ for the spiral-like ellipse, $q(t) = |\sin(t)|$ for "wobbly" curve, and $q(t) = |3\sin(4t)|$ for the flower-like curve (see Fig. 1A).

Curvature spectrum. Curvature frequency spectrum analysis is based on Huh and Sejnowski (2015), expanded to approximate also the frequency spectrum of non-monotonic angle profiles. We calculate the first derivative of the unwrapped local angle profile, then take its absolute value, and finally integrate. The profile is re-sampled to a uniform step in the local angle coordinate. We take the log of the profile, de-trend it, and apply the Fourier transform.

Generating power-law kinematics of any exponent from arbitrary geometries. Selecting an arbitrary power law between angular velocity and curvature is solved by recalculating the time period between each point of the discretized curve, so that the angular velocity fits a desired relationship with curvature (the power-law relation; $A = kC^{\beta}$), or equivalently, that tangential velocity fits equation ($V = kC^{\beta-1}$). First, we sample or construct the trajectory using a constant step in time (dt). We calculate the arc-length ds_i, and curvature C_i at each point (x_i, y_i) of the trajectory. Next we construct a new time-difference vector, where each dt_i follows equation $dt_i = ds_iC^{1-\beta}$. We then construct a time vector as a cumulative sum of all dt_i, and scale it by a factor k (as the desired duration divided by the total duration of the original vector) so as to set the total traversing duration of the trajectory equal to the desired duration, without changing the power law relationship. Then, using a cubic spline, we fit the existing (x_i, y_i) points to the new time vector. Finally, we sample the splined trajectory again with constant dt, obtaining a new vector of points (x_i, y_i) as a discrete approximation of an arbitrary power law trajectory.

2.3. Behavioral experiments

Ellipse trace. Using the methods developed in Matic and Gomez-Marin (2019), one of the authors traced an ellipse on an android tablet device in a fast and fluid manner. The data was recorded at 85 Hz. Raw data was smoothed with a low-pass, 2nd order Butterworth filter, with a cutoff at 8 Hz.

Homer's trace. A member of the lab traced a contour of Homer Simpson's head shown on a Wacom Cintiq interactive graphics monitor, using an electronic pen. The tracing movement was done without lifting the pen from the screen. Several practice traces preceded the trace used in this paper. The data was recorded at 150 Hz. Raw data was smoothed with a low-pass, 2nd order Butterworth filter, with a cutoff at 8 Hz.

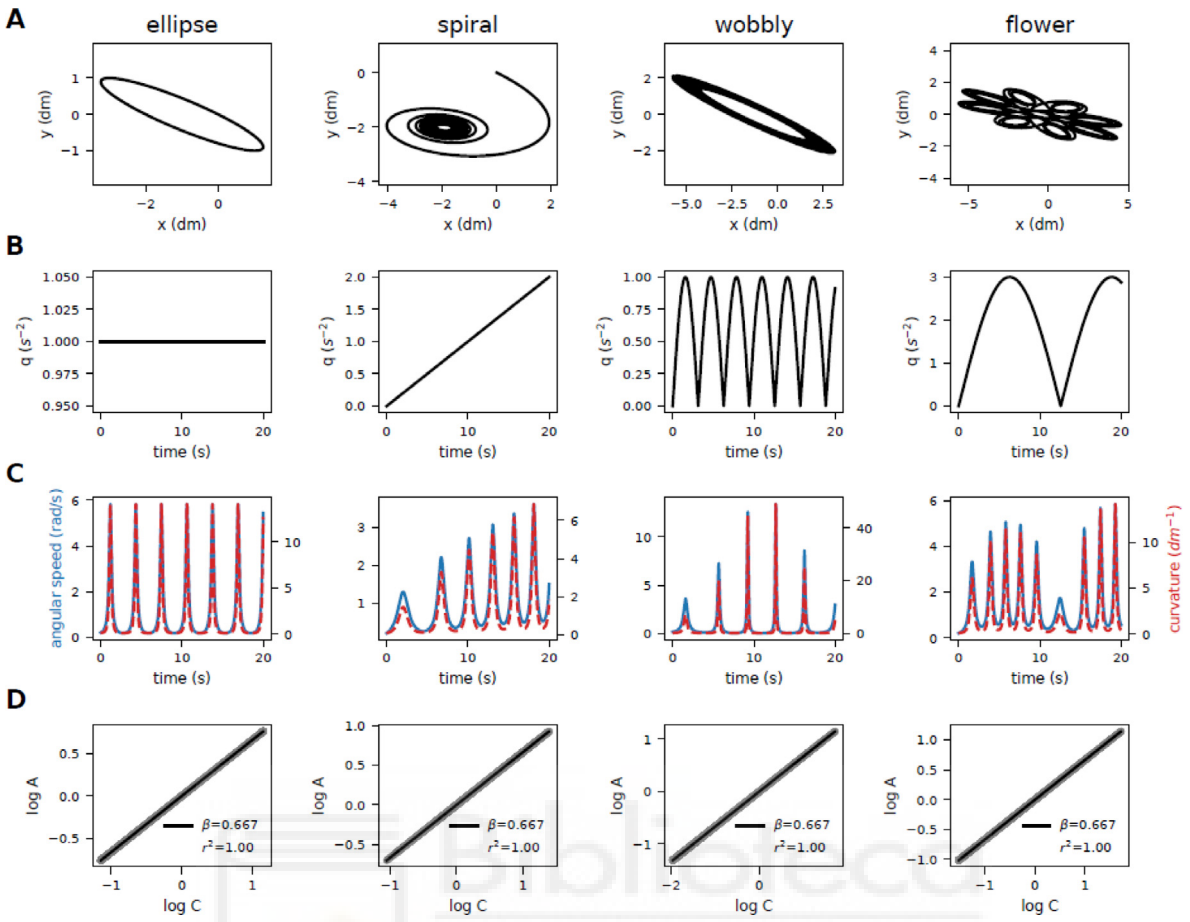

Fig. 1. A wide range of geometries beyond ellipses can have two-thirds power law kinematics. (**A**) The four main generated trajectories analyzed in this work: ellipse, elliptic spiral, wobbly ellipse and elliptic flower. (**B**) Time dependence of the function q(t), which generates those trajectories via the third order differential equation $d^3u/dt^3+q(t)u = 0$ satisfied for both x(t) and y(t). (**C**) Time course of instantaneous angular speed A and local curvature C for each curve. (**D**) The numerically estimated log–log plot of angular speed versus curvature reveals, as predicted, an exact power law relationship with exponent 2/3 for each of the curves. Thus an ellipse is not the only geometry that naturally admits kinematic scaling.

2.4. Codes

For more details please see the **Supplementary material** at the end of the manuscript with links to the code that generates all analyses, plots, and animations.

3. Results

3.1. A wide range of curves beyond ellipses naturally lead to a 2/3 power law

The speed-curvature power law is the relation $A = k \cdot C^{\beta}$, where A is the instantaneous angular speed (defined as $A = V/R$), C is the local curvature (defined as $C = 1/R$), V is the absolute instantaneous speed of movement and R the local radius of curvature of the trajectory. The term k is a proportionality factor that remains more or less constant empirically (and a precise constant theoretically), and β is the power law exponent. This relation is non-trivial since aspects of geometry (like curvature; which concerns only space) and aspects of kinematics (like speed; which concerns time) need not constrain one another in general (like in the motion of a pendulum).

Using the definition of the radius of curvature R as a function of the time derivatives of the trajectory (we are always referring to movement in two dimensions here), it is not difficult to show that, if the power law holds, the term $k = D^{1/3}$, where $D = |v_X a_Y - v_Y a_X|$. Note that v_i and a_i are the velocity and acceleration components in both orthogonal directions x and y. The 2/3 power law is often written as $A = D^{1/3}C^{2/3}$, with D constant.

Now, if k is constant (namely, if the 2/3 power-law holds), then the term $|v_X a_Y - v_Y a_X|$ should also be constant. This implies that its time derivative should be zero, and thus one gets: $a_X a_Y + v_X j_Y - v_Y j_X - a_Y a_X = 0$ (where "j", known as jerk, is the time derivative of acceleration; just as "a" is the time derivative of speed). Two terms cancel out, and thus we finally get that any trajectory that complies with the 2/3 power-law must satisfy the following differential equation: $j_X/v_X = j_Y/v_Y$. This geometric-kinematic constraint is very interesting because it dictates that both x(t) and y(t) must behave so that the ratio of their third and first time derivatives is equal which, without losing generality, can be expressed as $j/v = q(t)$, where q(t) is any arbitrary temporal function. In other words, one can choose any q(t) at will and, by means of the equation $d^3u/dt^3+q(t)u = 0$ – where u(t) here denotes both x(t) and y(t), although initial conditions can be different – generate geometric curves whose kinematics follow the 2/3 power law.

Following this mathematical reasoning (Lebedev et al., 2001), we generated four different trajectories (Fig. 1A). Selection of the q(t) function determines the shape of the trajectory: for the ellipse, it is constant, $q(t) = 1$; for the elliptic spiral $q(t) = t$; the wobbly ellipse, $q(t) = |\sin t|$; and for the elliptic flower we chose $q(t) = |3 \sin t/4|$ (Fig. 1B). Not only are curvature and angular speed of these trajectories strongly correlated (Fig. 1C), but they also in fact follow the 2/3 speed-curvature power law exactly (Fig. 1D).

Lebedev and colleagues explicitly listed the ellipse, hyperbola and parabola as the trajectories resulting from constant q(t), noting the relationship between constant q and the resulting geometry ($q = 0$ for parabola, $q < 0$ for ellipse, and $q > 0$ for hyperbola). In **Supplementary Figure 1** we analyzed those three curves in the same way as four mentioned curves in Fig. 1. Curvature and angular speed are visibly constrained, following a power law with the exponent of exactly 2/3.

To the best of our knowledge, nobody has analyzed the family of curves that are generated with a non-constant q(t). Some examples are shown in Fig. 1. In what follows, we will concentrate on such four curves to gain further insights into geometric purity, kinematic scaling, and dynamic optimality beyond ellipses. We will also correct an important physics error in Lebedev et al. (2001).

3.2. Two-thirds power law trajectories have quasi-pure geometrical spectra

Let us now concentrate on the geometry of the curves presented in the previous section. It has been recently shown that the speed curvature power laws (of different exponents, not just 2/3) are achieved for so-called "pure frequency curves" (Huh & Sejnowski, 2015). Actually, (as we will see in the last section of the Results) trajectories with "mixed curvature frequencies" cannot comply with the kinematic scaling of the power law, unless they give up dynamic optimality. So, how does one estimate the "geometric purity" of a curve?

Parametrization of local curvature can be done in many ways. To estimate power laws one usually parametrizes curvature in time, namely, C(t), so that it can be compared, moment to moment, with speed V(t), which is naturally defined as a function of time. Time parametrization of log curvature is convenient in the regression analysis with log angular velocity, also parametrized in time (as in Fig. 1D). In Fig. 2B we show curvature parametrized in time for the four study-case trajectories shown in Fig. 2A.

However, cumulative arc length (s) is the natural parametrization for curvature, since curvature is by construction a purely geometrical quantity, and so the time parametrization natural in kinematic quantities (such as speed) injects a temporal bias that geometry should be indifferent to. In Fig. 2C we re-parametrize curvature now in terms of arc length, C(s). Note the subtle change in the functions with respect to the time parametrizations in Fig. 2B.

There is a third way to parametrize curvature: rather than time or length, one can use angle. Based on Huh (2015) we can parametrize curvature in the local angle coordinate, as shown in Fig. 2D. This representation has many advantages in understanding essential properties of the curves, as well as revealing the connection between geometry and kinematics in power law constraints (Huh & Sejnowski, 2015).

In particular, once any curve is parametrized in the angle, one can detect a shared feature in the four curves studied here: note how the profiles of Fig. 2D are naturally rescaled with respect to those in Fig. 2C and B, so that now, every 2π, curvature undergoes exactly two complete oscillations. If these were temporal functions, a Fourier transform would immediately reveal a dominant frequency there.

Following Huh and Sejnowski (2015) we apply the Fourier transform to the log of the curvature profile, once parametrized in the local angle coordinate (Fig. 2E). The resulting amplitude profile shows curvature frequency spectrum in angle space. The frequency of a curve is the number of curvature oscillations per unit of local angle (full oscillation is 2π radians), and the local angle is defined as the angular direction of the velocity vector. Despite their very different appearance in X-Y space (Fig. 2A), all four curves share a main peak at $\nu = 2$ (which corresponds to Huh's pure ellipse; see below) as well as some ripples.

The quasi-pure spectrum of these geometries, and especially that of the ellipse shown on the left side of Fig. 2A, makes one wonder why they are not exactly pure (namely, with a single peak at $\nu = 2$, without any ripples). To better understand this, we went back to Huh's pure frequency curve with $\nu = 2$ (Huh, 2015), which is visually very similar to the classical ellipse, $(x/a)^2 + (y/b)^2 = 1$. Both curves are shown in **Supplementary Figure 2A**, together with ellipses empirically traced on a tablet.

Huh's ellipse (on the left) has a single strong peak at $\nu = 2$ by design, and no peaks at other frequencies, meaning that its log-curvature profile in angle space is a pure sinusoid. The classic ellipse, constructed with two orthogonal sine waves with 90 degrees of phase difference, has a few harmonics at frequencies multiples of $\nu = 2$ (4, 6, 8, etc.), but it is still quasi-pure. The empirically recorded ellipse trace, similarly, shows some harmonics and also peaks at other frequencies (**Supplementary Figure 2B**). It is also decently pure. In sum, this precise geometrical analysis of the spectrum of curvature is not only both informative as to whether we shall expect a power law and of what exponent, but also a necessary condition to know that we are dealing with a pure frequency curve in the first place, which is very important when trying to determine whether the speed-curvature power law holds empirically.

To gain even further insight into what these spectra are reflecting, we morphed an ellipse into a circle by reducing the eccentricity of the former (**Supplementary Figure 2C**). The amplitude of the peak at $\nu = 2$ is progressively reduced, as well as all the other harmonic frequencies, until the circumference does not show peaks at any frequency (as it should, since its curvature is constant). Finally, spectra for different parametrizations of curvature are shown in **Supplementary Figure 3**.

We can proceed now with kinematic and dynamic considerations on these curves.

3.3. The power law does not imply that mechanical work is constant nor minimal

For 2/3 power law trajectories, we have seen that D is constant. It turns out that D is actually the magnitude of the *cross* product between the velocity and acceleration vectors. For the trajectories displayed in (Fig. 3A) that cross product should be constant too (Fig. 3B). The magnitude of the cross product can be represented as the area of the parallelogram closed by both vectors.(Fig. 3D). So far, so good.

Remember that one can rewrite the 2/3 power law ($A = kC^{2/3}$) as $A = D^{1/3}C^{2/3}$, and then simply as $V = D^{1/3}R^{1/3}$, so that $V^3/R = D$. With similar mathematical manipulations Lebedev et al. (2001) arrive at this last same equation and, rewriting $D = V(V^2/R)$ realize that the term in parenthesis is the magnitude of centripetal acceleration (A_n), and so $D = V \cdot A_n$. The fatal error comes in their equation (5), when they say that "[t]his product is known in physics as mechanical power", which they call P. The essential mistake that invalidates the main claim of their paper is to equate D with P.

If that was the case (which is not), then a 2/3 power law would constraint movement along the trajectory to have constant mechanical power (because we have seen that D is constant). As we will unpack further below, the authors were understandably excited to discover that, mathematically, the time integral of D is minimal when D happens to be constant. In other words, the optimal way to move is to do so that D is constant, aka, the 2/3 power law. They are thrilled (as we would) because, if their physics were correct, the mathematics would prove that "drawing movements" [which fulfill the 2/3 speed curvature power law] are "an outcome

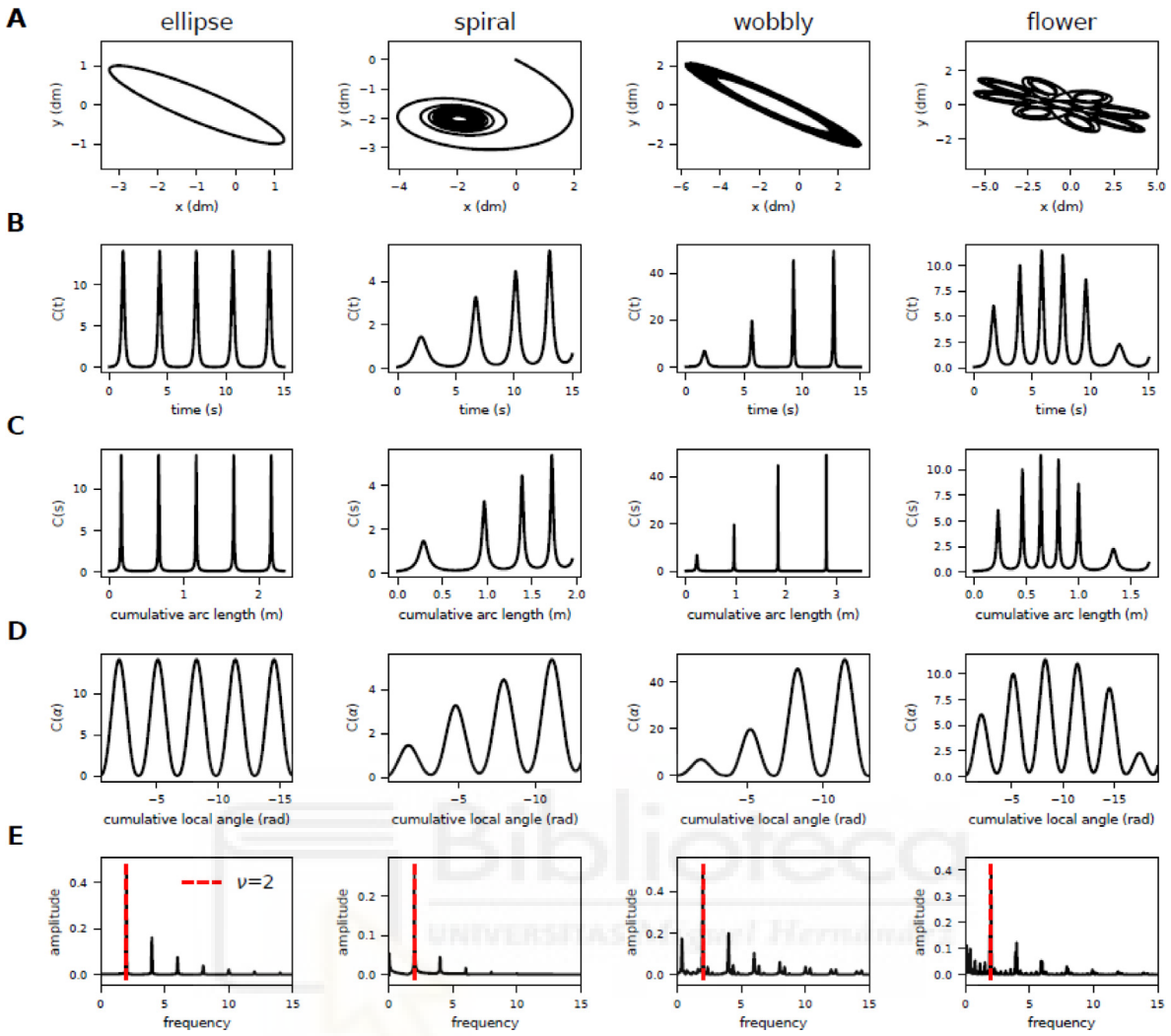

Fig. 2. Very different geometries can have the same quasi-pure curvature spectrum. (**A**) The four studied curves in Euclidean space. (**B**) Their local curvature parametrized in time as C(t). (**C**) Curvature parametrized in arc length space as C(s). (**D**) Curvature reparametrized in local angle as C(α). (**E**) Geometric spectrum of the curves – Fourier transform of the logarithm of C(α) – showing that all curves are quasi-pure with a dominant peak at frequency 2.

of the Principle of Least Action" (which is precisely the title of their paper). But if D is not the mechanical power, then the claim evaporates. Why is not D = P, then?

Lebedev and colleagues equate mechanical power with D, namely, the authors take the product of centripetal acceleration with the speed to be proportional to physical force that would push a particle moving along such 2/3 power law trajectories.

Mechanical power is the amount of mechanical work per unit of time. Mechanical work is the amount of energy transferred by a force. It is calculated as the integral of the force vector along the trajectory vector. Force is proportional to acceleration, and the trajectory vector can be rewritten as velocity times dt. Thus, in practice, mechanical work is proportional to the product of velocity and acceleration. But (and here comes the subtle mistake), it is the *dot* product (also called *scalar* product) of the vectors, rather than the simple product of their magnitudes. Put plainly, the dot product of two orthogonal vectors is zero, no matter how large they are; while the product of their magnitudes is large. In sum, mechanical work is calculated via the *scalar* product – rather than the *cross* product (which gives us D)— of velocity and acceleration. And thus, as shown in Fig. 3C, work is far from constant along the trajectory, as opposed to D (Fig. 3B).

Animated traversals of the spiral and elliptical trajectories are available in the *GitHub* repository as video files (see **Supplementary Material**). They show the constancy of the magnitude of the cross product D during the whole trajectory, and the changes in the position, acceleration, velocity and jerk vectors over time. See Fig. 3D for snapshots.

In sum, and contrary to what was claimed in Lebedev et al. (2001), the speed-curvature 2/3 power law of movement is *not* an outcome of the principle of least action whereby mechanical work is minimized.

3.4. Trajectories with constant D minimize the time integral of D

The mathematical derivation that, by means of a variational analysis, shows that the time integral of D is minimal when D is constant (Lebedev et al., 2001) is still valid and somewhat insightful. Agnostic about the existence of a meaningful physical or mathematical interpretation of the term D, next we sought to numerically demonstrate that constant-D prescribes the most "economical" way to move amongst the infinitely many ways to do so. To our knowledge, such minimization has not been done numerically.

Because we seek a numerical demonstration that trajectories complying with the 2/3 power law constrain their geometry (curvature) and kinematics (speed) so as to minimize the integral of D, we can only aspire to show local, rather than global, minima. To that end, we invented a way to systematically generate a

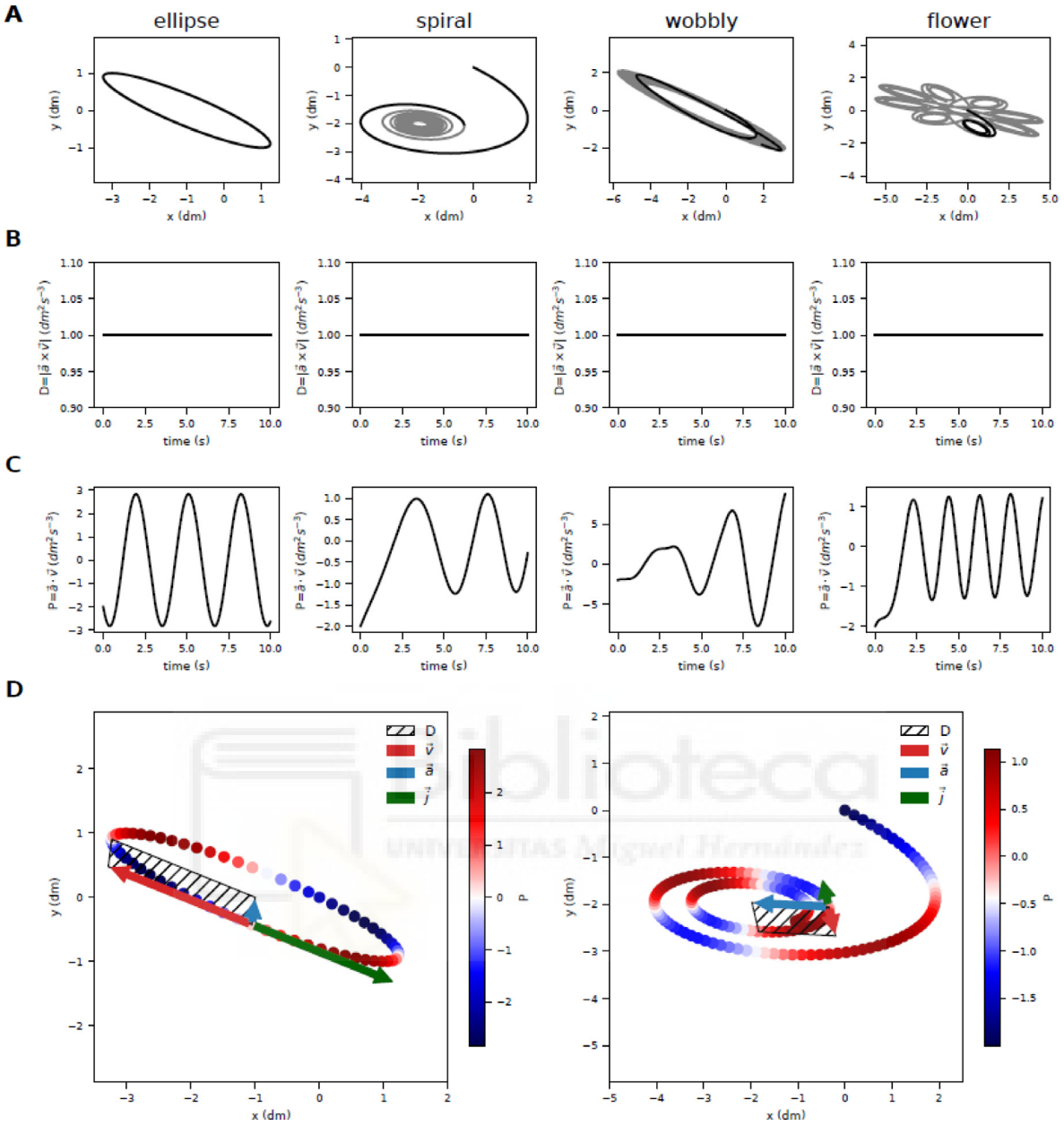

Fig. 3. Mechanical work is not constant for 2/3 power law trajectories, but the term D is. (**A**) Analyzed segments of the curves marked in solid black. (**B**) Magnitude of the cross product of the velocity and acceleration vectors (which is mathematically equal to D) as a function of time along the trajectory. It is constant for all curves. (**C**) Dot product of the velocity and acceleration vectors (which is technically the power divided by the mass, and in the present case proportional to mechanical work) over time. It is not constant for any curve (including the ellipse). (**D**) Velocity, acceleration and jerk vectors for two of the curves at a given time instant. Geometrically, the term D is the area of the parallelogram formed by velocity and acceleration, and it has the property of remaining constant along the trajectory. Moreover, the jerk and velocity vectors have opposite directions. Mechanical power (whose value is depicted in color) is not constant along the trajectory. It is actually zero at the extremes of the ellipse (since velocity and acceleration vectors are orthogonal there) but non-zero at other times. See also animations of panel (D) in the **Supplementary Material**.

range of different kinematics that would traverse the exact same geometry in the exact same total duration (see below).

We take a segment (of a trajectory that complies with the 2/3 speed curvature power law) with starting points A and B (Fig. 4A), and whose total time duration is T (vertical black line in the plots of Fig. 4B). We then maintain the geometry while rescaling the kinematics so that the same segment is traversed in the same amount of time but now with a kinematics that would still yield a power law with an exponent different than 2/3 (say, with hypo-natural exponent 1/3, and hyper-natural exponent equal to 1). We then numerically calculate D as we integrate it in time all the way to t = T (Fig. 4B) for such three different (power law) kinematics. Exponent 2/3 always yields the minimum value at the end of the segment. In Fig. 4C we can calculate I(t = T) for a whole range of values of β on the given path. Compared to trajectories with any other values of β, trajectories with $\beta = 2/3$ indeed have the minimal time integral of D.

In case it is not already clear by now, let us emphasize that a given geometry can in principle be traversed with any kinematics. Let us now have a brief interlude to explain and illustrate how to kinematically re-scale a given geometry with any kinematics to a power-law kinematics with our exponent of choice. For each β in the required range, we start with a generated path as an ordered list of points. Given the path, the β and k, we calculate the time periods between each point of the path, so that they satisfy the formula $dt = (ds/k)C^{1-\beta}$, derived as explained in the

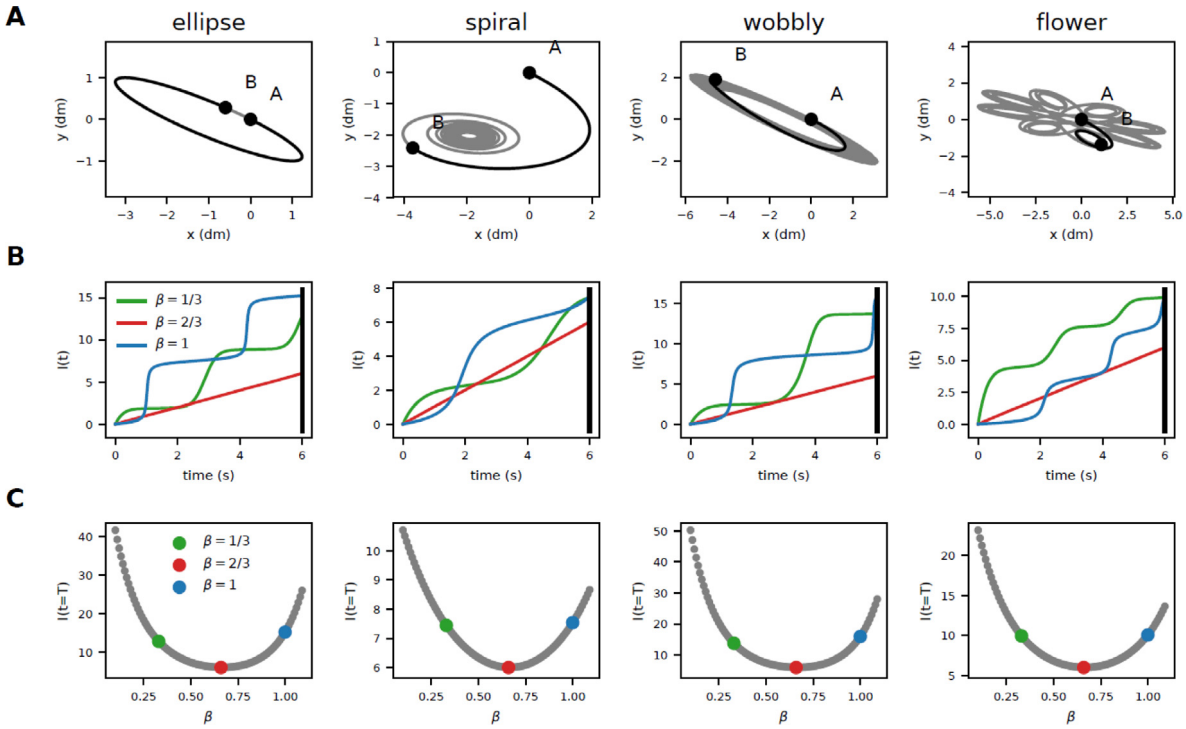

Fig. 4. Numerical evidence that the time integral of D is (locally) minimal when D is constant. (**A**) Start and end points of trajectory segments (of 6 s of duration) for each of the four main curves. (**B**) The time integral of D as time elapses from the beginning to the end of the segment. Respecting the same geometry and total duration of the movement, different kinematics were explored (generated by power laws with different exponents; depicted in green, red blue). (**C**) The integral of D, when numerically calculated for all exponents between 0 and 1 turns out to be minimal for $\beta = 2/3$ (red dot), for all curves. . (For interpretation of the references to color in this figure legend, the reader is referred to the web version of this article.)

Methods. The resulting trajectory does not necessarily have the desired average speed. The whole trajectory is then re-calculated with the same points and β, but with a different k parameter so that the total time elapsed is the same.

We illustrate the effects of the rescaling algorithm for the classical example of an ellipse (**Supplementary Figure 4A**). Generating an elliptical trajectory with orthogonal sine waves yields a $\beta = 2/3$ power law (**Supplementary Figure 4D**, red line). We can rescale this trajectory into $\beta = 1$ (blue line) and $\beta = 1/3$ (green line) power laws. The Y coordinate over time (**Supplementary Figure 4B**) of the $\beta = 2/3$ trajectory is shown in red, and is a pure sinusoid. A trajectory with exponent $\beta = 1$ is more 'round' in the Y coordinate, and a trajectory with $\beta = 1/3$ is more 'triangular'. The arc-length for the $\beta = 2/3$ trajectory changes over time: an object moving on such a trajectory slows down in more curved parts, and speeds up in straighter parts of the path (**Supplementary Figure 4C**). Because human participants produce speed profiles similar to these, the $\beta = 2/3$ trajectory is called 'natural'. In comparison, a trajectory with $\beta = 1$ is called 'hyper-natural' and has a constant arc length, because it has constant tangential speed. Trajectories with $\beta = 1/3$ are called 'hypo-natural', as they slow down more and speed up more than $\beta = 2/3$ 'natural' trajectories. Similar relationships are visible in the speed over cumulative arc length plot (**Supplementary Figure 4E**), illustrating the transformations made by the rescaling algorithm. When shortening the time period of crossing the same distance, we get higher speed, as illustrated by the peaks of the $\beta = 1/3$ (green) plot. For longer times, speed goes down, as in the valleys of the $\beta = 1/3$ plot. Angular speed over time (**Supplementary Figure 4F**) shows some inverted relationships. Here, the hyper-natural trajectory has the highest peaks and lowest valleys of the three trajectories.

3.5. Equi-affine displacement is invariant under different kinematics

We have seen how the time integral of the term D is minimal when D is constant. However, we have also seen that D does not correspond to mechanical power, and so the minimization of D does not imply that the power law is the outcome of the least action principle of physics. Mechanical work is not necessarily minimal for power-law kinematics with a 2/3 exponent (**Supplementary Figure 5**). Is there any other quantity whose integral, when minimized, lends itself to a meaningful interpretation?

The cubic root of D has been identified as the so-called equi-affine speed (Flash & Handzel, 2007; Pollick & Sapiro, 1997): $V_{EA} = D^{1/3}$. Of course V_{EA} is constant when D is constant. But note that the fact that the integral of D is minimal when D is constant does not mean that the integral of V_{EA} is minimal when V_{EA} is constant. And so we asked: what happens if we minimize the integral of V_{EA}?

We can answer the question mathematically by means of variational calculus. When deriving the Euler–Lagrange equation that results in minimizing the equi-affine speed as the Lagrangian, we found that the terms in that equation cancel out completely. To be concrete, first one needs to rewrite V_{EA} as (dx/dt) times a second term which is d^2y/dx^2 raised to the 1/3 power. This turns out to be a very convenient mathematical rewriting as shown in Lebedev et al. (2001). Then, the partial derivative of the Lagrangian with respect to the time derivative of x yields simply that second term. Finally, when calculating the time derivative of that term in order to obtain the second term of the Euler–Lagrange second-order partial differential equation, one realizes that it is exactly equal to the first term of the Euler–Lagrange equation, namely, the partial derivative of V_{EA} over x. Thus, both terms cancel out. So, are not there any particular solutions that make the functional an extremum?

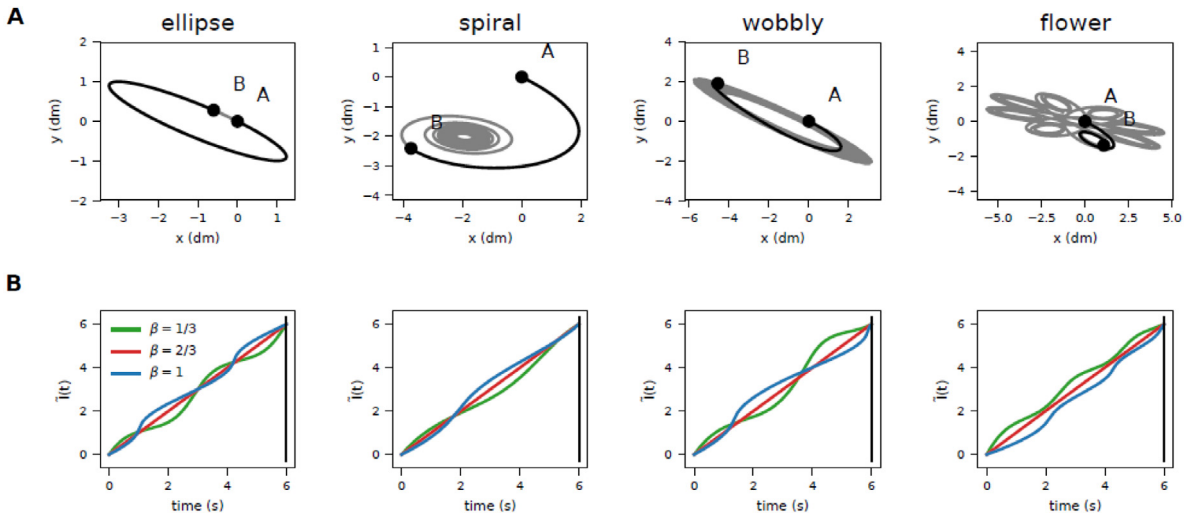

Fig. 5. The time integral of equi-affine speed is invariant for different kinematics with fixed geometry. (A) Trajectory segments of duration T (in black) with their start and end points. (**B**) Time integral of equi-affine speed for various kinematics (power laws of different exponents). Unexpectedly, all kinematics lead to the same value of the integral at t = T, for all curve segments.

We then answered the question numerically. We followed in Figure 5 the same procedure as in Figure 4. We took our four main curves and chose a segment of duration T (Fig. 5A) and numerically estimated the time integral of V_{EA} upon movement along the same geometry with three different kinematics (Fig. 5B), this is, power laws with different exponents. To our surprise, and as opposed to the integral of D in Figure 4, the integral of V_{EA} yields the same value at the end of the segment (t = T) regardless of the kinematics. There seems to be no minimum. Is it thus an invariant?

Note that, generally, the time integral of speed along a path is precisely its total displacement. In fact, the integral of affine velocity is known as the equi-affine arc-length or the special affine arc-length (Izumiya & Sano, 1998). Our analytical and numerical results thus indicate that affine arc-length is invariant under different power law kinematics.

Next we asked whether such invariance remains when the kinematics does not follow a power law (**Supplementary Figure 6A**) and/or when the geometry between A and B is different (**Supplementary Figure 6B**). In a similar analysis to Figure 5, we show that the affine arc-length is the same for power law and non-power law kinematics. An elliptical trajectory segment (Figure 5.1 A) is traversed with power law kinematics (with exponent $\beta = 2/3$) (in black) and non-power law kinematics (with ellipse's sine angle theta increasing with time squared) (in red). The integral of equi-affine speed is the same for both (**Supplementary Figure 6A**).

Let us note an interesting pathological case: in movement from A to B in a straight line at constant speed, there is no acceleration vector, and so V_{EA} is zero and so is its integral.

To explore the effect of different ways to get from one point to another in space (geometry), not just in time (kinematics), we also tested three pseudo-random paths from points A to B. Using the procedure described in (**Supplementary Figure 4**), we imposed power law kinematics (black lines), while colored lines had non-power law kinematics, as shown in the middle plot. The integral of equi-affine speed is the same for both kinematics, but not across different geometries (**Supplementary Figure 6B**).

Equi-affine speed is not invariant under arbitrary transformations. It has been shown that equi-affine length is invariant under affine transformations using the signed volume of the parallelepiped created by vectors of first, second and third derivatives with respect to time of the curve r, raised to the power 1/6 (Pollick et al., 2009). Equi-affine speed has also been shown to be piecewise constant along movement segments and so, rather than Euclidean, it becomes a natural geometric description of hand trajectories (Bennequin et al., 2009; Flash & Handzel, 2007; Meirovitch et al., 2016; Polyakov et al., 2009). However, we have not been able to find an explicit claim that the time integral of equi-affine speed is a kinematic invariant, as our findings suggest.

3.6. Pure curves with two-third power law scaling minimize jerk

Having found a way to numerically estimate whether certain functionals (such as D and V_{EA} respectively in Figure 4 and Figure 5), are (locally) minimal for a fixed geometry upon different kinematics, we now apply the method to confirm (Huh & Sejnowski, 2015) mathematical derivations: minimum of total jerk is achieved for pure frequency curves when their kinematics follow a speed-curvature power law (where the exponent value β depends on the frequency ν of the curve).

It is well known now that ellipses (which we have shown to have ν near to 2), when traversed with a power law kinematics of $\beta = 2/3$ (which is how they are traced by humans), have minimum jerk (Huh & Sejnowski, 2015; Viviani & Flash, 1995; Wann et al., 1988). But, our knowledge, nobody has estimated this numerically. Nor has this claim been shown for the large family of curves that, despite not being an ellipse, have $\nu = 2$ (like those in Fig. 6A).

To that end, we show that quasi-pure curves with a peak at $\nu = 2$, produce minimum jerk when kinematically traversed at $\beta = 2/3$ (Fig. 6B). This confirms and expands the findings in Huh and Sejnowski (2015), at the same time that provides a numerical method to estimate and predict the intricate relationship between geometric purity, kinematic scaling and dynamic optimality for any drawn movement beyond (the ultra-studied) ellipses.

3.7. The subtle relationship between curve purity, scaling and optimality

Let us end with a fun and illustrative example to recapitulate. Tracing the contour of Homer Simpson's face (Fig. 7A) was drawn on an interactive graphics tablet, tracing the original image shown on the screen, in a single movement, without lifting the pen from the screen. The raw data are smoothed before analysis

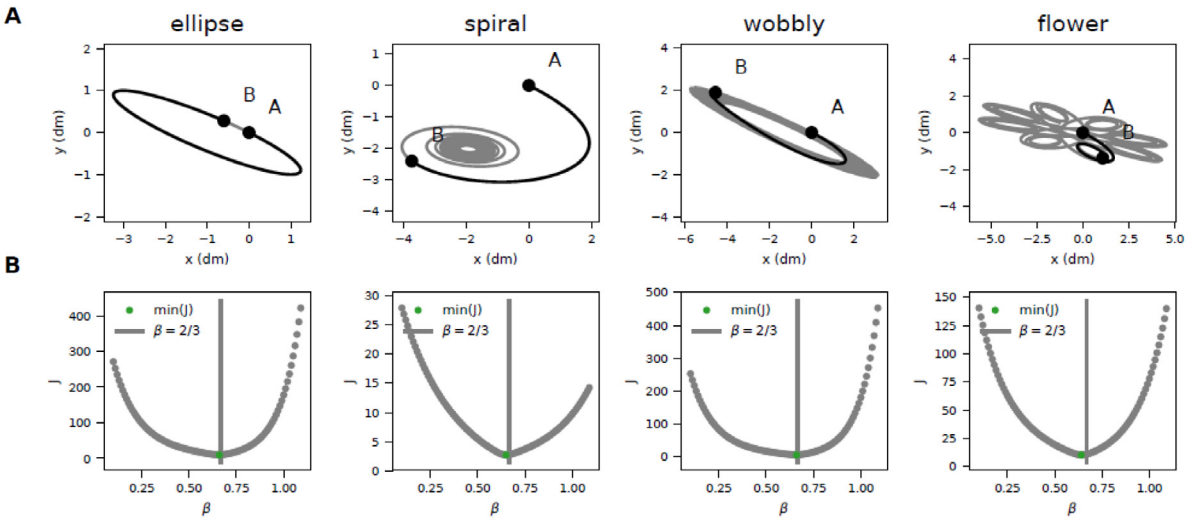

Fig. 6. Numerical estimation of minimum jerk for the four quasi-pure ($\nu = 2$) frequency curves. (**A**) Trajectory segments analyzed (in black). (**B**) Total jerk as a function of different power law kinematics shows a minimum near $\beta = 2/3$.

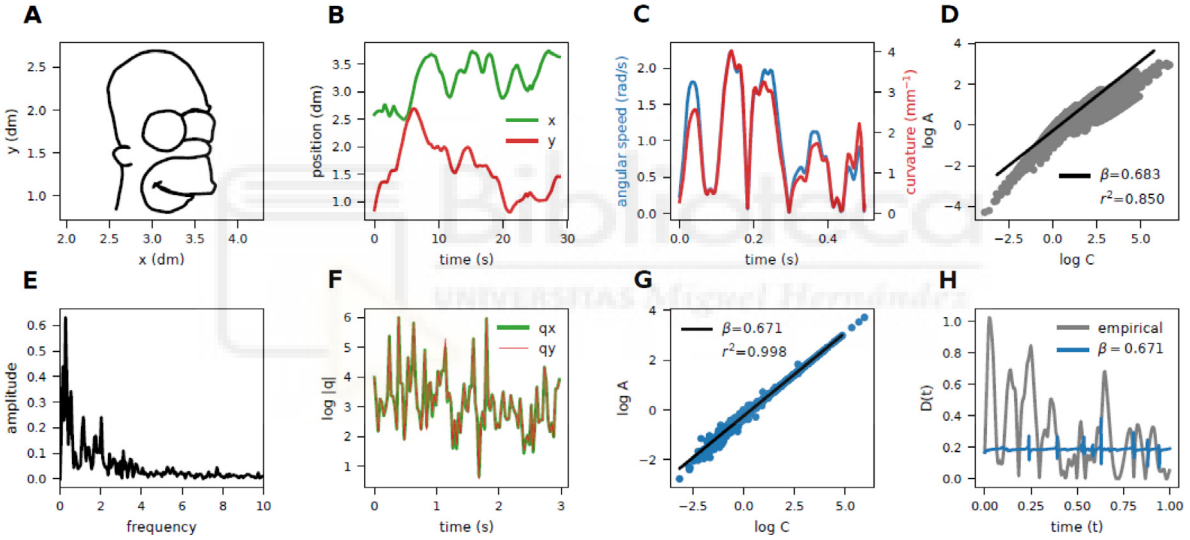

Fig. 7. Using Homer's face to illustrate purity, scaling and optimality in drawing movements. (**A**) Trace of Homer Simpson's face contours. (**B**) X and Y positions of the tip of the pen as a function of time. (**C**) Speed and curvature for a brief segment a function of time. (**D**) Log–log plot of speed and curvature reveals that kinematics does not comply with a power law. (**E**) Curve spectrum reveals that the drawing is not a pure-frequency geometry, having several peaks at low frequencies and a decreasing tail. (**F**) One can transform the original kinematics so that both X and Y follow the same third-order differential equation with the shared time-dependent parameter q(t), which can be calculated as the ratio between the third and first derivatives of position, shown here. (**G**) Homer's face now must follow a 2/3 power law. (**H**) The term D, as compared to the original drawing (gray) is quasi constant along the trajectory (blue). . (For interpretation of the references to color in this figure legend, the reader is referred to the web version of this article.)

(see **Methods**). The X and Y coordinates over time (Fig. 7B) show constant movement with no breaks. Curvature and velocity look fairly correlated (Fig. 7C), but do not exactly conform to a power law (Fig. 7D). In fact, the log–log plot seems to indicate multiple segments with different power law exponents, perhaps related to different segments of the drawing. The geometry spectrum analysis shows multiple peaks at low frequencies, and we can see that this is not a pure frequency curve (Fig. 7E).

The plots in Fig. 7F–H show a transformed trajectory: the geometry is the same (still Homer's face), but the empirical kinematics of drawing are transformed to strictly follow the 2/3 power law (Fig. 7G). From the same trajectory we can extract the function q(t), and we can see it is near-identical in X and Y dimensions (Fig. 7F) which, as we saw at the beginning of this article, is a hallmark of a 2/3 power law trajectory. Beyond ellipses, or the other three main curves systematically analyzed in this study, there are infinitely many ways to have a 2/3 power law trajectory (Homer's face included). As such, the magnitude of the cross product (the term D) is now near constant, unlike the empirical one, which is more variable (Fig. 7H).

Unfortunately for Homer, since its geometry is not pure (Fig. 7E), its tracing cannot enjoy both kinematic scaling (Fig. 7G) and dynamic optimality at the same time. In other words, if speed scales with curvature, drawing movements cannot be optimal in terms of jerk unless their curvature spectrum is pure. In fact, power-law kinematics do not produce minimum jerk dynamics if the curve geometry is not pure (**Supplementary Figure 7**). However, in general, one could have minimum jerk using some unknown minimization procedure for any non-pure geometry, with non-power law kinematics.

4. Discussion

Nearly forty years after its discovery, the two-thirds speed-curvature power law of human movement (Lacquaniti et al., 1983) is still puzzling. Moreover, evidence for the same scaling law with different exponents has recently been discovered empirically (Huh & Sejnowski, 2015), and demonstrated to be derivable from normative principles that require jerk (the time derivative of acceleration) accumulated along the trajectory to be minimal. Along those lines, it was claimed that the 2/3 speed-curvature power law of movement is a consequence of minimizing mechanical power (Lebedev et al., 2001). If so, the power law could be seen as both an outcome of minimum jerk (Flash & Hogan, 1985) and "an outcome of least action" (Lebedev et al., 2001). That would be interesting, were it true. However, here we have demonstrated that this is not the case. We have discovered a flaw in the derivation of Lebedev and colleagues, which is due to a basic physics error in interpreting mechanical work (to take the dot product of two vectors as that of their magnitudes). Thus, the connection the authors draw between the term D and mechanical work is inexistent. This invalidates the main claim of their paper. Drawing movements complying with the two-thirds power law do not minimize mechanical work.

The origins of the speed-curvature power law remain debated to date. Therefore, we deemed it necessary that the (to the best of our knowledge) undetected mistake in Lebedev et al. (2001) – and its corresponding unexpected link to equi-affine speed, in the line of the work by Flash and colleagues – does not continue unreported and uncorrected.

However, two pieces of their mathematical treatment are still valuable when expanded upon. They provide more insights to further understand the 2/3 speed-curvature power law observed in humans while drawing. First, their mathematical treatment demonstrates that drawing movements complying with the 2/3 power law must obey a third-order linear ordinary differential equation that only depends on a time-dependent coefficient q(t). The authors explored only the family of x(t) and y(t) solutions when q(t) is constant in time, which comprises ellipses, hyperbolas and parabolas. Here we exploited other non-trivial curves of the myriad of geometries that can stem from time dependencies in q(t). Second, the variational principle they put forth demonstrates that D (rather than the work) is minimal when it is constant. We tested it numerically, and reformulated it to show that equi-affine displacement of trajectories is invariant upon different power-law and non-power-law kinematics. We also demonstrated that $\beta = 2/3$ power laws with geometrical frequency ν close to 2 (namely, ellipses but other curves too) have minimum jerk.

Our work has limitations and poses some challenges. First, note that except the hand-drawn ellipse and Homer's face, the rest of our analysis is based on mathematics and numerically simulated curves. Further studies should mirror our findings in human experiments inspired by them. Second, all our numerical estimates regarding minimization demonstrate local, but not global, minima (we explored the space of β parameters). Third, a very interesting aspect remains fairly unexplored: while the equation that generates all possible 2/3 power law movement trajectories is a third-order differential equation, in physics virtually all equations of motion do not go beyond second-order. Fourth, while in most traces and drawings one constantly switches from clockwise to counter-clockwise movement, all trajectories explored in this manuscript (except Homer's) were monotonic in curvature. Fifth, it is still a challenge to robustly estimate jerk from empirically measured trajectories because of sensitivity to filtering and to noise in the derivatives.

To end, let us emphasize that the discovery of non-trivial constraints in nature – like a power law – is always as puzzling as rewarding. Kepler established one for the motion of orbiting planets. Lacquaniti and colleagues found another one for the movement of drawing hands. Both characterized by an exponent whose value is exactly 2/3. In 1981 Yoshio Koide uncovered a yet-unexplained relation between the masses of three elementary particles (the three charged leptons, namely, the electron, the muon, and the tau): their sum divided by the square of the sums of their square roots is approximately equal to 2/3. If that was not enough, the same relation holds for the masses of the three heaviest quarks. It is tempting to dismiss such phenomenological discoveries as mere numerology or, at best, as compressed descriptions awaiting the hard-core science to take place. This is even more so in biology, where mechanism is king while phenomena often enjoy epiphenomenal connotations. However, as we hope to have illustrated here, phenomena borrow from mechanisms the reasons by which they are explained. but restore those reasons to mechanisms in the form of scientific questions which they have stamped with their own meaning. The depth that an answer provides crucially depends on the quality of the question being asked in the first place. Science, in a way, is like good journalism.

CRediT authorship contribution statement

Adam Matic: Analyses, Figures, Manuscript. **Alex Gomez-Marin:** Idea and conceptualization, Analyses, Mathematical calculations, Figures, Manuscript.

Acknowledgments

We thank Regina Zaghi-Lara for drawing Homer's face.

Funding

The authors declare no competing financial interests. The work was supported by the Spanish Ministry of Science (grant BFU-2015-74241-JIN to AGM; pre-doctoral contract BES-2016-077608 to AM) and by the Severo Ochoa Center of Excellence programs (SEV-2013-0317 start-up funds to AGM).

Appendix A. Supplementary data

Supplementary material related to this article can be found online at https://doi.org/10.1016/j.jmp.2020.102453.

References

Bailly, F., & Longo, G. (2011). *Mathematics and the natural sciences: the physical singularity of life*. London: Imperial College Press.

Bennequin, D., Fuchs, R., Berthoz, A., & Flash, T. (2009). Movement timing and invariance arise from several geometry. *PLOS Computational Biology*, *57*, Article e100042. http://dx.doi.org/10.1371/journal.pcbi.10004266.

Flash, T., & Handzel, A. A. (2007). Affine differential geometry analysis of human arm movements. *Biological Cybernetics*, *96*(6), 577–601. http://dx.doi.org/10.1007/s00422-007-0145-5.

Flash, T., & Hogan, N. (1985). The coordination of arm movements: an experimentally confirmed mathematical model. *Journal of Neuroscience*, *5*(7), 1688–1703. http://dx.doi.org/10.1523/JNEUROSCI.05-07-01688.1985.

Flash, T., Karklinsky, M., Fuchs, R., Berthoz, A., Bennequin, D., & Meirovitch, Y. (2018). Motor compositionality and timing: Combined geometrical and optimization approaches. *Biomechanics of Anthropomorphic Systems*, *15*, 5–184. http://dx.doi.org/10.1007/978-3-319-93870-7_8.

Gomez-Marin, A. (2017). Causal circuit explanations of behavior: Are necessity and sufficiency necessary and sufficient? In A. Çelik, & M. Wernet (Eds.), *Decoding neural circuit structure & function*. Springer, http://dx.doi.org/10.1007/978-3-319-57363-2_11.

Huh, D. (2015). The vector space of convex curves: How to mix shapes. arXiv preprint: https://arxiv.org/abs/1506.07515.

Huh, D., & Sejnowski, T. J. (2015). Spectrum of power laws for curved hand movements. *Proceedings of the National Academy of Sciences*, *112*(29), 3950–3958. http://dx.doi.org/10.1073/pnas.1510208112.

Izumiya, S., & Sano, T. (1998). Generic affine differential geometry of plane curves. *Proceedings of the Edinburgh Mathematical Society*, *41*(2), 315–324. http://dx.doi.org/10.14943/83457.

Kepler, J. (1609). New astronomy astronomia nova aitIOΛoΓhTOΣ seu physica coelestis, tradita commentariis de motibus stellae martis ex observationibus g.V. Tychonis brahe.

Kepler, J. (1619). *The harmony of the world [harmonices mundi.*

Krakauer, J. W., Ghazanfar, A. A., Gomez-Marin, A., MacIver, M. A., & Poeppel, D. (2017). Neuroscience needs behavior: correcting a reductionist bias. *Neuron*, *933*, 480–490. http://dx.doi.org/10.1016/j.neuron.2016.12.041.

Lacquaniti, F., Terzuolo, C., & Viviani, P. (1983). The law relating the kinematic and figural aspects of drawing movements. *Acta Psychologica*, *54*(1–3), 115–130. http://dx.doi.org/10.1016/0001-6918(83)90027-6.

Lebedev, S., Tsui, W. H., & Van Gelder, P. (2001). Drawing movements as an outcome of the principle of least action. *Journal of Mathematical Psychology*, *45*, 43. http://dx.doi.org/10.1006/jmps.1999.1287, 52.

Matic, A., & Gomez-Marin, A. (2019). A customizable tablet app for hand movement research outside the lab. *Journal of Neuroscience Methods*, *328*, Article 108398. http://dx.doi.org/10.1016/j.jneumeth.2019.108398.

Meirovitch, Y., Bennequin, D., & Flash, T. (2016). Geometrical invariance and smoothness maximization for task-space movement generation. *IEEE Transactions on Robotics*, *32*(4), 837–853. http://dx.doi.org/10.1109/TRO.2016.2581208.

Newton, I. (1687). *Philosophiæ naturalis principia mathematica.*

Pollick, F. E., Maoz, U., Handzel, A. A., Giblin, P. J., Sapiro, G., & T., Flash (2009). Three-dimensional arm movements at constant equi-affine speed. *Cortex*, *45*(3), 325–339. http://dx.doi.org/10.1016/j.cortex.2008.03.010.

Pollick, F. E., & Sapiro, G. (1997). Constant affine velocity predicts the 1/3 power law of planar motion perception and generation. *Vision Research*, *37*(3), 347–353. http://dx.doi.org/10.1016/S0042-6989(96)00116-2.

Polyakov, F., Stark, E., Drori, R., Abeles, M., & Flash, T. (2009). Parabolic movement primitives and cortical states: merging optimality with geometric invariance. *Biological Cybernetics*, *100*(2), 159–184. http://dx.doi.org/10.1007/s00422-008-0287-0.

Schwartz, A. B. (1994). Direct cortical representation of drawing. *Science*, *265*, 540–542. http://dx.doi.org/10.1126/science.8036499.

Viviani, P., & Flash, T. (1995). Minimum-jerk, two-thids power law, and isochrony: convering approaches to movement planning. *Journal of Experimental Psychology: Human Perception and Performance*, *21*(1), 32–53. http://dx.doi.org/10.1037/0096-1523.21.1.32.

Wann, J., Nimmo-Smith, I., & Wing, A. M. (1988). Relation between velocity and curvature in movement: equivalence and divergence between a power law and a minimum-jerk model. *Journal of Experimental Psychology: Human Perception and Performance*, *14*(4), 622. http://dx.doi.org/10.1037/0096-1523.14.4.622.

West, G. (2011). *Scale: the universal laws of growth, innovation, sustainability, and the pace of life in organisms, cities, economies, and companies.* NY: Penguin Press.

Zago, M., Lacquaniti, F., & Gomez-Marin, A. (2016). The speed-curvature power law in Drosophila larval locomotion. *Biology Letters*, *12*, Article 201605. http://dx.doi.org/10.1098/rsbl.2016.0597.

Zago, M., Matic, A., Flash, T., Gomez-Marin, A., & Lacquaniti, F. (2018). The speed-curvature power law of movements: a reappraisal. *Experimental Brain Research*, *236*(1), 69–82. http://dx.doi.org/10.1007/s00221-017-5108-z.

Annex 4:

Matić, A., & Gomez-Marin, A. (2022). Angular speed should be avoided when assessing the speed-curvature power law of movement. bioRxiv. DOI: 10.1101/2022.06.27.497695

Angular speed should be avoided when assessing the speed-curvature power law of movement

Adam Matić & Alex Gomez-Marin

Behavior of Organisms Laboratory,
Instituto de Neurociencias CSIC-UMH, Alicante, Spain
(Correspondence to: adam.matic@gmail.com)

Abstract. The speed-curvature power law is an intriguing constraint between the geometry and the kinematics of a movement trajectory. It dictates, for instance, how much slower the hand should move in curves. The empirical phenomenon has led to various interesting theoretical proposals for its origin and possible generating processes. Its formulation based on tangential speed ($V \sim C^{\beta}$) is considered equivalent to its angular speed counterpart ($A \sim C^{\beta+1}$), with the corresponding change in the exponent. In the case of drawing ellipses, these relationships are respectively known as the "one-third power law" or the "two-thirds power law", after the values of the exponents. Here we show that using angular speed instead of tangential speed tends to result in much stronger data correlations, impacting on the interpretation of the strength of relationship, the putative value of the exponents, and even the very existence of the power law. We explain how and why this is the case, using both empirical and synthetic data. We conclude that angular speed should be avoided when expressing the speed-curvature power law.

Keywords: motor control, speed-curvature, power law, geometry, kinematics.

*

1. INTRODUCTION

The relationship between instantaneous speed and local curvature in human movement is a classic, fascinating, and well-studied phenomenon in the field of motor control. Its historical roots can be dated to the observations of Binet and Courtier (1893) and Jack (1895) that in 'natural handwriting' the speed of the pen tends to be lower in curved segments of the path and higher in the straight segments. Lacquaniti and colleagues (1983) proposed that the relationship can be expressed as a power law and reported its validity for a large class of hand movements. The law has since been observed also in human locomotion, speech, eye movements, and even in the trajectories of animals (Zago et al, 2016). For a recent review, see (Zago, Matić et al, 2017).

The speed-curvature power law is expressed in several ways, involving either tangential speed or angular speed as kinematic variables and curvature or radius of curvature as geometric variables. Different formulations are often explicitly considered to be *equivalent* (e.g. Lacquaniti et al. 1983; Viviani and Cenzato, 1985; Wann et al. 1988; Viviani and Schneider, 1991; Schaal and Sternad, 2001; Vieilledent et al. 2001; Ivanenko et al. 2002; Perrier and Fuchs, 2008; Maoz et al. 2009; Tesio et al. 2011; Huh and Sejnowski, 2015; Karklinsky et al. 2016; Zago, Matić et al. 2017; Rybarczyk and Carvalho 2019; Matić and Gomez-Marin 2020).

Indeed, examining the algebraic relationships shows that the exponents in different formulations of the power law are mathematically related. Namely, with angular speed A, curvature C, and a constant k (related to average speed, also called the velocity gain factor), one has the "AC power law" as:

$$A = kC^{\beta} \quad (1)$$

With tangential speed V, since A=VC, one gets the "VC power law":

$$V = kC^{\beta-1} \quad (2)$$

If instead of curvature C, one uses the radius of curvature $R = C^{-1}$, the exponent of the power law would simply be: $A = kR^{-\beta}$ or $V = kR^{1-\beta}$. See also Figure 1 for definitions of variables.

It turns out that, in drawing ellipses and scribbling movements, the exponent of the AC power law (equation 1) is empirically found to be $\beta \approx 2/3$ (Lacquaniti et al. 1983), a phenomenon known as the "2/3 power law". If one chooses to analyze the same trajectories with the VC power law (equation 2), the exponent is near -1/3, and the phenomenon is sometimes called the "1/3 power law". Regardless of the name used, most published research uses tangential speed and curvature, the VC power law, as expressed in equation (2). The use of angular speed is relatively rare, but it is frequent enough to warrant scrutiny (e.g. Lacquaniti et al. 1983, Ivanenko et al 2002; Zago, Matić et al. 2017; James et al. 2019).

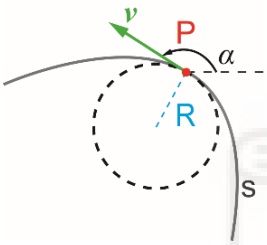

Figure 1. For a particle P moving along the path s, speed (V) is defined as the magnitude of the (tangential) velocity vector, $V = |\mathbf{v}| = \left|\frac{ds}{dt}\right|$, while angular speed (A) is the absolute rate of change of the direction of velocity, $A = \left|\frac{d\alpha}{dt}\right|$, and curvature (C) is the reciprocal of the radius of the osculating circle, or the rate of change of direction with respect to arc-length, $C = \frac{1}{R} = \left|\frac{d\alpha}{ds}\right|$. From this we see that, naturally, A=VC.

Crucially, these mathematical relationships show an equivalence of exponents between relationships, but not an equivalence of *strength* of the underlying relationship.

In the research on the power law of movement, power functions (1) and (2) are typically converted to linear functions by taking a logarithm of both sides. Next, the exponents β, the speed gain factor k and the strength of the relationship, expressed as the coefficient of determination r^2 are estimated by linear regression from models:

$$\log A \approx \log k + \beta_{AC} \log C \quad (3)$$
$$\log V \approx \log k + \beta_{VC} \log C \quad (4)$$

In linear regression, the coefficient of determination (r^2), shows how much variance in the outcome is explained by the predictors, expressing the strength of the linear relationship. When there are only two variables in a regression, the r^2 is the square of the correlation coefficient r (Pearson's or other). More generally, it is calculated as $r^2 = 1 - RSS/TSS$ where RSS is the sum of squares of residuals and TSS the total sum of squares of the outcome. If the relationship between variables has a high r^2 (near 1), one can predict with high accuracy the value of the outcome variable from the values of the predictors.

Here we look carefully at the differences between the coefficients of correlation and determination in the formulations of the power law involving different kinematic variables, tangential speed V and angular speed A. We show that there are big differences in empirical and synthetic data, explain why the differences exist, and suggest how to interpret different formulations of the power law.

2. EMPIRICAL DATA: Tracking elliptic targets at different frequencies

Methods

We analyzed pen trajectories recorded in a target tracking experiment (Matić and Gomez-Marin, *in preparation*).

Participants were seated, looking at a computer monitor, while holding an electronic pen in their dominant hand on a graphics tablet. There was a small circular target displayed on the screen. The pen determined the position of a circular cursor on the screen, and the task of the participant was to track the target with the cursor. Targets always moved in an elliptical pattern. Target trajectories varied across trials (i) in 9 different frequencies, from slow rhythms to fast, and (ii) in 3 different speed profiles: constant speed (β_{VC}=0), 'natural speed' (β_{VC}=-1/3) and 'extra slowing' (β_{VC}=-2/3). Each participant (three males) performed 27 trials of target tracking, lasting 16 seconds, presented in a random order.

The recorded trajectories were smoothed by a second-order, low-pass Butterworth filter with a cutoff at 10Hz, and differentiated to estimate speed and curvature. The power law exponents β and the coefficients of determination r^2 were estimated using linear regression. Conformity to the power law was chosen at an arbitrary point of $r^2 > 0.75$, considering that pure gaussian noise can produce a fit of up to $r^2 \approx 0.6$ (Maoz et al, 2005).

All of the data and the code in python for analysis and generating the figures are available in an online repository: https://github.com/adam-matic/AngularSpeedPowerLaw.

Results

The plot of the VC power law across frequencies (Figure 2) and the plot of the AC power law across frequencies (Figure 3) show that the values of exponents are equivalent; for each trajectory the following equality holds: $\beta_{AC} = \beta_{VC} + 1$. However, there is a dramatic difference in the coefficients of determination. For the VC power law, only the trajectories performed at fast rhythms of $f \geq 0.94$ conformed to the power law with the coefficient of determination of $r^2 \geq 0.75$. On the other hand, angular speed is strongly correlated to curvature across the entire frequency range, with only a few exceptions of the power law estimates with $r^2 < 0.75$, and even then, the lowest value is $r^2 \approx 0.5$.

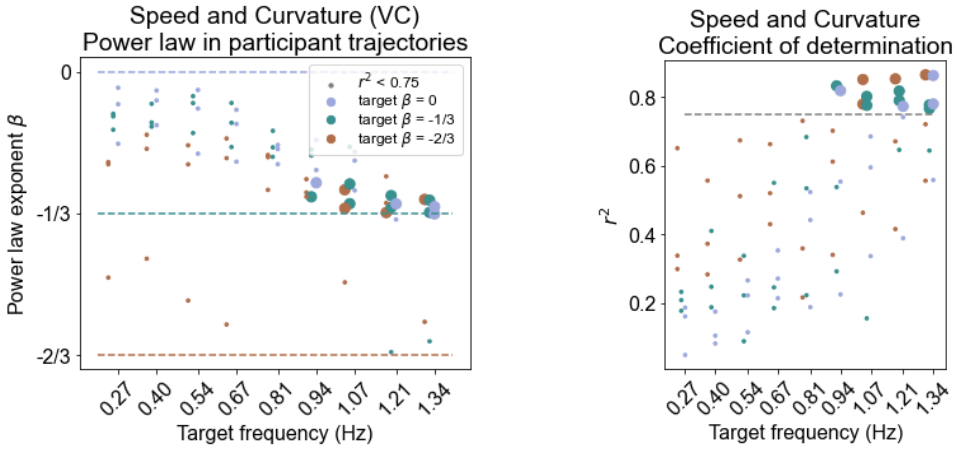

Figure 2. Using tangential speed and curvature to estimate the speed-curvature power law, only high-frequency participant trajectories (freq ≥ 0.94) conform to the power law with a coefficient of determination $r^2 \geq 0.75$. Many trajectories have a low r^2.

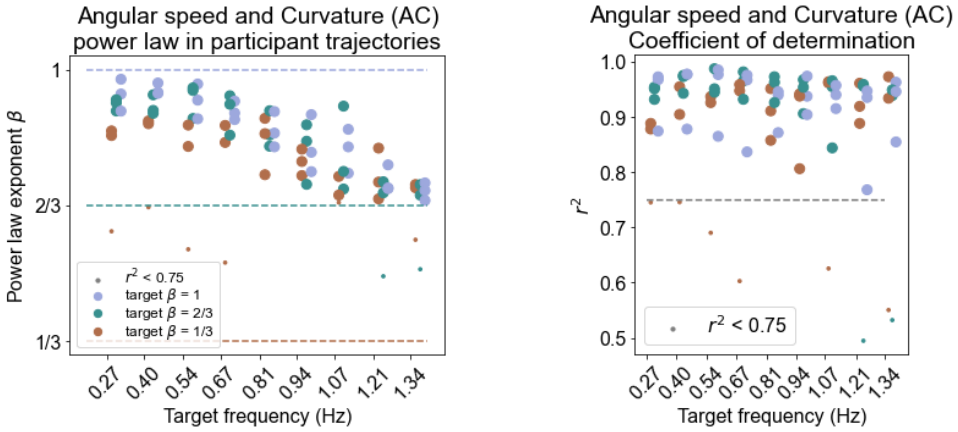

Figure 3. Using angular speed and curvature to estimate the speed-curvature power law, the r^2 is higher than 0.75 for most trials, making the AC power law apparently much stronger than the VC power law (see Figure 2).

Clearly, the VC and AC power laws are not equivalent (compare Figure 2 to Figure 3); the AC power law tends to be much stronger.

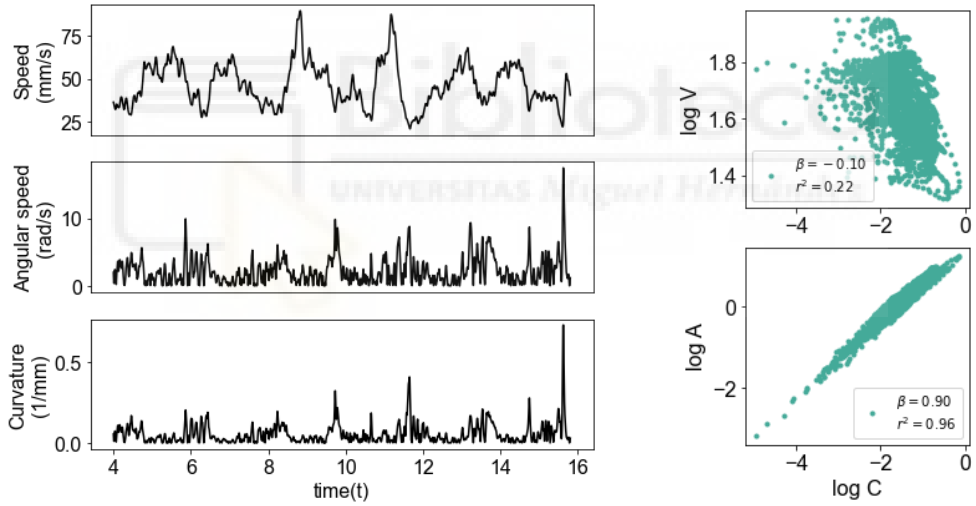

Figure 4. Example data from a single trial (target frequency = 0.27Hz), showing tangential speed, angular speed and curvatrue over time. The VC power law is fairly weak, showing that tangential speed is hardly related to curvatrue, while in this case the AC power law is very strong, angular speed being strongly correlated with curvature.

Figure 4 shows a common type of the differences in the estimated strength of the speed-curvature power law: when using angular speed, the power law is very strong while, for the same trajectory, tangential speed is very weakly related to curvature, apart from a slight tendency to slow down in more curved parts of the path.

In other words, there can be plenty of empirical cases in which the speed V of the cursor is hardly related to the curvature, while the speed of 'turning', or the rate of change of direction, is strongly related to curvature. In the following section we explore why this is the case by means of synthetic data.

3. SYNTHETIC DATA: Correlation between curvature and the two speeds

Methods

In simple linear regression, the coefficient of determination r^2 is equal to the square of Pearson's correlation coefficient r. The Pearson's correlation coefficient r is in turn defined as normalized covariance. To investigate the differences between the two power laws, here we focus only on the algebraic manipulations of correlations and covariances between the variables, and using simulations and random variables.

Elliptical trajectories were generated in the following way: first, we generated an elliptic trajectory with a given semi-minor and semi-major radius, frequency, and number of cycles. Next, we created a gaussian noise speed profile of the same length as the trajectory, smoothed it with a low-pass butterwort filter at 10Hz cutoff, and then generated a time profile for the elliptic trajectory by dividing the distances between the points with the desired speeds obtain from the random speed profile. Finally, we used a cubic spline to create constant time-sampling for the final elliptic trajectory.

Results

According to equation (4), in the VC power law one is correlating log C and log V; according to equation (3), for the AC power law one is correlating log C and log A. However, we also know that A=CV, and therefore log A = log C + log V. In considering the AC power law, we are, in effect, correlating log C with log C + log V.

Letting Cov = covariance, a = log A, c = log C, and v = log V, we can write:

Cov(c, a) = Cov(c, c+v) = Cov(c, c) + Cov(c, v) = Var c + Cov(c, v)

We can then see that Cov(c, a) will be dependent not only on the covariance of curvature and speed, but also on the variance of curvature. This means that the correlation coefficient will tend to be large when the curvature has a big variance relative to speed, regardless of the actual correlation between speed and curvature.

One can simply and effectively explore such a dependency as follows. Let us take two random normal variables x and y (Figure 5) and calculate the correlation coefficient between x and x + y, as an analogy to correlation of log C and log A. Letting Corr be equal to the Person's correlation coefficient, obviously, the correlation r = Corr(x, x+y) is *not equivalent* to the Corr(x, y), which is zero in all four cases. Instead, if we keep the standard deviation of y stable, the Corr(x, x + y) increases with the standard deviation of x.

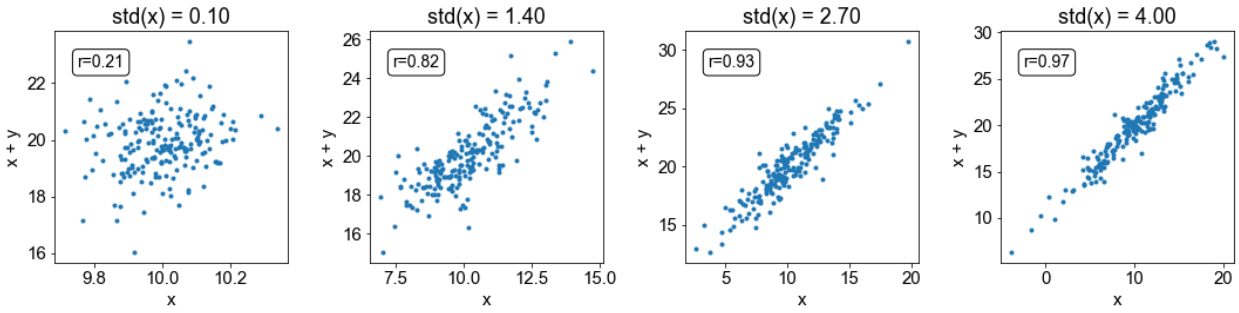

Figure 5. For two random normal variables x (mean 10, std in range [0.1, 4]) and y (mean 10, std 1), the variable x is not necessarily correlated to x+y, but it gets more strongly correlated as the variance of x increases.

The same effect of increasing the range of curvature can be illustrated with a random speed profile along a circular and along an elliptic trajectory. As shown on Figure 6A, the circular trajectory is designed to have a constant curvature profile and a random-smoothed speed profile. As expected, the correlation between logC and logV is very low, and so is the correlation between logC and logA. In the case of the ellipse (Figure 6B), the curvature profile has a bigger range, but the speed profile is identical to the circle. This single change was enough to increase the correlation between logC and logA to 1.

We further explore this effect in Figure 7. We show how the Pearson's correlation coefficient Corr(logC, logV) is near zero for all values the semi-major axis. This is expected, since the speed profile is randomized. However, for the correlation between angular speed and curvature, even a small increase in the semi-major axis, making the ellipse slightly eccentric, and making the curvature have slightly larger variance, increases the correlation Corr(logC, logA) to very high levels.

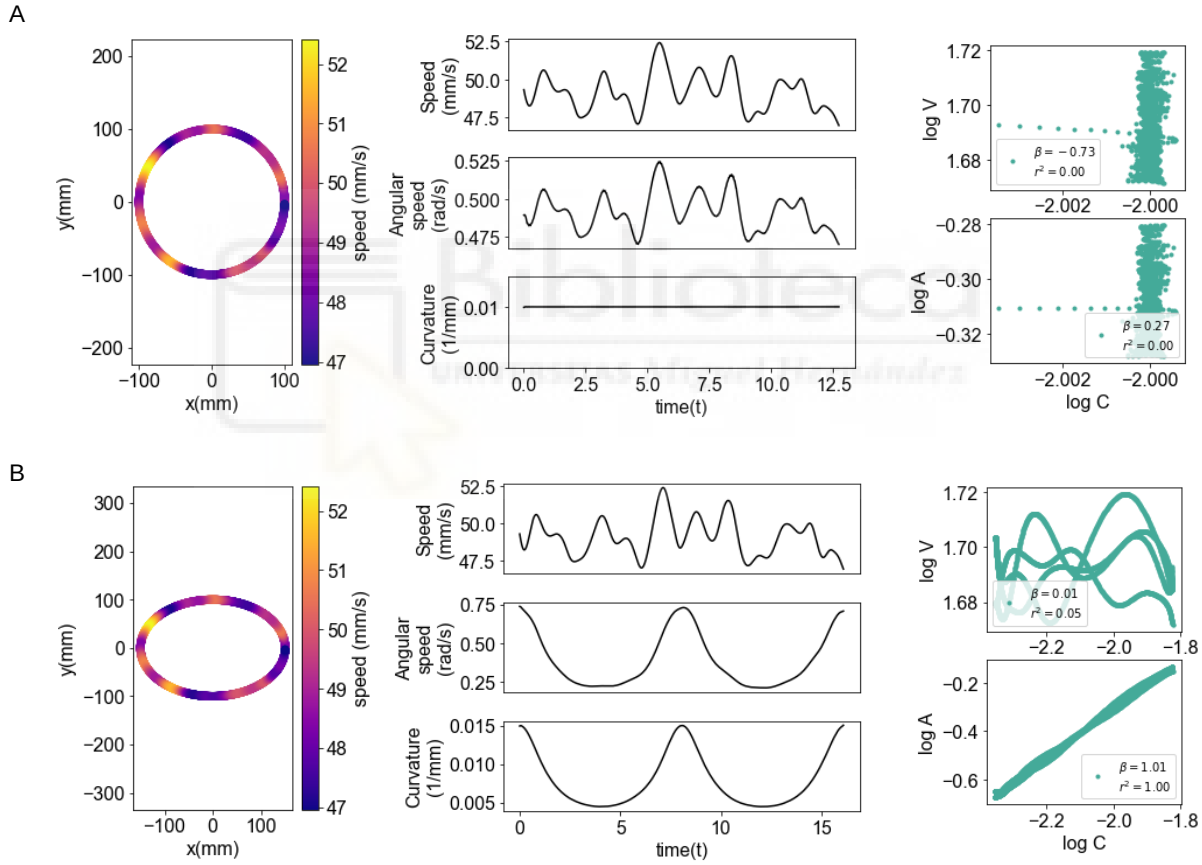

Figure 6. Correlation depends on the range of curvature in generated ellipses. **(A)** For a circular trajectory, radius of 100 mm, with a random-smoothed speed profile, both the logC-logV and logC-logA correlations are near zero. **(B)** For an elliptic trajectory, ra = 150 mm, rb =10 0mm, with the same speed profile, the logC – logV correlation is still low, while the logC-logA is very high. In this case, it is worth realizing that an exponent tending to β=1 for the AC power law already indicates, if one recalls the mathematics, that there will be no relation at all between tangential speed and curvature.

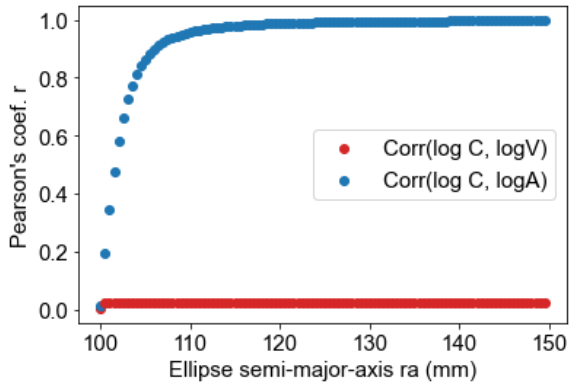

Figure 7. The correlation between logC and logA depends on the range of curvature, even in the absence of a speed-curvature power law. All ellipses had the same random-smoothed speed profile (see Figure 5), and the same semi-minor axis rb=100mm, while the curvature range was varied by increasing the semi-major axis. Note that, for instance, at 105 mm, which is 5% increase, the correlation is 0.87, and at 110 mm, which is a 10% increase, the correlation is 0.96.

4. DISCUSSION

Here we asked whether tangential speed and angular speed are equivalent in estimating the speed-curvature power law from data.

The analysis of empirical data from an experiment with human participants (Figures 2, 3 and 4) shows a huge difference between the two forms of the speed-curvature power law, generally considered to be equivalent. This difference can be explained in the following way: the VC version of the law is relating a purely kinematic variable (tangential speed) with a purely geometric variable (curvature), and is adequately reflecting the strength of the constraint in human movement. The correlation between angular speed and curvature, and the AC power law, have to be interpreted differently.

We also found that some types of movement (here fast drawing of ellipses at about 1s of cycle time or faster) show a strong speed-curvature power law, always with an exponent tending to $\beta vc \approx -1/3$. Other forms of movement don't show a strong speed-curvature power law, namely, drawing of slower ellipses (Figure 2).

We stress that this correlation is measuring a genuine phenomenon in movement, an invariance that needs to be explained by theories of human motor control. However, the correlation between angular speed and curvature will reflect the tendency that small-curvature segments have smaller angular speed; a generic fact we know a priori from A = CV.

Conceptually, one could think of the correlation between angular speed and curvature as the correlation between widths and areas of rectangles (area = width * height, or log area = log width + log height) in a set of rectangles of different sizes. In this idealized example, the correlation is not necessarily there, but in most cases, if we have a sufficient range of widths, the small-width rectangles can be associated with small areas, and large-width rectangles with large areas, regardless of their heights. The larger the range of widths, the stronger the correlation.

Although it is possible to measure (Figure 4) or construct (Figure 6) trajectories where angular speed and curvature that are hardly correlated at all, in most movement trajectories a great deal of the correlation between angular speed and curvature arises from the fact that the rate of change of

direction increases in direct proportion to curvature. As we have illustrated, a high correlation between logA and logC in an elliptical trajectory can arise it complete absence of kinematic-geometric constraints (Figure 6B and Figure 7).

Ever since the pioneering works of Binet and Courtier (1883), Jack (1895), and a century latter Lacquaniti et al (1983), one goal of movement science is to understand why there is a relationship between movement speed and curvature. In such a quest, the main message of this manuscript is that when estimating the correlation between kinematics and geometry of movement, one should better use mutually independent kinematic and geometric variables, such as tangential speed and curvature, avoiding angular speed, as it can often inject spurious correlations to curvature, leading to misinterpretations of the strength of the speed-curvature power law of movement.

*

Acknowledgements: We thank Roberto Montanari and Javier Alegre Cortés for their comments on earlier versions of the manuscript.

Author contributions. AM carried out the experiments, did the numerical simulations, performed the analyses, came out with the examples, and wrote the first draft of the manuscript. AGM supervised the research and edited the final version of the manuscript. All authors approved the final version.

Funding. AM was initially funded by the Spanish Ministry of Science (BES-2016-077608) and then self-funded. AGM is supported by the Spanish Ministry of Science.

Conflict of interests. The authors declare that the research was conducted in the absence of any commercial or financial relationships that could be construed as a potential conflict of interest.

*

REFERENCES

Binet, A., & Courtier, J. (1893). Sur la vitesse des mouvements graphiques. *Revue Philosophique de la France et de l'Etranger*, *35*, 664-671.

Ivanenko, Y. P., Grasso, R., Macellari, V., & Lacquaniti, F. (2002). Two-thirds power law in human locomotion: role of ground contact forces. *Neuroreport*, *13*(9), 1171-1174.

Jack, W. R. (1895). The analysis of voluntary muscular movements by certain new instruments. *Journal of Anatomy and Physiology*, *29*(Pt 4), 473.

James, L., Davies, T. E., Lim, K. S., & Reynolds, A. (2020). Do bumblebees have signatures? Demonstrating the existence of a speed-curvature power law in Bombus terrestris locomotion patterns. *PloS one*, *15*(1), e0226393.

Karklinsky, M., Naveau, M., Mukovskiy, A., Stasse, O., Flash, T., & Souères, P. (2016, June). Robust human-inspired power law trajectories for humanoid HRP-2 robot. In *2016 6th IEEE International Conference on Biomedical Robotics and Biomechatronics (BioRob)* (pp. 106-113). IEEE.

Lacquaniti, F., Terzuolo, C., & Viviani, P. (1983). The law relating the kinematic and figural aspects of drawing movements. *Acta psychologica*, 54(1-3), 115-130.

Maoz, U., Berthoz, A., & Flash, T. (2009). Complex unconstrained three-dimensional hand movement and constant equi-affine speed. *Journal of neurophysiology*, *101*(2), 1002-1015.

Maoz, U., Portugaly, E., Flash, T., & Weiss, Y. (2005). Noise and the two-thirds power law. *Advances in Neural Information Processing Systems*, *18*.

Matić, A., & Gomez-Marin, A. (2020). Geometric purity, kinematic scaling and dynamic optimality in drawing movements beyond ellipses. *Journal of Mathematical Psychology*, *99*, 102453.

Matić, A. & Gomez-Marin, A. (in preparation). Salient visual features in tracking elliptic targets and reproducing hand trajectories with a visuomotor phase-locked loop

Perrier, P., & Fuchs, S. (2008). Speed–curvature relations in speech production challenge the 1/3 power law. *Journal of neurophysiology*, *100*(3), 1171-1183.

Rybarczyk, Y., & Carvalho, D. G. (2019). Bioinspired implementation and assessment of a remote-controlled robot. *Applied Bionics and Biomechanics*, *2019*.

Schaal, S., & Sternad, D. (2001). Origins and violations of the 2/3 power law in rhythmic three-dimensional arm movements. *Experimental brain research*, *136*(1), 60-72.

Tesio, L., Rota, V., & Perucca, L. (2011). The 3D trajectory of the body centre of mass during adult human walking: Evidence for a speed–curvature power law. *Journal of biomechanics*, *44*(4), 732-740.

Vieilledent, S., Kerlirzin, Y., Dalbera, S., & Berthoz, A. (2001). Relationship between velocity and curvature of a human locomotor trajectory. *Neuroscience letters*, *305*(1), 65-69.

Viviani, P., & Cenzato, M. (1985). Segmentation and coupling in complex movements. *Journal of experimental psychology: Human perception and performance*, *11*(6), 828.

Viviani, P., & Schneider, R. (1991). A developmental study of the relationship between geometry and kinematics in drawing movements. *Journal of experimental psychology: human perception and performance*, *17*(1), 198.

Wann, J., Nimmo-Smith, I., & Wing, A. M. (1988). Relation between velocity and curvature in movement: equivalence and divergence between a power law and a minimum-jerk model. *Journal of Experimental Psychology: Human perception and performance*, *14*(4), 622.

Zago, M., Lacquaniti, F., & Gomez-Marin, A. (2016). The speed-curvature power law in Drosophila larval locomotion. Biology Letters 12: 20160597.

Zago, M., Matic, A., Flash, T., Gomez-Marin, A., & Lacquaniti, F. (2017). The speed-curvature power law of movements: a reappraisal. *Experimental brain research*, 236(1), 69-82.

*

Annex 5:

Matić, A., Valerjev, P., & Gomez-Marin, A. (2021). Hierarchical control of visually-guided movements in a 3D-printed robot arm. Frontiers in Neurorobotics, 149.
PMID: 34776921 DOI: 10.3389/fnbot.2021.755723

frontiers in Neurorobotics

ORIGINAL RESEARCH
published: 29 October 2021
doi: 10.3389/fnbot.2021.755723

Hierarchical Control of Visually-Guided Movements in a 3D-Printed Robot Arm

Adam Matić[1]*, *Pavle Valerjev*[2] *and Alex Gomez-Marin*[1]

[1] *Behavior of Organisms Laboratory, Instituto de Neurociencias CSIC-UMH, Alicante, Spain,* [2] *Department of Psychology, University of Zadar, Zadar, Croatia*

The control architecture guiding simple movements such as reaching toward a visual target remains an open problem. The nervous system needs to integrate different sensory modalities and coordinate multiple degrees of freedom in the human arm to achieve that goal. The challenge increases due to noise and transport delays in neural signals, non-linear and fatigable muscles as actuators, and unpredictable environmental disturbances. Here we examined the capabilities of hierarchical feedback control models proposed by W. T. Powers, so far only tested *in silico*. We built a robot arm system with four degrees of freedom, including a visual system for locating the planar position of the hand, joint angle proprioception, and pressure sensing in one point of contact. We subjected the robot to various human-inspired reaching and tracking tasks and found features of biological movement, such as isochrony and bell-shaped velocity profiles in straight-line movements, and the speed-curvature power law in curved movements. These behavioral properties emerge without trajectory planning or explicit optimization algorithms. We then applied static structural perturbations to the robot: we blocked the wrist joint, tilted the writing surface, extended the hand with a tool, and rotated the visual system. For all of them, we found that the arm *in machina* adapts its behavior without being reprogrammed. In sum, while limited in speed and precision (by the nature of the do-it-yourself inexpensive components we used to build the robot from scratch), when faced with the noise, delays, non-linearities, and unpredictable disturbances of the real world, the embodied control architecture shown here balances biological realism with design simplicity.

Keywords: robot arm, perceptual control theory, reaching, tracking, human movement

Edited by:
Claudio Castellini,
University of Erlangen Nuremberg, Germany

Reviewed by:
Ye Ma,
Ningbo University, China
Roberto Meattini,
University of Bologna, Italy

***Correspondence:**
Adam Matić
adam.matic@gmail.com

Received: *09 August 2021*
Accepted: *08 October 2021*
Published: *29 October 2021*

Citation:
Matić A, Valerjev P and Gomez-Marin A (2021) Hierarchical Control of Visually-Guided Movements in a 3D-Printed Robot Arm. Front. Neurorobot. 15:755723. doi: 10.3389/fnbot.2021.755723

INTRODUCTION

Pointing and reaching toward visual targets are nearly effortless human behaviors. However, an explanation of these processes at levels of detail and abstraction that would allow us to build equally capable artificial systems or to treat common disorders in hand and arm control remains elusive. An understanding of such simple motor behaviors should follow from a broader theory of sensorimotor control, while being consistent with the anatomical structure of the underlying system. Such an understanding would provide insights into the origin of laws, invariances, and principles in the behavior of organisms.

The anatomical structure of the nervous system, together with the behavioral analysis of organisms under different conditions and upon different perturbations, suggests that biological control is hierarchical. One of the earliest hypotheses on the hierarchical nature of the nervous system was proposed by Hughlings Jackson (1884, 1958), discussing the possible evolutionary development of the nervous system in layers (see also Prescott et al., 1999). In turn, neurophysiologist Nikolai Bernstein proposed a hierarchical organization of neural structures underlying movement, where each layer performs a specific function, increasing in abstraction as one ascends the hierarchy (see Profeta and Turvey, 2018). Arguments for the existence of hierarchy of control can also be made from the comparative evolutionary history of the nervous system (Cisek, 2019) and from early development in primates (Plooij and van de Rijt-Plooij, 1990).

However, some findings in spinalized preparations blur the line between the capabilities of different levels in motor control. Cats with a transected spinal cord or cats in a decerebrate preparation can learn to walk on a treadmill (Whelan, 1996); decerebrate ferrets can learn new locomotion trajectories (Lou and Bloedel, 1988, 1992); rats with lesions in the motor cortex can still move in stable, predictable, non-perturbing environments, but not if the environment is rapidly changing (Lopes, 2016). Those experiments show the existence of independent "lower levels" in the spinal cord, capable of relatively complex behaviors on its own, despite normally operating in accord with the higher levels. Therefore, while the consensus seems to be that biological control is hierarchical, it is still unclear what is the function of each particular level, what are their limits and relationship, or even why there is a hierarchy at all.

Hierarchical architectures have been used in robotics, famously by Brooks in the subsumption architecture (Brooks, 1986). More recently, Merel et al. (2019) listed core advantages of hierarchical control appearing in both biological and engineered systems. Hierarchies allow for modularization and simplification of individual controllers and training procedures. Each subsystem can deal with only a part of the incoming sensory information, and, having partial autonomy, can be trained separately with cost functions and performance requirements distinct from the task objective. In contrast, "flat" non-hierarchical controllers receive and process all the sensory information, and directly calculate the behavioral output. Such arrangements make the control algorithm complex, require extensive training, and result in rather incomprehensible information flows. Thus, at least from an engineering perspective, hierarchical architectures can be very beneficial for adaptive behavioral control.

A prominent normative approach to motor behavior is optimal feedback control (Todorov and Jordan, 2002a; Scott, 2004, 2012; Shadmehr and Krakauer, 2008). The theory predicts many of the features of human movement and corrects a long-standing bias against the importance of sensory feedback in online movement (e.g., Flash and Hogan, 1985; Uno et al., 1989). However, this theoretical framework does not necessarily suggest a neural substrate for implementation of the proposed control algorithms. In fact, it is still debated whether some features of the optimal feedback control architecture, such as internal forward and inverse models are necessary, computationally too complex, and whether they can be found in the brain or not (Loeb, 2012; McNamee and Wolpert, 2019; Hadjiosif et al., 2021). Briefly, forward models estimate the current state from a copy of the motor command and the delayed sensory signals, while the inverse models (also called controllers) provide a motor command that will achieve the desired state given the current state and an inverted model of the plant (Wolpert and Kawato, 1998). The theory does not explicitly address the hierarchical structure of motor control or the role of sensory feedback in subcortical levels and the spinal cord.

Exploring the computational principles that underlie eye-hand coordination and synergistic control in pointing and reaching, William T. Powers designed a series of distinct models of arm control. The first one (Powers, 1999) contained a model of muscles, an arm with three degrees of freedom (DOF) and a binocular vision control layer. The organization of this control system follows roughly the anatomical hierarchical organization of the spinal and some supra-spinal neural structures involved in human motor control and arm coordination. The second model (Powers, 2008) consisted of a 14 DOF arm with more fidelity in arm segment lengths and joint movement limits, but it lacked the muscle model. These models were built by cascading multiple layers of simple proportional and proportional-derivative feedback loops with low-pass filtering. Using hierarchically arranged controllers, and a selection of biologically-inspired controlled variables, Powers managed to avoid computationally expensive calculations of inverse models, unreliable estimates of load properties, and even inverse kinematics.

However, the behavioral capabilities of those models have not been assessed beyond the ideal world of numerical simulations. Our aim here is to test the *in silico* idea *in machina*, namely, to run those arm simulations in a robot arm, thus assessing not only the feasibility of the proposal in controlling a robot arm, but its biological realism in the context of human movement.

Why is this necessary and important? As with many simulations, Powers' arm models contain idealized representations of the nervous system, the body, and the environment. To name a few: there is no friction, no noise, no realistic transport delays (although there are some delays), no contact forces, etc. These idealizations are acceptable for initial testing and demonstration of principles, but as argued by Webb (2001), models of biological structures should be tested in terms of real problems faced by real organisms in the real world. Additionally, as claimed by Brooks (1992), there is a near certainty that programs that work well on simulated robots completely fail in real robots because of the differences between simulated and real-world sensing and actuation. Moreover, designing and building robots that work decently can generate insights about the function of structures in the nervous system that produce analogous behaviors in living organisms (Floreano et al., 2014; Morimoto and Kawato, 2015).

In sum, following this approach, in the present work we adapted and implemented the proposed hierarchical control architecture (Powers, 1999, 2008) to a 4 DOF robot arm in

order to examine its theoretical capabilities in the real world—dealing with noise, delays, non-linearities, and unpredictable environmental disturbances; as well as to generate insights about human control in basic task such as reaching or tracking. In the first part of the manuscript, we show that several fundamental invariant properties found in human hand trajectories—isochrony, bell-shaped velocity profiles and the speed-curvature power law—are also found in the robot arm trajectories without planning or optimization. In the second part, we demonstrate the motor equivalence phenomenon, where the robot arm can still perform reaching and tracking while the wrist joint is blocked, without learning or being reprogrammed. We also show spontaneous behavioral adaptation to the tilt of the writing surface, to the rotation of the visual field with respect to the arm segments, and to the extension of the robot hand with a "tool." We conclude by discussing the limitations of both the robot and its control architecture, specifically in the light of modeling fidelity and potentially higher and lower levels of control.

METHODS

Hardware: The Robot Arm

We designed and 3D-printed robot arm segments and its rotating base in PLA plastics. Several pictures of the arm and its diagram are shown in **Figure 1**. The robot has four degrees of freedom: shoulder rotation angle, shoulder pitch, elbow pitch, and wrist pitch. They are actuated via DC motors M0–M3, respectively (**Figure 1B**). The location of the shoulder pitch joint is 4 cm above the base level. The upper and lower arms are both 12 cm in length, while the hand spans 10 cm from the wrist joint to the hand tip. Each joint has a geared DC motor as the actuator and a potentiometer as a sensor to estimate the joint angle and angular velocity. The motors and gear trains come from RC servos: two HobbyKing 15298 in base and shoulder joints, Futaba S3003 in the elbow, and an N20 DC motor in the wrist. All the electronics and control circuits were removed from the servo motors and replaced by custom control software on the microcontroller. The potentiometers on the gear output shaft of the servos were kept to measure the angular position of the joints.

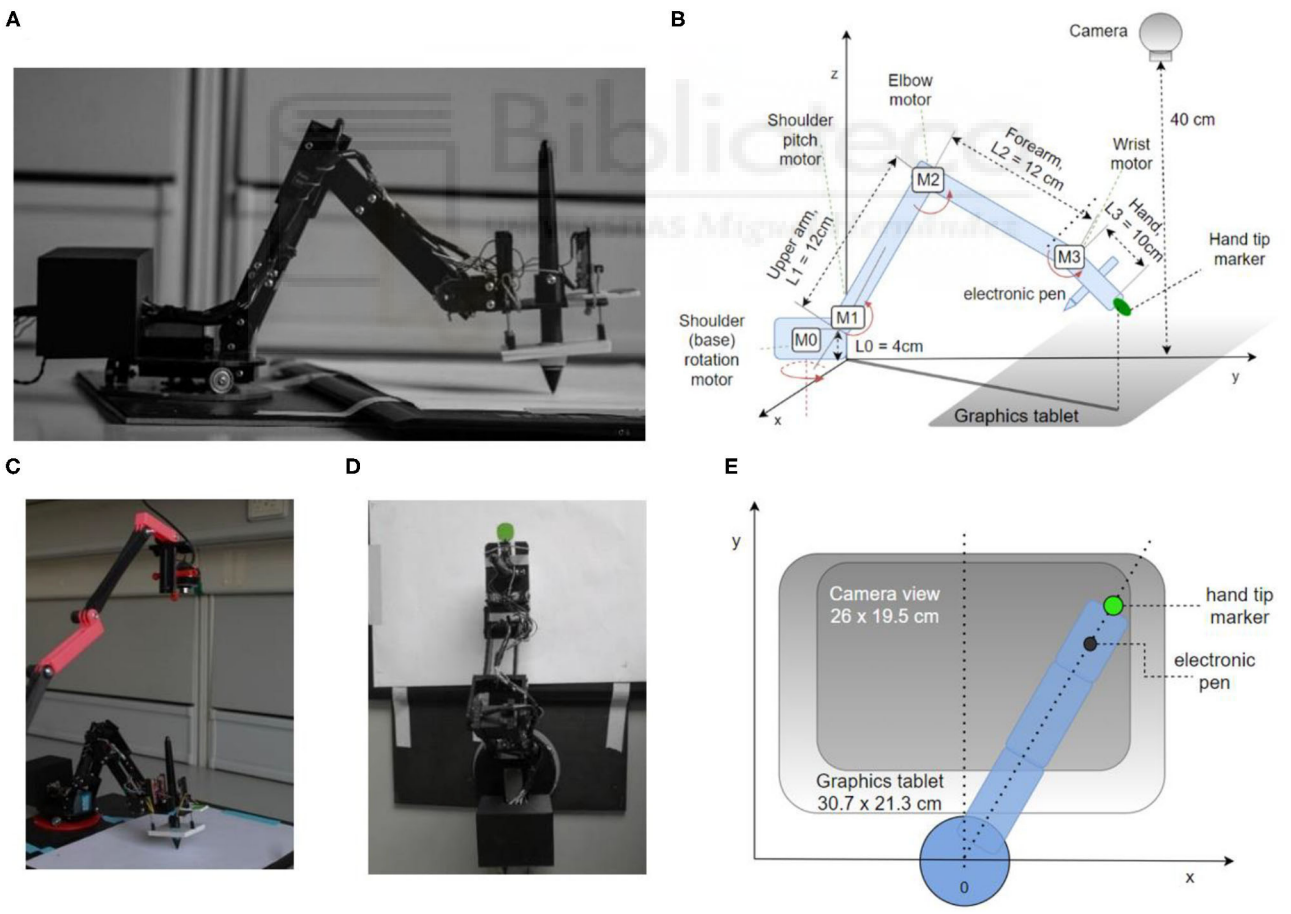

FIGURE 1 | The robot arm system design and implementation. **(A)** Side view showing the body of the robot, enclosed microcontroller, electronic pen, and tablet. **(B)** Diagram of the robot arm in perspective view with arm segments L0–L3, motors M0–M3, camera, tablet, pen, and marker of tip position. **(C)** Photo of the experimental setup, including the top camera. **(D)** Top view photo (camera's viewpoint), the green circle is used by the visual system as the marker of hand tip position. **(E)** Diagram of the robot from the top view.

The microcontroller used was Teensy 3.1, with a Cortex-M4 processor working at 96 Mhz and 3.3 V logic. It was programmed in C++ in Arduino IDE 1.8.6. It outputs four pulse-width modulated (PWM) signals to two TB6612FNG dual H-bridge 1A motor drivers, each connected to two motors and a 9 V 1A power supply, limited to 5 V in software. The sampling rate for angle potentiometers and control signal calculation rate on the microcontroller was 200 Hz.

To detect and measure the marker position, we used a generic webcam with a resolution of 640 × 480 px and a maximum frame rate of 30 Hz. The camera was placed at a height of ∼40 cm from the writing surface using a 3D printed stand (**Figure 1C**) The camera was pointed down toward the marker on the tip of the hand, covering the area of 26 × 19.5 cm, slightly smaller than the graphics tablet active area size (**Figures 1D,E**). The image from the camera was used to construct two controlled variables, the x and y position of the marker, and formed the basis of visual controlled loops.

To measure pen angle and pressure, we used a graphics tablet Wacom Intuos Pro Paper PTH-860, with an active surface of 30.7 × 21.3 cm, at a spatial resolution of 0.08 mm. The sampling rate of the tablet was 120 samples per second. However, we used 30 samples per second for pen pressure and pen angle control in order to be synchronized with the visual control loops that were limited by the temporal resolution of the camera to 30 Hz. The position of the pen as measured by the tablet itself was not used in arm control.

The PC we used for recording and visual processing had an Intel i5 processor, 8 GB of RAM, and runs on Windows 10 OS.

We initially designed and placed pressure sensors on the hand of the robot, using three linear sliding potentiometers measuring the stretch of an elastic rubber band when the hand is pressing on a surface (visible on the hand in **Figure 1A**). One sensor was placed at the tip of the hand, and two on the base. The sum of travel of all three potentiometers was therefore directly related to the pressure of the palm on a surface, and the difference between the front potentiometer and two back potentiometers was related to the pressure difference and tilt of the hand. However, the Wacom graphics tablet also reports the pressure of the pen on the tablet and the angle of pen tilt, and these readings proved to be more reliable than our custom sensors and were used in control loops.

Software and the Control Architecture

Hierarchical Control

In the arm models, Powers (1999, 2008) provides several simulations of hierarchical control architectures. However, those control systems are not proposals for the exact architecture of the human arm control systems, but rather conceptual models and demonstrations of principles. There are no rigorous rules or recipes given for construction of hierarchical systems. In his 1973 book, Powers proposes that the first, lowest-level control systems are in direct contact with the environment via receptors and effectors, forming fast negative feedback loops, with short transport delays. The reference values for the first level are supplied by the second level in the hierarchy, as outputs of a single control system or functions of outputs of multiple second-level control systems. The controlled variables of the second level in the hierarchy are constructed as functions of first-level controlled variables, have a different *level of abstraction,* and work with a longer signal transport delay. The next level up then continues the pattern of creating controlled variables as functions of lower-level controlled variables and provides the reference signals for the lower level. An example of the lowest level would be spinal loops controlling tendon tensions and muscle lengths, while supra-spinal or cortical loops would implement control of slower-changing, more abstract variables such as arm configurations of sequences of positions.

The control architecture of the present robot, as shown in the block diagram in **Figure 2A**, is not a verbatim copy of simulated systems. It is adapted to a 4 DOF arm using the guidelines and rules of thumb described in the literature. In addition to proprioceptive and visual variables, it also uses control of pressure, not found in the simulations. The architecture is composed of two levels with four control systems at each level. Starting from the bottom (body, plant), each degree of freedom of the robot contains a DC motor and a potentiometer for joint angle measurements. The voltages activating the motors are proportional to the net signal arriving from the outputs of lower-level controllers; i.e., *the same motors are used by multiple controllers, creating joint torque-coupling at the controller level.* The gears, potentiometers and housing of the motors come from RC servos, but the servo circuitry has been stripped away (see section Hardware: the Robot Arm for details).

The lower level of control (**Figure 2A**, blue box) is implemented on the microcontroller, it is faster (200 Hz cycle) and has a short signal transport delay (5–10 ms). It is controlling proprioceptive variables, with a relatively low gain. The proprioceptive variables *R, xp, z*, and δ are constructed from low precision and noisy potentiometer readings and stored arm segment lengths. Their geometric meaning is shown in the **Figure 2B**. Note that joint angles are measured and used in forward kinematics equations, but they are not controlled.

The higher level (**Figure 2A**, yellow box) is implemented on the PC, it is slower (30 Hz cycle) and has a longer transport delay (180–190 ms). The variables controlled at the higher level are visual and tactile, constructed from camera images and graphics tablet and pen recordings. Their geometric meaning is shown on **Figure 2B**. The controllers at this level are slower, but have a higher gain than controllers on the lower level, i.e., they are more sensitive to errors. The errors x_e and y_e between the reference for the visual position (top level signal provided by the experimenter) and the sensed visual (x, y) position of robot arm sets the reference for the proprioceptively sensed endpoint positions *xp* and *R*. The tactile variable *pen pressure error* z_e sets the height (z) reference; and the *pen angle error* t_e sets the reference for the hand angle δ.

Proportional-Derivative Controller With a Low-Pass Filter

The basic unit of the control architecture (**Figure 2A**) is the proportional-derivative (PD) controller with a low-pass filtering element (LPF) on the controller output. All of the controllers of

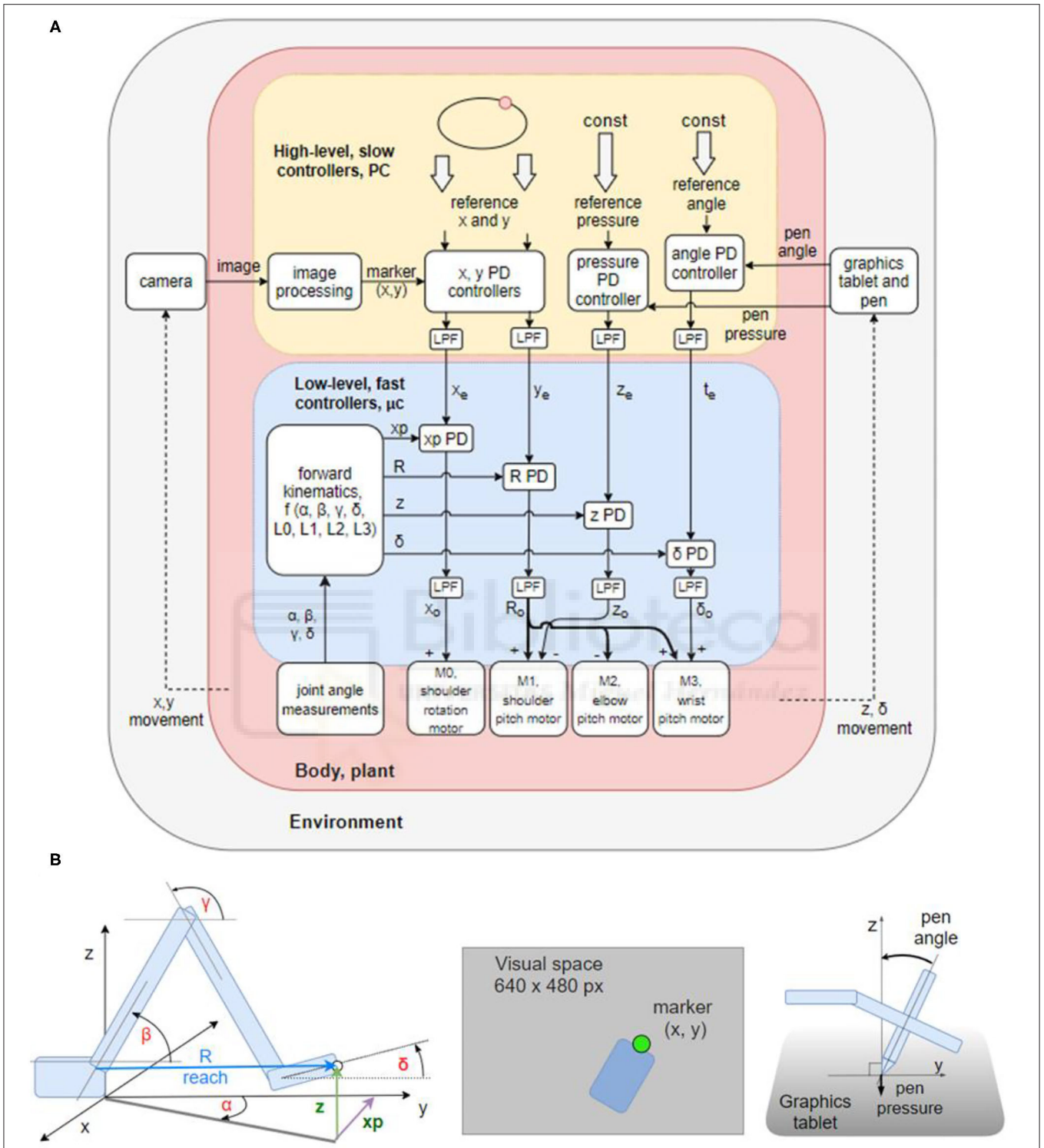

FIGURE 2 | Block diagram of the robot arm control systems and geometric definitions of the variables involved. **(A)** Block diagram of two levels of feedback loops, high level (yellow) and low level (blue). There are four high-level controlled variables: position of the marker in (1) *x* and (2) *y* dimensions in the visual field, (3) *angle of the pen* to the tablet, and (4) *pressure of the pen* to the tablet. The references for those variables are supplied by the experimenter at each run. The outputs from higher-level loops are references for the lower-level loops controlling four proprioceptive variables: (1) *xp*: the x coordinate of the hand tip in proprioceptive space; (2) reach, R: the distance from the shoulder base to the hand tip; (3) *z:* the height of the hand tip; and (4) *delta (δ)*: the angle between the x-y plane and the hand. All controllers are proportional-derivative (PD) with a low-pass filter (LPF) in controller output. **(B)** Diagrams showing the geometric definitions of variables in the block diagram, the visual space, and a diagram of the pen angle and pressure variables.

the hierarchy can be described by the following equations in the time domain:

$$o = K_p\left(i_{ref} - i\right) - K_v\frac{di}{dt} \quad (1)$$

$$\frac{dy}{dt} = \frac{o - y}{tc} \quad (2)$$

where (1) is the PD controller equation with controlled variable *i,* reference input i_{ref}, output *o,* the derivative of the controlled variable *di/dt*, proportional gain *Kp*, and derivative gain Kv. Equation (2) models the low-pass filter with input *o* and output *y*, and *tc* is the open-loop time constant of the low pass filter.

The purpose of the low pass filter is to modify the bandwidth of the system. In the presence of delays and noise, high-frequency disturbances might cause positive feedback and instability. The low-pass filter attenuates the amplitudes of high-frequency components or completely removes them from the controller output, preserving stability of the loop. At the same time, the proportional and derivative gain can be kept high to maintain error sensitivity and good performance at low frequencies.

Construction of Controlled Variables

Robot arms are usually built with a servo motor in each degree of freedom. Consequently, at the lowest level, controlled variables are joint angles, its derivatives—joint velocities and accelerations—or joint torque. Building the robot arm from scratch enabled the experimentation with alternative control architectures that create coupling between multiple joint motors and skip joint angle control, which is arguably more biologically realistic. Instead of joint angle control, we constructed the controlled variables at the first level using standard forward kinematics equations, stored arm segment lengths and joint angle measurements obtained from potentiometers placed at each joint. Due to imprecise measurements, noise, gear backlash, and flex in the plastics of the arm segments, the gain of control systems on the first level was relatively low.

There are four controlled variables at the first level: (1) xp, the x coordinate of the hand tip in proprioceptive space; (2) R or reach, the distance from the base to the hand tip; (3) z, the height of the hand tip or z coordinate in proprioceptive space; and (4) δ (delta), the angle of the hand with respect to the x-y plane. The position in x dimension of the hand tip in kinesthetic space (xp) is controlled by activating the shoulder rotation motor M0. This configuration limits the work area of the arm to $<180^\circ$ in the upper half-plane (y>0). Reach R is controlled by simultaneously activating shoulder (M1), elbow (M2), and wrist (M3) motors, with the elbow being activated in the opposite angular direction from the other two. Height z of the hand tip is controlled by moving the shoulder motor M1. Angle delta between the hand and the x-y plane is controlled by moving the wrist motor M3. All the variables are controlled simultaneously. For instance, if correcting the height variable creates an error in δ angle, it will be treated as a disturbance to the δ angle control system and will be corrected simultaneously to the height error, creating a coupling between control systems. Joint angles are not calculated before starting the movement as in traditional inverse kinematics. Joint motors move until all the errors are reduced. These calculations are performed on the microcontroller.

At the second level, there are also four controlled variables: (1) x and (2) y positions of the marker in visual space, (3) pen pressure and (4) pen angle (**Figure 2B**). These control systems are implemented on the PC, in a script written in Python. The image processing algorithm uses the OpenCV library to find the location of a green marker placed on the tip of the hand of the robot (**Figure 2B**). The image from the camera is first converted from BGR color space to HSV; then an inRange filter is applied to extract the green-colored areas. The filtered image is eroded and dilated to remove noise. Finally, the location of the marker is taken to be the center of the largest contour found on the image. The location of the marker is reported in pixels. Each variable is sampled or calculated at ∼30 Hz, determined by the sampling rate of the camera. Signal transport delays in visual loops are ∼180–190 ms. Pen pressure and pen angle are read-out from the Wacom tablet using the PyQt5 tabletEvent api, with pressure being measured in percentages and angle in degrees.

Tuning the Control Systems

We first tuned the lower-level, proprioceptive loops. The tuning procedure started with setting proportional and derivative gains to zero, and the time-constant of the low pass filter to a low value. Next, we increased the proportional gain until oscillations appeared after a step reference, and then we increased the derivative gain until the oscillations would stop. If the precision were not high enough, then we would increase the time constant of the LPF and retune the proportional and derivative gains to a higher value, trading bandwidth for precision and stability. The time constant *tc* of the low-pass filters was 80 ms for all the controllers at the lower level. For tuning the higher levels, we applied step references and aimed for a critically damped response using the same trial and error procedure as described. The PD controllers at the higher level are identical to lower-level controllers expressed in Equations (1) and (2). They differ only in parameters. Loop gains and open-loop time constants are much larger in higher-level loops in order to achieve stability and precision in conditions of large loop delays and noise from the marker location finding algorithm.

Data Analysis

Robot hand trajectories were extracted from the camera-recorded positions and estimated hand marker locations. We did not use the position of the pen on the tablet since the position of the hand-tip marker was not identical to the position of the pen. The experimental signals were smoothed with low-pass second-order Butterworth filter, with the cutoff frequency specified for each analysis, in order to tame the relatively high levels of noise, aiming for the preservation of position and velocity profiles, and taking into account the speed of arm movement. Trajectories of the computational model were not smoothed.

RESULTS

Beyond computer simulations and blackboard mathematics, we studied the robot arm as an "embodied control architecture"

in the real world to see how it can deal with tasks commonly performed by humans and other primates, while adaptively managing noise, delays, non-linearities, unpredictable disturbances, and perturbations.

Having built the robot arm hardware from scratch and having implemented the hierarchical control algorithms as described above, our main goal was 2-fold: first, to examine the behavior of the system in its own right, and second, to compare the behavioral features of the robot arm to known properties and invariances of human arm movement.

Task I: Straight Movements in a Reaching Task

The first test is a reaching paradigm similar to the center out reaching task (**Figure 3A**) often used in primate and human movement research (e.g., Cisek and Kalaska, 2002; Inoue et al., 2018). We applied the step reference signal simultaneously to x and y visual tracking loops. There was no central stopping point: for one size of the task, there were 10 movements in each direction, done in sequence, for a total of 40 movements, with a 5-s pause on the endpoints. The task was repeated 4 times with different lengths of movement at 4, 8, 12, and 16 cm (**Figure 3B**). We did not randomize the movement directions, since the robot did not have any learning capabilities that might have influenced the reaction time or movement trajectories.

We found that the robot performs straight movements across different lengths and different directions in approximately the same time: 1.45 s (**Figure 3C**). For the shortest movements (4 cm) there was a deviation of 50 ms from the average duration of longer length movements. The speed profile (**Figure 3D**) was

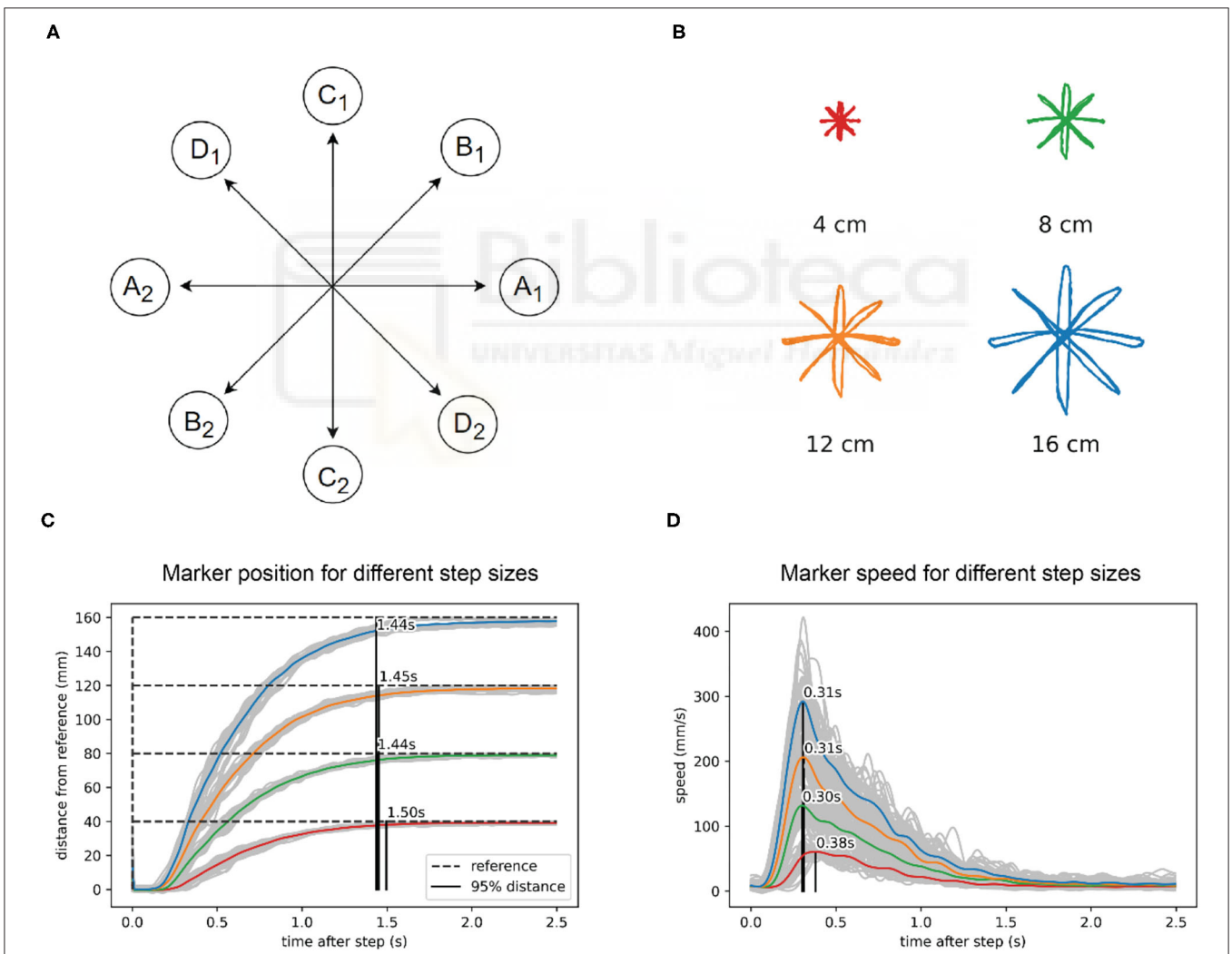

FIGURE 3 | In reaching to a visual reference, the robot arm shows isochrony and bell-shaped speed profiles. **(A)** Task diagram. The reference jumps between points A1 and A2, with a pause of 5 s at each point. Then repeats the same pattern at points B1 and B2, C1 and C2, and D1 and D2. **(B)** Marker position data for four different sizes of the reference step. **(C)** Marker position in visual space calculated as the distance from the previous marker position. The marker reaches 95% of the distance to the reference after a step in about 1.45 s, regardless of the distance or direction traveled. **(D)** Speed calculated from the same data shows a bell-shaped profile, scaled in height to step distance. The position data in plots B and C and was low-pass filtered with a 2nd order Butterworth filter with a cutoff at 15 Hz, while the speed data filter had a cutoff at 5 Hz.

roughly bell-shaped with a shorter rise and longer fall segment and scaled with the length of movement. In all movements, the maximum speed was achieved at approximately the same time after the reference step (peak at 0.33 s, **Figure 3D**), except in the shortest movement of 4 cm, where the peak of maximum speed was 70 ms later than the average of the other movements. Robot position data were low-pass filtered using a second-order Butterworth filter with a cutoff at 15 Hz, while the speed data filter had a cutoff at 5 Hz.

Task II: Curved Movements in a Tracking Task

Producing elliptic traces or drawings in humans in a fast and fluid manner results in a speed-curvature relationship known as the 2/3 speed-curvature power law (or 1/3 power law, depending on the variables used), first described by Lacquaniti et al. (1983). In the second task, we tested the production of curved movements. We used a continuously moving reference point, and we report on the situation where the reference moved at a constant speed along an elliptic path.

An elliptic trajectory with a constant tangential speed is a non-power law trajectory ($\beta \approx 0$, $r^2 \approx 0$); the x and y components are not pure sinusoids, but also contain higher frequency components. In the low frequencies, the speed of the robot was close to the reference speed, but at higher frequencies, the speed of the robot was not constant and had a sinusoidal profile and a lower average than the reference speed. At the highest frequency of input ($f = 0.826$ Hz, speed ≈ 406 mm/s), the output trajectory followed a speed-curvature power law with an exponent of $\beta \approx -1/3$ and $r^2 = 0.78$ (**Figure 4C**).

This seems to support the hypothesis that the power law is a consequence of the physical limitations of the human arm, and not a planned invariance. However, the size of the drawn shape was smaller than the reference shape because both x and y components of the reference are attenuated in the output. Additionally, the position data was smoothed with a low-pass filter with a cutoff at 3 Hz and differentiated, which increased the coefficient of determination (r^2) of the power law. To further probe the question of the origin of reaching and tracking invariances, and to minimize the effect of noise, we created and fitted a model of visual loop behavior described in the next section.

Modeling and Characterization of the *in Machina* System

The system controlling the visual y variable (**Figure 5A**) is non-linear because increasing reach affects the y position differently depending on the angle of rotation of the base (α). The three motors involved in changing reach (**Figure 5A**) are different in power and mechanical linkage; they have a different effect on changes in reach depending on the position they are in. Despite non-linear elements, the behavior of high-level visual loops can be described fairly well by a set of linear second-order equations, modeled in the block diagram (**Figure 5B**), the free-body diagram (**Figure 5C**), and a system of equations:

$$e_t = {y^{ref}}_{t-d} - y_{t-d} \tag{3}$$

$$\ddot{y}_t = \frac{k}{m} e_t - \frac{b}{m} \dot{y}_t \tag{4}$$

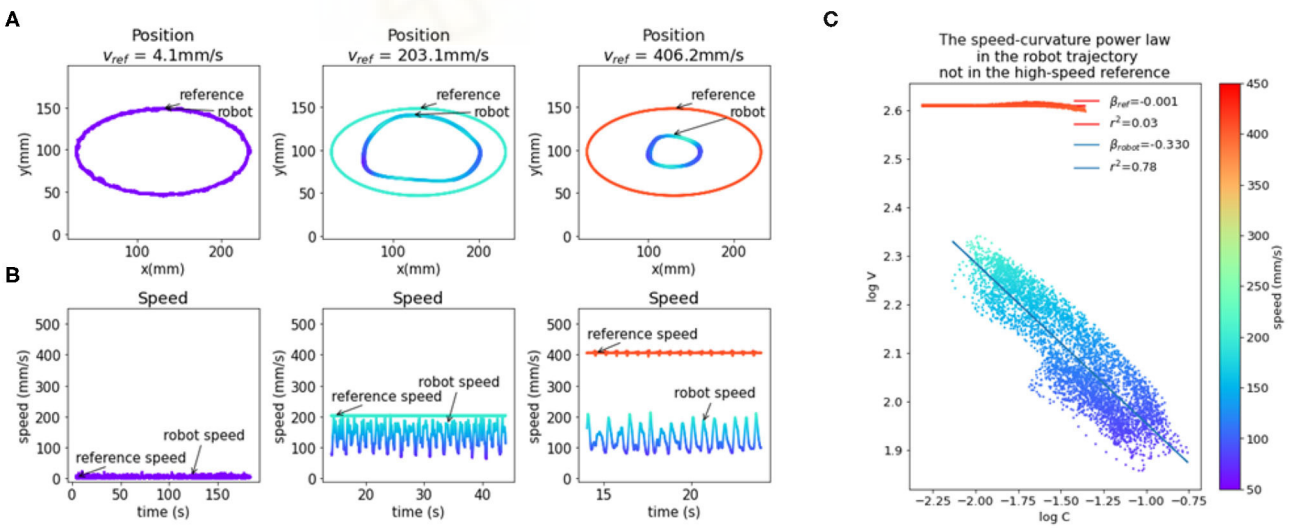

FIGURE 4 | The emergence of the speed-curvature power law at high speed. **(A)** Reference and robot positions. When the reference speed is low, the position of the robot hand tip marker in visual space matches the speed of the reference. At higher speeds, there is a magnitude attenuation—the ellipse shape is smaller. **(B)** Plot of reference and robot speeds. At low speed, the robot speed matches the reference. When the reference speed is high, the speed of the robot is lower and oscillates, even though the input speed is constant. **(C)** Oscillations in robot speed for the highest speed input are regular and correlated with local curvature of movement, following the speed-curvature power law with the exponent of $\beta \approx -1/3$ and $r^2 = 0.78$. The reference speed is constant (400 mm/s), and there is no power law ($\beta \approx 0$, $r^2 \approx 0$). In all the plots colors indicate speed, as shown in the color bar on the right. Position data were smoothed with a 2nd order Butterworth filter with a 3 Hz cutoff and differentiated to generate speed data.

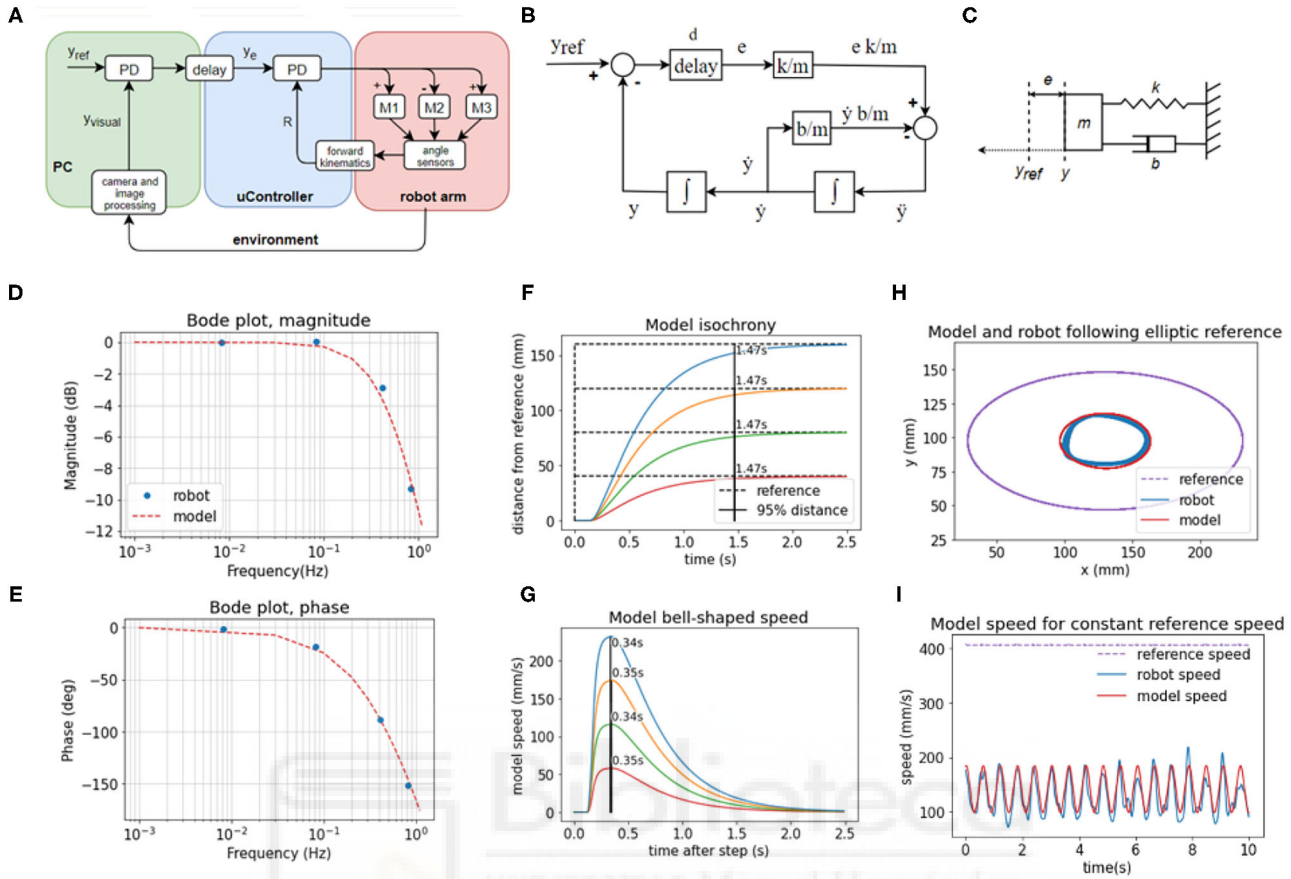

FIGURE 5 | The behavior of visual feedback loops can be represented by a second-order model. **(A)** Diagram of the elements in the control of the position of the hand in visual space in y dimension, including the lower-level control of reach distance. **(B)** Block diagram of the model with variables, parameters, and functions. **(C)** Free body diagram of a mechanical setup analogous to the model mass on a spring with damping. **(D)** Bode magnitude plot shows how the amplitude of output signals at high frequencies is attenuated in relation to the input signals. **(E)** Bode phase plot showing the frequency-dependent phase difference between the input and the output. The model reproduces the frequency-dependent properties of the robot's visual loop. **(F)** The model produces a similar pattern of isochronous movement independent of distance in the step reference task; as well as **(G)** bell-shaped speed profiles in the same task **(H)** The model produces an ellipse smaller than the reference ellipse, similar to the robot, due to attenuation of high-frequency inputs. The frequency of the input here is 0.826 Hz, and the attenuation is ∼9.5 dB. **(I)** In the same task, the speed of the model follows the same sinusoidal pattern as the speed of the robot, even with the constant speed of the reference. Model trajectory was not smoothed in any of the plots.

where t is time, e is position error, y_{ref} the position reference, y position, d is loop transport delay. The values of the coefficients used are k/m = 40, b/m = 27.5, and d = 0.185 s, which were found by fitting the behavior of the model to the behavior of the robot in the step reference task with a 12 cm step distance. The best fit values indicate a slightly overdamped second-order system. We modeled the x and y control loops as independent systems with equal parameters.

The model in Equations (3) and (4) is analogous to a mass-spring-damper system (**Figure 5C**) with a movable equilibrium position and a pure delay element. The approach trajectory of the marker on the hand of the robot to the visual reference in the step-reference task is similar or analogous to the approach trajectory of an object of mass m on a spring with stiffness k and damping b toward its equilibrium position y_{ref}, where the displacement of the equilibrium position happens after a delay of d seconds. The spring constant is an analog of the visual gain or sensitivity to error; the damping coefficient b is an analog of the combined effect of visual velocity gain (damping term in the visual PD controller), gains at the proprioceptive level, and friction between the pen and the tablet; the mass in the mass-spring-damper system is an analog of the combined contribution of the mass of the robot arm, time constants in the visual loops and inertia of electromotors; and the delay is the total duration of the travel of the signal around the visual loop, combining camera latency, frame rate, and transmission delays of the serial protocol between the PC and the microcontroller.

We examined the behavior of the robot in response to sinusoid inputs across a range of frequencies (0.008, 0.083, 0.413, 0.826 Hz). We applied input as the visual reference signals and measured the output as the position of the marker in the visual field over time. We calculated the relation of output

amplitude A_{out} to input amplitude as 20 $\log_{10}$ (A_{out}/A_{in}) for the Bode magnitude plot, and we calculated the phase difference between the input and output sinusoids for the phase plot. We then interpolated the plot using the second-order mass-spring-damper model (**Figures 5D,E**, model interpolation in red, experimental values in blue).

Looking at the Bode plot (**Figures 5D,E**), we can see that the system is stable for all input frequencies. At the gain crossover frequency of ∼0.1 Hz, the system has a large phase margin of about 160°, and at the phase crossover frequency at ∼1 Hz the magnitude attenuation is 11 dB, which satisfies the stability criterion of having both the phase and gain margins positive. The bandwidth is limited by the large transport and processing delays in the visual loops, approximated at 185 ms. The delays cause a phase shift that takes an increasingly longer part of the sine period with the increase in frequency and are compensated by low pass filtering the controller output (see Equations 1 and 2 in Methods section).

We repeated the step-reference task with the model (**Figures 5F,G**). The duration of movement is isochronous across different distances: it takes the same amount of time, 1.47 s, to cross 95% of the distance to the reference. The speeds are bell-shaped and scaled with distance, but they all reach a peak after 0.37 s, replicating very nearly the behavior of the robot arm.

Finally, in the ellipse tracking task (**Figures 5H,I**) at the highest frequency of 0.826 Hz of input, the model replicated the size of the robot trajectory, and also the properties of the speed profile. Even when the reference speed was constant, at this frequency, the speed profile of the model was sinusoidal. Model trajectory followed a speed-curvature power law with the exponent $\beta = -0.40$, $r^2 = 0.98$.

Model trajectories in panels (**Figures 5D–I**) were produced by a model with the same, constant coefficients, simulated with a time step of 5 ms and Euler integration. Model trajectories were not low-pass filtered.

Task III: Robustness to Blocking the Robot Arm's Wrist Joint

The hallmark of biological motor control is robustness to perturbations. In further testing of the robot arm, we applied different perturbations to the controlled variables, keeping them constant for the duration of the task and not changing any of the parameters in the controllers or other parts of the software of the robot. We blocked the wrist, tilted the writing tablet, added a tool that extended the arm, and rotated the visual field.

In the first trial, we blocked the wrist joint and compared the performance of the robot in visual tracking tasks to the performance in normal operation where the wrist was moving freely. Without any changes to the code or parameters of the control systems, the robot arm performed the tasks even with the wrist blocked. In normal operation, the variable *reach* (**Figures 6A,B**) is affected by three motors—in the shoulder (M1), elbow (M2), and wrist (M3). The time-plot of the variables in normal operation in the step reference task (**Figure 6D**) shows joint angles that illustrate how all three motors contribute to the movement. When the wrist is blocked, reach is maintained at the same desired value as in the normal situation. However, here reach is not affected by three motors, but only by two: the elbow and shoulder motor automatically pick up or compensate for the work normally done by the wrist motor because their activation is proportional to the reach error.

The block diagram shows the flow of information in the reach synergy (**Figure 6B**). We can describe the system using the terminology of Latash (2008) or Latash et al. (2007): the performance variable is *reach*, and it is maintained at its reference level y_e by varying elemental variables—activations o1, o2 and o3, of motors M1, M2, and M3, respectively. The activations are calculated by weighting the output R_o of the controller, and summing the signals with outputs from other systems, here control of height z and wrist angle δ. These sums (o1, o2, and o3) are used as activations of motors, as pulse-width-modulated signals from the microcontroller to the motor driver chip.

Task IV: Further Perturbations: Tilting the Tablet, Using Tools, Rotating Point-of-View

We applied static disturbances or perturbations to controlled variables either directly or indirectly to examine the adaptiveness and robustness of the robot control architecture. In the normal condition, without additional perturbations (**Figure 7A**), the writing tablet is horizontal, the wrist is mobile, the marker is on the tip of the hand of the robot, and the visual coordinate system is roughly aligned with the proprioceptive coordinate system along the × and y axes. The angle of the pen to the tablet is sensed and maintained at 0 degrees (pen is perpendicular to the tablet, while the hand is parallel to the tablet) by moving the wrist joint. The pressure of the pen to the tablet is sensed and maintained at or near 50%.

In the tilted tablet condition (**Figure 7B**), the end of the tablet distal to the robot was lifted to make the tablet close an angle of 30° to the surface. This perturbation challenged the pen pressure and pen angle control systems because the pressure control system needs to continuously modify the height of the hand in order to keep the pressure at 50% and still move toward the reference in the visual space. The pen angle control system needs to modify the wrist angle so that the pen is always orthogonal to the tablet surface. The plots of pen angle and pressure show that those variables were maintained near their reference values despite the perturbation, with somewhat more error than in the normal condition.

In the tool use task (**Figure 7C**), we added a 12 cm long plastic piece to the tip of the arm and moved the marker forward to the end of the plastic piece, creating a situation resembling tool use, as now the tip of the "tool" was tracking the reference. We moved the camera about 12 cm forward to keep the workspace in the visual field. The robot performed the task without learning or reprogramming visual transformations. In the next task, we rotated the visual field by 30° (**Figure 7D**) by rotating the camera and keeping the robot in place. This amount of rotation is near the limits of performance—the robot performed the task with higher amounts of error, visible on the patterns (red) on the plots.

The perturbations summary plot shows the average absolute error as the average distance of the hand marker from the

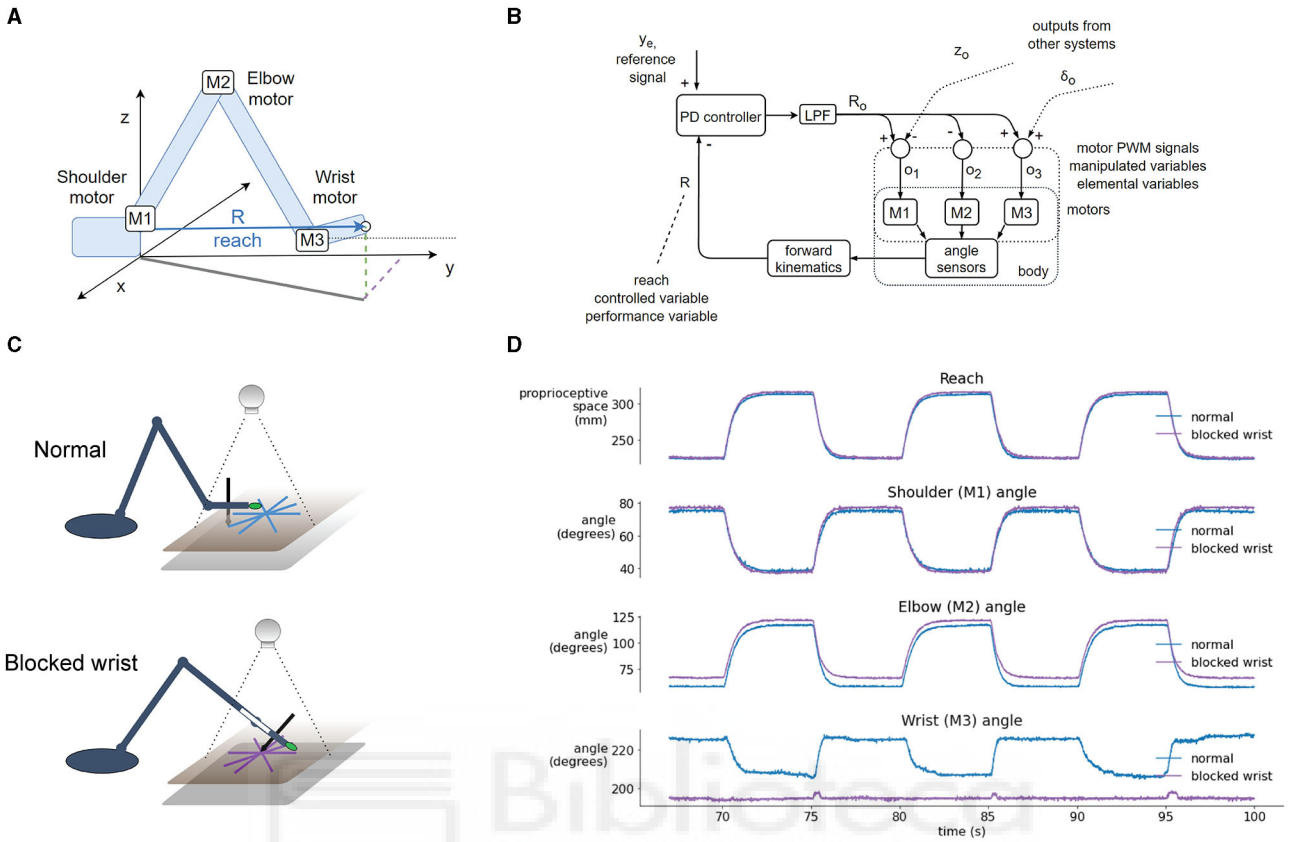

FIGURE 6 | Blocking the wrist is compensated by the reach synergy. **(A)** Geometric definition of *reach*—the distance from shoulder base to the tip of the hand, and locations of joint motors. **(B)** Block diagram of computational and physical processes in the reach synergy, with marked performance and elemental variables. **(C)** Diagram of the normal and blocked wrist setup. In the normal setup, the wrist moves freely, keeping the hand parallel to the tablet (and the pen perpendicular). In the blocked-wrist setup, the motor of the wrist is not powered, and the wrist is locked at ∼180° to the forearm. **(D)** Segment of a reaching task with a step reference, comparing the normal and blocked-wrist situation. With the wrist blocked, reach is nearly identical to reach in the normal situation, but shoulder and elbow motors are activated more to compensate. Shoulder and especially elbow angle show differences in both situations.

reference in all perturbation tests across different tasks. The error grows with distance or the size of the step in the step-reference task. In pseudorandom tracking, the error grows with "difficulty," where more difficult tasks have a higher magnitude of high-frequency signals. In the ellipse tracking task, the error grows with frequency or with the speed of the reference. Thus, our robot arm is highly robust to external perturbations, akin to human movement.

DISCUSSION

We have demonstrated how and explained why a custom-made robot arm (**Figure 1**) with a hierarchical control architecture (**Figure 2**) based on simulations by Powers (1999, 2008) displays basic features characteristic of biological movement. Being robust to noise and delays, the robot's behavior complies with isochrony and displays bell-shaped velocity profiles in a reaching task (**Figure 3**). In tracking a moving target at high speeds, the robot complies with the so-called speed-curvature power law of human movement (**Figure 4**).

We must acknowledge that the proposed control architecture does not fully explain the production of reaching and tracking trajectories since (i) the reaching trajectories of the robot are isochronous for different reach distances, while humans may change the reaching duration according to speed or accuracy demands of the task (Fitts, 1954); and (ii) the tracking of elliptic reference trajectories does not reproduce the geometrical trace or exact speed profile of the reference, with the amplitude of movement falling with frequency, and the shape reducing in size.

However, it is clear that the hierarchical organization of the control systems afford a lot of flexibility to the robot arm even without learning algorithms or online optimization. Moreover, we have demonstrated adaptive behavior to structural perturbations such as blocking the robot's wrist (**Figure 6**) and to environmental configuration disturbances such as tilting the writing tablet, extending the hand with a tool, or rotating the visual field (**Figure 7**). The main reason for such a robust behavioral emergence seems to be the choice of the controlled variables and the hierarchical arrangement of the control systems. We further discuss these findings below.

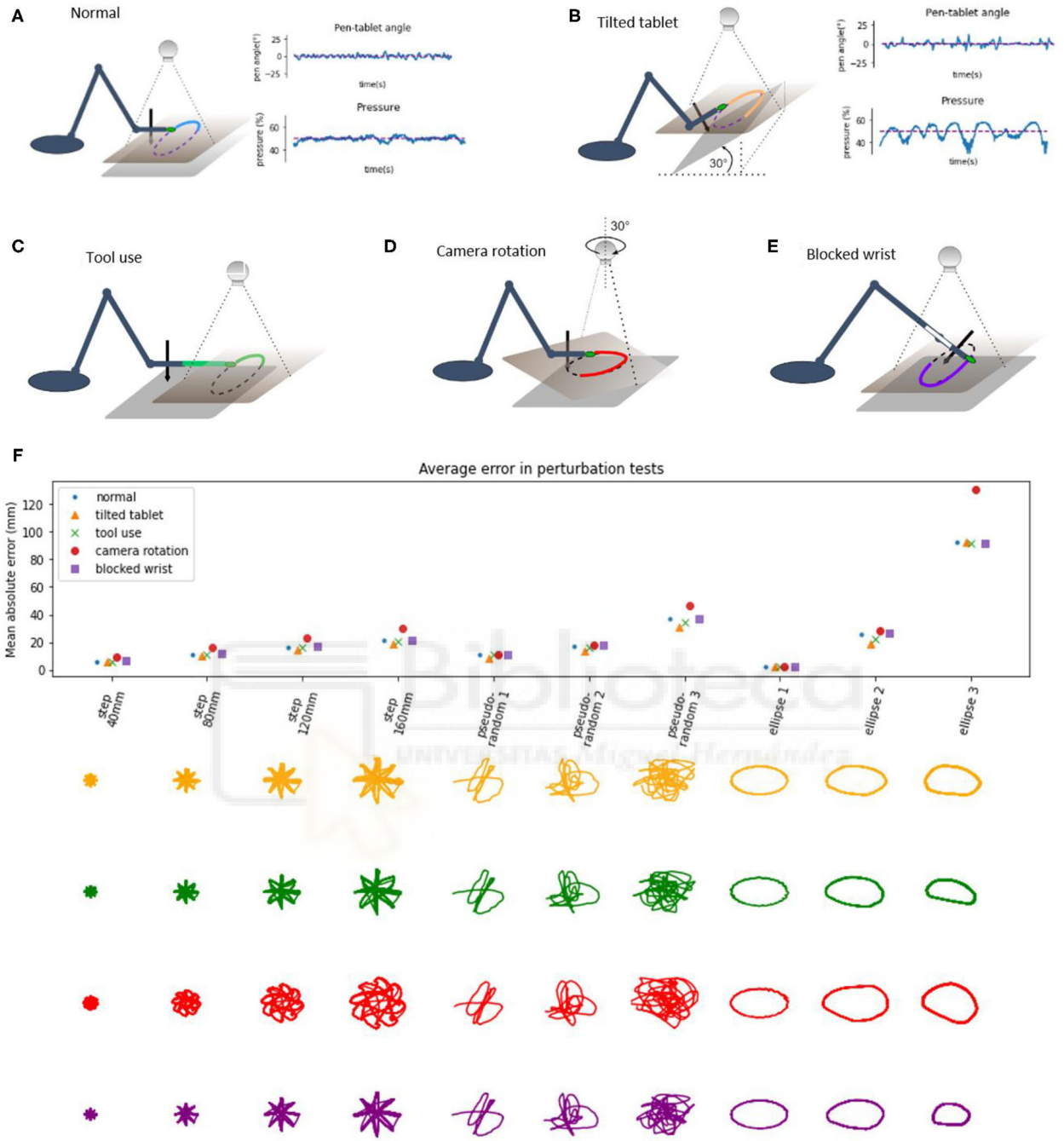

FIGURE 7 | Diagrams of perturbation conditions and a plot of tracking performance in different tasks. **(A)** the normal condition diagram and plots of pen angle and pressure from a pseudorandom tracking task, reference in red and measured variable in blue. **(B)** The tablet is tilted 30°, distal part is lifted, plots show the pen angle, and pressure in a pseudorandom tracking task, reference in red and measured variable in blue. **(C)** Diagram of the tool use task, a 12 cm plastic piece is attached to the hand of the robot, and the maker placed on the end. **(D)** Diagram of the camera rotation task; the camera is rotated by 30° when compared to the "normal" conditions. **(E)** Diagram of the blocked wrist. **(F)** Average distance (absolute error) between the marker and the reference in the visual space, across different conditions and tracking tasks. Bellow the plot are robot trajectories for each perturbation condition and task.

Frequency Response and Stability Despite Noise and Delays

The frequency response of the robot's visually guided behavior (**Figure 3**) shows how the arm behaves in response to input signals of different frequencies, where the "input" is the reference or setpoint input to the hand tip position in the visual space, and the "response" is the hand tip position in visual space. We can see that the system is stable for inputs of any frequency because

both the phase and gain margins are positive. The system has a slightly overdamped second-order response (simplified model of the robot arm discussed later in more detail), and it acts as a low pass filter with the gain crossover frequency of ∼0.08–0.1 Hz. This means that magnitudes of all input signals above this frequency will be attenuated.

Transport delays in the human visuo-manual loops in tracking pseudorandom targets are approximated at 100–150 ms (Viviani et al., 1987; Parker et al., 2017). Visual loops of the present robot also contain large signal transport delays, 180–200 ms, that come from camera latency and refresh rate, as well as serial protocol communication delays between the microcontroller and the PC. Delays in feedback loops cause a frequency-dependent phase shift so that at high frequencies of input, the phase shift might cause the actuator action to add to the error, creating positive feedback as opposed to negative feedback where the error is reduced, which may cause instability and oscillation. Long transport delays are often cited as the main reason for relatively complex delay-compensation schemes such as forward models (e.g., Miall et al., 1993; Kawato, 1999; Desmurget and Grafton, 2000). A forward model, given the efference copy of the motor command, estimates the state of the arm at current time, instead of waiting for the delayed feedback signals. However, we show that an alternative, simpler scheme might work.

Stability can be achieved by reducing the bandwidth of the system—trading the bandwidth for stability—using low pass filter elements in the outputs of controllers (**Figure 2**). This maintains the visual loop gain high when the input frequency is low and reduces the effective gain for high-frequency inputs to avoid positive feedback (Powers, 2008). Additionally, the "real world" is highly unpredictable, and various disturbances acting on the arm would invalidate any prediction made by the forward model that takes only the motor command into account. The present architecture avoids the problem by always using feedback signals, affected by both motor action and environmental disturbances, as representations or parameters in calculation of actual state.

The robot arm is still capable of producing movements with high peak speed (**Figure 3**), while movements with both a short duration and a high peak speed might be produced if the movement was stopped by an obstacle. This might be a mechanism involved in fast, short movements of human hands in e.g., pressing piano keys.

Most of the effects of sensory noise in the high-gain visual level systems seem to be averaged over time by the low-pass filter and do not affect the movement, especially at low speed, and don't require additional compensation mechanisms. In the lower levels, sensory noise does not affect movement because the gains are low.

Isochrony, Bell-Shaped Velocity, and the Speed-Curvature Power Law

In humans, isochrony was found in drawing figures of different sizes (Viviani and McCollum, 1983; Viviani and Flash, 1995). It was also found in macaques in natural settings (Sartori et al., 2013), but not consistently in laboratory settings (Castiello and Dadda, 2019). In the Fitts tapping task, the time of movement is related to the so-called index of difficulty, and isochrony is present not for all movements, but for tasks of the same index of difficulty (Guiard, 2009). The tapping task illustrates the speed-accuracy tradeoff: the faster we move, the less accurate our movements will be. Then, in order to preserve accuracy, presumably, when aiming for smaller targets, we slow down our movements.

We have found that the robot performs isochronously all movements in the step-reference task, regardless of travel distance or direction (**Figure 3**); for all movements in this task, the average reaching time was 1.47 s. In comparison, e.g., Fitts (1954) reports times from 0.180 to 0.580 s for reaching across comparable distances; depending also on the size of the target or the required accuracy. This illustrates that for a direct comparison with human movement, the robot arm would need to have (1) higher force-producing capabilities and (2) presumably a higher-level system that would be able to perceive target sizes and modify produced speeds accordingly. The arm might also be made closer in size to the human arm: with 12 cm forearm and 12 cm upper arm it is approximately a third of the size of the adult human arm.

In humans, during rapid straight-line hand movements, the speed profile is not constant. The movement starts slow, accelerates to a point, then decelerates to a stop, forming a bell shape over time or distance. Some researchers report symmetrical bell shapes where the peak speed is in the middle of the movement (Flash and Hogan, 1985), and some report less symmetrical profiles, namely short acceleration and longer deceleration phase in human (Soechting, 1984; Atkeson and Hollerbach, 1985) and in primate reaching (Inoue et al., 2018). In the step-reference task, we found that the speed profiles are bell-shaped, asymmetrical with a short acceleration phase and longer deceleration, and with the maximum speed scaled with the extent of the movement (**Figure 3**). The peak speeds for the robot arm were in the range from 50 mm/s for 4 cm distance to 300 mm/s for 16 cm distance; while in human reaching peak speeds are higher, e.g., Soechting (1984) reports speeds of 650–1,300 mm/s for reaching across 30 cm. Without the modifications to the robot arm system mentioned in the previous paragraph, it is not possible to make more direct comparisons.

We interpret this speed profile emerging as a consequence of programming visual level loops as proportional-derivative controllers. Since there was no trajectory planning or online optimization, our results show that it is possible to achieve such profiles with a simple control architecture, supported also by our mass-spring-damper simulation.

There were no accuracy requirements, but we found that increasing the frequency and speed in the ellipse tracking task decreased the accuracy, suggesting a speed-accuracy tradeoff in the movement of the robot. This tradeoff seems to be caused by several factors: (i) the low-pass filtering properties of the arm, resulting from its inertia, relatively low power of the actuators and also explicit low-pass filter elements, and (ii) the increased influence of lower-level non-linearities and control system interactions on the behavior of the robot because the errors on the lower levels were not corrected fast enough.

The speed-curvature power law with a two-thirds coefficient is observed in rapid elliptical movement in humans. This phenomenon can be roughly described as movement at lower

speed in areas of high curvature and relatively higher speed in areas of low curvature (Viviani and Terzuolo, 1982; Lacquaniti et al., 1983). The production of a power law trajectory is not obligatory in principle because the hand might take many of the infinite possible trajectories along the same path. However, the set of possible trajectories is limited by the physical properties of the hand and the environment. For instance, the hand will never move instantaneously from point A to point B, as there is a limit to the force produced by muscles.

Remarkably, when the robot was tracking a high-frequency elliptic reference, we found the speed-curvature power law in the measured movement, even when it was not present in the reference input. This result is consistent with the optimization of jerk in the movement planning phase (Viviani and Flash, 1995; Huh and Sejnowski, 2015). However, we seem to be getting an optimal jerk trajectory "for free," without an explicit optimization algorithm. This result shows that the speed-curvature power law can be achieved without explicitly optimizing jerk or smoothness either in the planning phase or online.

However, the robot did not accurately follow the path component of the reference. It seems that the emergence of the power law comes from the *failure* of the robot to accurately follow the high-frequency non-power law position reference, which is interesting. This can be viewed as a consequence of low-pass filtering the reference signal by the robot arm system. The position references in x and y dimensions have high-frequency components that get filtered out, leaving single-frequency sinusoid fundamentals, conforming to the power law. Similar results were obtained in simulations by Gribble and Ostry (1996) and Schaal and Sternad (2001) where low-pass filtering non-power-law input signals produced power law trajectories.

Related to this result, several studies with human participants have shown that it is difficult to accurately track targets that don't follow the speed-curvature power law (Viviani et al., 1987; Viviani, 1988; Viviani and Mounoud, 1990). However, the subjects did accurately follow the path component of the trajectory and the rhythm of the target. We further discuss possible mechanisms in the section "higher levels."

A Second Order Simple Model Accounts for the Robot's Behavioral Features

Human behavior in tracking pseudorandom targets can be accurately modeled by a first-order model with three constant parameters (see review in Parker et al., 2020). The step-response and frequency response in humans is also modeled by second-order models, bang-bang control, surge control, or the Crossover model (compared in Müller et al., 2017) with various tradeoffs in simplicity and accuracy of modeling.

Here, in turn, we modeled the behavior of the robot itself with a second-order system, a mass on a spring with damping, with three constant parameters (**Figure 5**) described by the system of Equations (3) and (4). Once the parameters were estimated, the model closely reproduced robot position and velocity in visual space in the frequency response task, in the step-reference task, and in tracking elliptic references. The model displayed isochrony and bell-shaped speed profiles in the step-reference reaching task and the power law in the ellipse tracking task (**Figure 5**).

The fact that the model captures all these features of robot behavior with just three parameters is surprising given the multi-level control architecture, the non-linearities in the lower levels, and differences in motors in each joint. This finding points to an interesting property of hierarchical systems: higher-order loops may appear as linear systems regardless of non-linearities at lower levels. Higher levels provide reference signals to the lower-level systems, so the lower systems are part of the "plant" from the perspective of the higher systems. A certain range of variations and non-linearities in the plant will be hidden in the behavior of the high-level loop.

If the system for tracking a visual target appears to higher levels of the brain just like the robot arm visual control systems appear to us as experimenters, movement control might be relatively simple for the higher brain structures. As postulated by Viviani and Mounoud (1990), all voluntary movement might be a special case of pursuit tracking, where the only difference from conventional tracking is that the target is internal. The hypothetical higher-level system would only need to specify the virtual target, which is identical to the hand position reference in the robot arm.

Higher Levels of Control

In optimal feedback control theory, as well as in industrial robotics control, the solution to the problem of producing a trajectory might involve forward or inverse models, online optimization with a changing horizon, and similar schemes. Those methods are very powerful, especially when coupled with modern computers, precise actuators, and relatively noise-free environments. However, from an academic perspective, they are criticized for not being empirically refutable or biologically plausible (Powers, 2008; Scott, 2012; Feldman, 2015). In the framework of hierarchical perceptual control (Powers, 1973), higher levels should be controlling variables more abstract than lower levels, and also work more slowly having a larger time constant and longer transport delays.

One hypothesis arising from the analysis of straight and curved movements of the robot arm is that the present architecture is missing higher levels of control. In the present architecture, the visual position references are set by the experimenter. A hypothetical higher level would be taking the role of the experimenter and would attempt to control or maintain a high-level variable at a desired value by using the position reference as the manipulated variable, much like the current visual position control loops manipulate references to proprioceptive variables to bring visual position to the desired value. The visual position reference would be equal to the produced visual position in the steady state, but not necessarily during transients.

Harris and Wolpert (1998) show that minimizing the variance of the hand trajectory from the desired path over a set of movements (accuracy) for a given speed, or minimizing the speed for a given desired accuracy, reproduced the bell-shaped speed profiles and the two-thirds power law. Their result was achieved in the framework of planning an optimal trajectory and

executing it in an open-loop manner; however, we propose that their cost functions for speed and accuracy might be treated as explicit higher-order controlled variables that set visual position references. This would amount to independent control of path accuracy and average speed.

Alternatively, elliptic or straight-line movement can be produced rhythmically. There is some evidence that control of movement amplitude and frequency are developed independently. For instance, 5-year-old children occasionally produce sinusoidal movements that match the amplitude but not the frequency of the target, while other children match the frequency but not the amplitude (Mounoud et al., 1985). This might suggest a closed-loop pattern generator, similar to a phase-locked loop, that produces a patterned reference for the position control system (see Matic and Gomez-Marin, 2019). More research is needed to further elucidate these questions.

Controlled Variables in a Hierarchy Explain Adaptivity to Perturbations

The ability of humans and animals to achieve the same task outcome using different motor means has been termed as the phenomenon of *motor equivalence*. The problem it poses to motor control theories is the apparent rapid selection of correct means from the space of all possible means. While motor synergies and hierarchical control are proposed as the solution for the problem (Bernstein, 1967), the concept of synergy in motor control literature is defined in many different ways (see review by Bruton and O'Dwyer, 2018). Our reach control system fits the definition of Latash et al. (2007), and we termed it the *reach synergy*.

To probe the system, we blocked the wrist of the robot and put it through the same battery of tests as in the normal condition: the step reference reaching task and tracking pseudorandom and elliptic targets. Without any reprogramming or autonomous learning algorithms, the robot still performed the task with similar performance to the normal condition (**Figure 6**), with the exception of pen angle not being controlled (as the pen was fixed perpendicularly to the hand, and the wrist was blocked). Wrist blocking was also modeled in the DIRECT model (Bullock et al., 1993) where they argued that fast adaptations to losing a degree of freedom probably exclude complex planning as a relevant mechanism as it would take too much time, and the same effect can be achieved by simpler schemes. Our result seems to be consistent with the *minimum intervention principle* (Todorov and Jordan, 2002b) where the task-level variable of reaching toward a goal is maintained, and the variability caused by blocking the wrist is taken up by task-irrelevant variables of elbow and shoulder joint angles. The minimum intervention principle may emerge from an online movement optimization algorithm; however, here we achieve the same result without optimization, by having a flexible control hierarchy.

Maintaining pen pressure and angle are indeed important skills in handwriting. Measures of quality of control have been linked, for instance, to dysgraphia as a diagnostic criterion (Mekyska et al., 2017). Modeling contact forces in model-based control and optimal feedback control is still an open problem. Control systems for pen pressure and pen angle were implemented for this robot as slow, but precise systems in the higher level. The precision afforded by the pressure control was compensating the lack of precision in the lower-level proprioceptive systems. We tested pressure and angle control systems by tilting the graphics tablet by 30° and keeping the reference for the pen angle toward the tablet at 0° and the reference for pressure at 50%. Next, the robot performed the battery of tracking tests (**Figure 7**), and we found the performance close to the normal condition. The robot automatically adjusted the height of the tip of the hand and the angle of the wrist in order to maintain the angle and pressure references. In this case, we can see that precise pressure control is crucial for maintaining the pen on the tablet, similarly to human handwriting.

The visual coordinate system was "retina-based" in the sense that the two-dimensional visual field recorded by the camera was the working space of the robot. It was somewhat primitive, as it could only find the location of a green marker in two dimensions. However, it was robust to perturbations. The robot arm and the camera, and their respective proprioceptive and visual coordinate systems were only roughly aligned to begin with, and this was sufficient for normal operation. In the first test, we extended the arm with a 12 cm long piece of plastic and put a marker on the tip of the plastic instead of the tip of the hand, simulating writing with a longer pen or reaching with a stick. The visual system had no information about the size of the stick, or for that matter, the size of the robot arm or the configuration of its angles, but only the location of the marker. This was sufficient to enable the robot to track the reference with this "tool."

In the second test, we rotated the camera by 30°. This made the relationship between visual location proprioceptive location variables more non-linear than in normal operation. The performance in this test was somewhat worse than in normal condition (**Figure 7**), but the tasks were still successfully performed: in the step-reference condition, the hand tip reached the reference position and settled at that position, and in target tracking, the hand tip followed the reference signal in a similar manner to the normal situation.

These perturbations to the visual system do not greatly affect performance because there are no explicit coordinate transformations between the visual and kinesthetic loops. All transformations are implicit: the higher levels tell the lower levels to "move until the higher-level reference state is achieved." Moving in approximately the right direction seemed to be enough. As discussed, most non-linearities in the lower levels were absorbed by the high-gain higher-level control systems, at least in the low frequency, low-speed movement.

The geometric and kinematic definitions of controlled variables used in the arm were selected and adapted to fit with this specific robot arm, largely based on the previous computer simulations. While we suspect similar variables might be found in human arm control, we have no direct evidence to support the claim. Following the performance of the robot arm in this study, we suggest that an architecture featuring hierarchical arrangement of controlled variables might be a plausible solution for biological arm control.

Limitations and Perspectives

A limitation of the present study is the lack of direct comparison of robot behavior to human behavior in the same tasks, and instead comparing invariances and trends. The mechanical and sensory properties of the arm were not on par with the human sensory-motor system to allow such a comparison. With the aim of creating a higher fidelity model of a visually, tactually, and proprioceptively controlled human arm, the improvements would make the arm slightly faster and the sensors more numerous, but maybe not more precise. The improvements would not remove transport delays or noise, because those properties are present in biological arm control systems.

Mechanically, backlash in the geartrain of the motors (also known as slop or play) seems to be a major obstacle for human-like movement, as it puts a hard limit on the precision and bandwidth of the system that cannot be improved by higher quality sensors. With all the non-linearities, slowness, and fatigability in human muscles, human joints are backlash-free. Therefore, a higher fidelity model should put an emphasis on removing the backlash from the joints, perhaps by tendon-driven actuators.

The visual system of the present robot is a crude approximation of the human visual system's object detection in two dimensions. Accurate modeling of visual delays should be maintained, but the resolution and refresh rate could be improved, as well as adding stereo vision for three-dimensional localization. Improvements in the same direction could be made to proprioceptive and haptic sensory systems. In sum, such improved systems would allow testing hypotheses of lower, spinal-level sensorimotor loops, and their interaction with higher-level visual or proprioceptive loops, multi-sensory integration etc.

Additionally, as in studies of human movement, the results are influenced by low-pass filtering the data in the analysis stage, and should be taken with some reserve.

CONCLUSION

This research has shown that in a robot arm system with a hierarchical control architecture based on simulations by Powers (1999, 2008) several features characteristic of biological movement naturally emerge. The robot is robust to noise, delays and some nonlinearities. We found isochrony and bell-shaped velocity profiles in straight reaching movements and the speed-curvature power law in the fast drawing of ellipses. We showed how they can be achieved without trajectory planning, learning or online optimization. We also showed that a hierarchy of controlled variables can produce a motor equivalence phenomenon, where the robot performs the same visual task either with the wrist freely moving or with the wrist blocked. The system also adapts to different angles of the graphics tablet tilt by relying on pressure and pen angle control. Moreover, the system adapts to extending the arm with a tool, and to rotations of the visual field. Overall, we have demonstrated that our 4 DOF robot arm reproduces important features of human movement and therefore presents an appealing platform upon which to build and test further models of adaptive behavior, while providing insight into feasible mechanisms of human arm control.

DATA AVAILABILITY STATEMENT

The raw data supporting the conclusions of this article will be made available by the authors, without undue reservation.

AUTHOR CONTRIBUTIONS

PV and AM conducted a preliminary study. AG-M and AM redesigned the project in its current form and edited the final version of the manuscript. AG-M supervised the research. AM built the arm system, wrote the control software, did the experiments, analyzed the data, performed the modeling, and wrote the first complete manuscript draft. All authors approved the final version of the manuscript.

FUNDING

This work was supported by the Spanish Ministry of Science (pre-doctoral contract BES-2016-077608 to AM; Severo Ochoa of Excellence program SEV-2013-0317 start-up funds to AG-M; Ramón y Cajal grant RyC-2017-23599 to AG-M).

ACKNOWLEDGMENTS

We thank Javier Alegre-Cortés, Regina Zaghi-Lara, Roberto Montanari, Max Parker, and especially Kevin Caref for valuable comments on the manuscript. We are grateful to Regina Zaghi-Lara for photos of the robot arm.

REFERENCES

Atkeson, C. G., and Hollerbach, J. M. (1985). Kinematic features of unrestrained vertical arm movements. *J. Neurosci.* 5, 2318–2330. doi: 10.1523/JNEUROSCI.05-09-02318.1985

Bernstein, N. A. (1967). *The Co-ordination and Regulation of Movements*. Oxford: Pergamon Press.

Brooks, R. (1986). A robust layered control system for a mobile robot. *IEEE J. Robotics Automat.* 2, 14–23. doi: 10.1109/JRA.1986.1087032

Brooks, R. A. (1992). "Artificial life and real robots," in *Proceedings of the First European Conference on Artificial Life*, Cambridge, MA. 3–10.

Bruton, M., and O'Dwyer, N. (2018). Synergies in coordination: a comprehensive overview of neural, computational, and behavioral approaches. *J. Neurophysiol.* 120, 2761–2774. doi: 10.1152/jn.00052.2018

Bullock, D., Grossberg, S., and Guenther, F. H. (1993). A self-organizing neural model of motor equivalent reaching and tool use by a multijoint arm. *J. Cogn. Neurosci.* 5, 408–435. doi: 10.1162/jocn.1993.5.4.408

Castiello, U., and Dadda, M. (2019). A review and consideration on the kinematics of reach-to-grasp movements in macaque monkeys. *J. Neurophysiol.* 121, 188–204. doi: 10.1152/jn.00598.2018

Cisek, P. (2019). Resynthesizing behavior through phylogenetic refinement. *Attent. Percept. Psychophys.* 81, 2265–2287. doi: 10.3758/s13414-019-01760-1

Cisek, P., and Kalaska, J. F. (2002). Modest gaze-related discharge modulation in monkey dorsal premotor cortex during a reaching task performed with free fixation. *J. Neurophysiol.* 88, 1064–1072. doi: 10.1152/jn.00995.2001

Desmurget, M., and Grafton, S. (2000). Forward modeling allows feedback control for fast reaching movements. *Trends Cogn. Sci.* 4, 423–431. doi: 10.1016/S1364-6613(00)01537-0

Feldman, A. G. (2015). *Referent Control of Action and Perception. Challenging Conventional Theories in Behavioral Neuroscience*. Springer Science+Business Media, New York. doi: 10.1007/978-1-4939-2736-4

Fitts, P. M. (1954). The information capacity of the human motor system in controlling the amplitude of movement. *J. Exp. Psychol.* 47:381. doi: 10.1037/h0055392

Flash, T., and Hogan, N. (1985). The coordination of arm movements: an experimentally confirmed mathematical model. *J. Neurosci.* 5, 1688–1703. doi: 10.1523/JNEUROSCI.05-07-01688.1985

Floreano, D., Ijspeert, A. J., and Schaal, S. (2014). Robotics and neuroscience. *Curr. Biol.* 24, R910–R920. doi: 10.1016/j.cub.2014.07.058

Gribble, P. L., and Ostry, D. J. (1996). Origins of the power law relation between movement velocity and curvature: modeling the effects of muscle mechanics and limb dynamics. *J. Neurophysiol.* 76, 2853–2860. doi: 10.1152/jn.1996.76.5.2853

Guiard, Y. (2009). "The problem of consistency in the design of Fitts' law experiments: consider either target distance and width or movement form and scale," in *Proceedings of the Sigchi Conference on Human Factors in Computing Systems*, Boston, MA. 1809–1818. doi: 10.1145/1518701.1518980

Hadjiosif, A. M., Krakauer, J. W., and Haith, A. M. (2021). Did we get sensorimotor adaptation wrong? Implicit adaptation as direct policy updating rather than forward-model-based learning. *J. Neurosci.* 41, 2747–2761. doi: 10.1523/JNEUROSCI.2125-20.2021

Harris, C. M., and Wolpert, D. M. (1998). Signal-dependent noise determines motor planning. *Nature* 394, 780–784. doi: 10.1038/29528

Hughlings Jackson, J. (1884). The Croonian lectures on evolution and dissolution of the nervous system. *Brit Med J.* 1:703. doi: 10.1136/bmj.1.1213.591

Hughlings Jackson, J. (1958). "Evolution and dissolution of the nervous system," in *Selected writings of John Hughlings Jackson*, Vol. 2, ed J. Taylor (London: Staples Press), 45–75.

Huh, D., and Sejnowski, T. J. (2015). Spectrum of power laws for curved hand movements. *Proc. Natl. Acad. Sci. U.S.A.* 112, E3950–E3958. doi: 10.1073/pnas.1510208112

Inoue, Y., Mao, H., Suway, S. B., Orellana, J., and Schwartz, A. B. (2018). Decoding arm speed during reaching. *Nat. Commun.* 9:5243. doi: 10.1038/s41467-018-07647-3

Kawato, M. (1999). Internal models for motor control and trajectory planning. *Curr. Opin. Neurobiol.* 9, 718–727. doi: 10.1016/S0959-4388(99)00028-8

Lacquaniti, F., Terzuolo, C., and Viviani, P. (1983). The law relating the kinematic and fgural aspects of drawing movements. *Acta Psychol.* 54, 115–130 doi: 10.1016/0001-6918(83)90027-6

Latash, M. L. (2008). *Synergy*. New York, NY: Oxford University Press. doi: 10.1093/acprof:oso/9780195333169.001.0001

Latash, M. L., Scholz, J. P., and Schöner, G. (2007). Toward a new theory of motor synergies. *Motor Control* 11, 276–308. doi: 10.1123/mcj.11.3.276

Loeb, G. E. (2012). Optimal isn't good enough. *Biol. Cybern.* 106, 757–765. doi: 10.1007/s00422-012-0514-6

Lopes, G. C. (2016). A robust role for motor cortex. *bioRXiv*. PhD Thesis. doi: 10.1101/058917

Lou, J. S., and Bloedel, J. R. (1988). A new conditioning paradigm: conditioned limb movements in locomoting decerebrate ferrets. *Neurosci. Lett.* 84, 185–190. doi: 10.1016/0304-3940(88)90405-3

Lou, J. S., and Bloedel, J. R. (1992). Responses of sagittally aligned Purkinje cells during perturbed locomotion: synchronous activation of climbing fiber inputs. *J. Neurophysiol.* 68, 570–580. doi: 10.1152/jn.1992.68.2.570

Matic and Gomez-Marin (2019). "Trajectory production without a trajectory plan," in *9th International Symposium on Adaptive Motion of Animals and Machines (AMAM 2019)*. Lausanne, Switzerland.

McNamee, D., and Wolpert, D. M. (2019). Internal models in biological control. *Ann. Rev. Control Robotics Autonomous Syst.* 2, 339–364. doi: 10.1146/annurev-control-060117-105206

Mekyska, J., Faundez-Zanuy, M., Mzourek, Z., Galaz, Z., Smekal, Z., and Rosenblum, S. (2017). Identification and rating of developmental dysgraphia by handwriting analysis. *IEEE Transact. Human-Machine Syst.* 47, 235–248. doi: 10.1109/THMS.2016.2586605

Merel, J., Botvinick, M., and Wayne, G. (2019). Hierarchical motor control in mammals and machines. *Nat. Commun.* 10:5489. doi: 10.1038/s41467-019-13239-6

Miall, R. C., Weir, D. J., Wolpert, D. M., and Stein, J. F. (1993). Is the cerebellum a smith predictor? *J. Mot. Behav.* 25, 203–216. doi: 10.1080/00222895.1993.9942050

Morimoto, J., and Kawato, M. (2015). Creating the brain and interacting with the brain: an integrated approach to understanding the brain. *J. R. Soc. Interface* 12:20141250. doi: 10.1098/rsif.2014.1250

Mounoud, P., Viviani, P., Hauert, C. A., and Guyon, J. (1985). Development of visuomanual tracking in 5-to 9-year-old boys. *J. Exp. Child Psychol.* 40, 115–132. doi: 10.1016/0022-0965(85)90068-2

Müller, J., Oulasvirta, A., and Murray-Smith, R. (2017). Control theoretic models of pointing. *ACM Transact. Computer-Human Interact.* 24, 1–36. doi: 10.1145/3121431

Parker, M. G., Tyson, S. F., Weightman, A. P., Abbott, B., Emsley, R., and Mansell, W. (2017). Perceptual control models of pursuit manual tracking demonstrate individual specificity and parameter consistency. *Attent. Percept. Psychophys.* 79, 2523–2537. doi: 10.3758/s13414-017-1398-2

Parker, M. G., Willett, A. B., Tyson, S. F., Weightman, A. P., and Mansell, W. (2020). A systematic evaluation of the evidence for Perceptual Control Theory in tracking studies. *Neurosci. Biobehav. Rev.* 112, 616–633. doi: 10.1016/j.neubiorev.2020.02.030

Plooij, F. X., and van de Rijt-Plooij, H. H. (1990). Developmental transitions as successive reorganizations of a control hierarchy. *Am. Behav. Sci.* 34, 67–80. doi: 10.1177/0002764290034001007

Powers, W. T. (1973). *Behavior: The Control of Perception*. Chicago, IL: Aldine.

Powers, W. T. (1999). A model of kinesthetically and visually controlled arm movement. *Int. J. Hum. Comput. Stud.* 50, 463–479. doi: 10.1006/ijhc.1998.0261

Powers, W. T. (2008). *Living Control Systems III: The Fact of Control*. Simulations accompanying the book. Available online at: http://www.livingcontrolsystems.com/lcs3/content_lcs3.html (accessed October, 2021).

Prescott, T. J., Redgrave, P., and Gurney, K. (1999). Layered control architectures in robots and vertebrates. *Adapt. Behav.* 7, 99–127. doi: 10.1177/105971239900700105

Profeta, V. L., and Turvey, M. T. (2018). Bernstein's levels of movement construction: a contemporary perspective. *Hum. Mov. Sci.* 57, 111–133. doi: 10.1016/j.humov.2017.11.013

Sartori, L., Camperio, A., Bulgheroni, M., and Castiello, U. (2013). Reach-to-grasp movements in *Macaca fascicularis* monkeys: the Isochrony Principle at work. *Front. Psychol.* 4:114. doi: 10.3389/fpsyg.2013.00114

Schaal, S., and Sternad, D. (2001). Origins and violations of the 2/3 power law in rhythmic three-dimensional arm movements. *Exp. Brain Res.* 136, 60–72. doi: 10.1007/s002210000505

Scott, S. H. (2004). Optimal feedback control and the neural basis of volitional motor control. *Nat. Rev. Neurosci.* 5, 532–545. doi: 10.1038/nrn1427

Scott, S. H. (2012). The computational and neural basis of voluntary motor control and planning. *Trends Cogn. Sci.* 16, 541–549. doi: 10.1016/j.tics.2012.09.008

Shadmehr, R., and Krakauer, J. W. (2008). A computational neuroanatomy for motor control. *Exp. Brain Res.* 185, 359–381. doi: 10.1007/s00221-008-1280-5

Soechting, J. F. (1984). Effect of target size on spatial and temporal characteristics of a pointing movement in man. *Exp. Brain Res.* 54, 121–132. doi: 10.1007/BF00235824

Todorov, E., and Jordan, M. (2002b). A minimal intervention principle for coordinated movement. *Adv. Neural Inf. Process. Syst.* eds Becker, Thrun, Obermayer, MIT Press (2003). 15, 27–34.

Todorov, E., and Jordan, M. I. (2002a). Optimal feedback control as a theory of motor coordination. *Nat. Neurosci.* 5, 1226–1235. doi: 10.1038/nn963

Uno, Y., Kawato, M., and Suzuki, R. (1989). Formation and control of optimal trajectory in human multijoint arm movement. *Biol. Cybern.* 61, 89–101. doi: 10.1007/BF00204593

Viviani, P. (1988). "Two-dimensional Visuo-manual Tracking Beyond The System Analysis Approach," in *Proceedings of the 1988 IEEE International Conference on Systems, Man & Cybernetics*, Vol. 1, (IEEE), Beijing, China. 404–412.

Viviani, P., Campadelli, P., and Mounoud, P. (1987). Visuo-manual pursuit tracking of human two-dimensional movements. *J. Exp. Psychol.* 13, 62–78. doi: 10.1037/0096-1523.13.1.62

Viviani, P., and Flash, T. (1995). Minimum-jerk, two-thirds power law, and isochrony: converging approaches to movement planning. *J. Exp. Psychol.* 21, 32–53. doi: 10.1037/0096-1523.21.1.32

Viviani, P., and McCollum, G. (1983). The relation between linear extent and velocity in drawing movements. *Neuroscience* 10, 211–218. doi: 10.1016/0306-4522(83)90094-5

Viviani, P., and Mounoud, P. (1990). Perceptuomotor compatibility in pursuit tracking of two-dimensional movements. *J. Mot. Behav.* 22, 407–443. doi: 10.1080/00222895.1990.10735521

Viviani, P., and Terzuolo, C. (1982). Trajectory determines movement dynamics. *Neuroscience* 7, 431–437 doi: 10.1016/0306-4522(82)90277-9

Webb, B. (2001). Can robots make good models of biological behaviour?. *Behav. Brain Sci.* 24, 1033–1050. doi: 10.1017/S0140525X01000127

Whelan, P. J. (1996). Control of locomotion in the decerebrate cat. *Prog. Neurobiol.* 49, 481–515. doi: 10.1016/0301-0082(96)00028-7

Wolpert, D. M., and Kawato, M. (1998). Multiple paired forward and inverse models for motor control. *Neu net.* 11:1317–1329. doi: 10.1016/S0893-6080(98)00066-5

Conflict of Interest: The authors declare that the research was conducted in the absence of any commercial or financial relationships that could be construed as a potential conflict of interest.

Publisher's Note: All claims expressed in this article are solely those of the authors and do not necessarily represent those of their affiliated organizations, or those of the publisher, the editors and the reviewers. Any product that may be evaluated in this article, or claim that may be made by its manufacturer, is not guaranteed or endorsed by the publisher.

Annex 6:

Matić, A., & Gomez-Marin, A. (2021). Elbow angle and stiffness control by twisted string actuators and nested feedback. The 9.5th international symposium on Adaptive Motion of Animals and Machines. Ottawa Canada (Virtual Platform), DOI 10.18910/84845

Elbow angle and stiffness control by twisted string actuators and nested feedback

Adam Matić, Alex Gomez-Marin
Instituto de Neurociencias CSIC-UMH, Alicante, Spain
adam.matic@gmail.com

1 Introduction

We can voluntarily control at least two variables at the elbow joint – the angular position of the elbow, and the stiffness or tone of the muscles articulating it. The connectome of sensory-motor loops in the spinal cord is mostly known; a recent primer on stretch reflexes summarizes current knowledge: spinal pathways form nested feedback loops [1]. However, we don't fully understand the computational principles of neural control that would allow us to create equally able artificial systems.

Twisted string actuators (TSAs) are tendon driven actuators that convert the rotary motion of a motor shaft to linear motion of the load by twisting a string. TSAs are an emerging technology with promising uses in exoskeletons and robotic hands [2][3][4]. They are light, efficient and flexible, but the transmission of force via string twisting is highly nonlinear. To compensate for nonlinearities and ensure good performance and high bandwidth, model-based control architectures are commonly proposed (e.g. [5][6]).

Here, we use two TSAs to create a mechanical model of the elbow joint, and we design a control architecture inspired by known anatomical connections in spinal sensorimotor loops, and by a simulation of a hierarchy of feedback loops [7]. As a proof of concept, we demonstrate low bandwidth, but high precision angular position control.

2 Methods

2.1 Hardware

We placed two TSAs in parallel, with one end fixed to a board and the other end connected to the elbow joint (Fig. 1), so that two TSAs acted as antagonists; with ~1.5cm of distance from joint center. Each TSA was composed of a small geared DC motors (N20), a string (~1mm diam.), a stationary sliding potentiometer for measuring string contraction (10KOhm linear, 6cm travel) and another moving potentiometer placed in series with the string (10KOhm, linear, 1cm travel), measuring the stretch of a rubber band (Fig 1, zoom-in). By Hooke's law, the output of the second potentiometer is approximately proportional to the tension of the rubber band and therefore the tension of the tendon. The angle of the joint is measured by a magnetic angular position sensor (ams as5047, 14bit resolution). Sensors are read out by an Arduino Pro Mini (5V, 16Mhz), at 30ms sampling time. The microcontroller sent the output PWM signals to a motor driver (TB6612FNG) with maximum output of 12V.

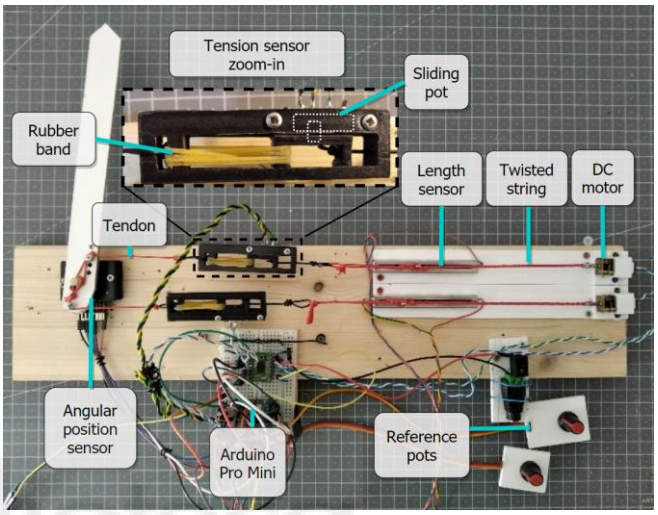

Figure 1: Hardware setup

2.2 Control architecture

The diagram (Fig. 2) shows the nested or hierarchical control architecture of the system. The outer-most loop controls angular position of the joint measured in degrees. The controller is proportional-derivative (PD) with a low pass filter. In the time domain, the equation is:

$$\dot{o} = [K_p(\theta_{ref} - \theta) - K_v\dot{\theta} - o]/tc, \qquad (1)$$

where o is controller output, Kp and Kv the position and velocity gains, θ the measured joint angle, θ_{ref} the reference for joint angle and tc the time constant of the first order low pass filter. Both gains are large (Kp=-20K, Kv=5K) and the time constant is 15s, ensuring high gain at low frequencies and reducing the bandwidth to avoid instabilities at high frequencies. The output o of the controller is a reference signal for the inner control loop (low gain, Kd=1) that senses and controls *tension difference*. The algebraic difference between measured tendon tensions of the two TSAs is proportional (approximately) to the torque acting on the joint. In other words, an angle error will create a torque reference, and this will cause one of the TSAs to increase the tension of the tendon, pull more strongly, and correct the angle error. Similarly, the stiffness of the joint is approximated as the *sum of measured tendon tensions*, and controlled in a low-gain loop (Ks = 3). The outputs of the sum comparator and the difference comparator are combined to form reference signals for the inner loops. The string length control loops are the inner-most loops in the hierarchy, with a loop gain of one.

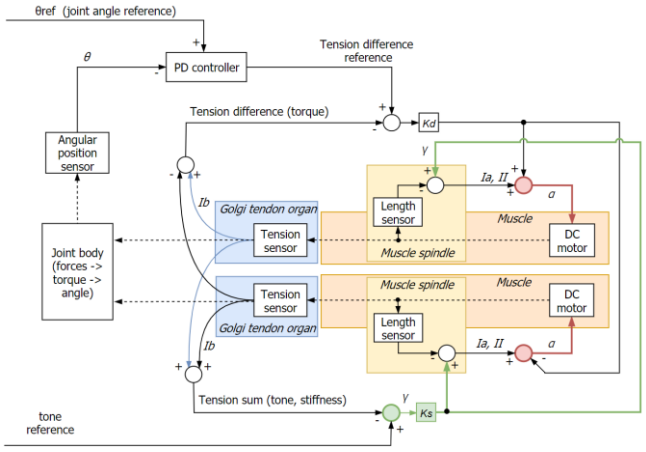

Figure 2. Block diagram of the control hierarchy with hypothetical biological analogs (in cursive)

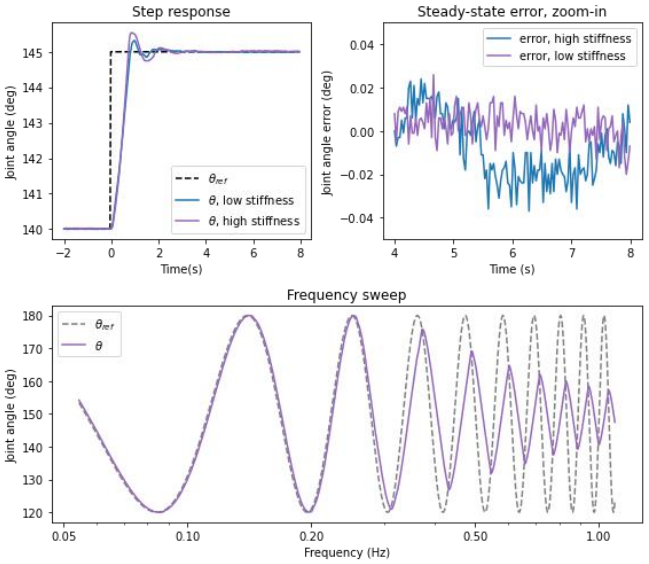

Figure 3. Step response, steady-state error and frequency sweep for measured joint angle

2.3 Biological analogs

The two TSAs are analogs of opposing muscles in the joint (Fig 2). Both mechanisms can only produce a pulling force and need an opposing force to elongate and control muscle length measured by the length sensor. If the sum of tensions is too low (low muscle tone and joint stiffness), joint angle control does not work – this seems to parallel the biological phenomenon of alpha-gamma co-contraction. The muscle spindle is modelled by the combined length sensor and the comparator receiving input from gamma motor neurons (green circle and line). The Ia and II fibers carrying the length error signal are entering the alpha motor neuron (red circle and line) that sends its axon to the extrafusal muscle fibers. The tensions sensors are analogs of Golgi tendon organs, and their outputs type Ib fibers connect to contralateral interneurons to form the tension sum and difference signals. The magnetic angle sensor is an analog of high-resolution visual angle sensing in humans, although with a shorter delay. The loop sampling time of 30ms is analogous to spinal reflex signal transport delay.

3 Results

In the initial test, we analyzed the movement range, speed, and precision using the step response and frequency seep in situations of low and high stiffness (Fig. 3); keeping stiffness constant during the task.

The total movement range was limited to 60 degrees (from 120° to 180°). Maximum movement speed was approximately 12 deg/s. The high stiffness step response had a higher overshoot than the low stiffness response, both settling down at about 3 seconds after the reference step. The bandwidth was low, with attenuation of position signal at frequencies above ~0.2Hz.

However, the precision was relatively high, approaching the limits of the angular position sensor, with the steady state error of only +/-0.03 degrees in low stiffness and +/-0.04 degrees in high stiffness situation.

4 Conclusion

The hierarchical control architecture working with noisy tension and length sensors, relatively long loop delays and affordable low-precision components is capable of high-precision control of joint angle, with up to +/-0.03° error. The source of this precision is the removal of backlash in the joint by using opposing TSAs with a constant sum of tensions, coupled with the high-gain angular position control loop (eq. 1). While the high precision might be satisfactory, the speed and bandwidth of the system are low. In future work we will attempt to improve them by using faster motors and a lower gear ratio. From the biological modelling side, a single joint with opposing muscles is the simplest arrangement, and more research is needed to verify that the control scheme can handle e.g. multiple partial agonists and antagonists. Also, we plan to incorporate biologically plausible transmission delays into different hierarchical levels of control and compare the behavior of the robot to human behavior.

References

[1] Reschechtko S, Pruszynski JA. Stretch reflexes. Current Biology. 2020 Sep 21;30(18):R1025-30.
[2] Palli G, Natale C, May C, Melchiorri C, Wurtz T. Modeling and control of the twisted string actuation system. IEEE/ASME Transactions on Mechatronics. 2012 Jan 25;18(2):664-73.
[3] Popov D, Gaponov I, Ryu JH. Bidirectional elbow exoskeleton based on twisted-string actuators. In2013 IEEE/RSJ International Conference on Intelligent Robots and Systems 2013 Nov 3 (pp. 5853-5858). IEEE.
[4] Shin YJ, Lee HJ, Kim KS, Kim S. A robot finger design using a dual-mode twisting mechanism to achieve high-speed motion and large grasping force. IEEE Transactions on Robotics. 2012 Jul 24;28(6):1398-405.
[5] Rodriguez AS, Hosseini M, Paik J. A hybrid control strategy for force and precise end effector positioning of a twisted string actuator. IEEE/ASME Transactions on Mechatronics. 2020 Dec 24.
[6] Nedelchev S, Gaponov I, Ryu JH. Accurate dynamic modeling of twisted string actuators accounting for string compliance and friction. IEEE Robotics and Automation Letters. 2020 Jan 30;5(2):3438-43
[7] Powers WT. The nature of robots. Part 3: A closer look at human behavior. Byte. 1979 Aug;4(8):94-116

Annex 7:

Matić, A. (2022). Visuomotor phase-locked loop reproduces elliptic hand trajectories across different rhythms. bioRxiv. DOI: 10.1101/2022.07.20.500761

Visuomotor phase-locked loop reproduces elliptic hand trajectories across different rhythms

Adam Matić, Instituto de Neurociencias, UMH-CSIC, Alicante, Spain

Correspondence: adam.matic@gmail.com

Abstract

A well-known phenomenon in human hand movement is the correlation between speed and curvature, also known as the speed-curvature power law ($V \approx kC^{\beta}$). In drawing elliptic shapes, the exponent is often found to be $\beta \approx -1/3$, however it is not clear why the power law appears and why the exponent is near -1/3. More fundamentally, it is not clear how do people track elliptic targets. In answering these questions, I've analyzed trajectories of participants' cursors while they tracked visual targets moving along elliptical paths, across different target speed profiles and cycle frequencies. The speed-curvature power law emerged when drawing ellipses at about 1 Hz or faster, regardless of the target speed profile, and it did not emerge for lower frequency movements. Analysis of the position frequency spectrum shows that the target-cursor trajectory transformation may be seen as a low-pass filter. Comparison of different hypothetical salient features of the visual field shows that phase difference (angular difference between the cursor and the target) and size difference (difference in the sizes of the elliptic paths) are the features most likely used in the task. The next experiment confirmed that phase and size difference could be controlled variables because participants kept them stable even under direct pseudorandom disturbances. A numerical model simulating the sensorimotor processes of the participant, similar to a phase-locked loop, using the visual features of phase and size difference as controlled variables, performed the same target tracking tasks as the participants. When fitted, the model closely replicated position and speed profiles of the participants across all trials, as well as the emergence of the power law at high frequencies. The model also reproduced the trajectories of participants in the experiment with direct pseudorandom disturbances. In conclusion (1) the speed-curvature power law emerges as a side effect of movement system properties, namely low-pass filtering in the sensorimotor loop; (2) people could be tracking elliptical targets by varying the frequency and amplitude of an internal pattern generator until the produced phase and shape size match the target's phase and shape size. The model generates new hypotheses about the neural mechanisms of rhythmic movement control.

Introduction

Hand movement is created in the continuous and closed loop interaction between the brain, body and environment. An often-studied phenomenon in hand movement is the correlation between speed and curvature, first noticed by Binet and Courtier (1893) and Jack (1895) in handwriting as slower movements of the pen in areas of high curvature, and faster movements of the pen in areas of low curvature. The phenomenon was later studied by Viviani and Terzuolo (1982) and formalized as the 'speed-curvature power law' by Lacquaniti et al (1983). The name "power law" comes from the empirical relationship $V \approx kC^{\beta}$ where speed V is approximately equal to curvature C raised to the power β, times a constant k. Speed, or tangential speed, is defined as the magnitude of the velocity vector, $V = |\boldsymbol{v}| = \sqrt{\dot{x}^2 + \dot{y}^2}$ and curvature as the reciprocal of the radius if the osculating circle, $C = \frac{1}{R} = \frac{|\ddot{y}\dot{x} - \ddot{x}\dot{y}|}{V^3}$, where x and y are coordinates of the point P in the plane (Figure 1A). In rhythmical elliptic movement, the exponent β is often found to be -1/3 (Figure 1B). The value of the exponent β expresses the degree of "slowing down in curves": for β=0, there is no slowing, the speed is constant (Figure 1C); for β=-1/3, the speed is slightly lower in curves than in straight parts, and for β=-2/3, the speed is much lower in curves than in straight parts.

An alternative form of the law uses angular speed, defined as the rate of change of the direction of the velocity vector, instead of tangential speed. The two forms have equivalent exponents, however, angular speed tends to have much higher correlations to curvature than tangential speed, as well as higher coefficients of determination in the regression estimate of the power law, and should be avoided when estimating the speed-curvature power law (Matić and Gomez-Marin, 2022). In further analysis, I will be using tangential speed and curvature.

Numerous studies found support for the law, from manually tracking visual targets (Viviani and Mounoud, 1990), drawing ellipses in water (Catavittelo et al, 2017), walking trajectories (Vieilledent et al, 2001) to changes in the exponent during child development (Viviani and Schneider, 1991). When drawing different shapes, the exponent has a spectrum of values different from -1/3 (Huh and Sejnowski, 2015). The power law was also found in movements of hands of monkeys and in population codes in their motor cortex (Schwartz, 1994), as well as in movements of the drosophila larvae (Zago et al. 2016). For a recent review of the evidence for the speed-curvature power law, the statistics used and hypotheses of its origin, see Zago, Matić et al. (2017).

Hypotheses aiming to explanation the emergence of the power law may be divided into two broad groups - central origin theories and emergence theories. The central origin group argues that, since the speed-curvature relationship is found in so many different types of movements, it is likely a part of the planning strategy for every movement. For example, it could be a result of minimizing jerk (Viviani and Flash 1995), maximizing smoothness (Huh and Sejnowski, 2015) or minimizing endpoint variance (Harris and Wolpert, 1998). The second group of explanations favors emergence

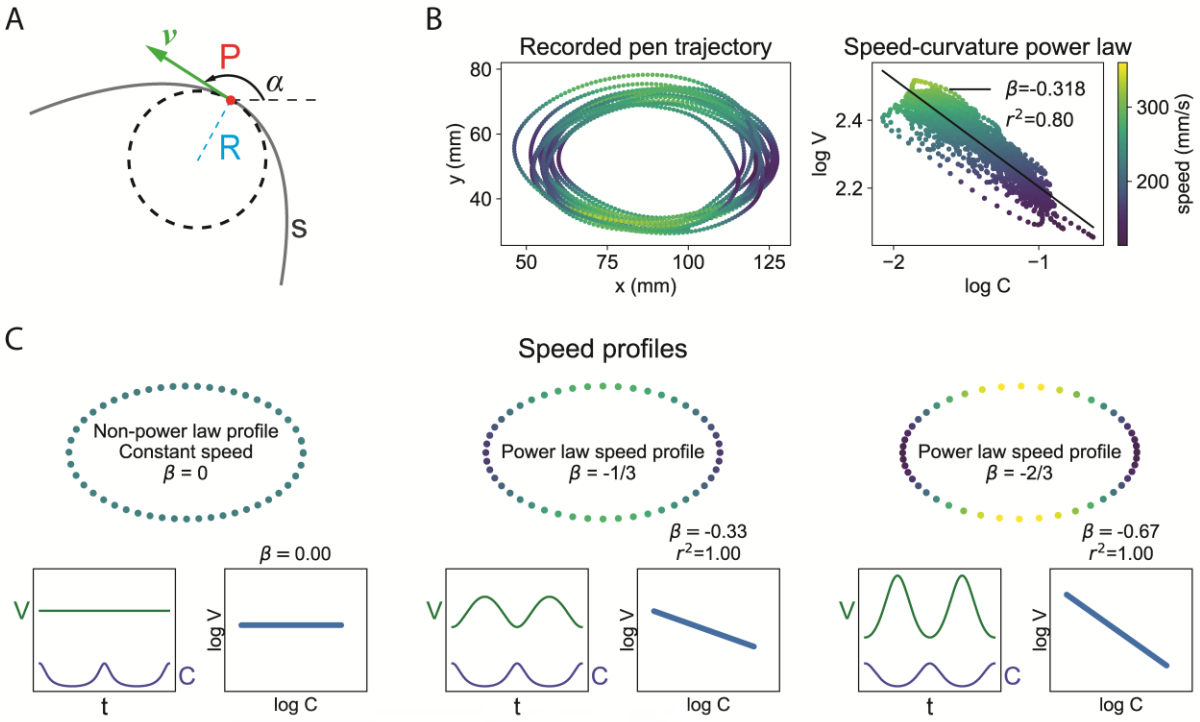

Figure 1. The hand movement speed-curvature power law*, $V \approx kC^{\beta}$, or $\log V \approx \log k + \beta * \log C$.* ***A)*** *Geometric and kinematic definitions of the variables: the point P moves along the curve s; at each instant of time, its velocity can be described by the vector* ***v****, speed V is the magnitude of velocity, and curvature C is the reciprocal of the radius R of the osculating circle (C = 1/R). The direction of movement with respect to the x-axis is* ***α****, and its first time-derivative is the angular velocity A. The variable k is a constant related to average speed.* ***B)*** *An example of an empirical trajectory conforming to a speed-curvature power law: a participant moves the pen faster (bright green) in areas of low curvature and slower (dark green) in areas of high curvature. On a log-log plot, the relationship between speed and curvature is linear, with the slope β, intercept log k and coefficient of determination r^2* ***C)*** *Examples of the speed-curvature relationships for equal curvature profiles, but different speed profiles. In the first case, the speed is constant, and there is no power law. In the second case, the speed is slightly lower in areas of high curvature, with the exponent β= -1/3 (~0.33) and r^2=1. This profile is often found in elliptic human hand movements. In the third case, the speed is much lower in areas of high curvature than in areas of low curvature, with the exponent β= -2/3 (~0.67) and r^2=1.*

of the power law in the interaction of the brain, body with the environment, mainly due to low pass filtering (Gribble and Ostry 1996; Schaal and Sternad, 2001).

The relationship of average speed or rhythm of drawing and the exponent of the power law has not been explored in detail, although Lacquaniti et al (1983, Figure 4) reported different values of the exponent for three different rhythms of drawing, and Wann et al (1988) reported two different exponents for two different rhythms, all of relatively fast movement.

Here, I explore target tracking over a wider range of rhythms for a constant size elliptic trajectory, and the relationship between the rhythm and the power law exponent and the coefficient of determination. Next, I estimate salient visual features used by the participant in the task, and build a numerical model, based on the findings, that performs the same task.

My basic assumption was that during the task, participants observe and maintain (control) certain visual variables at their respective reference values. It was not obvious what these variables were, and how to describe them mathematically. The deceptively simple strategy, suggested by Powers (1973, 1978) is to find variables that remain stable despite being disturbed by the experimenter.

The search starts by generating precise mathematical definitions of the hypothetical controlled variables. This definition needs to make clear what are the effects of the experimenter-generated disturbances on the controlled variable, and the effects of participant-generated behavior on the controlled variable. For instance, the controlled variable may be defined as a distance between the target and the cursor, the disturbance is, therefore, the position of the target, and the behavior of the participant is the position of the cursor. Both the target and the cursor can affect the controlled variable in a precisely defined way. The experimenter can directly perturb this hypothetical controlled variable by generating a target trajectory and then observe corrective actions by the participant; or alternatively the experimenter can insert a disturbance between the pen and the cursor on the screen.

If the hypothetical controlled variable is stable relative to the variance of the perturbation, it might be a good approximation for the variable controlled by the participant. If it is not stable, there are several possibilities – (1) the variable is not controlled, (2) the variable is controlled, but the bandwidth of the disturbance is too wide (the task is too difficult), (3), the variable is controlled, but the reference level was not stable, etc. The task should be designed to be not too difficult, and the reference level should be stable, or with a known variation.

Aside from the stability of the controlled variable, another useful statistic is a *low* correlation between the potential controlled variable and the disturbance variable – meaning that a controlled variable is unaffected by the disturbance, and as a consequence it is uncorrelated to it.

When a sufficiently good and precise definition of the hypothetical controlled variable is found, then a generative numerical model, a simulation of the participants' sensorimotor loop in the can be built, and fitted to each participant individually. For further validation, the behavior of the model can be compared to the behavior of the participants in new tasks where the model was not fitted. Good performance of the model in new tasks would support the explanatory and predictive power of the model and the conclusion that the mathematical definition of the controlled variable is a good approximation of the variable controlled by the participant. There is always a possibility of finding a better approximation.

The model should be made as computationally simple as possible in order to be biologically plausible. Signals generated by the numerical model may be direct correlates of neural signals in the nervous system of the participant, and this might be verified in an independent experiment.

Strong invariances in participants' movements, such as the speed-curvature power law, may be used to verify a model of rhythmic behavior: the power law needs to appear in the same conditions

for the model as for the participants, and also it needs to *not* appear in the same conditions for the model, where it does not appear for the participants.

Data and code availability

The data collected in this research, along with jupyter notebooks and python code used to analyze the data and prepare the figures is available at https://github.com/adam-matic/visuomotor-phase-locked-loop

Experiment 1: Tracking targets along rhythmic elliptical trajectories

Method

In the first experiment, participants tracked a target with a cursor on the computer monitor. Participants (N=3, male, right-handed, age 30-36, including the author of the paper) were seated, looking at the computer monitor showing a cursor and a target. They were holding an electronic pen in their dominant hand, pen positioned on the graphics tablet (Wacom Intous PTH S). They were instructed to keep the cursor and target as close as possible. Target trajectories had three different speed profiles: (1) $\beta=0$, constant speed, (2) $\beta=-1/3$, 'natural' speed with slight slowing in the curved areas, and (3) $\beta=-2/3$, excessive slowing in the curved areas, (see Figure 1C). All three profiles were generated for nine fundamental frequencies of the target: 0.27, 0.40, 0.54, 0.67, 0.81, 0.94, 1.07, 1.21, and 1.34Hz corresponding to average speeds of the target: 44, 67, 91, 113, 135, 158, 180, 203, 227 mm/s. The target always moved in a counter-clockwise direction. The trials were presented in a random order. Each trial started when the participant pressed the space key, and lasted for 20 seconds, after which the participant could rest. The monitor displayed the target and cursor at 60Hz, while the tablet recorded the pen position data at 200Hz.

Target trajectories were formed by first generating a high-resolution elliptical path, and then rescaling the temporal distances between the points so that the speed conformed to a desired speed-curvature power law. The resulting target trajectory was splined and resampled to have the points equally spaced in time, and rescaled for desired total time. For analysis, pen position data was low-pass filtered with a second-order Butterworth filter with a cutoff at 10Hz; target positions were converted from screen coordinates (px) to tablet coordinates (mm). The speed-curvature power law was estimated using orthogonal linear regression because both speed and curvature contained measurement uncertainties.

Results

For slow, low-frequency movements, the position error (Fig. 2B and Fig. 2E) and velocity errors (Fig 2E) were low, meaning that the participants' pen position stayed fairly close to target position,

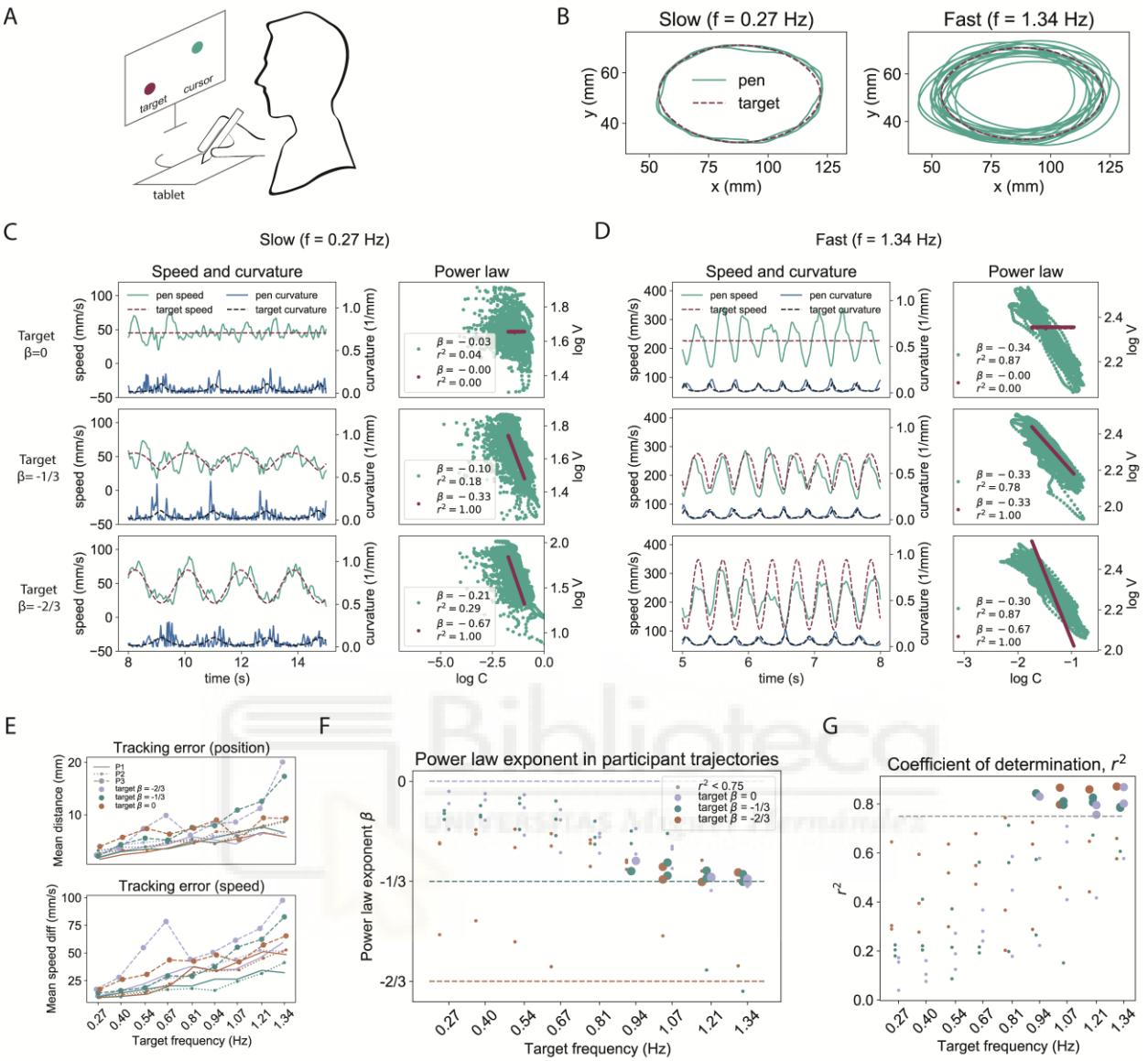

Figure 2. Experiment 1, when tracking elliptic targets, the speed-curvature power law only emerges at high frequencies ***A)*** *Diagram of the task* ***B)*** *Target and pen paths in slow movement (f=0.27Hz, period=3.7s) and in fast movement (f=1.34Hz, period=0.75s). Target ellipse dimensions were 68x39mm, measured from the shape the pen needed to traverse on the tablet.* ***C)*** *Segment of the pen and target speed and curvature over time for low-frequency movements, across three different speed profiles; participant's pen speed seems to track target speed, but pen logC and logV are not strongly correlated* ***D)*** *Segment of the pen and target speed and curvature over time for high-frequency movements. The exponent of the pen's trajectory is β=-1/3, regardless of the exponent of the target's trajectory.* ***E)*** *Participants are more accurate in tracking low frequency targets' positions and speeds and less accurate in tracking positions and speeds of high-frequency targets, regardless of target speed profile, suggesting poor trajectory control at high frequencies* ***F)*** *The speed-curvature power law is only strong enough ($r^2 \geq 0.75$, arbitrary cutoff) for some high frequency movements ($f \geq 0.94$Hz), and has the same exponent of β≈-1/3, regardless of target power-law exponent. Each point represents a tracking trial, with the color signifying the target speed profile and size the crossing of threshold of r^2* ***G)*** *The coefficient of determination (r^2) rises with the frequency of drawing the ellipses, and crosses the arbitrary threshold of 0.75 at f=0.94Hz.*

and pen speed is also very similar to target speed for all participants. As an example, Fig 2C shows segments of low-frequency tracking speed and curvature time profiles. For each of the target speed profiles (β=0, β=-1/3 and β=-2/3) the participant stays close to the target speed and curvature. However, the speed and curvature of the pen vary more than the speed and curvature of the target. This variance can be seen as the 'spread' on the power-law plot (low r^2). Target log-speed and log-curvature have a strong linear relationship (by design), but participant pen log-speed and log-curvature are uncorrelated.

High-frequency target tracking was very different. There are large errors in position (Fig. 2B, 2E) and large errors in speed (Fig. 2E); however, most participant pen trajectories conform to a speed-curvature power law with the same exponent, $\beta \approx -1/3$, and a high coefficient of determination $r^2 \geq 0.75$, even though target exponents are different.

An example segment plotted on Figure 2D shows that participant speed had very similar range and mean across different target speed profiles. The power law plots show very similar exponents and high r^2s in participants' trajectories, regardless of target exponent. Position and speed tracking accuracy gets worse with the increase in target frequency (Figure 2E), and since the ellipse sizes were always equal, higher frequency meant higher average speed. This result is consistent with the speed-accuracy tradeoff, and suggests poor trajectory control at high average speeds, if trajectory is the controlled variable.

The main results of the first experiment are summarized in Figure 2. Panels F and G: the exponent of the power law of the participants trajectories converges toward β=-1/3 at high frequencies of movement, regardless of target speed profile. The power law was only strong enough ($r^2 \geq 0.75$, arbitrary cutoff) for some trajectories with drawing frequency $f \geq 0.94$ Hz (period smaller than ~1.06s), and did not appear for slower movements. The frequency where the power law crosses the threshold of 0.75 also depends on the data filtering procedure, here a second order Butterworth filter with a 10Hz cutoff was used to smooth the position data, and the smoothed data was used estimate curvature and velocity.

Experiment 2: Is the cursor-target distance a salient visual feature and a controlled variable?

The instruction to participants in the first experiment was to *keep the cursor as close as possible to the target*. The first guess for the salient visual feature (or visual cue, or visual controlled variable) was the distance between the cursor (C) and the target (T). However, the Euclidean distance is unsigned (always positive), and cannot be used in a proportional feedback control system. In random pursuit tracking it is established that the x and y components of the Euclidean distance (dx and dy) are good approximations for controlled variables (Viviani and Mounoud 1990, Parker et al 2017). In the first test, I've analyzed weather dx and dy could be controlled, where dx=Cx – Tx, and dy = Cy – Ty (see the diagram in Figure 2E) in each point in time.

Method

For experiment 2, the target trajectory was generated as a smoothed pseudorandom trajectory in two dimensions, and used in a pursuit tracking task (Figure 3A). One participant (male, right-handed) performed the task of following the target with the cursor by moving a pen on an electronic tablet (Huion 610ProV2, recording at 60Hz), with the instructions to keep the cursor as close as possible to the target. The behavior of participants in the ellipse tracking task was first compared to the behavior in the random pursuit tracking task, with the following hypothesis: if the participant controlled the same variables in both tasks, then those variables will have the same relationships to the target position and cursor position, namely dx and dy will be stable and uncorrelated to Tx and Ty, respectively, in both tasks. Next, a numerical model was designed to control dx and dy and then fitted to participant behavior in the pursuit tracking task. The model then performed the ellipse tracking task. If the participants also control dx and dy, their behavior in ellipse tracking should be as well approximated by the model in ellipse tracking task as it is in the random pursuit task.

Results

In the pursuit tracking task, the distance (dx and dy) between the target and the cursor in stable (Figure 3B) and uncorrelated to the target (T), r(dx, Tx)=0.05, r(dy, Ty) = 0.04. Similarly, in tracking elliptic trajectory targets, the distance between the cursor and the target is relatively stable (Figure 3C). However, across all trials, the variables dx and dy are not consistently uncorrelated to Tx and Ty (Figure 3D). This is suggesting there might be better approximations for salient visual features in this task than dx and dy.

In the second line of evidence, a first-order, distance control model with delay (Figure 3E) was fitted to the behavior of the participant. The best fit values for the parameters were found to be: gain K=-10, damping B=0.02 and delay tau=0.100s, similar in x and y. The model accounts for the pursuit tracking behavior fairly well (Figure 3F). However, when the fitted model is tracking the same elliptic trajectory target as the participant, the behavior of the model differs from the behavior of the participant – the distance dy is much larger (Figure 3G), there is phase delay in the model cursor with respect to the target, not seen in participant trajectories, and the amplitude of the model cursor movement is larger than participant amplitude. When the two large-amplitude movements in x and y are combined (Figure 3H), the model cursor trajectory creates a larger elliptic shape than that of the target; while participants maintain the drawn shape on average equal in size to the target-drawn shape.

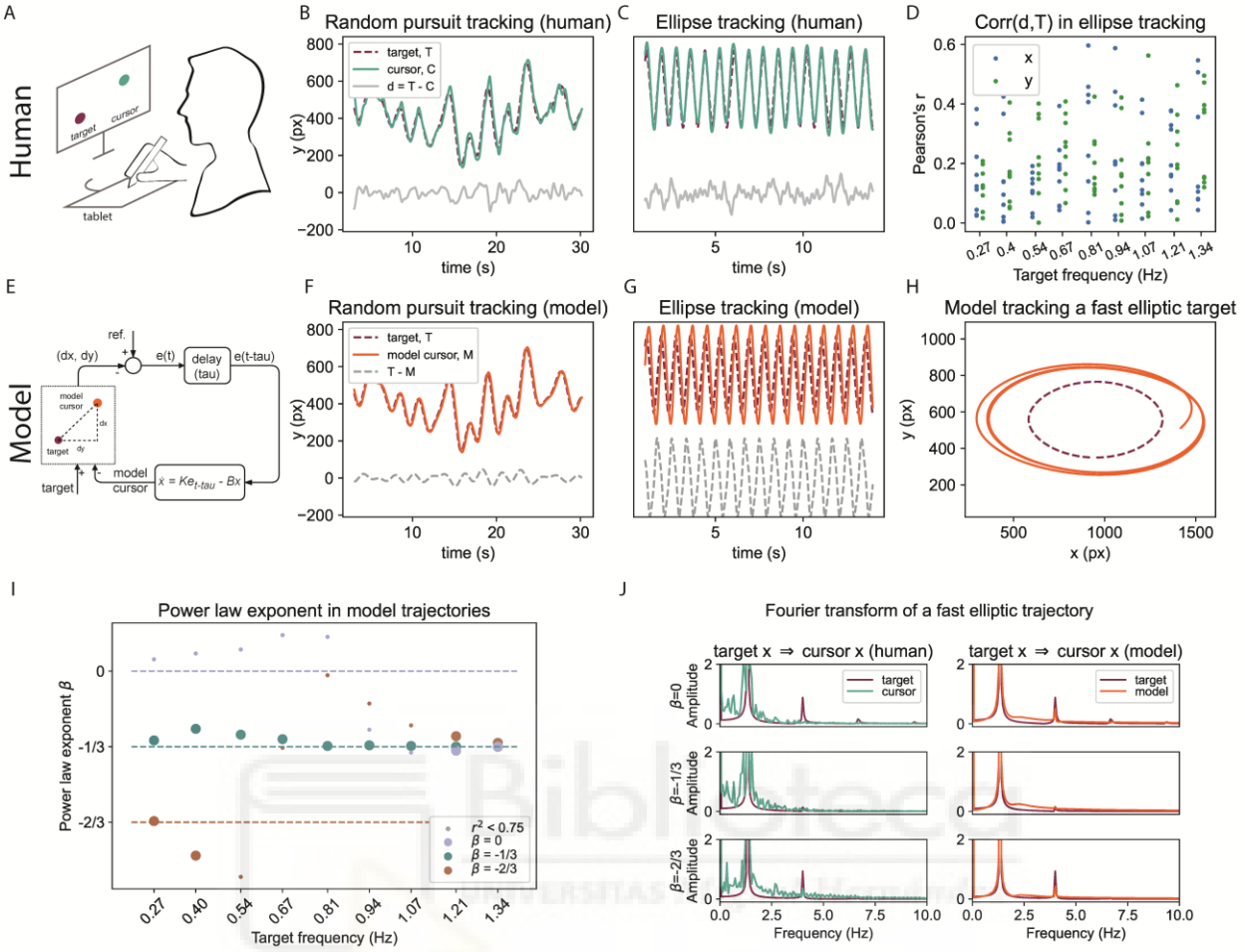

Figure 3. Experiment 2: The cursor-target distances (dx and dy) are controlled variables when tracking pseudorandom targets, but not when tracking elliptic targets*. Still, the distance tracking model partially reproduces the β-frequency relationship because of low-pass filtering.* ***A****) Diagram of the experimental setup.* ***B****) In a pursuit tracking task, the participant closely follows the target; variables d and T and uncorrelated.* ***C****) When tracking an elliptic trajectory, the participant is still closely following the target, however,* ***D****) across the trials in Experiment 1, the correlations between variables dx and Tx, and dy and ty, are not low.* ***E****) Diagram of a first-order model with delay, parameters fitted in a random pursuit task.* ***F****) The model controlling the C-T distance follows the target and reproduces participant trajectory in a random pursuit task.* ***G****) The same model does not account for participant behavior in ellipse tracking, as the dy is larger than in participant's trajectory and* ***H****) The elliptic path of the model is larger than the path of the target for fast movements* ***I****) However, the trajectories of the model converge toward β≈-1/3 power law at high frequencies.* ***J****) Both the human participant and the numerical model can be seen as low-pass filters of the target signal, passing the low-frequency fundamentals and attenuating the higher-frequency components.*

From these two lines of evidence, we can conclude that dx and dy are not the salient visual features in tracking elliptic targets; they are not controlled in this task, and there might be better approximations for the controlled variables.

While the dx-dy distance model does not account for the behavior of participants in the elliptic target tracking task, model trajectories do show some interesting properties. The exponents of

model trajectories, like those of participants, converge to the value of β=-1/3 at high frequencies (Figure 3I). This convergence may be a consequence of low-pass filtering properties of both the model and human participant, as shown by the Fourier transform plot (Figure 3J). Target trajectories that contain harmonics of a frequency higher than the filter's cutoff frequency will be 'transformed' to cursor trajectories that contain only the fundamental frequencies. Similarly, target trajectories with the exponent β=-1/3 across all trials are already single-frequency sinusoids, and when passed through the filter they were phase shifted and amplitude-modulated, they remained single-frequency sinusoids, and their 2D elliptic trajectory conformed to the power law.

Phase difference and size difference as controlled variables in tracking elliptic targets

After the confirmation that the cursor-target distances dx and dy are not controlled in tracking targets along elliptic paths, I've tested several other hypotheses of controlled variables, and here I report on the most likely ones – phase difference and size difference. The analysis was performed using data from experiment 1.

Method

The phase difference (dφ) is here defined as the angle closed by the cursor, the center of the ellipse and the target (Figure 4A), or equivalently, as the difference between the cursor angle (or phase) φ_C and the target angle φ_T. In terms of control systems, dφ is the proposed controlled variable, with the assumed reference value of zero radians, meaning 'cursor on target'. This controlled variable is disturbed by the changes in the target angle, so the disturbance is φ_T, and the participant's behavior acts to bring back the phase difference to zero radians by changing the cursor angle φ_C. The expectation was that participants maintained the controlled variable stable and uncorrelated to the disturbance variable. Since the variables were measured in radians, the circular coefficient of correlation was used.

The second proposal for the controlled variable is the size difference (ds), defined as the difference between the semimajor axis a of the target ellipse (the 'x-radius') and the semimajor axis r_C of an ellipse with the same center, but passing through the cursor point (Figure 4A). The axis of the cursor ellipse is calculated as $r_C = r\sqrt{\cos(\varphi_C)^2 + ((a/b)\sin\varphi_C)^2}$, where r is the instantaneous distance of the cursor to the center, and a/b is the constant ratio of target ellipses' major and minor semiaxes. The value is expected to be stable if it is controlled. However, the correlation coefficient is not defined when one of the variables is a constant (the size of the target ellipse a), so the correlation was not calculated.

Results

As shown on the figure 4B, the phase difference is maintained stable in the slow trial as well as in a fast trial. Analyzing all the correlations between dφ and φ_T, for all trials and participants, we can

see extremely low values (Figure 4C), supporting the proposal that the phase difference was a controlled variable in the elliptic target tracking task in experiment 1.

Similarly, participants maintained the size difference stable in both slow and fast trials (Figure 4D), supporting the proposal that the size difference was also a controlled variable in experiment 1.

Experiment 3: Direct pseudorandom disturbances to phase and size differences

I've verified the proposed controlled variables further in a new experiment where the both the size difference and the phase difference were simultaneously disturbed with pseudorandom disturbances, while the participant attempted to maintain them stable. Here, the disturbance to the controlled variable are the target's angular position and target ellipse size: the participant tracked a target moving along an ellipse in a random-smoothed fashion. Alternatively, the experiment could be performed using the same task as experiment 1 – tracking a target that has a constant rhythm and draws and ellipse of constant size – and the disturbances could be added to the pen position.

Method

One participant performed the task of following the target with the cursor by moving the pen on an electronic tablet (Huion 610ProV2, recording at 60Hz), with the instructions to keep the cursor as close as possible to the target. Both the angle of the target and the size of target ellipse varied randomly (Figure 4E). The participant performed 8 trials; the trial number does not signify a progression in any of the task properties.

Results

Figure 4E shows a segment of both cursor and target paths in experiment 3. Next, Figure 4F shows participant performance in trials 1 and 8 - the participant maintained the phase difference stable and near zero. The participant also maintained the size difference relatively stable and near zero, or in other words the size of the ellipse shape drawn by the cursor was close to the size of the ellipse shape drawn by the target (Figure 4G).

The correlations of disturbance and the controlled variable are very low in the case of phase angles (Figure 4H), using the circular correlation coefficient. This again indicates that the phase difference is a very good candidate for a controlled variable in tracking elliptic targets. In the case of the size difference, the correlations were moderately low (Figure 4I), using the Pearson's correlation coefficient, indicating that size difference might be a controlled variable simultaneously with phase difference.

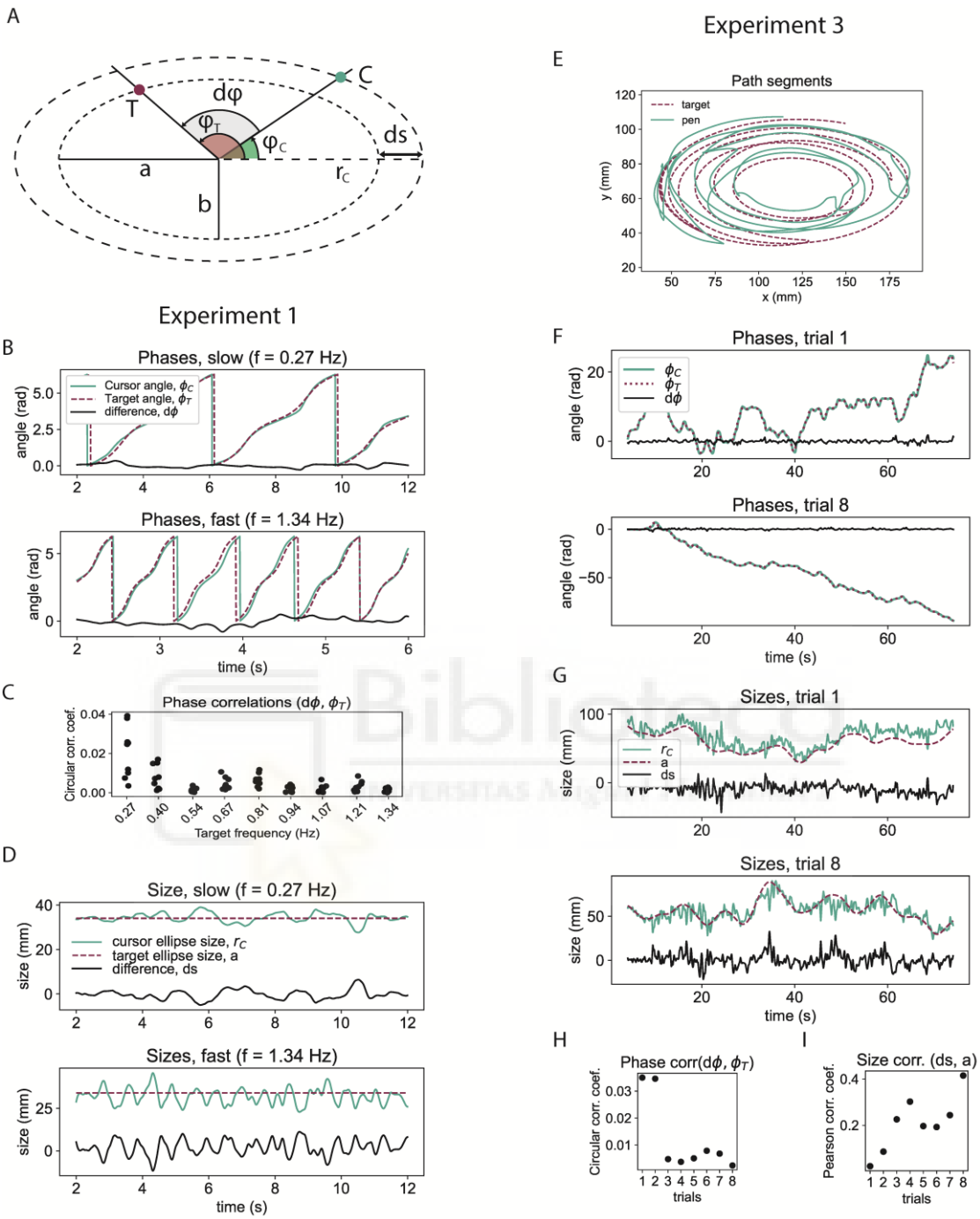

Figure 4. Phase difference (dφ) and size difference (ds) are good candidates for controlled variables in following elliptic trajectory targets. ***A***) *dφ is the difference between the cursor angle (φ_C) and target angle (φ_T) measured from the x-axis; ds is the difference between the x-axis radius of the target path (a), and the x-axis radius of the cursor path (r_C). The ratio a/b is constant.* ***B***) *Examples from Experiment 1: dφ is stable.* ***C***) *Phase correlations across all tasks in Experiment 1 are very low, using the circular correlation coefficient.* ***D***) *The size of target path (a) is constant, and the size of the cursor path (r_C) is nearly equal, with low variance.* ***E***) *Experiment 3: cursor and target path segments – target trajectory varies randomly in phase and size.* ***F***) *The participant maintains dφ stable, near zero* ***G***) *The participant maintains ds stable, near zero.* ***H***) *Variables dφ and target angle φ_T are uncorrelated* ***I***) *the variables ds and a are only weaky correlated.*

Numerical model, sensorimotor phase-locked loop with amplitude control

Having found two good candidates for controlled variables, I've constructed a numerical model that controls them, and fitted the parameters of the model to participant behavior in experiment 1. The aim of this model was to reproduce participant behavior in measures such as position, speed, and curvature over time and the exponent β and coefficient of determination r^2 of the speed-curvature power law. For further validation, the model performed the experiment 3 in the same conditions as the participants, with the same pseudo-random elliptic target trajectories.

Method

The model simultaneously controls phase difference and size difference in tracking an elliptically moving target (Figure 5A). It directly incorporates the dx-dy tracking model in the lower level - the loop on the lower right of Figure 5A is the same model seen in Figure 3E. The output of two high-level controllers, phase difference and size difference, is combined to generate the reference signal for the lower-level system. The reference is a point in 2D space acting as a virtual target for the dx-dy tracking system. This control system is aiming to keep the model cursor near the virtual target, using the same controller equation as in experiment 2, and the same parameters obtained when fitting the model to participant behavior.

The phase control loop in this model is a version of the phase-locked-loop (PLL), a very common control system in radio communication and information technology used to synchronize phases and frequencies of signals. Keeping the phases of two signals in 'lock', where their difference is a constant value (not necessarily zero), means that their frequencies will be equal.

The main parts of the phase control loop appear on the diagram (Figure 5A) starting with the phase difference 'detector'. Given positions of the center of the ellipse, the target and the cursor, the phase difference detector finds dφ: the angles of φ_T and φ_C are calculated as arctangents of the x and y components of their positions relative to the center and unwrapped. The output of the phase difference detector is $d\varphi = \varphi_T - \varphi_C$. The value dφ is passed to a pure delay element and used as an input to a proportional-derivative controller (PD) with an implicit reference of zero, so the phase difference is maintained at zero. The error is integrated as passed to the harmonic oscillator as the frequency parameter f. The oscillator is implemented as a rotating unit vector with instantaneous frequency f and angular velocity $\omega=2\pi f$, described by the equations $\dot{x} = -y\omega$ and $\dot{y} = x\omega$ with initial angle set to the target angle φ_T.

The size difference control loop maintains the size of the cursor-drawn ellipse equal to the size of the target drawn ellipse. The size r_C is calculated as $r_C = r\sqrt{\cos(\varphi_C)^2 + ((a/b)\sin\varphi_C)^2}$, where r is the instantaneous distance of the modelled cursor to the center, and a/b is the constant ratio of target ellipses' major and minor semiaxes. The controlled variable ds is the difference between the target ellipse size determined by the parameter **a**, and the size of the cursor ellipse r_C. The difference is passed to a pure delay element, then a PD controller gives values rx and ry, where ry

= (a/b) rx. The values rx and ry are multiplied with oscillator output to generate the 2D location of the virtual target.

The lower-level loop aims to maintain the cursor on the virtual target. It is identical to the dx and dy control loop from experiment 2, has the same parameters and therefore identical low-pass filtering properties, presumably matching those of the participant. The difference is that the 'target' is an internal reference signal, and not an external stimulus. In experiment 2, we observed that the dx and dy control model lagged in phase behind the target, and that the size of the ellipse drawn by the model was different than the size of the ellipse drawn by the target. The role of the virtual target was to automatically compensate for the attenuation or amplification of amplitude produced by the low-pass filtering process. The size of the ellipse drawn by the virtual target was automatically increased when there was a size difference between the cursor and the 'real' target. Similarly, the virtual target was automatically advanced in phase to compensate for the phase lag produced by the low pass filter.

Another important part of this model is the simulated measurement noise. This a is a small-amplitude, normally distributed pseudorandom signal (mean=0mm, std=0.06 mm), added to cursor in x and y position independently during the task. This signal was primarily aimed at modelling the noise arising in the electronic tablet and pen instruments during recording.

The model performed the same task as the participants of first tracking the target across elliptic trajectories from experiment 1, and second across randomly varying phase and size from experiment 2. Recorded position trajectories were smoothed with a 10Hz cutoff low-pass, second-order Butterworth filter. The simulation step was 5ms, using Euler integration. Time derivatives of signals were approximated as differences between current and previous time-step signal values, divided by the time-step length.

Results

The parameters of the model – the gains and delays of the phase and size difference control loops – were found by fitting the behavior the model to the behavior of one participant. The parameters of the inner loop were found in experiment 2, and they remained the same (K=10, B=0.018 and delay=100ms). The size difference loop had a delay of 250ms: 150ms on top of 100ms from the inner loop, while the phase difference had a delay of 100ms; no additional delay on top of the inner loop. The phase difference proportional-derivative (PD) controller had Kp=0.5 and Kd=0.3, while the size difference PD controller had Kp=1.33 and Kd=0.016, and an additional slowing term with B=0.033.

Figure 5 shows the performance of the model in the same tracking task performed by the participants, analyzed in the same way as participant performance (Figure 2), while Figure 6 shows a direct comparison between one participant and the model.

The model closely approximates the behavior of the participants – the speed curvature power law emerges only for high-frequency target tracking, where $r^2 \geq 0.75$ only for trials where the target frequency was $f \geq 0.81$Hz (Figure 5F and 5G), while for participants the power law was present for $f \geq 0.94$Hz.

In a slow trial (target f=0.27 Hz, period=3.7s, Figure 5C), for different target speed profiles (β=0, β=-1/3, β=-2/3), the model cursor seems to be tracking the low-frequency fundamental, and there is some higher-frequency noise, in both speed and curvature profiles. Speed and curvature are only weakly related and the power law does not reach $r^2 \geq 0.75$. This is similar to participant speed and curvature profiles for the same task - compare Fig. 5C to Fig. 2C.

In a fast trial (target f=1.34Hz, period=0.75s, Figure 5D), for different target speed profiles, the model has the same speed profile, with the exponent β≈-1/3, and with high r^2. This is similar to the participant speed profiles, and the relationship between speed and curvature in participant trajectories – compare Fig 5D to Fig 2D.

The position and speed errors across trials with different frequencies were not the same as participants (Figure 5E, compare to Figure 2E). The model has lower errors, lowest when the target speed profile conforms to β=-1/3 power law. This distinction does not appear strongly in participant position and speed errors plot (Figure 2E). The absolute value of the errors is also smaller in the model than in participant trajectories. In the given range of target frequencies, the position error for targets with β=0 and β=-2/3 is relatively large even for slow targets, and does not have a clear trend.

The similarity of the behavior of the model is to the behavior of the participants is best seen in direct comparison of several time profiles: position, speed, phase difference and size (Figure 6). In the slow, low frequency trial (Figure 6A) the position of the model closely matched participant position in the same task. Speed profiles contain similar amounts of high-frequency components, mostly coming from the modelled low-amplitude measurement noise.

In phase difference and size, the participant's profiles seem to contain more randomness, while model phase difference and size are more repetitive. Direct comparison between the participant and the model in fast movement (Figure 6B) reveals very similar position and speed profiles, while phase difference and size seem to be more variable in participants trajectories than in the model trajectories.

Without changing the parameters, the model performed a tracking trial identical to experiment 3 (Figure 6C and 6D). The model maintained simultaneously the phase difference (Figure 6C) and the size difference (Figure 6C) stable and near zero, in a very similar range to that of participants, even when both target phase and ellipse sizes had a randomly-varying time profile.

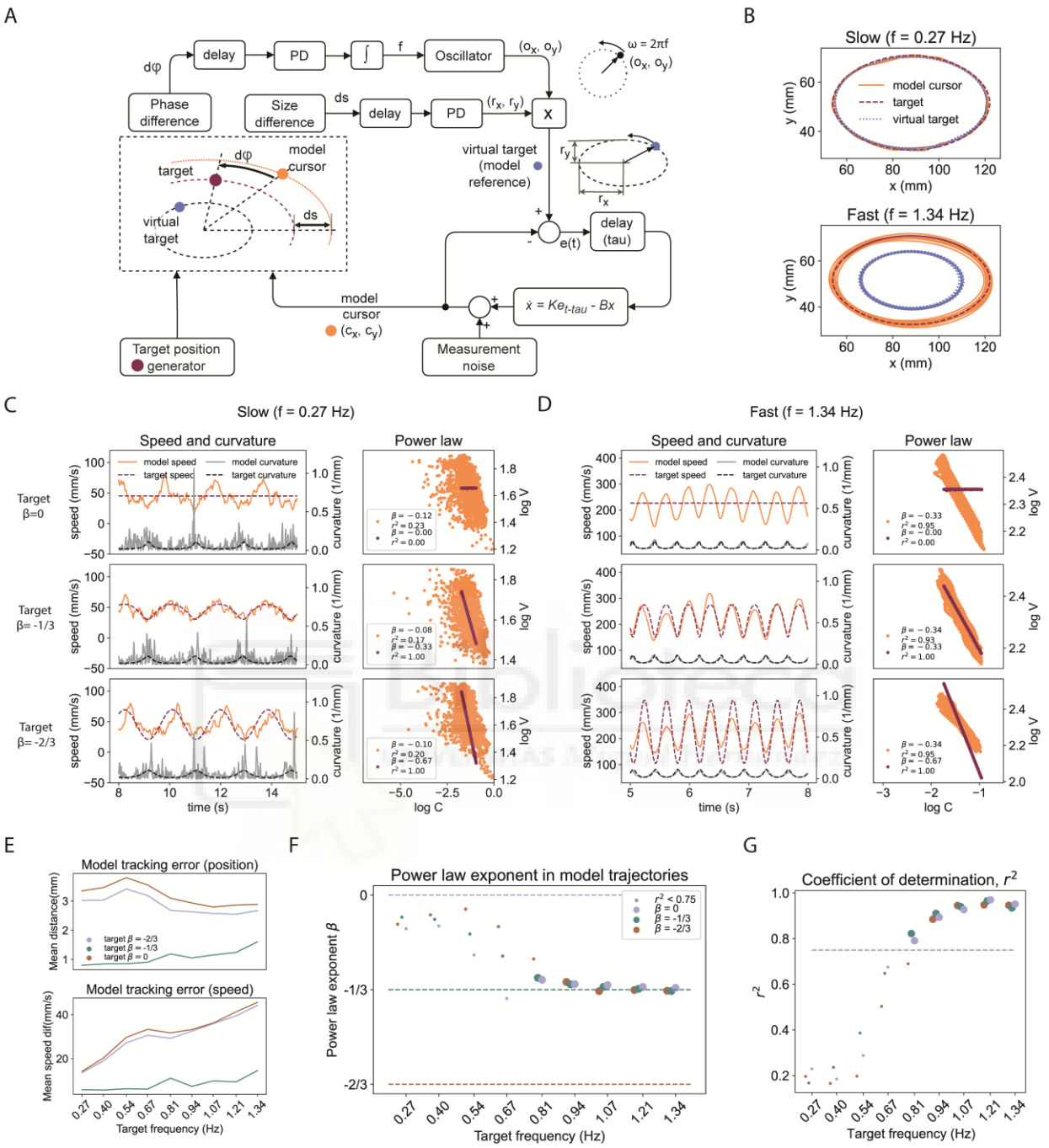

Figure 5. The numerical model reproduces participant trajectories and the dependence of the power law exponent on target frequency found in experiment 1 (Figure 2) A) *Diagram of the model: a visuomotor phase-locked loop with amplitude control* ***B)*** *Model maintains the size of the cursor path equal to the size of the target path for both slow and fast targets by modifying the amplitude of the virtual target* ***C)*** *For slow movements, the model's speed and curvature are similar to participants, including the non-conformity to the speed-curvature power law.* ***D)*** *In fast movement, all model cursor trajectories follow the β=-1/3 speed curvature power law, regardless of the target speed profile.* ***E)*** *In the given frequency range, the model is much more accurate than participants in both position and speed* ***F)*** *The model is reproducing the relationship between the power law exponent β and the movement frequency found in Experiment 1, as well as* ***G)*** *the relationship between the coefficient of determination r^2 and movement frequency.*

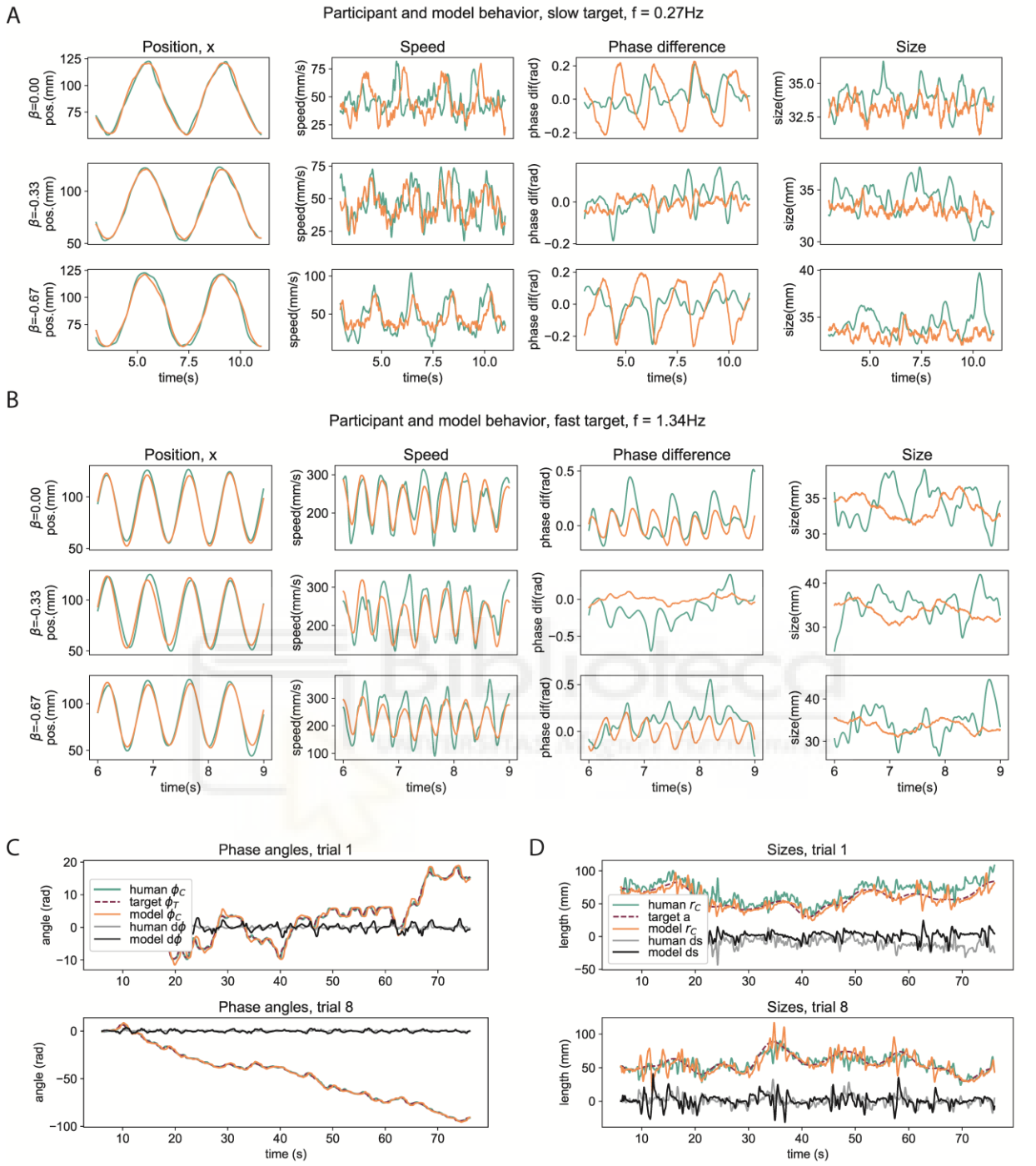

Figure 6. Direct comparison of one participant and model behavior in the same tasks *(model in orange, participant in green).* ***A****) In tracking a low frequency (slow) target, model and participant behave similarly in measures of position in the x dimension, speed, phase difference and ellipse size.* ***B****) In tracking a high-frequency (fast) target, the model shows more regularity, while the participant shows more randomness in behavior, however the positions and speeds are very similar* ***C****) The model also reproduces participant phase angles from Experiment 3, where the target phase varied randomly* ***D****) The model reproduces participant ellipse sizes from Experiment 3, where the target size varied randomly.*

Discussion

The power law does not necessarily appear for low-speed trajectories. The main empirical finding in experiment 1 (Figure 2) was that the speed-curvature power law appeared ($r^2 \geq 0.75$) only for high frequency movements, when the fundamental frequency was larger than 0.94Hz, or equivalently, when the period of drawing an ellipse was shorter than 1.04 seconds, and average speed higher than 158mm/s. For higher rhythms, participants did not track instantaneous target speeds well. Instead, participants' speed profiles were nearly the same from trial to trial, following the β=-1/3 speed-curvature power law, regardless of the target's power law exponent. In other words, for fast rhythms, participants always moved slightly slower in the curves than in the straight parts, even when the target moved at a constant speed (β=0) or had a higher speed difference profile (β=-2/3) (Figure 2D). In contrast, for low frequencies, (low average speed, cycle periods longer than 1.04s) the fit to the speed-curvature power law was poor. Participants roughly tracked instantaneous positions and speeds of the targets (Figure 2E) but the curvature and speed profiles contained a lot of high-frequency components, possibly coming from movement noise and measurement noise.

The limit where the power law fit (r^2) reaches 0.75, at period time of 1 second, or frequency of 1Hz, might be specific to small-size elliptic trajectories of the hand, since the target ellipse had a constant size, 6.8cm in width and 3.7 cm in height. It has already been reported that drawing larger elliptic shapes does not always result in a good fit to the power law (Schaal and Sternad, 2001). Future research should look into the interaction of average speed, size of the trajectory and rhythm or period of drawing, and their influence on the exponent and the strength of the speed-curvature power law.

At low speeds, the participants did closely reproduce the low-frequency target trajectories in both speed and position (Figure 2E). If participants can explicitly track or control trajectories, this ability seems to have a fairly low bandwidth, as the errors steadily increase with frequency, and yet, the size of the elliptic shape and the rhythmic synchronization to the target were still preserved. This seems to suggest a non-trivial control scheme, where *trajectory is not the controlled variable*.

Cursor-target lineal distance is not controlled. In experiment 1, participants were instructed to *'keep the cursor as close to the target as possible'*, and the first approximation for the controlled variables were the x and y components of the cursor-target distance, variables called dx and dy. There are several independent lines of evidence suggesting dx and dy are *not* controlled in ellipse tracking. First, in random pursuit tracking, dx and dy are demonstrably good approximations for controlled variables (Parker, 2017), and as expected, there are very low correlations between dx and Tx, as well as between dy and Ty in experiment 2 (random pursuit, Figure 3B). However, those correlations were higher in ellipse tracking, suggesting that dx and dy are not controlled in ellipse tracking (Figure 3D).

Second, the dx-dy model made much bigger ellipse drawings than the participants, and created a large phase lag, again suggesting that dx and dy are not controlled in ellipse tracking.

Low-pass filtering accounts for the power law. The low-pass filtering properties of the dx-dy model may account for the convergence of the power-law exponents toward a value of β=-1/3 at high speeds (Figure 3I and 3J). A similar result was found by Gribble and Ostry (1996), where they concluded that the power law may arise from the low-pass filtering properties of the musculoskeletal system of the arm. Schaal and Sternad (2001) found that even a simple Butterworth filter with an appropriate cutoff frequency can produce power-law trajectories out of constant-speed trajectories. Recently, we have shown that a robot arm following a constant-speed visual target can also produce power law trajectories because it behaves as second order system with delay, also a low-pass filter (Matić et al., 2021). Similarly, as recognized by Lacquanity et al (1983), an ellipse composed of pure sinewave components, without any harmonics, will conform to the -1/3 speed-curvature power law. Low-pass filtering creates smooth trajectories for frequencies below the cutoff, and this alone might explain the speed-curvature relationship – if the target trajectory is the input signal, the visuomotor and proprioceptive-motor loops are filters that smooth it out, and create pure sinewaves in the cursor (or pen) trajectory as output.

The difficulty with this explanation is that low-pass filters distort the input signal by introducing amplitude modulation and phase lags – filtered trajectories in Schaal and Sternad (2001), Gribble and Ostry (2003) and Matić et al (2021) all show that output ellipses have a different size than input ellipses. Participants in experiment 1 generally maintained the size of the cursor trajectory equal to that of the target's trajectory, and followed the targets without phase lags – similar results were found by Viviani and Mounoud (1990) when tracking ellipses and by Parker (2020) when tracking one-dimensional sine waves.

A possible solution is that higher-order systems somehow compensate for the distortions introduced by the filter.

Phase and size difference may be controlled. I've proposed that higher order systems directly observe and control the visual phase difference and the size difference between the ellipses drawn by the cursor and the target. In experiment 1, the phase difference was maintained stable, and also had a very low correlation with disturbances (Figure 4B, 4C), which means it was unaffected by the disturbances and likely controlled. Participants also maintained the size of the cursor-drawn ellipse relatively constant (Figure 4D), which means that the size difference was also likely controlled.

In experiment 3, direct disturbances were applied to the phase difference and size difference variables by designing an elliptic target trajectory that had a randomly changing phase and size. The stability and correlation measures confirmed the findings from the first experiment (Figure 4E, 4F, 4G, 4I).

Instead of creating new target trajectories, an alternative strategy might be to apply random perturbations in the pathway between the pen and the cursor, making the disturbances invisible to the participants, and maintaining task visually equal to experiment 1, but altering the pen movement patterns necessary to maintain phase difference and size difference stable.

Numerical model reproduces participant trajectories. For the next verification step, I've created a numerical model, a simulation of the perceptual and control processes of participants. It is implemented as a two-level hierarchical control system that perceives and controls the cursor-target phase difference and the cursor-target ellipse size difference (Figure 5A). The phase difference is integrated in time and used as a frequency parameter to a harmonic oscillator. The output of the oscillator is multiplied by the size difference error to create a virtual target – a phase-advanced and amplitude-corrected reference for the inner loop. When the model cursor follows the virtual target, the phase difference and size difference can be kept low in the whole range of target frequencies tested; making the behavior of the model similar to human participants. The low-pass filtering properties of the dx-dy model are maintained because the inner loop has the same structure and parameters.

The model replicated some important measures of participant behavior – namely the absence of the speed-curvature power law at low frequencies and the emergence of the power law at high frequencies, with the same exponent $\beta \approx -1/3$, and $r^2 \geq 0.75$ for higher frequencies ($f \geq 0.84$Hz). For participants this frequency was $f \geq 0.94$Hz, and the difference is possibly a consequence of unmodelled, multiplicative noise (Faisal et al., 2008). Speed and position profiles of the model cursor were also similar to participants (Figure 6). On the other hand, the speed and position errors (the distance between the cursor and the target) in the model (Figure 5E) were lower than the speed and position errors in participant trajectories (Figure 2E) - the model was more accurate. This might suggest some changes in the model that would make it less accurate in speed and position tracking, while still maintaining a good fit in other measures.

The model also replicated participant behavior in non-rhythmical target trajectories, namely when both the phase of the target and size of the target ellipse had pseudorandom profiles (experiment 3, Figure 6D and 6E), suggesting that the model might be more general – the target trajectory does not need to be rhythmical, and the size of the target ellipse does not need to be constant. The model performed all the tasks without any changes in the parameter after initial fitting.

Parameter measurement implications. If model parameters represent some internal characteristics of the participant, their values might be informative about the characteristics of the participant. The delay parameter represents the time it takes for a signal to make a 'full trip' around the loop, and longer delays might indicate longer computational processing or longer nerve pathways, implying hierarchically higher systems. As expected for a hierarchically higher system - the size difference control loop has a large delay (250ms), but the phase difference loop is only at 100ms, the same as the inner control loop. This might indicate that the model needs some reorganizing. I've proposed the phase control loop as superordinate to the inner cursor position

loop, but those two loops might also be on the same organizational level. The proposed oscillator is 'cortical', since it sends outputs downstream to the visual system, however it might be a spinal or a brainstem central pattern generator. This proposal could be verified in a future study.

Alternative and additional controlled variables. As mentioned in the introduction, there are always potential improvements to the approximation of the controlled variables. Similar measures to phase and size difference might also be used, such as the arc-length distance instead of the phase difference. This might be a more useful measure when the target path is not elliptical. The size of the ellipse, as proposed, might be split into the horizontal and vertical amplitude components, allowing the control of elliptic paths of independently varying width and height. Alternatively, path accuracy might be controlled more locally, by perceiving the distance between the cursor and the path, and altering the direction of movement. The velocity of the target itself might play a role, as in one-dimensional sinewave tracking (Parker et al., 2021). An additional control variable in the task might be the center of the oscillation.

Limitations of the study. Participants were not trained to perform the task. The task was not difficult, however, training until there is no more improvement should remove the influence of learning on performance and make the participant trajectories less variable from cycle to cycle.

There were only three participants in the first experiment, and a single participant in the second and third. A larger number of participants who would perform all three experiments would allow fitting the model to each participant individually, and then testing how well the model predicts their behavior in a new task. While I have not used any statistical inference tests that would require a large number of participants, a higher number of participants might still be useful to gather the ranges and consistency measures of model parameters, such as gains and delays, in the sample.

Summary and outcome. In this study, I've attempted to answer why there is a relationship between speed and curvature in elliptic hand movement, why is the exponent of the speed-curvature power law often found to be -1/3, and more broadly – how people track elliptic trajectories.

I've found that the power law only appears in fast movement, here when elliptic paths are traversed in less than 1 second, for relatively small elliptic shapes (6.8 cm width and 3.7 cm height).

Based on the recorded data, I've proposed phase difference and size difference as controlled variables in the ellipse tracking task and supported the hypothesis by finding that participants can maintain them stable when they are directly perturbed in a tracking task. Also, there are low correlations between controlled variables and disturbance variables in two different tasks.

Finally, a numerical model that controlled phase and size difference reproduced many of the behavioral measures found in participants' hand trajectories, such as the emergence of the speed-curvature power law, as well as position and speed profiles of participants' hand trajectories.

In conclusion, it appears that in ellipse tracking, the speed-curvature power law emerges because of the low-pass filtering properties of the whole visuomotor loop, including visual processing and musculoskeletal elements. The effects of the low-pass filter – phase delay and amplitude modulation – are compensated by two higher level loops that maintain the phase of the cursor equal to the target and the size of the drawn ellipse equal to the size of the target ellipse by modulating the frequency and amplitude of a simple harmonic oscillator.

Acknowledgements. I would like to thank Alex Gomez-Marin for his involvement in the design of Experiment 1, and the comments of the figures.

References

Binet, A., & Courtier, J. (1893). Sur la vitesse des gestes graphiques [On the speed of voluntary movements]. Revue Philosophique, 35, 664-671

Catavitello G, Ivanenko YP, Lacquaniti F, Viviani P (2016) Drawing ellipses in water: evidence for dynamic constraints in the relation between speed and path curvature. Exp Brain Res 234:1649–1657

Faisal, A. A., Selen, L. P., & Wolpert, D. M. (2008). Noise in the nervous system. Nature reviews neuroscience, 9(4), 292-303.

Gribble, P. L., and Ostry, D. J. (1996). Origins of the power law relation between movement velocity and curvature: modeling the effects of muscle mechanics and limb dynamics. J. Neurophysiol. 76, 2853–2860. doi: 10.1152/jn.1996.76.5.2853

Harris CM, Wolpert DM (1998) Signal-dependent noise determines motor planning. Nature 394:780–784

Huh D, Sejnowski TJ (2015) Spectrum of power laws for curved hand movements. Proc Natl Acad Sci 112:E3950–E3958 doi: 10.1073/pnas.1510208112

Jack, W. R. (1895). On the analysis of voluntary muscular movements by certain new instruments. Journal of Anatomy and Physiology, 29, 473-478

Matić, A., Valerjev, P., Gomez-Marin, A. (2021). Hierarchical Control of Visually-Guided Movements in a 3D-Printed Robot Arm. Front. Neurorobot. 15:755723. doi: 10.3389/fnbot.2021.755723

Matic, A., & Gomez-Marin, A. (2022). Angular speed should be avoided when assessing the speed-curvature power law of movement. bioRxiv.

Lacquaniti, F., Terzuolo, C., & Viviani, P. (1983). The law relating the kinematic and figural aspects of drawing movements. Acta psychologica, 54(1-3), 115-130.

Parker, M. G., Tyson, S. F., Weightman, A. P., Abbott, B., Emsley, R., and Mansell, W. (2017). Perceptual control models of pursuit manual tracking demonstrate individual specificity and parameter consistency. Attent. Percept. Psychophys. 79, 2523–2537. doi: 10.3758/s13414-017-1398-2

Parker, M. G., Weightman, A. P., Tyson, S. F., Abbott, B., & Mansell, W. (2021). Sensorimotor delays in tracking may be compensated by negative feedback control of motion-extrapolated position. Experimental brain research, 239(1), 189-204. https://doi.org/10.1007/s00221-020-05962-0

Powers, W. T. (1973). Behavior: The Control of Perception. Chicago, IL: Aldine

Schaal, S., and Sternad, D. (2001). Origins and violations of the 2/3 power law in rhythmic three-dimensional arm movements. Exp. Brain Res. 136, 60–72. doi: 10.1007/s002210000505

Schwartz AB (1994) Direct cortical representation of drawing. Science 265:540–542

Vieilledent S, Kerlirzin Y, Dalbera S, Berthoz A (2001) Relationship between speed and curvature of a human locomotor trajectory. Neurosci Lett 305:65–69

Viviani P, Flash T (1995) Minimum-jerk, 2/3 power law, and isochrony: converging approaches to movement planning. J Exp Psychol Hum Percept Perform 21:32–53

Viviani, P., and Mounoud, P. (1990). Perceptuomotor compatibility in pursuit tracking of two-dimensional movements. J. Mot. Behav. 22, 407–443. doi: 10.1080/00222895.1990.10735521

Viviani, P., and Terzuolo, C. (1982). Trajectory determines movement dynamics. Neuroscience 7, 431–437 doi: 10.1016/0306-4522(82)90277-9

Viviani P, Schneider R (1991) A developmental study of the relationship between geometry and kinematics in drawing movements. J Exp Psychol Hum Percept Perform 17:198–218

Wann J, Nimmo-Smith I, Wing AM (1988) Relation between speed and curvature in movement: equivalence and divergence between a power law and a minimum-jerk model. J Exp Psychol Hum Percept Perform 14:622–637

Zago M, Lacquaniti F, Gomez-Marin A (2016) The speed-curvature power law in Drosophila larval locomotion. Biol Lett 12(10):20160597